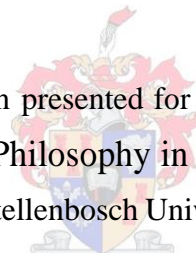


# **The Mechanical Behaviour of High-Performance Concrete with Superabsorbent Polymers (SAP)**

by

**Babatunde James Olawuyi**

Dissertation presented for the degree of  
Doctor of Philosophy in Engineering  
at Stellenbosch University



Promoter: Prof. William Peter Boshoff  
Faculty of Engineering

March 2016

## *Declaration*

By submitting this dissertation electronically, I declare that the entirety of the work contained therein is my own, original work, that I am the sole author thereof (save to the extent explicitly otherwise stated), that reproduction and publication thereof by Stellenbosch University will not infringe any third party rights and that I have not previously in its entirety or in part submitted it for obtaining any qualification.

November, 2015

Copyright © 2016 Stellenbosch University

All rights reserved

# *Abstract*

High performance concrete (HPC) is known to be of low water-binder ratio (W/B) and exhibits high strength, durability and elastic modulus amongst many other properties. HPC is susceptible to autogenous-shrinkage-caused-cracking under restraints while previous research efforts directed at mitigating autogenous-shrinkage in HPC by the introduction of IC agents have reported superabsorbent polymers (SAP) to be the most promising. This study seeks to fill the existing gap on proper understanding of the effect of SAP addition on the mechanical behaviour of HPC.

The work studied the mechanical properties of HPC containing SAP as internal curing agent (IC-agent) using two grain sizes of SAP ( $< 300 \mu\text{m}$  and  $< 600 \mu\text{m}$ ) at varied SAP contents (0%; 0.2%; 0.3%; and 0.4%  $b_{\text{wob}}$ ) in four reference HPC mixtures ( $M_{1F}$ ,  $M_{1S}$ ,  $M_2$  and  $M_3$ ) after 7, 28, 56 and 90 days of curing in water. SAP absorption in cement pore solution (CPS) was determined using the tea-bag test and the 25 g/g absorption in CPS obtained after 10 minutes of immersion was used for provision of additional water in the HPC mixtures. Experimental works were carried to study the impact of SAP addition on the rheology of the HPCs, as well as identify and establish the effect of varying sizes and volume of SAP on rate of cement hydration and strength development. The work involved quantifying and modelling the mechanical behaviour (strength in compression, tension, elastic and fracture properties) of the low W/B (0.2 – 0.3) HPC (C55/67 – C100/115) with SAP. Microstructure and molecular interaction of the internal constituent of the HPC were also investigated using the X-ray computed tomography (CT) scanning and scanning electron microscopy (SEM).

The study observed a slight decrease in the compressive strength of HPC as SAP content increases but there is no such effect on the elastic and fracture properties of the concrete. The 25 g/g SAP absorption result of the teabag test over-estimates the actual amount of water used up by SAP in the internal curing of HPC. The 3D void analysis of the HPC via CT scanning revealed that SAP created voids in the HPC is only about half (i.e. 12.5 g/g) of the teabag test result of 25 g/g and affirms that the required additional water for SAP's effective internal curing of the low W/B HPC is 12.5 g/g. The

study concludes that the optimum additional water for SAP addition in the low W/B HPCs at no negative effect on mechanical properties is 12.5 g/g.

# Opsomming

Hoë verrigting beton (HVB) is bekend as 'n beton met 'n lae water/binder (w/b) verhouding en vertoon 'n hoë sterkte, duursaamheid en elastiteitsmodulus. HVB is egter geneig om krake te vorm weens outogene krimp wanneer dit verhinder word om te krimp. Vorige werk het gewys dat die gebruik van superabsorberende polimere (SAP) hierdie outogene krimp kan verminder as dit gebruik word as 'n interne kuur metode. Hierdie studie poog om die gebreke in die navorsing van HVB met SAP te vul, naamlik die verstaan van die meganiese eienskappe van hierdie materiaal.

Hierdie werk het die meganiese eienskappe van HVB met SAP van twee groottes ( $< 300 \mu\text{m}$  en  $< 600 \mu\text{m}$ ) ondersoek teen verskillende inhoude (0%; 0.2%, 0.3%, 0.4% bgvb) met drie verskillende meng klasse ( $M_{1F}$ ,  $M_{1S}$ ,  $M_2$ ,  $M_3$ ) na 7, 28, 56 en 90 dae van kuur in water. Eksperimentele werk was uitgevoer om die impak van SAP byvoeging op die reologie van die HVB, die effek van verskillende groottes SAP, die volume van SAP op die hidrasie tempo en sterkte ontwikkeling te ondersoek. Die werk het behels die kwantifisering en die modellering van die meganiese gedrag (sterkte in druk, trek en die elastiese en fraktuur eienskappe) van lae W/B HVB (0.2 tot 0.3) (C55/67 tot C90/C105) wat SAP bevat. Die mikrostruktuur en molekulêre interaksie van die interne bestanddele was ook ondersoek met twee nie-destruktiwe toetsmetodes naamlik CT skandering en elektronmikroskopie.

Die studie wys 'n minimale verlaging van die druksterkte van HVB indien die SAP inhoud verhoog word, maar geen effek was opgemerk op die elastiese en fraktuur eienskappe van die beton nie. Die 25 g/g SAP absorpsie kapasiteit bepaal deur die sogenaamde teesakkie-toets oorskat die eintlike hoeveelheid water opgeneem deur SAP in HVB. Die 3D leemte bepaling d.m.v. die CT skandering het getoon dat die leemtes veroorsaak deur die SAP is nader aan die helfte as verwag, naamlik 12.5 g/g. Dit bevestig die addisionele water wat benodig word vir interne kuur met SAP is eerder 12.5 g/g. Indien meer as 12.5 g/g water addisioneel bygevoeg word sal dit 'n verlaging van die druksterkte veroorsaak. Die optimale addisionele water byvoeging vir interne kuur doeleindes vir HVB met SAP is dus 12.5 g/g.

# *Acknowledgements*

I acknowledge with profound gratitude my supervisor, Prof. W.P. Boshoff, for his guidance, and immense contributions throughout the course of this study. Accepting me as research student was a good gesture on itself, not to talk of working with a student that has no financial support for the programme. I am indeed very grateful to you. I appreciate the Head of Department, Prof. G.P.A.G Van Zijl, for his time spent in reading through and contributions made on my initial proposal towards presentation for Senate's approval when my Supervisor was un-avoidably on leave due to ill-health. His concern and timely words of encouragement are indeed immeasurable.

I say thank you to the Management of the Department of Civil Engineering, Stellenbosch University and the industry partners, the Pretoria Portland cement Company (PPC) for the Departmental Bursary offered me for the 2014 and 2015 Sessions of the programme and the materials (CEM I 52.5 N and Corex slag) provided for the laboratory work. Also of note is the supply of the superplasticiser (Premia 310) by Chryso, silica fume (SF) by SiliconSmelters of the FerroAltantica group and fly ash (FA) from AshResources.

I appreciate the support and assistance of the staff of the laboratory and workshop of the Civil Engineering Department, University of Stellenbosch offered during the design and fabrication of the Wedge Splitting test setup and the entire laboratory work. My special thanks also go to the following people: Mr. Guillaume Jeanson (Construction Product Manager) SNF Floerger - ZAC de Milieux, 42163 ANDREZIEUX Cedex – FRANCE; Davy Penhard, FEI Visualisation Science Group; Dr. Anton du Plessis and Stephan le Roux, CT Scanning Unit; Mrs. Madelaine Frazenburg and Dr. Angelique Laurie, Electron Beam Unit; both of Central Analytical Facilities (CAF); and Mrs. Hanlie Botha of Process Engineering Department, Stellenbosch University, South Africa for the assistance received in materials procurement, use of facilities, softwares and time input in the analysis.

I am grateful to my employer, Department of Building, Federal University of Technology, Minna, Nigeria, for releasing me on study fellowship in pursuit of a PhD degree at Stellenbosch University,

South Africa. I also say thank you to TETFUND, Nigeria for the financial support received for my Benchwork.

I seize this opportunity to acknowledge the grace of God upon the following people of God around me here in Cape Town and Stellenbosch environment: Pastor Obiajulu Onyia and his Wife, Pastor Prince Mathebula and his Wife, Pastor Shedrack Shu, Pastor Oyeleke Oyebamiji and everyone in the Ministerial Team of the Winners Chapel International, Cape Town. Thank you all for giving me an opportunity to serve the Lord in your midst. Worthy mentioning here is the family of Dr. Dominic Bass, for making their car available for my use in meeting up with the demands of my Academic work and God's assignment. This investment will surely speak in your life and that of your children. I say thank you to Pastor, Dr. Funlola Olojede for her prayers, support and privileged opportunity to learn and minister in Bible Study with my special Brethren at Stellenbosch assembly (Desire of Nations) of The Redeemed Christian Church of God. God bless you all.

To my first Family in Stellenbosch, Br. Femi Olaoye, Chidi Ofoegbu, my friend and brother, John Babafemi Adewumi (Dcn., Bldr., Dr.), I say thanks you. God will strengthen the bound of love within us. Special love and appreciation goes to my spiritual children in Cape Town (Samuel Asante, Michell, Bukky, Vimbai, Debby, Success and Nonkululeko); Br. Smith, Emmanuel, Godspower, Sis. Favour, Reezy and the Youth of Winners Chapel International, Cape Town; Br. Richards Kamutando, Papa Vukile and the entire congregation of Winners Chapel International, Khayelitsha. It has been a privilege and great opportunity to see you receive God's word through me and work with it in Faith. Your followership in Kingdom service is really amazing. The grace of God will be multiplied upon you all.

I am grateful to all my Parents, Parents-in-law and siblings (maternal and in-love) for their love, prayers and support. I say thank you to all my friends, colleagues, loved ones and all who contributed in one way or the other who might not have been mentioned.

Finally, I am eternally grateful to God for my Wife, Stella Funmilayo and three children, Gladness, Joyful and Glory for their love, good health, grace, sacrifices and fore-bearing during my over three

years of stay in Stellenbosch. You were all strong, supportive and always gave me reasons to go all the way. Dear, I am proud of you and will always love you. God bless and keep you all for me.

## *Dedication*

This dissertation is dedicated to the Almighty God and Father of our Lord Jesus Christ for grace, inspiration and enablement enjoyed in the course of this study and my stay in South Africa. To him alone is the glory forever (Amen).

# Table of Contents

<i>Declaration</i> .....	<i>ii</i>
<i>Abstract</i> .....	<i>iii</i>
<i>Opsomming</i> .....	<i>v</i>
<i>Acknowledgements</i> .....	<i>vi</i>
<i>Dedication</i> .....	<i>ix</i>
<i>Table of Contents</i> .....	<i>x</i>
<i>List of Figures</i> .....	<i>xvi</i>
<i>List of Tables</i> .....	<i>xxi</i>
<i>List of Symbols</i> .....	<i>xxiv</i>
<i>List of Abbreviations</i> .....	<i>xxvi</i>
1 Introduction.....	1
1.1 Statement of Research Problem.....	3
1.2 Aim and Objectives of the Study .....	5
1.3 Research Proposition .....	6
1.4 Significance of Study.....	6
Outline of the Dissertation .....	7
2 HPC with SAP: Properties and Mechanical Behaviour .....	9
2.1 Concrete .....	9
2.2 High Performance Concrete.....	10
2.2.1 Application of HPC.....	11

2.2.2	Characteristics of HPC.....	14
2.2.3	Classes of HPC .....	15
2.2.4	Materials for HPC.....	16
2.3	Mix Design for HPC .....	18
2.4	Superabsorbent Polymers.....	23
2.4.1	Water Absorption and Desorption of SAP.....	24
2.4.2	Absorption in pore solution.....	25
2.4.3	Desorption in pore solution.....	29
2.5	Superabsorbent Polymer in Concrete.....	31
2.5.1	Previous Studies on Superabsorbent Polymer in Concrete .....	32
2.5.2	Effect of SAP on Workability of Concrete and Mortar .....	32
2.5.3	Binder Hardening and Microstructure Development.....	35
2.5.4	Effect of SAP on Concrete Shrinkage.....	38
2.5.5	Effect of SAP on Mechanical Properties of Concrete.....	46
2.6	Mechanical Behaviour of HPC .....	53
2.7	Existing Models on Mechanical Properties of HPC .....	55
2.7.1	Powers' Model.....	55
2.7.2	Bolomey's Model.....	59
2.7.3	Constitutive Relations of Mechanical Properties of Concrete .....	61
2.8	The modified Wedge Splitting Test Setup for Fracture Energy .....	66
2.9	Summary .....	67
3	Materials and Experimental Procedures.....	69

3.1	Materials .....	69
3.1.1	Superabsorbent Polymers.....	69
3.1.2	Binders .....	70
3.1.3	Aggregate.....	70
3.1.4	Water.....	71
3.1.5	Admixtures.....	71
3.1.6	HPC Mixtures .....	71
3.2	Experimental Procedures .....	72
3.2.1	Preliminary Tests .....	72
3.2.2	Concrete Production.....	75
3.2.3	Early-age strength properties of HPC .....	76
3.2.4	Mechanical Properties Tests .....	79
3.2.5	Non-destructive tests on HPC mixtures .....	83
3.3	Characterisation of Constituent Materials.....	87
3.3.1	Results.....	88
3.3.2	Inferences.....	94
3.4	Summary .....	95
4	Fresh and Early - Age Strength Properties of HPC with SAP .....	96
4.1	SAP Absorption and pH-value of CPS .....	96
4.1.1	Results.....	96
4.1.2	Inferences.....	98
4.2	Fresh Properties of HPC Mixtures .....	98

4.2.1	Results of Tests on Fresh Properties .....	99
4.2.2	Inferences .....	101
4.3	Setting Times and Early-Age Strength Development .....	101
4.3.1	Results.....	102
4.3.2	Inferences .....	111
4.4	Microstructure and Chemical Composition .....	113
4.4.1	SEM images of the binders and SAP particles.....	113
4.4.2	Chemical composition of constituent materials and HPC mortar .....	120
4.5	Discussion .....	121
5	Mechanical Properties of HPC with SAP .....	126
5.1	Compressive Strength of HPC with SAP.....	126
5.1.1	Results.....	126
5.1.2	Discussion .....	130
5.1.3	Curve – Fitting and Modelling.....	137
5.2	Elastic Modulus .....	141
5.2.1	Results.....	141
5.2.2	Discussion .....	144
5.3	Splitting Tensile Strength and Fracture Energy .....	148
5.3.1	Results.....	148
5.3.2	Discussion .....	152
5.4	Summary .....	158
6	Non Destructive Tests on HPC with SAP.....	159

6.1	X-ray CT Scanning .....	159
6.1.1	Influence of SAP Contents on Air Void Distribution .....	165
6.1.2	Influence of W/B, Binder Type and Curing on Air Void Distribution .....	171
6.1.3	Inferences.....	174
6.2	Scanning Electron Microscopy of HPC .....	175
6.2.1	Micro-morphology and crystalline structure.....	175
6.2.2	Quantitative Analysis of HPCs and cement pastes .....	177
6.2.3	Cement Hydration Products.....	182
6.2.4	Inferences.....	187
7	Conclusion and Recommendations.....	189
7.1	Fresh and Early–Age Strength Properties.....	189
7.2	Mechanical Properties of HPC with SAP .....	190
7.3	Non Destructive Tests on HPC with SAP.....	190
7.4	Recommendation .....	191
8	References.....	192
Appendix A: Attachments to Chapter Four .....		209
Table A1: for Specimen Designation of HPC Mixtures .....		209
Table A2: SAP Absorption .....		210
Table A3: Setting Times and Strength Developments of HPC Mixtures .....		210
Appendix B: Attachments to Chapter 5 .....		211
B1 Duncan Multiple Range Test Results for Early Age Properties.....		211
B2 Influence of SAP addition Compressive Strength of HPCs .....		212

B3 Duncan Multiple Range Test Results for E-modulus of HPC.....	216
B4 Duncan Multiple range Test for Fracture Energy.....	217
Appendix C: SEM image analysis of HPCs.....	218
C1 Summary of SEM Quantitative Analysis for M <sub>2</sub> – HPC Series .....	218

## *List of Figures*

Figure 2-1: Mix Design Process for HPC (Aïtcin, 1998) .....	22
Figure 2-2: SAP polymer network based on polyacrylic acid (courtesy of BASF) cited in RILEM STAR TC 225 (Mechtcherine & Reinhardt, 2012).....	24
Figure 2-3: Schematic representation of water migration in cement-based systems, after Mönning (2009).....	25
Figure 2-4 : Compressive strength, $f_c$ of 50 mm cement-paste cubes as a function of relative strength ( $w/w$ ), Low-alkali cement (Persson, 1996).....	57
Figure 2-5: Compressive strength vs. gel-space ratio for cement-sand mortars .....	58
Figure 2-6: Principle of wedge splitting test: (a) specimen on two linear supports, (b) LVDT on both sides of the specimen, (c) steel holding devices with roller bearings, (d) transversers with wedges .....	67
Figure 2-7: Modified wedge splitting test setup according to RILEM: AAC 13.1. (a) One single line support at the end of the theoretical crack path. (b) Two line supports under the mass concentration points under each half specimen .....	67
Figure 3-1: ACV mould used as mortar and pestle for milling hardened HPC mortars .....	78
Figure 3-2: Compressive strength test setup .....	80
Figure 3-3: E-modulus test setup for HPC with SAP .....	81
Figure 3-4: Test setup for wedge splitting test – (a) shows the plastic clip (LVDT holder) glued to concrete specimen; (b) the groove (30mm x 20mm) and notch (20 mm deep); (c) the complete wedge splitting setup and (d) the crack propagation on the cube specimen.....	82
Figure 3-5: 100 $\mu$ m scan of HPC cylinder - (a) 3D visualisation and (b) thresholding applied to 2D image.....	84

Figure 3-6: 3D Image of separated dry SAP particles with colour indicating sizes classification (a) and (b) Centrally cropped CT image of dry SAP particles obtained from 3D VGI file .....	85
Figure 3-7: Plot of sieve analysis of available and blended fine aggregates.....	88
Figure 3-8: Particle size distribution of binders.....	91
Figure 3-9: Particle of SAP obtained from X-ray CT Scanning .....	92
Figure 3-10: Snapshot of filtered central portion of VGI file of dry SAP particles (blue) under analysis .....	93
Figure 4-1: Setting times (initial and final) plot of M <sub>2</sub> -HPC mixture.....	102
Figure 4-2: Initial and Final setting times for M <sub>2</sub> -HPC mixtures made from binary cements.....	103
Figure 4-3: Initial and Final setting times of M <sub>1S</sub> - HPC mixtures made from ternary cements.....	104
Figure 4-4: Initial and Final setting times of HPC mixtures with SAP1.....	104
Figure 4-5: Degree of hydration of M <sub>2</sub> -HPC (binary cements) with SAP .....	106
Figure 4-6: Degree of hydration of M <sub>1S</sub> -HPC (ternary cements) with SAP.....	106
Figure 4-7: Early-age strength development of control HPC mixes.....	108
Figure 4-8: SP <sub>1</sub> influence on early-age strength development of M <sub>2</sub> - HPC.....	109
Figure 4-9: SP <sub>1</sub> influence on early-age strength of M <sub>3</sub> -HPC .....	109
Figure 4-10: SP <sub>1</sub> influence on early-age strength of M <sub>1F</sub> -HPC.....	110
Figure 4-11: SP <sub>1</sub> influence on early-age strength of M <sub>1S</sub> -HPC.....	110
Figure 4-12: SP <sub>2</sub> influence on early-age strength of M <sub>1S</sub> – HPC.....	111
Figure 4-13: SEM image of microstructure of CEM I 52.5 N (a) 50 X and (b) 500 X magnifications .....	114
Figure 4-14: SEM image of microstructure of SF (a) 50 X and (b) 500 X magnifications .....	115
Figure 4-15: SEM image of microstructure of CS (a) 50 X and (b) 500 X magnifications.....	116

Figure 4-16: SEM image of FA (a) 50 X and (b) 500 X magnifications .....	117
Figure 4-17: SEM image SAP particles (a) SP <sub>1</sub> and (b) SP <sub>2</sub> .....	118
Figure 4-18: Typical spectra image of SEM/WDS analysis of Binders (CEM I 52.5 N52.5 N).....	119
Figure 4-19: Fourier Infra-Red (FRIR) spectroscopy spectra of the binders (CEM I 52.5, SF, FA and CS) .....	120
Figure 4-20: Early-age compressive strength of all HPC mixtures .....	121
Figure 5-1: Compressive Strength of M <sub>2</sub> - HPC (a) with SP <sub>1</sub> and (b) with SP <sub>2</sub> .....	128
Figure 5-2: Compressive Strength of M <sub>3</sub> - HPC (a) with SP <sub>1</sub> and (b) with SP <sub>2</sub> .....	128
Figure 5-3: Compressive Strength of M <sub>1F</sub> - HPC (a) with SP <sub>1</sub> and (b) with SP <sub>2</sub> .....	129
Figure 5-4: Compressive Strength of M <sub>1S</sub> - HPC (a) with SP <sub>1</sub> and (b) with SP <sub>2</sub> .....	129
Figure 5-5: Influence of SAP contents on the density of HPC .....	130
Figure 5-6: Compressive strength of HPC versus binder type as influenced by curing age.....	134
Figure 5-7: Compressive strength versus binder type as influenced by W/B .....	134
Figure 5-8: Mean compressive strength of HPC against SAP contents.....	135
Figure 5-9: Compressive strength of reference mixtures - HPCs on log time scale .....	136
Figure 5-10: Compressive strength of HPC – mortars cubes corrected for both air and SP <sub>2</sub> voids....	138
Figure 5-11: Compressive strength of HPC mortar cubes corrected for both air and SP <sub>1</sub> voids .....	139
Figure 5-12: Compressive strength against the gel / space ratio for HPC mortar cubes.....	140
Figure 5-13: E-modulus of binary cements HPC against curing age; (a) M <sub>2</sub> SP <sub>1</sub> - HPC; (b) M <sub>2</sub> SP <sub>2</sub> - HPC; (c) M <sub>3</sub> SP <sub>1</sub> - HPC and (d) M <sub>3</sub> SP <sub>2</sub> - HPC.....	143
Figure 5-14: E-modulus of binary cements HPC against curing age; (a) M <sub>1F</sub> SP <sub>1</sub> -HPC; (b) M <sub>1F</sub> SP <sub>2</sub> -HPC; (c) M <sub>1S</sub> SP <sub>1</sub> -HPC and (d) M <sub>1S</sub> SP <sub>2</sub> -HPC.....	143
Figure 5-15: Mean E-modulus of HPCs against curing age .....	144

Figure 5-16: Mean E-modulus of HPCs (a) against SAP contents (b) against SAP type .....	146
Figure 5-17: Mean E-modulus of HPCs (a) against binder type (b) against W/B .....	146
Figure 5-18: Typical plot of data extracted from Wedge Splitting Test for $W_f$ and $G_f$ Calculation ...	148
Figure 5-19: Fracture Energy ( $G_F$ ) of $M_{1F}$ – HPC .....	151
Figure 5-20: Fracture Energy ( $G_F$ ) of $M_{1S}$ – HPC .....	151
Figure 5-21: Fracture Energy ( $G_F$ ) of $M_2$ – HPC .....	151
Figure 5-22: Fracture Energy ( $G_F$ ) of $M_3$ – HPC .....	152
Figure 5-23: Mean Splitting Force ( $F_{sp}$ ) against SAP content .....	154
Figure 5-24: Splitting Force ( $F_{sp}$ ) vs. W/B as influenced by SAP type .....	154
Figure 5-25: Fracture Energy vs. SAP contents as influenced by binder type.....	156
Figure 5-26: Compressive Strength vs. Fracture Energy as influenced by SAP contents .....	157
Figure 5-27: Compressive Strength vs. Fracture Energy as influenced by W/B .....	157
Figure 6-1: Centrally cropped - 25 mm x 25 mm (air-threshold) HPC with air voids in blue colour	160
Figure 6-2: Histogram Plot of Air Void Distribution of (25 x 25 x 50 mm <sup>3</sup> ) $M_{1F}$ – HPC Samples....	161
Figure 6-3: Histogram Plot of Air Void Distribution of (25 x 25 x 50 mm <sup>3</sup> ) $M_{1S}$ – HPC Samples....	162
Figure 6-4: Histogram Plot of Air Void Distribution of (25 x 25 x 50 mm <sup>3</sup> ) $M_2$ – HPC Samples .....	163
Figure 6-5: Histogram Plot of Air Void Distribution of (25 x 25 x 50 mm <sup>3</sup> ) $M_3$ – HPC Samples .....	164
Figure 6-6: SAP void% against SAP content% (a) $Sp_1$ ; (b) $Sp_2$ .....	168
Figure 6-7: Cumulative SAP voids range vs curing age for $M_{1F}$ – HPC (a) $SP_1$ ; (b) $SP_2$ .....	169
Figure 6-8: Cumulative SAP voids range vs curing age for $M_{1S}$ – HPC (a) $SP_1$ ; (b) $SP_2$ .....	169
Figure 6-9: Cumulative SAP voids range vs curing age for $M_2$ – HPC (a) $SP_1$ ; (b) $SP_2$ .....	169
Figure 6-10: Cumulative SAP voids range vs curing age for $M_3$ – HPC (a) $SP_1$ ; (b) $SP_2$ .....	169

Figure 6-11: Cumulative SAP voids range vs curing age for triplicate  $M_2$  – HPCs (a)  $Sp_1$ ; (b)  $Sp_2$ .. 171

Figure 6-12: Cumulative SAP voids range vs curing age (triplicates specimen) for (a)  $M_3$  (b)  $M_{1F}$ .. 173

Figure 6-13: General morphology and crystalline structure of the HPCs ( $M_{1F}$  as a sample)..... 176

Figure 6-14: Spectrum of Quantitative Analysis for Coarse Aggregates in  $M_{1F}$  – HPC..... 178

Figure 6-15: Typical SEM image of HPC paste portion ( $M_2$  as sample)..... 180

Figure 6-16: Atomic ratio plot (Si/Ca vs Al/Ca) for  $M_2$  - HPC ..... 184

Figure 6-17: Atomic ratio plot (S/Ca vs Al/Ca) for  $M_2$  - HPC ..... 184

Figure 6-18: Si/Ca vs Al/Ca plots of calcium silicates phases in the three HPCs ..... 186

## *List of Tables*

Table 2-1: Strength classes for normal weight concrete according to BS EN 206-1:2001 and classification according to <i>fib</i> Model Code 2010 (Dehn, 2012) .....	10
Table 2-2: Classification of HPC (Mehta & Monteiro, 2014) .....	15
Table 2-3: Effect of maximum aggregate size $d_{max}$ on base value of fracture energy $G_{FO}$ (CEP FIP MC 90).....	64
Table 2-4: Effect of type aggregates on the modulus of elasticity $E_{ci}$ ( <i>fib</i> MC 2010).....	65
Table 2-5: Tangent modulus and elastic modulus of elasticity ( <i>fib</i> MC 2010).....	65
Table 3-1: Mix constituents of reference HPC mixtures .....	72
Table 3-2: Summary of particle size distribution of available fine aggregates.....	88
Table 3-3: Summary of particle size distribution and BET surface area .....	91
Table 4-1: pH-values of CPS .....	97
Table 4-2: Mix constituents and fresh properties of HPC mixtures from binary cements.....	99
Table 4-3: Mix constituent and fresh properties of HPC mixtures from ternary cements .....	99
Table 4-4: Influence of SAP and binder type on degree of hydration of HPC .....	107
Table 4-5: Oxides composition of the binders obtained through SEM/BSE .....	119
Table 4-6: Test between Subject Effects.....	122
Table 4-7: Duncan's multiple range test (W/B effect on Early-age Compressive Strength).....	124
Table 4-8: Duncan's multiple range test (Binder type effect on Early-age Compressive Strength) ...	124
Table 4-9: Duncan's multiple range test (SAP contents effect on Early-age Compressive Strength). 124	124
Table 4-10: Duncan's multiple range test (SAP type effect on Early-age Compressive Strength).....	124
Table 4-11: Duncan's multiple range test (Curing Age effect on Early-age Compressive Strength) .	124

Table 5-1: Density of Binary cements - HPC with SAP .....	127
Table 5-2: Density of Ternary cements - HPC with SAP .....	127
Table 5-3: Compressive Strength of Binary cements - HPC with SAP .....	128
Table 5-4: Compressive Strength of Ternary cements – HPC with SAP.....	129
Table 5-5: Between Effect Test for Density .....	131
Table 5-6: Between Effect Test on Compressive Strength .....	133
Table 5-7: Summary of Trend Line ( $A + B \log t dt1$ ) for Compressive Strength of HPCs with SAP .	136
Table 5-8: Correction factor for Reference HPCs.....	138
Table 5-9: E-modulus of Binary cements - HPC with SAP.....	142
Table 5-10: E-modulus of Ternary cements - HPC with SAP .....	142
Table 5-11: Between Test Effects on E-modulus .....	147
Table 5-12: Summary of Fracture Energy Results for Ternary Cement HPCs.....	149
Table 5-13: Summary of Fracture Energy Results for Binary Cements HPCs .....	149
Table 5-14: Tests of Between-Subjects Effects for Splitting Force ( $F_{sp}$ ) .....	153
Table 5-15: Tests of Between-Subjects Effects for Fracture Energy.....	155
Table 6-1: Summary of Influence of SAP contents and curing age on void distribution for $M_{1F}$ – HPC .....	165
Table 6-2: Summary of Influence of SAP contents and curing age on void distribution for $M_{1S}$ – HPC .....	165
Table 6-3: Summary of Influence of SAP contents and curing age on void distribution for $M_2$ – HPC .....	166
Table 6-4: Summary of Influence of SAP contents and curing age on void distribution for $M_3$ – HPC .....	166

Table 6-5: Summary of void distribution in triplicate HPC - M <sub>2</sub> with both SAP types.....	170
Table 6-6: Summary of curing age influence and W/B on void distribution using triplicate specimens .....	173
Table 6-7: Quantitative Analysis of Typical concrete Polished Section (M <sub>1F</sub> as Sample).....	177
Table 6-8: SEM Quantitative Analysis of Aggregates in M <sub>1F</sub> – HPCs by Weight% .....	179
Table 6-9: Quantitative Analysis of a Typical M <sub>2</sub> – HPC SEM Image by Element Weight% .....	181
Table 6-10: Summary of Quantitative Analysis of Spectrum B .....	185
Table 6-11: Summary of Quantitative Analysis of Spectrum D .....	185

## *List of Symbols*

$a$	Actual air content (% relative to volume of concrete)
$a_0$	Reference air content
$\alpha_c$	Degree of hydration of binder
$\alpha_{max}$	Ultimate degree of hydration
$f_{c,cube}$	Cube compressive strength (N/mm <sup>2</sup> )
$f_{c,cube28}$	28 <sup>th</sup> day cube compressive strength (also known as $f_{c28}$ )
$f_{c,cyl}$	Cylinder compressive strength (N/mm <sup>2</sup> )
$E_{ci}$	E-modulus (N/mm <sup>2</sup> ) at concrete age of 28 days
$E_{co}$	E-modulus value of $21.5 \times 10^3$ N/mm <sup>2</sup>
$G_F$	Fracture energy (N/m)
$G_{FO}$	Base value of fracture energy (N/m)
$K_{Bolomey}$	Material constant given by the Bolomey's formula (A)
$R_{c28}$	Compressive strength of standard mortar after 28 days of curing (N/mm <sup>2</sup> )
$V_m$	Total surface area of the solid phases is related to the computed cement composition
$X_{pc}$	Gel-space ratio of the HPC mortar paste
$d_{max}$	Maximum size of aggregate
$f_c$	Characteristic strength obtained (also known as $f_{ck}$ ) - (N/mm <sup>2</sup> )
$f_{cm}$	Mean cylinder compressive strength (N/mm <sup>2</sup> )
$f_{cr}$	Target strength at maturity (often 28 days) - (N/mm <sup>2</sup> )
$f_{ct,fl}$	Flexural tensile strength

$f_{ct.sp}$	Splitting tensile strength
$f_{ctk}$	Characteristic tensile strength
$f_{ctm}$	Mean value of tensile strength (N/mm <sup>2</sup> )
$v_c$	Specific volume of anhydrous binder (i.e. binary or ternary)
$w_n$	Non-evaporable water
$\rho_c$	Relative density of the cementitious material
$B$	Second material constants by Bolomey
$\sigma$	standard deviation

## *List of Abbreviations*

2D	Two Dimensional
3D	Three Dimensional
ACV	Aggregate crushing value
BET	Brunauer–Emmett–Teller
BSE	Backscattered electron
$b_{woc}$	by weight of cement
$b_{wob}$	by weight of binder
C&CI	Cement and Concrete Institute of South Africa
CD	crusher dust
CEM I	cement type I
CMOD	crack mouth opening displacement (mm)
COD	crack opening development
CPS	CPS
CS	corex slag
C-S-H	Calcium-silicate-hydrate
$C_c$	Coefficient of gradation
$C_u$	Coefficient of uniformity
D.O.E	Department of Environment in United Kingdom
D10	Cumulative 10% passing
D50	Cumulative 50% passing

D90	Cumulative 90% passing
EA	Expansive additives
EDX	Energy Dispersive X-ray
FA	fly ash
FHWA	Federal Highway Administration of United States Department of Transport
FM	fineness modulus
F <sub>sp</sub>	splitting force (kN)
FTIR	Fourier Transmission Infra-red Spectroscopy
GGBS	ground granulated blast-furnace slag
HDC	high-durability concrete
HES	high early strength
HESC	high-early strength concrete
HPC	High performance concrete
HPM	High performance mortar
HSC	High strength concrete
HVFA	high-volume fly ash concrete
IC-agent	IC agent
LOI	Loss on ignition
LVDT	linear variable displacement transducers
LWA	Lightweight aggregates
M <sub>1F</sub>	0.2 W/B HPC reference mix containing fly ash as additional cementitious material
M <sub>1S</sub>	0.2 W/B HPC reference mix containing corex slag as additional cementitious material

M <sub>2</sub>	0.25 W/B HPC reference mix
M <sub>3</sub>	0.3 W/B HPC reference mix
mFabs	SAP absorption in solution
MK	metakaolin
mSAP, t	swollen SAP after a time of immersion in a solution
mTBT, f	mass of moist tea bag
N	natural sand
NSC	Normal strength concrete
OPC	ordinary Portland cement
PCE	Polycarboxylate Ether
pH	power of hydrogen (it has a numeric value defined as a negative base 10 logarithm of the molar concentration of hydrogen ions). This is a measure of acidity (< 7) and alkalinity (> 7).
PPC	Pretoria Portland cement
PR	penetration resistance
PSD	Particle size distribution
PVA	polyvinyl acetates
PVC	polyvinyl chloride
RH	Relative humidity
<b>RH</b> <sub>7</sub> factor	Rate of hydration based on 7 <sup>th</sup> day degree of hydration for reference mixtures
RPC	reactive powder concrete
SAP	Superabsorbent Polymers
SCC	self-consolidating concrete

SCM	Supplementary cementitious materials
SEM	Scanning Electron Microscopy
SF	silica fume
SFRHPC	Self-compacting Fibre Reinforced High Performance Concrete
SHRP	Strategic Highway Research Program
SHRP	Strategic Highway Research Programme
SN <sub>1</sub>	sieved natural sand type one ( $\geq 300 \mu\text{m}$ )
SN <sub>2</sub>	sieved natural sand type two ( $\geq 150 \mu\text{m}$ )
Sp <sub>1</sub>	SAP size I
Sp <sub>2</sub>	SAP size II
SPSS	Statistical Package for Social Sciences
SRA	Shrinkage reducing agent
STAR	State-of-the-art-report
t <sub>1</sub>	early age at time of one day curing
t <sub>d</sub>	early age duration of curing after casting taken as greater than 1 and up to day 10
UHPC	Ultra-high performance concrete
VES	very early strength
VGI	volume graphics image
VHS	very high strength
W	mixing water
W <sub>e</sub>	entrained water
W/B	water: binder ratio

W/C	water: cement ratio
$W_{ic}/C$	inter curing water: cement ratio
WDS	Wavelength Dispersive Spectroscopy
$W_f$	work of fracture
X-ray CT	X-ray computed tomography

# 1

## *Introduction*

Concrete is a versatile material for construction work and its production process requires adequate mix proportioning, materials handling and curing for effective development of strength, durability and other mechanical characteristics. In normal strength concrete (NSC) the curing methods of immersion in water, sprinkling and other approaches as outlined in the codes of concrete practices (ACI, 308-01, 2008; BS EN 12390 - 2, 2009) suffices for prevention of moisture loss from the concrete surface.

High performance concrete (HPC) on the other hand is defined by ACI (1999) as concrete meeting special combinations of performance and uniformity requirements that cannot always be achieved routinely using conventional constituents and normal mixing, placing, and curing practice (ACI THPC/TAC, 1999). It is a type of concrete specially designed to meet a combination of performance and requirements which specifically includes high strength or high early strength, durability and high elastic modulus (Kosmatka, et al., 2002; Neville, 2012). Its application includes precast pylons, piers and girders of many long span bridges in the world; tunnels, tall and ultra-high buildings; shotcrete repairs, poles, parking garages and agricultural applications (Kosmatka et al., 2002).

HPC is made with conventional materials as used in normal concrete, carefully selected high quality ingredients and optimised mixtures involving high standard of production processes. It comprises very high cement content and low water cement-cementitious materials (i.e. water/binder, W/B) ratio which, according to Kosmatka et al., (2002), can be at a range of 0.20 to 0.45 while Aïtcin (1998) and Neville (2012) believe that HPC is a concrete with a W/B equal to or lower than 0.35.

HPC is performance oriented and often defined on the basis of specific requirements encountered for a particular application, the most common being compressive strength. Although strength alone is not the required characteristic, it is noted to be almost always of higher strength than normal concrete (Kosmatka et al., 2002). On their part, Beushausen & Dehn (2009) state that the terminology of high-

strength concrete (HSC) is sometimes used for HPC. The meaning of high strength concrete based on 28 day compressive strength ( $f_{c,cube28}$ ) varies significantly over the years as pointed out by Neville (2012).  $f_{c,cube28}$  of 40 MPa was considered high at one time while 60 MPa became the minimum benchmark later on. HSC generally can be considered HPC for certain applications. However, Beushausen & Dehn, (2009) are of the view that high performance does not necessarily mean high strength. Typical HPC, according to them, has compressive strength ranges of 60 to 130 MPa while Kosmatka et al., (2002) places a threshold on strength requirement of HPC as 28 day cube strength ( $f_{c,cube28}$ ) of 70 MPa and Neville (2012) thinks HPC has concrete with compressive strength in excess of 80 MPa. South Africa envisaged the adoption of Eurocode 2: Design of concrete structures (EC2 - (British Standard Institution, 2004)) which includes HSC up to 90 MPa cylinder strength / 105 MPa cube strength (C90/C105).

Issues of serious concern in HPC production are its workability and inadequate curing. The use of superplasticiser has been identified by previous researches (Aïtcin, 1998; Beushausen & Dehn, 2009; Kosmatka et al., 2002; Neville, 2012) as enhancing good workability in HPC while effort is also being intensified at achieving good internal curing (IC) in HPC as a means of improving the curing needs.

Schrofl, et al., (2012) stated that HSC/HPC is particularly susceptible to autogenous-shrinkage-caused-cracking under restraints. Autogenous shrinkage is defined by Jensen, et al., (2010) as the bulk deformation of a closed (sealed), isothermal, cementitious material system not subject to external forces.

Conventional concrete curing methods are noted (ACI 363R-92; ACI, 308R-01, 2008) to be insufficient for mitigating autogenous shrinkage in HPC, even with intensive wet curing applied. Typical HPC has very dense microstructure even at an early age, which hinders the possibility of sufficient rapid transportation of curing water into the interior of concrete members especially those with relatively large dimensions. Hence the need for IC in HPC through the use of high water storing materials as admixtures in concrete especially HPC, thereby supplying water to the surrounding matrix soon as self-desiccation begins (Schrofl et al., 2012).

Researchers have introduced different materials as IC-agents in concrete with pre-soaked light weight aggregates (LWA) and superabsorbent polymers (SAP) been the most acceptable (ACI (308-213) R13, 2013; RILEM Rep 041 - Jensen and Lura (eds.), 2006).

The use of Super-absorbent polymers (SAP) as IC-agent has been adjudged to be effective for mitigation of self-desiccation and autogenous shrinkage in concrete especially HPC/ ultra-high performance concrete (UHPC) via its absorption and desorption of water internally as concrete hydrates (Siriwatwechakul, et al., 2010).

The works of Jensen & Hansen (2001 & 2002), have generated increased research interests on utilisation of SAP as concrete admixture thus leading to the establishment of the RILEM Technical Committee (TC) 225-SAP “Application of Superabsorbent Polymers in Concrete Construction” in 2007. The State-of-the-Art Report (Mechtcherine & Reinhardt, 2012) prepared by this committee summarised the available knowledge on SAP application in concrete and provided a basis for further study.

## **1.1 Statement of Research Problem**

Shrinkage deformation in normal concrete is well documented and understood in literature with less work on autogenous shrinkage especially when drying is prevented by sealing or curing by immersion in water. The emergence of HPC has brought to the fore the problem of autogenous shrinkage caused by insufficient water for complete hydration (Braam et al., 2006; Schrofl et al., 2012).

HPC with low W/B ratio experience considerable chemical shrinkage and self-desiccation during hydration resulting in high autogenous shrinkage deformation and hence early age cracks which can adversely affect the durability of the concrete. Research efforts in the past two decades had thereby been directed towards enhancing IC by introducing materials such as pre-soaked light weight fine aggregates (LWA) and super-absorbent polymers (SAP).

SAP has been identified to be the most appropriate and promising material as IC-agent in concrete. This is evident in the State-of-the-Art-Report (STAR) published by RILEM TC 225 which was constituted in 2007. The STAR summarised all the available knowledge on SAP effectiveness as a

source of water for mitigating self-desiccation and autogenous shrinkage in concrete (Mechtcherine & Reinhardt, 2012). The application of SAP in concrete was extensively discussed at various conferences held by researchers in the field (Jensen et al., 2010; Kovler & Jensen, 2007; Mechtcherine & Schroefl, 2014).

The views of the various researchers revealed that more research effort is required to provide better understanding on the utilisation of SAP in concrete construction. Although the researchers unanimously agreed that SAP addition is beneficial in the mitigation of autogenous shrinkage in cement paste, mortar and concrete, several other issues are yet to be resolved, some of which include:

- Level to which SAP addition prevents autogenous shrinkage
- Side effects of SAP in concrete such as loss of strength, stiffness, inappropriate fresh properties including workability, associated segregation and porosity
- Determination of the optimum size and volume of SAP in cement paste, mortar and concrete (especially HPC) and
- An understanding of the micro-structure of the calcium-silicate-hydrate (C-S-H) and intermolecular relations of the concrete constituent particles

To unravel the issues identified above, the research works of Hasholt et al., (2010a & b) are of particular interest to this study and therefore considered a point of departure for this research. Their studies investigated the mechanical properties of concrete with emphasis on the compressive strength and elastic modulus using concrete specimens with W/B ratio ranges of 0.35 - 0.50 varying the proportion of SAP ranging between 0% and 0.6% cured in water up to 28 days. The studies modelled the effect of SAP on concrete strength and elastic modulus by combining Bolomey's formula and Powers' model and observed that the net effect of SAP (negative or positive) depends on the mix design and curing age. The research concluded that SAP has little effect on hydration and hence leads to reduced strength when the W/B is high ( $> 0.45$ ) especially at early ages and large SAP additions. It was argued by Hasholt et al., (2010a) that concrete specimens with low W/B ratio and low SAP addition exhibit compressive strength increase at later ages.

However, Hasholt et al., (2010b) further stated on the modulus of elasticity that there is need for care on deduction with more empirical models despite their observations that the theoretical models for mechanical properties work as well for concrete with SAP as for concrete without. This study examines the effect of SAP on the mechanical properties of HPC specifically with W/B ratio range 0.2 – 0.3 having 28<sup>th</sup> day strength above 70 MPa (i.e. C55/67 – C100/115).

The trend of developments in concrete research as highlighted in the recent ACI convention is a call for more coordinated research into cement hydration with the use of kinetics for an understanding of life cycle performance of concrete (Kenter, 2012). The cohesive strength of concrete is believed to be governed by the micro-molecular interaction of its constituents as influenced by the properties of the hydration product calcium-silicate-hydrate (C-S-H) while this is said to determine the mechanical behaviour of the cement paste and hence concrete (Masoero, et al., 2012). A study of the micro-structure of HPC having SAP incorporated can thereby be seen as timely in understanding the effect of SAP on its mechanical behaviour.

This study provides answers to the following pertinent questions:

- What impact will the addition of SAP and its absorption capacity have on the rheology of the HPC?
- What effect will grain sizes and volume of SAP have on rate of hydration and long term strength development?
- How will the addition of SAP influence the mechanical behaviour (i.e. strength and stiffness properties, micro-structure and molecular interaction) of HPC?

## **1.2 Aim and Objectives of the Study**

This study aims at investigating the mechanical behaviour of HPC containing varying sizes and volume of SAP with a view to evaluating the effect of the performed IC.

The specific objectives are to:

- Examine the impact of SAP addition on the rheology of HPC containing varying sizes and volume of SAP.
- Identify and establish the effect of varying sizes of SAP and its volume on rate of hydration and strength developments in HPC.
- Quantify and model the mechanical behaviour (strength in compression, tension, fracture energy and stiffness) at both short and long term for low W/B (0.2 – 0.30) HPC (C55/67 – C100/115) with SAP.
- Investigate the micro-structure and molecular interaction of the material constituent of HPC.

### 1.3 Research Proposition

This study proposes that size and volume of SAP in concrete (specifically HPC) have a direct influence on the micro-structure and molecular interaction of the constituents materials and hence the mechanical behaviour of HPC.

The sub-propositions are:

- The fresh properties (i.e. workability, temperature and demoulded density) are altered by the increase in particle size and volume of SAP added to HPC.
- The higher the SAP particle size and volume added in HPC, the lower the strength and elastic properties.
- The existing Powers' model can still be adopted for prediction of strength and elastic properties of HPC with the SAP swelling rate simulated into it.
- SAP inclusion in HPC has a significant effect on the micro-structure of the C-S-H of cement paste and hence the hydration rate and strength development and mechanical behaviour of HPC.

### 1.4 Significance of Study

There is a growing trend in the utilisation and adoption of HPC and UHPC in the construction industry while these concrete types are known to be susceptible to self-desiccation and autogenous

shrinkage. Curing is therefore very important and the fact that the real site situation can hardly offer effective curing by complete immersion in water to prevent drying in actual concrete elements calls for an intensive study of the IC-agents being introduced in concrete. Any material for use as an IC-agent ought to be of appropriate type and optimum proportion while its addition should not result in any detrimental effect on the required properties of the concrete. The outcome of this study provides a good basis for appropriate choice and efficient proportioning of SAP for use in high performance concrete of low W/B (0.2 – 0.3) having minimum 28 day cube strength specification of 70 MPa. It will offer a prediction on the behaviour of these concrete types at ages beyond the 28 day as required for high-performance concrete according to the postulations of some authors (Beushausen & Dehn, 2009; Neville, 2012; Portland Cement Association, 2012).

This work intends to further enhance the utilisation of HPC for provision of improved ways of handling constraints with long span bridges; cable stay bridges and more high rise and ultra-tall buildings in concrete works. This will be enabled by providing information on mechanical behaviour, and guidelines towards sound design.

## **Outline of the Dissertation**

This dissertation on “understanding the mechanical behaviour of high performance concrete with superabsorbent polymer (SAP)” is presented in seven chapters. It begins with a comprehensive introduction stating the motivation for the study, the research aim and objectives and the expected contribution to the field of concrete in general.

A detailed review of existing literature on HPC and its application in construction coupled with utilisation of SAP in concrete construction is presented in Chapter 2.

In Chapter 3, a description of the methods adopted for carrying out the experiments for an understanding of the mechanical behaviour of these concrete types which have SAP incorporated as IC-agent is reported. The test methods described includes those for physical properties of the constituent materials (particle size distribution, specific surface area, chemical analysis for determination of oxide contents, pH value determination of cement pore solutions (CPS) and the tea-

bag test for SAP swelling rate), fresh properties of the HPC mixtures (slump flow test, concrete temperature, setting times of concrete, rate of hydration and early age strength development), mechanical properties of hardened concrete (strength in compression, tension, fracture energy and elastic modulus) and image analysis (Scanning electro-microscopy (SEM) - two dimensional and x-ray computer tomography (x-ray CT) scanning –three dimensional) of the hardened HPC to study the effect of SAP on the products of hydration, microstructure, air voids created and pore distribution.

Chapter 4 presents the results and discussion of the materials and fresh properties of the HPC mixtures coupled with the effect of SAP on its hydration and early age strength development process.

In Chapter 5, the results of mechanical properties (compressive strength, elastic modulus, splitting tensile and fracture energy tests) are presented with statistical software used to examine the data generated for a discussion on the influence of SAP on the characteristics of the HPC. The several dependent variables were regressed against the independent variables to assess which variable has influence and to what level of significance on the concrete behaviour. They were thereby curve-fitted into the Powers' model for an inference of the effect of SAP on the HPC mixtures.

Chapter 6 reports on the image analysis tests (back scattered electron (BSE) image analysis via SEM and 3D air void analysis via x-ray CT-scanner). This was used to explain the effect of SAP on the change in the microstructural properties of the HPC and hence the reason for observed mechanical behaviour as influenced by the SAP inclusion in the concrete type.

Finally, Chapter 7 highlights the conclusions of this study on the mechanical behaviour of HPC with SAP as an IC-agent with recommendations made for practitioners based on the findings from this study for utilisation of SAP as IC-agent in HPC with areas for future studies also enumerated.

## 2

### *HPC with SAP:*

## *Properties and Mechanical Behaviour*

This chapter presents a general review on concrete, HPC, properties of concrete at the fresh state and performance requirements. A detailed discussion is presented on the mechanical properties of concrete and internal curing of concrete in general, and HPC in specific. The Chapter further touches on a review of existing works on SAP's influence on concrete (with emphasis on HPC) and cementitious materials. Existing models on the mechanical behaviour of cement pastes, mortar and HPC are also presented.

### **2.1 Concrete**

Concrete is a composite construction material and is composed primarily of aggregates, cement and water. Its production requires a good understanding of the basic processes of materials handling, mixing, transporting and curing to achieve a 'good concrete'. The requirements generally in the fresh state are a consistent mix that can be compacted with available means; cohesive enough to be transported and placed without segregation (Neville & Brooks, 2010; Neville, 2012).

The classification of concrete is often based on application type, performance requirements and additional ingredients (i.e. admixtures) incorporated. In a broad classification based on 28-day strength ( $f_{c,cube28}$ ) we can have; normal strength concrete ( $f_{c,cube28} \leq 50$  MPa) and high performance / high strength concrete ( $f_{c,cube28} > 50$ MPa) (International Federation for Structural Concrete (fib), 2012) - *fib* Model Code 2010). This classification is further divided into low strength ( $f_{c,cube28} \leq 20$  MPa); moderate or normal strength ( $f_{c,cube28} = 20$  to 50 MPa); high strength ( $f_{c,cube28} = 50$  to 100

MPa); ultra high strength ( $f_{c,cube28} = 100$  to 150 MPa) and Special ( $f_{c,cube28} > 150$  MPa) (Mehta & Monteiro, 2014; Neville & Brooks, 2010; Neville, 2012). Concrete can also be classified on the basis of density (*fib* Model Code 2010) as lightweight aggregate concrete (800 – 2000 kg/m<sup>3</sup>), normal weight concrete (>2000 – 2600 kg/m<sup>3</sup>) and heavy weight concrete (> 2600 kg/m<sup>3</sup>). Table 2.1 extracted from the work of Dehn (2012) present strength classes of normal weight concretes according to BS EN 206-1: 2001 (reviewed 2013) and *fib* Model Code 2010.

**Table 2-1: Strength classes for normal weight concrete according to BS EN 206-1:2001 and classification according to *fib* Model Code 2010 (Dehn, 2012)**

Concrete type	Strength class $f_{ck,cyl}/f_{ck,cube}$						
Low strength concrete	C8/10	C12/15	C16/20				
Normal strength concrete	C20/25	C25/30	C30/37	C35/45	C40/50	C45/55	C50/60
High strength concrete	C55/67	C60/75	C70/85	C80/95	C90/105	C100/115	
Ultra-high strength concrete*		C110/130, C120/140					

\*not included in BS EN 206-1:2001

Another basis for classification of concrete as offered in literature (Aïtcin, 1998; Kosmatka et al., 2002; Neville, 2012) is the water/binder (W/B) ratio as concrete with W/B below 0.40 behaves differently from normal strength concrete (NSC). The discussion in this section centres on high performance concrete.

## 2.2 High Performance Concrete

HPC is a generic term for all concrete exhibiting properties and constructability which exceeds that of NSC (Kosmatka et al., 2002). This is a type of concrete specially designed to meet combinations of performance and requirements which specifically include high workability, high strength, high early strength; durability and high modulus of elasticity amongst other properties (Aïtcin, 1998; Malhotra, 1994; Mehta & Monteiro, 2014; Neville, 2012). It is alternatively referred to as “speciality concrete”, HSC and is often defined according to the specific property for which performance requirement is placed in its design (Beushausen & Dehn, 2009; Mehta & Monteiro, 2014; Portland Cement Association, 2012).

The American Concrete Institute (ACI THPC/TAC, 1999) defines HPC as “a concrete meeting special combination of performance and uniformity requirements that cannot be achieved routinely using conventional constituents and normal mixing, placing and curing practices”.

Mehta & Monteiro (2014) present a definition of HPC on basis of basic requirements of HPC in Strategic Highway Research Programme (SHRP) in the United States of America as follows:

- HPC is a concrete that has been designed to be more durable and if necessary, stronger than conventional concrete.
- HPC mixtures are essentially composed of the same materials as conventional concrete mixtures, but the proportions are designed or engineered to provide the strength and durability needed for structural and environmental requirements of the project.

### 2.2.1 Application of HPC

Application of HPC as observed in literature (Aïtcin, 1998; Schrofl et al., 2012) came into the limelight about three decades ago with the Water Tower Place, built in 1970 in Chicago, Illinois, USA (adopting 60 MPa concrete with lingosulfonate based water reducers), as the first building structure made with HPC (Aïtcin, 1998). HPC use is now adopted extensively for the fabrication of precast pylons, piers and girders of many long span bridges in the world (Mehta & Monteiro, 2014). HPC has been primarily used in tunnels, bridges, and tall buildings for its strength, durability, and high modulus of elasticity. The use now includes shotcrete repair, poles, parking garages, and agricultural applications.

Some known structures (with dates) which adopted HPC as found in Aïtcin (1998) are outlined below:

- Water Tower Place built in 1970 in Chicago, Illinois, USA. This involved concrete of  $f_{c,cube28} = 60$  MPa having a lingosulfonate based water reducer added.
- Norway’s Gullfaks offshore platform built in 1981. It is made of concrete with average  $f_{c,cube28} = 79$  MPa and a slump of 240 mm in the fresh state.

- Sylans and Glacières viaduct built in France in 1986. This utilised concrete of  $f_{c,cube28} = 60$  MPa and 50 MPa at different portions of the structures as against the initial design strength of 40 MPa.
- Scotia Plaza, built in 1988 in Toronto, Canada, made of concrete with average tested strength of 93.6 MPa at the 91 days.
- Île de Ré bridge, built in 1988 in France. The girders of the bridge was designed for 40 MPa target strength and built with concrete of  $f_{c,cube28} = 59.5$  MPa; this was chosen due to the need for 20 MPa compressive strength at 10 to 12 hrs age to enhance stripping off box girders formwork.
- Two Union Square, built in 1988 in Seattle, Washington, USA. Constructed with a concrete having a W/C of 0.22, utilising naphthalene based super-plasticizer; outstanding aggregates of 10 mm maximum size and coarse graded sand of 2.80 fineness modulus; its  $f_{c,cube28} = 131$  MPa.
- Joigny bridge, built in 1989 in France. The concrete used for construction of the bridge deck had tested compressive strengths of 3 days = 26.2 MPa; 7 days = 53.6 MPa; 28 days = 78.0 MPa. The design was actually for  $f_{c,cube28} = 60$  MPa against the usual 35 – 40 MPa.
- Montée St-Rémi bridge built near Montreal, Canada in 1993. The bridge has two continuous 40 m spans made of HPC with  $f_{c,cube28}$  of 60 MPa.
- The ‘Pont de Normandie’ bridge, completed in 1993. This was the longest cable-stay bridge in the world when it was built having an overall length of 2141 m and a centre span of 856 m. It has approximately 35, 000 m<sup>3</sup> of HPC of  $f_{c,cube28} = 60$  MPa used for construction of the pylons and cantilever beams.
- Hibernia offshore platform, completed in Newfoundland, Canada in 1996. It was built with a ‘modified normal weight’ HPC having W/B ratio of 0.31 for the splash zone and 0.33 for the submerged zone for a design  $f_{c,cube28}$  of 69 MPa. The design constraints included unit mass of between 2200 and 2250 kg/ m<sup>3</sup> for buoyancy and meeting an elastic modulus  $\geq$  of 32 GPa.

- Confederation Bridge completed between Prince Edward Island and New Brunswick in Canada in 1997. It consists of 44 main spans of 250 m length each and massive main pier shaft and foundation elements fabricated on land. The approach pier foundation and some mass concrete sections, requiring control of thermal cracking, were built with Class C ( $f_{c,cube28} = 30$  MPa and  $f_{c,cube90} = 40$  MPa) concrete which contained cement partially replaced with approximately 32% fly ash (FA) in addition to 7.5% silica fume (SF) by weight of cement content. The Class A concrete in this work had  $f_{c,cube28} = 55$  MPa and a maximum of 1000 coulombs chloride permeability at 28 days. Some piers with an abrasion resistance shield were built with  $f_{c,cube28} = 80$  MPa concrete (Mehta & Monteiro, 2014).

Many structures adopting HPC in particular variants are either ongoing or recently completed all over the world. Some worth of mention in this work are:

- Burj Khalifa Towers in Dubai, United Arab Emirates. The 829.84 m high, World tallest building, completed in October, 2009 had its foundation made of a high density, low permeability concrete while ice was added to the mixing water to combat the excessively high temperature (about 50 °C) of the environment.
- Abraj Al-bait Towers (formerly Makkah Clock Royal Towers), Saudi Arabia completed in 2012 is now the World's second tallest building (601 m tall). It is made of similar concrete as those used in Burj Khalifa.
- The Moses Mabhida Stadium in Durban, South Africa is a structure on the continent which must enter this list. The main bowl of the stadium comprises of 1750 columns and 216 raking beams while the façade has 100 columns of varied heights; the highest being with 46 m.
- One World Trade Centre in New York City is another example of utilisation of HPC in recent times. The tower height and slenderness imposed stringent demand on the overall strength and stiffness of the structure. HSC of C95/105 and E-modulus of 48 GPa specified are the dual requirements (Rahimian & Eilon, 2012).

The demands of concrete structures as in the projects mentioned above will continually make a case for the utilisation of HPC with specifics in design requirements for strength, durability, low permeability and special concepts and approach in materials handling, mixing, transporting and curing to meet the job demands.

### 2.2.2 Characteristics of HPC

HPC comprise of a very high cement content and low W/B placed in the range of 0.20 to 0.45 (Kosmatka et al., 2002). Aïtcin (1998) and Neville (2012) placed the W/B as equal to or lower than 0.35. Its compressive strength is usually greater than NSC even though the alternative use of HSC for HPC is not totally correct, high compressive strength value is also a characteristic of HPC (typical compressive strength values of HPC ranges between 55 MPa and 115 MPa). The benchmark of  $f_{c,cube28}$  to be adopted in this study shall be 70 MPa minimum as specified in recent literature (Aïtcin, 1998; Beushausen & Dehn, 2009; EC 2, 2004; Mehta & Monteiro, 2014; Neville, 2012).

The characteristics of HPC considered critical for particular application in practice often differ but may range within the following properties as outlined in literature (Aïtcin, 1998; Beushausen & Dehn, 2009; Kosmatka et al., 2002; Mehta & Monteiro, 2014; Neville, 2012):

- high workability
- high-early strength
- high-strength
- high-elastic modulus
- high-durability and long life in severe environments
- Low permeability and diffusion
- Resistance to chemical attack
- High resistance to frost and deicer scaling damage
- Toughness and impact resistance
- Volume stability
- Ease of placement

- Compaction without segregation
- Inhibition of bacterial and mold growth

### 2.2.3 Classes of HPC

The SHRP in USA has four types of HPC for highway structures on basis of minimum strength, maximum W/B and minimum durability criteria (Mehta & Monteiro, 2014). This classification of SHRP with their requirement is as presented in Table 2.2.

**Table 2-2: Classification of HPC (Mehta & Monteiro, 2014)**

HPC Type	Minimum Strength Criteria	Water/Binder (W/B) Ratio	Minimum Durability Factor for Cycles of Freezing and Thawing
Very Early Strength (VES)	14 MPa in 6 hours	$\leq 0.4$	80%
High Early Strength (HES)	34 MPa in 24 hours	$\leq 0.36$	80%
Very High Strength (VHS)	69 MPa in 28 days	$\leq 0.35$	80%
Fibre Reinforced	HES + (steel or PVA)	$\leq 0.35$	80%

Mehta & Monteiro (2014) had an additional class of HPC called high-volume FA concrete (HVFA) said to be more durable and resource efficient than those made with conventional Portland – cement material. The HVFA is said to comprise of FA content above 50 percent of the cementitious material as component of blended cement.

Portland Cement Association (2012) also presents five classifications of HPC as high-early strength concrete (HESC); high-strength concrete (HSC); high-durability concrete (HDC); self-consolidating concrete (SCC) and reactive powder concrete (RPC).

The five classes of HPC given by Aitcin (1998) are based on 25 MPa strength increments derived from a combination of experience and the present state-of-the-state-art in practice. These are Class I (50 MPa); Class II (75 MPa); Class III (100 MPa); Class IV (125 MPa) and Class V (150 MPa). The focus of this study shall be high early strength to very high strength concrete types of FHWA (2012) same as Class II – IV of Aitcin (1998).

## 2.2.4 Materials for HPC

HPC being concrete of low W/B (specifically  $\leq 0.4$ ) is prone to autogenous shrinkage (also called self-desiccation or chemical shrinkage) which can occur when cement hydrates. According to Aïtcin, (1998), a 0.38 W/B concrete is not much stronger nor exhibits much better performance than 0.42. If the W/B deviates significantly from the 0.40 value, the compressive strength, microstructure and overall performance of HPC differs significantly from that of the NSC (Aïtcin, 1998). At this stage it becomes difficult, if not impossible to achieve a workable and place-able concrete without introduction of superplasticisers. The lower the W/B, the stickier the concrete and the more difficult the handling, mixing and transportation becomes. The concrete becomes so dense and impermeable that even with wet curing by immersion, the internal regions hardly get enough water for complete hydration hence the need for internal curing.

Chemical admixtures (i.e. superplasticisers, accelerators, retarders and air-entraining agents) and supplementary cementitious materials (SCM) application in HPC has been noted in literature (Aïtcin, 1998; Beushausen & Dehn, 2009; Mehta & Monteiro, 2014; Neville, 2012) to be a way of controlling the workability and placeability. Common SCM in use for HPC includes silica fume (SF), fly ash (FA), ground granulated blast-furnace slag (GGBS) and Metakaolin (MK). The selection and appropriate proportioning of the SCM is influenced by the specific properties requirements for the HPC at both the fresh and hardened state (Beushausen & Dehn, 2009).

Special attention is thus required in material handling, mixing and manufacturing procedures of HPC for achieving consistently high quality concrete. Specific material performance requirement must be ascertained as met by the mix ingredients prior to selection. The recommendation from literature (Aïtcin, 1998; Beushausen & Dehn, 2009; Neville, 2012) can be summarised as follows:

### 2.2.4.1 Cementitious Material

All cement conforming to SANS 50197-1 or BS EN 197 -1-2000 is adjudged suitable for HPC (Beushausen & Dehn, 2009), once compactibility between cement clinker and superplasticisers is ascertained. However, CEM I 42.5 R is recommended based on its suitability for required workability

and strength development to a long term limit of up to 105 MPa. CEM I 52.5 R is on the other hand excellent for higher strength but might show higher water demand and heat of hydration thereby necessitating the use of retarding agent for prevention of rapid hardening (Beushausen & Dehn, 2009; Neville, 2012). SF, generally of 5 to 15% by weight of total binder and sometimes other SCM such as FA, GGBS, MK and corex slag (CS) are always necessary additions (Aïtcin, 1998; Beushausen & Dehn, 2009; Neville, 2012). Binder content ranges of 380 – 550 kg/m<sup>3</sup> are common in HPC with a consequence high heat of hydration and autogenous shrinkage during hydration resulting in early-age cracking if volume changes are restrained.

HPC's properties of high strength and low permeability although not necessarily concomitant, are linked to one another since high strength requires a low volume of larger capillary pores. This requirements warrants making the mix to contain particles graded down to the finest size which is achieved by the use of SF. The SF fills the spaces between the aggregates and the cement particles (Neville, 2012). Aside the filler effect of the SF is its high pozzolanic reaction which according to Detwiler and Mehta (1989) is dominant in improving concrete compressive strength. The need for a sufficiently workable mixture in low W/B concrete, for solids to be well dispersed towards achieving a dense packing and deflocculation of cement particles often necessitates addition of other SCM. This is in addition to the use of large dosage of a compatible superplasticizer.

#### **2.2.4.2 Aggregates**

In HPC the mechanical properties of the aggregates are of great importance, so are the shape, grading and chemical reactions between aggregate and cement paste. Water demand of the aggregates used in HPC has to be checked and controlled stringently. This is expected to be made as low as possible through selection of rounded aggregates and optimised grading of different sizes (Beushausen & Dehn, 2009).

The fine aggregate ought to be of low fine content ( $\geq 150 \mu\text{m}$ ) since HPC is rich in fines as a result of the high cement content. A sand of fineness modulus (FM) of 2.7 – 3.0 is recommended (Aïtcin, 1998; Beushausen & Dehn, 2009; Kosmatka et al., 2002; Mehta & Monteiro, 2014; Neville, 2012).

ACI 363R-92 recommends fine aggregate with rounded particle shape and smooth texture surface for less mixing water requirement in HPC. The State-of-the-Art-Report (ACI 363R-92) also affirms that sand with an FM of about 3.0 gives best workability and compressive strength. For high packing density and avoidance of stress concentrations due to lack of homogeneity in the concrete matrix, Beushausen & Dehn (2009) specify a maximum aggregate of 8 to 16 mm size, preferably crushed stone (andesite, dolerite and dolomite) as the most suitable coarse aggregate for HPC.

#### **2.2.4.3 Admixture**

The required low W/B in HPC will always warrant the use of high quality superplasticisers. The specific project demands might also place a need on the incorporation of other common admixtures such as retarders or air-entraining agents (Beushausen & Dehn, 2009). There is the need for a proper understanding of the compatibility of the superplasticisers with the cement type while optimum dosage for the required workability has to be established from field or laboratory trials. Issues of consideration here are the ambient temperature and required slump retention time of concrete. The saturation point of the superplasticisers as specified by the manufacturer is of importance as addition beyond this point can result in segregation (Beushausen & Dehn, 2009; Neville, 2012).

### **2.3 Mix Design for HPC**

Mix design refers to the appropriate selection of different ingredients of concrete to be designed for specific purpose (Addis & Goodman, 2009). This exercise must result in a mixture that:

- In the fresh state, can be transported without segregation, placed, compacted and finished (if necessary) with available equipments.
- In the hardened state, satisfactorily meet the required strength, durability and dimensional stability (Beushausen & Dehn, 2009; Neville, 2012).

The various mixture proportioning methods has the following objective as highlighted by (Aïtcin, 1998).

- Determine an appropriate and economical combination of concrete constituents that can be used for a first trial batch to produce a concrete close to that which can achieve a good balance between the various desired properties of the concrete at the lowest possible cost.

Neville (2012) pointed out that a generalised systematic approach of mix proportioning for high-performance concrete is yet to be developed. McIntosh also stated succinctly that a precise relationship has not been established between the properties of concrete, and even the more specific characteristics of the mix such as water: cement ratio; aggregate: cement ratio and grading let alone such elusive qualities as aggregate particle shape and texture (cited in Addis and Goodman, 2009). The data used in selecting mix proportions thereby serve only as a guide. Mix design is therefore said to be a matter of trial and error. The calculations based on design data are really just a means of making an intelligent guess towards arriving at a trial mix (Addis & Goodman, 2009).

Despite the above-cited draw-backs, a good concrete practitioner can combine the science of mix design with experience and intuition to obtain proportions which will be close to the requirements with only one or two trial mixes. The art requires proper care during sampling and more importantly the materials have to be as uniform as possible to obtain a representative sample (Addis & Goodman, 2009).

The common approaches to mixture proportioning can be placed under two basic classifications namely

- The American Mix design (ACI 211-1) method and
- The British Mix design method (or the Department of Environment (D.O.E) method).

The ACI 211-1 method comprises of eight steps as listed in Neville (2012), namely

- Step 1: Choice of slump
- Step 2: Choice of maximum size aggregate
- Step 3: Estimate of water content and air content
- Step 4: Selection of water/cement (W/C) ratio
- Step 5: Calculation of cement content

- Step 6: Estimate of coarse aggregate content
- Step 7: Estimate of fine aggregate content
- Step 8: Adjustment to mix

The British mix design method is however presented to comprise five steps as follows.

- Step 1: Compressive strength for the purpose of determining the W/C ratio. This thereby brought to fore the concept of target strength
- Step 2: Determination of water content based on required workability recognising influence of the maximum aggregate size and type
- Step 3: Determination of cement content
- Step 4: Determination of total aggregate content
- Step 5: Determination of fine aggregate content from the total aggregate content. The governing factors here are the maximum size of aggregate, level of workability required, the water/cement ratio and the percentage of fine aggregate passing the 600  $\mu\text{m}$  sieve.
- The method also makes provision for casting trial mixes and adjustment made to the mix proportioning till the slump range chosen is arrived at. This serves as a check at the fresh state of the concrete (Neville, 2012).

In South Africa, the Cement and Concrete Institute (C&CI) has a mix design approach derived from the ACI 211-1 method and this is what is adopted for proportioning of concrete mixtures (Addis & Goodman, 2009). A close study of the C&CI method reveals it as an expanded form of the ACI 211-1. Both the D.O.E method and the ACI 211-1 often result in similar proportions of ingredients of same properties if used for the same target strength.

The peculiarity and performance requirements in HPC have however made the known mix design approaches to be inadequate due to the following reasons identified in literature (Aïtcin, 1998; Addis & Goodman, 2009; Neville, 2012).

- The use of superplasticisers now, enhances low W/B in HPC.

- HPC often contains one or more SCM which in many cases replaces a significant amount of cement.
- The presence of SF in HPC causes significant changes in properties of fresh and hardened concrete.
- Workability of HPC can be adjusted using superplasticisers without altering the W/B.

A recent concept in use for mix proportioning in concrete and cement paste is the particle packing model as discussed in the works of Fennis, et al., (2012). The approach is adjudged not to be effective for situations where the material constituent can undergo change in shape, nature, or state during the mixing process (Fennis et al., 2012), hence it can not be considered in this work with SAP expected to absorb water during the mixing of the HPC. The approach is also for now being used for concrete materials basically comprising fine particles only while this study has coarse aggregate incorporated.

The American Concrete Institute offers a method of design for HSC in their state-of-the-art-report on high-strength concrete (ACI 363 R-92, reapproved in 1997). The procedure like the known method for normal strength concrete (the D.O.E and ACI 211-1) specified the required target strength  $f_{cr}'$  (MPa) same as in ACI 211-1 as:

$$f_{cr}' = f_c + 1.34\sigma \quad (2.1)$$

$$f_{cr}' = f_c + 2.33\sigma - 3.5 \quad (2.2)$$

Where:  $\sigma$  is standard deviation;  $f_{cr}'$  is target strength at maturity (often 28 days) and  $f_c$  is the characteristic strength obtained from previous onsite data, making reference to ACI 318 and ACI 322.

Equation 2.1 ensures that there is a 99% probability that the average of all sets of three consecutive compressive strength tests will be equal to or greater than  $f_c$ . The second equation ensures that there is a 99% probability that no single test will have a compressive strength lower than  $f_c - 3$  MPa (ACI 363 R-92).

Mehta & Monteiro (2014) also proposed a simplified mixture proportioning procedure applicable for normal weight concrete of compressive strength range 60 MPa to 120 MPa. It is suitable for coarse aggregate having maximum size range of 10 to 15 mm and slump range of 200 to 250 mm. It assumes

a 2% entrapped air volume for non-air entrained HPC, which can be increased to 5 to 6% and suggested an optimum aggregate volume of 65%.

Aïtcin (1998) on the other hand presented a design approach for HSC said to be initiated by five different mix characteristics beginning with decision on W/B ratio. The sequence is as follows:

- No. 1 – the W/B;
- No. 2 – the water content;
- No. 3 – the superplasticiser dosage;
- No. 4 – the coarse aggregate content and
- No. 5 – the entrapped air content (assume value).

The procedure is presented in the chart shown in Figure 2.1.

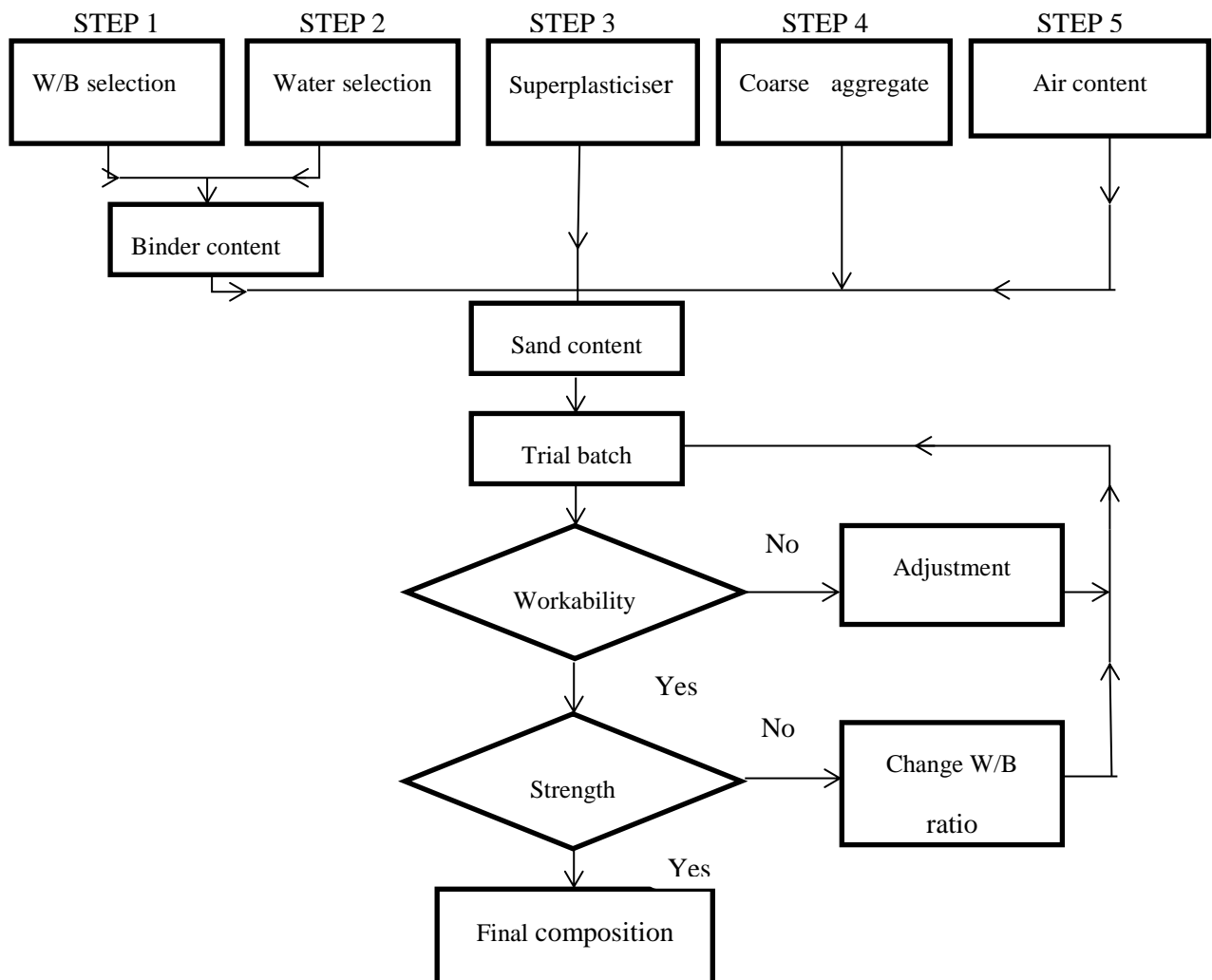


Figure 2-1: Mix Design Process for HPC (Aïtcin, 1998)

This study adopts the above mix design method with proper attention given to choice and treatment of the constituent materials before use in production of the HPC mixes. The specified cement content in literature for HPC is adhered to while compatibility and the manufacturers guide on superplasticiser determines the superplasticiser's choice and dosage. The W/B became the first guiding principle for this design while preliminary tests on available fine sand as presented in Section 3.3.1 led to the decision of sieving the natural sand available to reduce the high dust content and the retained on 300  $\mu\text{m}$  used in the trial mixes for a reduced quantity of mixing water.

## 2.4 Superabsorbent Polymers

Superabsorbent polymer (SAP) is defined by Siriawatwechakul et al., (2010) as a general term referring to polymers that are able to retain a large amount of water. SAPs are cross-linked polyelectrolytes which starts to swell upon contact with water or aqueous solutions, resulting in the formation of a hydrogel (Mechtcherine & Reinhardt, 2012). The two main categories of SAPs are thermoplastic polymers (or linear polymers) and thermoset polymers (or cross-linked polymers). Thermoplastic polymers are noted to be of high molecular weight, having overlapping polymer chains with the junctions acting as physical cross-links which form pseudo-three dimensional structures. Thermoset polymers, on the other hand, are three-dimensional polymer networks with chemical cross-links which hold polymer chains together, thus preventing their being dissolved when soaked in solvents (Siriawatwechakul et al., 2010). This study focuses on thermoset polymers in general, and, specifically on, the covalently cross-linked polymers of acrylic acid and acrylamide, neutralised by alkali hydroxide which, according to Mechtcherine & Reinhardt (2012), have been proven to be efficient as IC-agents in concrete.

The main driving force for the swelling of SAP as reported in the RILEM State-of-the-Art Reports (STAR) Volume 2 by the TC 225 is the osmotic pressure which is proportional to the concentration of ions in the aqueous solution (Mechtcherine & Reinhardt, 2012). As the ions in SAP are forced closely together by the polymer network, there exists a very high osmotic pressure within. By absorption of water, the osmotic pressure is reduced by diluting the charges (Figure 2.2). The reset force of the

polymer network and the external osmotic pressure thus work together to offset the osmotic driving force. Other external pressure such as from the swelling of SAP or retention of water against external mechanical forces, reduces the absorption capacity of the SAP. The swelling is thereby in equilibrium when all forces are equal (Mechtcherine & Reinhardt, 2012).

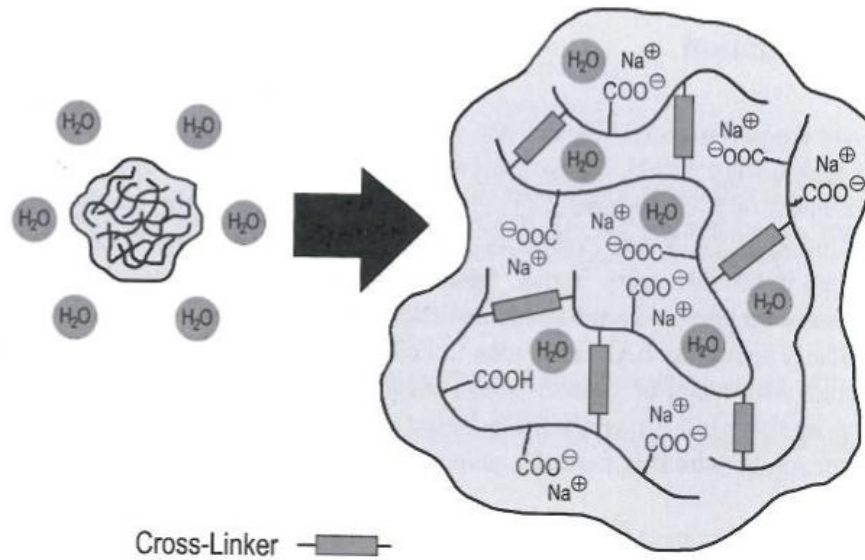


**Figure 2-2: SAP polymer network based on polyacrylic acid (courtesy of BASF) cited in RILEM STAR TC 225 (Mechtcherine & Reinhardt, 2012)**

The absorption of a SAP is argued Mechtcherine & Reinhardt (2012) to be strictly dependent on the concentration of ions in the swelling medium. Kinetics of water migration in cement-based materials systems containing SAP is thereby of importance to this study with focus on the behaviour of HPC with SAP as IC-agent. The RILEM STAR volume 2 (Mechtcherine & Reinhardt, 2012) has a summary of studies on this topic which is presented in the following sections.

### 2.4.1 Water Absorption and Desorption of SAP

The effectiveness of IC by SAP, as argued by Siramanont et al. (2010) is dependent on the swelling ratio of SAP. This is defined as the rate at which SAP absorbs and releases water and the spacing within the SAP particles in concrete. These factors are noted to be heavily related to the structure and polymerisation technique of the SAP.

The kinetics of water migration in cement-based systems containing SAP as shown in Figure 2.3 can be discussed on two basic concepts of absorption and desorption with previous studies as summarised by Mechtcherine & Reinhardt (2012) as follows:

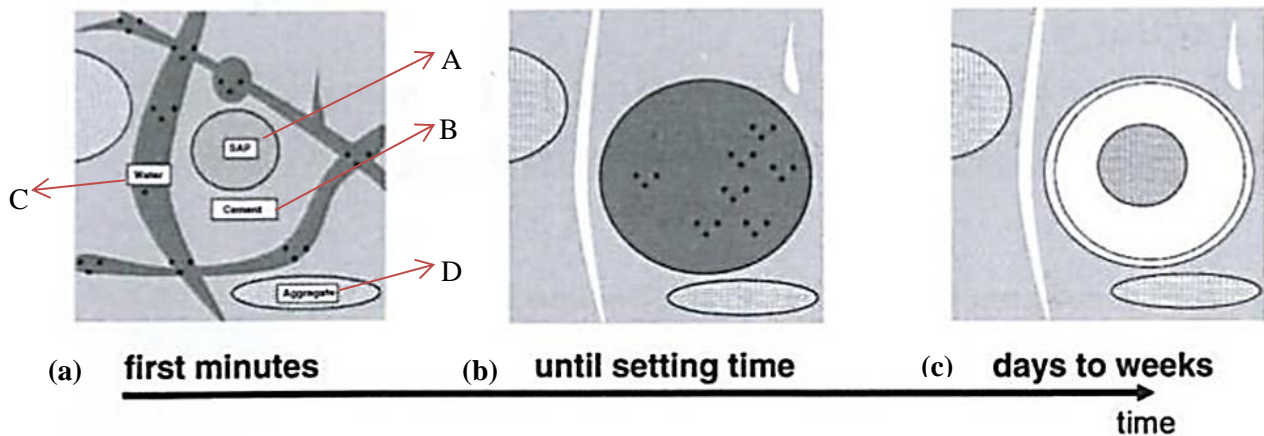


Figure 2-3: Schematic representation of water migration in cement-based systems, after Mönning (2009).

The item labelled A in Figure 2.3 above is the SAP, B is the cement, C is the water, and D is the aggregate. Figure 2.3(a) is the initial condition which shows homogenous dispersion of cement particles, water, SAP and aggregates. Figures 2.3(b) represent the state when SAP has reached final absorption and Figure 2.3(c) refers to the state after desorption when the water has been transported into the cementitious matrix and almost empty pore remains (Mechtcherine & Reinhardt, 2012).

#### 2.4.2 Absorption in pore solution

Absorption of pore fluid into the SAP is the result of a competitive balance between expansive and shrinkage forces. The two main factors responsible are the high concentration of ions existing inside the SAP leading to a water flow into the SAP by osmosis and the increase in the swelling due to water solvation of hydrophilic groups present along the polymer chain (Mechtcherine & Reinhardt, 2012). Also of importance depending on the SAP architecture, is the ionic strength of the aqueous solution which change the interaction (inter- and intra-molecular) of the polyelectrolytes due to the shielding of charges on the polymer (Jensen & Hansen, 2001). Mönning (2009) observed that the calcium ( $\text{Ca}^{2+}$ ) ions present in the pore solution of concrete can cause additional interlinking of the polymer and limit their swelling. Increase in the concentration of the ions outside the SAP results in decrease in the osmotic pressure inside the gel and hence a reduced swelling of the SAP (Jensen & Hanse, 2001). The

SAP particle size also influences the absorption of pore fluids. Very large SAP particles may have a reduced efficiency due to insufficient time for water uptake during mixing while very small SAP particles on the other hand, may also show reduced absorption as caused by less active surface zone compared to the bulk (Jensen & Hansen, 2002). Esteves (2010) confirmed the significant influence of SAP particle size on both the amount of pore solution absorbed and the rate of water absorption. He used Fick's second law of diffusion to describe the kinetics of absorption within a group of SAP as dependent on its particle size distribution.

Lothenbach & Winnefeld's Thermodynamic modelling of the hydration of Portland cement (2006) is one of the many studies carried out on concentration of different ions in the pore solution of cement pastes as a function of hydration time. The potassium ( $K^+$ ), sodium ( $Na^+$ ) and sulphate ( $SO_4^{2-}$ ) ions are the highest concentration commonly found. High concentrations has been reported by Lura & Lothenbach (2010) to develop immediately after mixing and remains roughly constant until the setting time. The ionic strength decreases at later ages as a result of precipitation. According to Lura & Lothenbach (2010), the ionic strength of CPS differs considerably among Portland cements depending on their alkali contents and SCM is argued to further influence the ionic strength.

Many research reports of SAP absorption of synthetic pore fluids exists. Notable amongst them is the work of Jensen & Hansen (2002) with absorption of 20 g/g in 60 minutes for suspension-polymerised SAP (round particles of average 200  $\mu m$  size), while a solution-polymerised SAP (crushed irregular particles of 125 – 250  $\mu m$  size) was reported to absorb 37 g/g in 30 minutes. The SAP swelling in cement pastes gave a total absorption of about half the amount shown in the CPS which in turn is several times less than the absorption in distilled water (Jensen & Hansen, 2002).

Craeye & De Schutter (2006), using SAP particles sizes of 100 to 800  $\mu m$  arrived at 130 g/g in distilled water after 5 minutes but above 500 g/g water absorption after 24 hours. The latter absorption level was then used to estimate the SAP to be added to concrete by Craeye & De Schutter (2006) with no account taken for the SAP's much less absorption in CPS than in water. Esteves (2010) using optical microscope observed the growth of individual SAP particles in the CPS over time. The work

concludes that particle size had a significant influence on both the absorption kinetics and total amount of absorbed fluid.

SAP absorption in cement paste is more difficult to determine when compared to absorption in CPS. Partial answers have been offered by previous studies on the amount of fluid absorbed and the kinetics of absorption. According to Mechtcherine & Reinhardt (2012), there is no information available on the differential swelling of different-sized particles in cement pastes. Jensen & Hansen (2002) are of the opinion that large particles may not have enough time for full expansion. The distribution of the SAP particles in concrete is also an issue of concern, as the particles can form clusters or agglomerate (Mönnig, 2009). Mechtcherine & Reinhardt (2012), in addition to issues raised above identify the need to investigate crushing possibility of swollen SAP, especially the larger particles during vigorous mixing.

A popular approach adopted by researchers in estimating SAP absorption in cement pastes and concrete is by observing the changes in rheology of mixtures containing SAP. Mönnig (2005 & 2009) compared the slump flow as a function of additional mixing time (up to 15 minutes) of concrete mixtures containing SAP to arrive at absorption of 10 ml/g and 45 ml/g for two SAP types. Most water uptake by the SAP was judged to occur in the first five minutes (Mönnig, 2005). Dudziak & Mechtcherine (2008) estimated SAP absorption in a coarse-grained fibre-reinforced UHPC by adjusting the water to obtain the same slump flow of a reference mixture.

Many approaches have been developed by researchers for determination of SAP absorption capacity in cement pastes and concrete such as:

- i) those based on the principle of stereology (Jensen, 2005);
- ii) collection of digital images from polished paste surface using a high resolution scanner in combination with SEM images for comparing particle size distribution of SAP at both the dry and swollen state at 2D image analysis level (Mechtcherine et al., 2006; Dudziak & Mechtcherine, 2008; Mechtcherine et al., 2009); and
- iii) use of X-ray micro-tomography (3D images) for dry SAP particle size distribution and their distribution in high-performance mortars (Lura et al, 2008).

Lura et al. (2008) characterised the pore structure of a mortar with SAP with round pores at a peak diameter of 150  $\mu\text{m}$  which was clearly different from a plain mortar. They also performed a micro-tomography study of SAP in UHPC producing an image of the 3D distribution of the voids without quantitative analysis.

Neutron tomography was used by Trtik et al. (2010) to observe the water uptake of a large SAP particle (about 1 mm size in dry state) inserted in a fresh cement paste with W/C of 0.25. The study reports 12 g/g SAP absorption of the CPS at 3 hours with about 90% of the uptake taking place at 35 minutes after casting, which was the time of completing the first tomography (Trtik et al., 2010). Nuclear magnetic resonance (NMR) relaxation is another technique used to study water absorption by SAP in fresh concrete. The NMR experiments with high time resolution shows a fast water uptake of SAP, within less than five minutes after water addition (Nestle et al., 2009).

The fluid absorbing capacity of SAP is expressed as the swelling ratio i.e. the ratio of the weight of swollen SAP (swollen state) to the dried SAP (collapsed state). This is also referred to as absorbency in the works of Esteves (2014). This is a basic property of SAP which determines the final characteristics (i.e. microstructure, pore structure and the nature of hydration products) of concrete and mortar pastes. The values adopted by previous researchers ranges between 45 g/g (Craeye, et al., 2011) and 12.5 g/g (Hasholt, et al., 2012) for SAP swelling capacity in concrete. The most popular approach for the determination of SAP absorbency is the “Tea-Bag test” which according to Mechtcherine & Reinhardt (2012) is simple and easy to carry out on-site and in a laboratory. Researchers have reported SAP absorbency through the tea-bag test of 20 g/g to 35 g/g in CPS depending on the SAP ionic concentration (Jensen and Hansen, 2002; Schroefl, et al., 2012; Assmann, et al., 2014). SAP swelling capacity in cement pastes is judged as about half the amount shown in cement pore fluid (Jensen and Hansen, 2002). Esteves (2014) however proposed the use of the laser diffraction particle method for measurement of SAP absorbency in cement-based materials and reported an absorbency value of 13.8 ml/g using a stimulated exposed liquid (a CPS) at a certainty level of 0.1 ml/g. He however pointed out some factors such as the storing condition and the choice of optical model or the refractive index which could influence the accuracy and reproducibility of the

result. It then follows that there is also a possibility of the influence of solid contents of concrete in SAP absorption and desorption of the CPS or available water in concrete. The need for determination of SAP absorbency thereby becomes an important factor in research on its influence on concrete properties especially HPC.

### **2.4.3 Desorption in pore solution**

The covalently cross-linked thermoset polymers type of SAP absorbs water when brought in contact with water thereby causing water molecules to diffuse into the void space inside the polymer network to the hydrated polymer chain resulting in a swollen polymer gel (Siriwatwechakul et al., 2010). This process can be reversed by removing water and the SAP will return to the collapsed state. The driving force for desorption is the gradient in water activity generated within the concrete between the SAP absorbed water and the pore fluid in the cement paste resulting from self-dessication of the paste due to cement hydration (Mechtcherine & Reinhardt, 2012). Capillary pressure develops in the pore fluid by part of the gradient of water activity causing emptying of the pore due to hydration or external drying (Lura et al., 2006; Friedemann et al., 2006). Osmotic pressure caused by difference in the composition of the absorbed solution in SAP and that of the pore solution in the cement paste at the setting time and later also is a contributory factor. The desorption process can be described as a competition for water between the SAP and the cement paste (Mönnig, 2009).

Determination of the desorption of water and pore solution by SAP is more difficult than the SAP absorption. Among the few attempts at determining desorption is the work of Jensen & Hansen (2002) which presented desorption isotherm of a solution-polymerised SAP. The report shows that the SAP retained only 3 g/g of pore fluid and less than 1 g/g at 86% RH from the 350 g/g free liquid uptake in distilled water and 37 g/g in CPS recorded at 98% RH (Jensen & Hansen, 2002). This implies that almost all the pore solution absorbed in the SAP will be released within the first day of hydration in a low W/B concrete known for rapid self-dessication.

Mönnig (2009) conducted a study to measure desorption rate of SAP particles through mass loss at different RH of layers of saturated SAP particles with a thickness of one particle. The result shows

that the water close to the surface of the polymers is lost rapidly but water closer to the core of the polymer has to overcome more side-chains in the polymer, which interact with the water molecules through the Van-der-Waal's forces.

The factors influencing the desorption kinetics of the SAP in cement paste are properties of the SAP, kinetics of hydration, microstructure of the cement paste and the interface between the SAP and the cement paste, through which the water transport takes place. Mechtcherine & Reinhardt (2012) presents some experimental techniques for quantifying the amount of water remaining in the SAP (or lost from SAP) at a given point during cement hydration. They however make a case for further studies on understanding the desorption process of SAP including the determination of transport distance of water into the hardening cement paste.

Mönnig (2009) in his observation of water transport from a single SAP in cement paste (W/C = 0.5) with an optical microscope shows a water transport distance from the SAP of at least 50 – 60 µm (SAP original section of 168 µm had an influence zone of 280 µm diameter). Pieper (2006) in his study of SAP made to absorb water with dye added, reports that during mixing of cement paste, the SAP particles released some part of the absorbed water. Low-field NMR relaxation had also been used to study hydration in hardening cement paste with and without SAP (Friedemann et al., 2009; Nestle et al., 2009). Nestle et al. (2009) reports that there is about 15% contribution of the curing water in the SAP to the total water content of the cement paste. The work further infers that the water transfer from the SAP into the cement matrix is almost completed after 1 day. Performing pulse field gradient NMR diffusion to study water mobility of SAP particles as a function of water content, as well as SAP inside hydrating cement paste. It was reported that self-diffusion coefficients in SAP decrease slightly with increasing weight fraction of SAP, but remains high in the range of free water which equals  $10^{-9} \text{ m}^2/\text{s}$  (Nestle et al., 2009; Friedemann et al., 2006). This implies that a fast exchange of water molecules exists between the SAP gel particles and the interface with the cement matrix. The research report on diffusion length determined by NMR in the above studies (Nestle et al., 2009; Friedemann et al., 2006) is found to be in good agreement with water transport measurements from saturated LWA to cement paste (Lura et al., 2006; Henkensiefken, et al., 2011; Trtik, et al., 2011).

Synchrotron X-ray micro-tomography and Neutron radiography, as used in the study of water transport from saturated LWA to cement paste (Benz et al., 2006; Maruyama, et al., 2009), are also possible techniques as suggested by Mechtcherine & Reinhardt (2012) for application to IC with SAP. Trtik et al., (2010), from their study using Neutron tomography to monitor water release in large particles, observe emptying of absorbed fluid by the SAP around the setting time and that about 80% of the water was released in the first day of the cement hydration.

Another approach is to derive indirect evidence on the kinetics of water desorption of SAP from the measurements of degree of hydration, heat of hydration, internal RH and autogenous deformation in the cement-based system (Mechtcherine & Reinhardt, 2012). The works of Jensen & Hansen (2002) and Pierard et al., (2006) are examples which adopted measurement of autogenous deformation approach with an inference that the development of autogenous deformation in cement pastes followed the trend in RH development. Lura et al., (2006) observed higher non-evaporable water ( $w_n$ ) at 28 days in cement pastes with SAP compared to reference pastes. The work of Klemm (2009) on measurement of rate of heat of liberation on white Portland cement paste (W/C = 0.3, 20% SF), with or without SAP, observed significant influence due to SAP addition on the dormant period of the paste. Water release by SAP was observed to correspond to the main hydration peak and up to the first couple of days of hydration.

## 2.5 Superabsorbent Polymer in Concrete

SAP are primarily used as absorbent for water and aqueous solution in baby diapers, feminine hygiene products and other applications. The use in concrete and cement-based materials as IC-agent is well documented in literature (Khare and Peppas, 1995; El-Dieb, 2007 cited in Siritwatwechakul et al., 2010) with the works of Jensen, et al., (2001 & 2002) being the most extensive studies. This has led to an increased research interest on utilisation of SAP as concrete admixture thus leading to the establishment of the RILEM Technical Committees; TC 196 – ICC: Internal Curing of Concrete, TC 225-SAP: Application of Superabsorbent Polymers in Concrete Construction and TC RSC: Recommendations for the use of Superabsorbent Polymers in Concrete. These committees have

brought researchers together for discussions on IC of concrete, SAP and its applications in concrete at different fora with RILEM Conference proceedings (RILEM *Pro* 052, 2006; *Pro* 074, 2010 and *Pro* 095, 2014) coupled with State-of-the-Art Reports (RILEM Report 41 by TC 196 – ICC - (Kovler & Jensen (eds.), 2007) and TC 225-SAP - (Mechtcherine & Reinhardt, 2012)) summarising the available knowledge on IC of concrete and SAP application in concrete. Highlights of these reports are thus presented in the following sections as basis for further study on SAP application in concrete.

### **2.5.1 Previous Studies on Superabsorbent Polymer in Concrete**

The RILEM Report 41 by TC 196-ICC (Kovler & Jensen (eds.), 2007) highlights the positive effects of the use of SAP in HSC as an efficient IC-agent. Self-dessication and resulting autogenous shrinkage of these low W/B concretes were adjudged to be reduced or even totally prevented by providing internal water reservoirs. LWA and SAP were identified as the prominent materials in use as IC-agent in HPC (Kovler & Jensen, 2007), while SAP is seen as more effective in mitigating autogenous shrinkage due to their high water absorption capacity following evidence from a pilot project executed with SAP as IC-agent applied to HPC on a large scale (Mechtcherine et al., 2006). The work of the RILEM TC 196-ICC brought about broader research on the topic of SAP with many researchers investigating effects of SAP addition on concrete's rheological behaviour, shrinkage, strength, durability and other properties which are summarised in the STAR volume 2 by RILEM TC 225-SAP (Mechtcherine & Reinhardt, 2012). The previous discussion in Section 2.4 centred on the kinetics of absorption and desorption of SAP while the following sections will review the available previous studies on effects of SAP on the rheological behaviour, shrinkage, strength, durability, and other properties as well as change in concrete's microstructure.

### **2.5.2 Effect of SAP on Workability of Concrete and Mortar**

HPC and UHPC are materials with exceptional mechanical properties and enhanced durability. They are low W/B mixtures susceptible to high autogenous shrinkage and early age cracking potential when the deformation is restrained (Mechtcherine et al., 2009). SAP addition in the HPC/UHPC is primarily as IC-agents to mitigate autogenous deformation due the polymers' capacity to absorb liquids many

times their own weight, with a resultant gel forming. This characteristic can, on the other hand, considerably change the rheology of concrete containing SAP and hence the workability of the fresh concrete. Jensen & Hansen (2002) reported that a 0.4% ( $b_{woc}$ ) addition of a particular SAP type led to a lowering of the free W/C by 0.06. The change in the W/C produces an increase in the yield stress and the plastic viscosity of concrete. Contributing to the pure binding effect on the yield stress and plastic viscosity increase is the physical presence of the swollen SAP particles (Jensen, 2008).

The works of Mechtcherine et al., (2006) is among the few results available in literature on influence of SAP on the workability of concrete. They developed a special UHPC for the construction of the FIFA World Cup pavilion in Germany. Examining four UHPC mixtures, two without SAP at similar mixture composition (Reference and Pavilion at W/C of 0.24 and 0.25 respectively) and the other two made of 0.4% SAP ( $b_{woc}$ ) with additional water for SAP absorption increasing the W/C to 0.28 (Reference with SAP) and 0.29 (Pavilion with SAP). The fresh properties of concrete were measured using the slump flow spread and the V-funnel time tests. Increases in slump flow and a decrease in V-funnel flow time values was reported for SAP addition in the reference mixtures, while the Pavilion mixtures (with or without SAP) presented same slump flow values. The V-funnel flow time reading on the other hand show a slight difference with higher values observed for the mixture containing SAP (Mechtcherine et al., 2006).

Dudziak & Mechtcherine (2010a) also measured the workability of fresh concrete containing SAP using the slump flow test with two types of UHPC reference mixtures. A fine-grained UHPC enriched with steel fibres and a fibre-free UHPC containing coarse aggregate. The work involves five UHPC mixtures containing SAP of varying contents (0.3 – 0.4%  $b_{woc}$ ) with additional water (0.04 - 0.07%  $b_{woc}$ ). Slump flow values of 750 mm and 830 mm were recorded for fine-grained UHPC with or without SAP and additional water respectively, while an average slump flow value of 680 mm and 695 mm were reported for both reference UHPCs made from coarser particles and fibre and its SAP-containing mixture respectively. The outcome of the various studies by Mechtcherine et al., (2006, 2009, 2010a & b); Dudziak & Mechtcherine (2008) led to the conclusion that adding an extra W/C content of 0.015 is required for every 0.1% of SAP addition for the same workability to be

maintained. This is however said to be valid only for the acrylamide/acrylic acid polymer, spherical shape type of SAP with approximately 150 µm diameter size in the dry state and water uptake of approximately 16±1 g/g used in their studies. The results revealed that all UHPC mixtures with SAP experienced an increase in air content. All the UHPC mixtures with SAP were reported to show some decrease in density at the fresh state. Results from the work of Paiva et al., (2009) were also in good agreement, showing that SAP addition with extra water resulted in decreased density and an increase in the air content of fresh mortar.

Mönnig (2005 & 2009) studied the time evolution of the spreading flow of mortar mixtures containing varied contents of different SAP materials. Slump flow measurements were expressed as a function of additional mixing time with 2 or 5 minute intervals. The work suggested that some SAP materials had significant influence on the workability of cement-based materials, enhancing longer slump retention time. Mönnig (2009) also reported results on air content and density as recorded for numerous combinations of mortars and concrete. The presence of varied SAP types, particle size distribution and content as well as the magnitude of total W/C are parameters of interest in the above listed research works.

The limitations of the various studies, examining SAP influence on concrete workability using slump flow measurement is the inability to derive answer to the extent to which SAP incorporation changes the rheological behaviour. Slump flow is arguably an insufficient tool for quantitative assessment of rheological variables (Mechtcherine & Reinhardt, 2012).

Use of rheometer and V-funnel tests was reported in Mechtcherine & Reinhardt (2012) as adopted to examine the rheological behaviour of fibre-free finely grained UHPC. The results showed that the effect of SAP addition in UHPC is beneficial. It was further pointed out that an underestimation of SAP absorption capacity in one of the experiments led to pronounced loss of workability. A slight overestimation of SAP absorption can on the other hand, provoke a pronounced decrease in concrete viscosity (Mechtcherine & Reinhardt, 2012). SAP addition in cement-based systems without additional water is equivalent to removing water from the system and thus increases the yield stress and viscosity values, causing a thickening action (Mechtcherine & Reinhardt, 2012). Jensen (2008)

believes that the thickening effect caused by SAP in cement-based systems can be used with advantage in some practical applications such as pumping.

### **2.5.3 Binder Hardening and Microstructure Development**

The mechanism behind reduction of self-desiccation in HPC containing SAP is the free water release from saturated SAP leading to an increasing RH and promoting further cement hydration. The added SAP changes the kinetic of the hydration process and the development of microstructure in concrete. Issues of interest therefore are the degree of cement hydration as influenced by SAP addition and influence of SAP on the development of microstructure characteristics. That is, porosity, pore size distribution, morphology and connectivity of bulk cement paste, interfacial transmission zone (ITZ) between the cement pastes and SAP and the voids introduced by SAP (Mechtcherine & Reinhardt, 2012). The following sections present a discussion of the available studies on SAP influence on degree of hydration and microstructure development in cement paste.

#### **2.5.3.1 Degree of hydration of cement paste**

The rate of change of the degree of hydration due to IC provided by SAP is influenced by the size and amount of SAP in the mixture, the original W/C and the procedure of SAP addition in the concrete or mortar mixture (Reinhardt et al., 2008). The procedures of SAP addition are: i) addition of dry SAP particles without extra water; ii) addition of SAP particles along with the dry constituents and extra water added for SAP absorption; iii) addition of saturated SAP particles to the concrete, mortar or cement paste. The mechanisms of SAP's water uptake in cement paste and the rate of water desorption by SAP directly control further hydration (as discussed in Section 2.4 above).

Reported influence of SAP on the hydration process to date had been only in few studies (Lam, 2005; Ingarashi & Watanabe, 2006; Lura et al, 2006). Ingarashi & Watanabe (2006), through BSE image analysis, observed no significant difference on degree of hydration for 0.25 W/C cement paste (with or without SAP) till an age of 14 days, while that SAP addition as IC-agent led to increased degree of hydration after the 14 days. Lura et al. (2006) measured  $w_n$  content and noted a 10% increase in the relative degree of hydration for SAP-modified cement paste at the 56 days age. Esteves (2009)

reported the measured degree of hydration of cement pastes and mortar containing SF with or without SAP. He stated that use of SAP as IC-agent promotes both the cement hydration and the pozzolanic reaction, especially in the first few days of hydration.

### **2.5.3.2 Pore structure**

The main reason for changes in the microstructure, especially the pore structure of concretes (NSC or HPC) containing SAP as highlighted by Mechtcherine & Reinhardt (2012) are:

- i. SAP acts as soft aggregate when fully filled with water, but as air void when empty.
- ii. Non-uniformity of the dispersion of SAP during concrete mixing operation.
- iii. SAP water absorption changes the effective W/C in the early hydration stage while the water desorption by swollen SAP affects the further hydration of cement.
- iv. More pores may be induced by the interface between SAP and the cement paste matrix.

The effect of SAP on the pore structure therefore can be total porosity as well as the pore size and the pore size distribution.

Mechtcherine et al., (2009) showed that SAP increases the total porosity of concrete due to voids introduced by SAP particles. The total porosity measured by mercury intrusion porosity (MIP) on the concrete containing 0.6% ( $b_{woc}$ ) SAP (with extra water) at all ages was 6% higher than plain concrete and 2% higher than the mixture with 0.3% ( $b_{woc}$ ) SAP (plus extra water). The extra water added in the SAP-enriched mixtures compensated for the expected loss of workability due to water absorption by SAP particles and thus changed the total W/C in these mixtures. Mönnig (2005), MIP results showed no difference or even lower porosity at 1 day for SAP-modified mixtures with no additional water compensating the change in the rheological properties. According to Mechtcherine et al., (2009), the pore diameter measured by MIP technique ranges between few nanometres (nm) to about 120  $\mu\text{m}$ , while the voids introduced by SAP particles in concrete on average should be above 150  $\mu\text{m}$  size. The MIP is thus limited to measuring only a part of the SAP created voids (those with smaller size). The need for improved technique examining SAP created voids in concrete as adopted in this research

will be an important contribution to the available knowledge on influence of SAP addition on the behaviour of concrete specifically HPC.

Pore size and pore size distribution of surrounding cement matrix can be affected by SAP addition. Mechtcherine et al., (2009) found no significant effect of SAP addition on the most frequent pore diameter of the UHPC investigated for different ages. Ingarashi & Watanabe (2006) revealed that pastes with SAP as IC-agent have smaller porosity and more cement gel than paste without SAP. This was shown using a BSE image analysis on volume fraction of constituent phases in the cement pastes made with or without SAP. This suggests that the water released from SAP further enhanced continued hydration of cement and hence a decrease in porosity at later ages, especially in the range of capillary pores. Results of the studies by Dudziak & Mechtcherine (2010a) on UHPC samples with SAP (plus extra water) corroborates this finding. The BSE image analysis by Ingarashi & Watanabe (2006) revealed little change in the pore diameter in the pastes without SAP after 24 hours while pores in SAP-enriched pastes appreciably decreased with time. It was thus suggested by Ingarashi & Watanabe (2006) that addition of saturated SAP particles decreased the volumes of large pores in the coarse pore structures of the paste.

Lam (2005) through SEM image analysis with a BSE detector reported that SAP-modified mortar had empty voids seen as black spots with dark greyish rim which were the remains of the spherical SAP particles. The remnant of the SAP particle had some cement paste on its outer surface which had likely broken away from the cement matrix due to drying at the sample preparation leaving a gap (Lam, 2005). Also noticed were large voids, greater than 300  $\mu\text{m}$  which according to Lam (2005) is due to non-uniform distribution of the SAP particles in the samples. Different techniques and different preparation methods were reported to show the interfacial transition zone (ITZ) differently. The ITZ observed by SEM in a gaseous secondary electron (GSE) mode can be completely different from that obtained in a BSE detector mode. Reports from both the GSE mode based SEM and the X-ray diffraction conducted by Mechtcherine et al., (2009) were in agreement, stating no visible difference in element distribution between the microstructure formed directly in the surrounding of SAP pores and the other matrix.

The structure of SAP introduced as IC has a significant positive influence on the frost/thaw resistance in concrete (Lausten et al., 2008). Lura et al., (2008) presented micro-CT images of 3D distribution of SAP in mortars which revealed a number of large, spherical pores in SAP-containing mixtures. The SAP induced pores were noted to be evenly distributed over the concrete volume (Mechtcherine et al., 2009). Mechtcherine et al., (2006) showed that the final pores correspond well to the spherical shape of dry SAP particles as observed before addition to the mixture but are considerably larger. Ye (2003) used 3D micro-CT images to examine the pore size and structure for quantitative characterisation of the microstructure. Grey level histograms were adopted for classifying the black parts which represent the voids and pores volume was distinguished. The volume of pore images was assessed by multiplying the number of pixels with the image resolution and calculations made using the equivalent diameter of a sphere to obtain the cumulative pore volume fraction against the equivalent pore diameter.

#### **2.5.4 Effect of SAP on Concrete Shrinkage**

Shrinkage deformation leads to volume changes in concrete with resultant instances of cracking. Four common types of shrinkage which are relevant in the context of the study, are: i) plastic shrinkage – occurring during the first few hours after mixing the concrete (before the concrete sets); ii) autogenous shrinkage of hardening concrete – this is the apparent (external, macroscopical, bulk ) volume reduction resulting from the cement hydration process; iii) drying shrinkage – caused by the loss of water to the surrounding environment; and iv) carbonation shrinkage – resulting from carbon dioxide reaction with water (Mechtcherine & Reinhardt, 2012). Discussions on the first three shrinkage types with reference to current state of research on effect of SAP are presented in the following sections.

##### **2.5.4.1 Plastic Shrinkage**

Plastic shrinkage is the volumetric change in concrete occurring at very early age of concrete after mixing and casting before hardening. It refers to the concrete's exhibition (in the plastic state) of its properties of drying suspension consisting of densely-packed solid particles in a liquid phase. This

results from rapid water loss from the concrete surface by evaporation (Mechtcherine & Reinhardt, 2012). Insufficient curing as a result of lack of protective cover for concrete surfaces exposed to strong winds, high temperatures and/or low humidity are the major causes of plastic shrinkage in concrete. According to Mechtcherine & Reinhardt (2012), available information on particular effect of SAP addition in cement-based materials on plastic shrinkage is limited.

The work of Dudziak & Mechtcherine (2010b) is among the few attempts made at determining the plastic shrinkage behaviour of fresh cement pastes containing SAP. The authors reported a reduction in the plastic deformation and capillary pressure due to SAP addition with extra water, but settlement deformation was found to increase compared to the control mixture. Set retardation was also observed for the cement paste with SAP and extra water (Dudziak & Mechtcherine, 2010b). Dudziak and Mechtcherine (2010b) are of the view that the less pronounced settlement of the reference mixture was due to two phenomena acting simultaneously. These are: i) early and high rise of temperature due to heat of hydration; and ii) high positive autogenous deformation within the first hour or two after casting.

Kratz et al. (2007) observed a common behaviour of expansion or low plastic deformation for SAP-enriched mixes (with additional water) while SAP-free mixes showed pronounced plastic shrinkage. Results obtained by the authors for the mixes with SAP without additional water were less conclusive while some apparent inconsistencies in the result of mass loss measurement gave some difficulties in interpretation of their findings. As noted by Kratz et al. (2007), there is need for further investigation before a comprehensive discussion of the shrinkage mechanism.

#### **2.5.4.2 Autogenous shrinkage**

Autogenous shrinkage is defined as the external bulk deformation of a closed (sealed), isothermal cement-based system, not subject to external forces (RILEM Report 41, 2007). This is an important phenomenon in young concrete especially at low W/C (less than about 0.42), in which all the water is rapidly drawn into the hydration process and the demand for more water creates very fine capillaries. The surface tension within the capillaries leads to autogenous shrinkage (through two mechanisms –

chemical shrinkage or self-desiccation) which can lead to cracking. HPC due to their fine pore structure and low W/B are very susceptible to self-desiccation-caused autogenous shrinkage.

Lyman (1934) was the first to describe this deformation type, observing a decrease in concrete volume without any notable change in its mass or temperature. The subject of autogenous shrinkage in NSC, being considerably smaller than drying shrinkage, however received little attention until application of HPC in construction became popular in recent times. At the fresh state of concrete (before setting), the internally occurring and externally measurable volume changes are alike, hence autogenous shrinkage has been regarded as equal to chemical shrinkage.

Chemical shrinkage is defined in by Mechtcherine & Reinhardt (2012) as the internal microscopical volume reduction due to a resultant lower absolute volume of the hydration products as compared to that of the reacting constituents (i.e. binders and water). Chemical shrinkage (being the change in absolute volume) is distinct from autogenous shrinkage deformation which is defined as the change in apparent volume (Jensen & Hansen, 2001). Although chemical shrinkage has drawn less attention in research than autogenous shrinkage, it is said to be the main driving mechanism behind the macroscopically observed autogenous shrinkage after a commencement of solid skeleton development in concrete (Mechtcherine & Reinhardt, 2012). Mechtcherine & Reinhardt (2012) offers assessment of hydration reactions of the main mineral components of cement as the most straightforward approach to study the absolute volumetric changes in concrete.

Nawa & Horita (2004) showed that reaction of Tricalcium silicate with water resulted in 16.5% reduction in the absolute volume (166.4 cm<sup>3</sup> of reagents produced 138.9 cm<sup>3</sup> of hydrates). In the study, the density of the reactants and the products of the chemical reaction as well as the molar weight of the compounds were incorporated in the input parameters for the calculations. Kratz et al. (2007) suggests adoption of the same approach for calculating the chemical shrinkage with further calculations made for the secondary reactions (e.g. ettringite formation). It is however the view of researchers that chemical shrinkage (as a rule of thumb) is equal to 0.06-0.07 ml/g of Portland cement reacted (Powers & Brownyard, 1948) while for SF it increases to 0.22 ml/g of SF reacted (Jensen, 1993). Absolute volume of unhydrated cement is noted to increase from 1 cm<sup>3</sup> to approximately 2.2

cm<sup>3</sup> after the hydration process is finished (Powers & Brownyard, 1948; Hansen, 1986). According to Lura (2003), the global reduction of volume takes place at the expense of water while the solid volume increases.

According to Mechtcherine & Reinhardt (2012), all commonly used approaches for chemical shrinkage assessment ensures constant water saturation of the pores within the cement-based system under examination. This makes the amount of water needed to replace the volume decrease a key principle of the measurement while chemical shrinkage is determined by normalising the volume change to the solid mass in the measured sample. Mechtcherine & Reinhardt, (2012) observed that there is currently no experimental evidence suggesting need to adjust the measurement protocol of chemical shrinkage characterisation in SAP-free systems for verification of changes caused by use of an IC-agent. No study in literature is noted to provide conclusive information on chemical shrinkage due to incorporation of IC-agents. Esteves (2009) and Lura (2003) arrived at similar results in their respective experiments on SAP-enriched cement pastes of W/C of 0.3% and 0.4% SAP content  $b_{woc}$ . They used similar protocols, although the pastes in Esteves (2009) work had a 15%  $b_{woc}$  SF content. They reported that all the SAP-enriched pastes mixtures showed higher chemical shrinkage compared to the SAP-free paste. This was said to be clearly driven by the highest rate of hydration. SAP addition was adduced to be responsible for the change as a result of the higher moisture content present as entrained water in the paste (RILEM Report 41, 2007).

The cement-based material in a liquid-like state is unable to sustain internal voids created by chemical shrinkage. As the solid skeleton forms of the hydration products, the bulk deformations of the entire concrete system observed (macroscopically) are smaller than the changes in the internal volume of the materials. Examining this in a microscope, shows formation of a large number of fine pores in the cement paste referred to regarded as significant volume changes due to hydration. The measured reduction in concrete specimen (macroscopically) – autogenous shrinkage, is therefore, only a fraction of the real material (i.e. chemical) shrinkage.

The extent to which chemical shrinkage is converted to autogenous shrinkage depends on the water content and the pore distribution resulting from hydration. In NSC, mainly for reason of workability,

the mixing water provided is more than required for complete hydration of cement. Thus, pores formed due to chemical shrinkage are either filled with water or at least the concrete air pore has a RH of 100%. In this case, there is no significant self-desiccation during the entire hydration process and the thermodynamic equilibrium of the system is undisturbed. The adjoining pressure between the particles of C-S-H gel experience can be offered similar consideration, hence no pronounced driving force for autogenous deformations (Mechtcherine & Reinhardt, 2012).

The amount of water in the low W/B HPC is insufficient to achieve complete hydration of cement. Hence, this concrete type experience pronounced decrease in RH within the pore system. This leads to a resultant self-desiccation-caused shrinkage deformation based on two mechanisms: i) a decrease in the disjoining pressure between the particles of the C-H-S gel, and, ii) a decrease in the menisci radii of the pore water, causing tension increase both within the pore water and at its surface. The second phenomenon is known to result in simultaneous development of compressive stresses in the solid skeleton of the system towards restoring equilibrium by compensating the tensile stresses in the fluid phase. The extent to which either of the two phenomena stated above dominates the material behaviour observed is yet to be ascertained by further experiment of studies (Mechtcherine & Reinhardt, 2012).

Contributory factors to the increased autogenous shrinkage in this low W/B HPC is the fact the mixtures usually contain superplasticiser and SF. SF incorporation in HPC mixtures leads to finer pore structure and thus increased capillary stress. The pozzolanic reaction of SF involves chemical shrinkage and thus higher bulk shrinkage of SF-concretes (Mechtcherine & Reinhardt, 2012).

Investigations on approaches to mitigate autogenous shrinkage by adding materials with high water storing capacity to the mixture, which would supply water to surrounding matrix as soon as self-desiccation occurs has identified the use of saturated LWA and SAP as appropriate (ACI (308-213) R13, 2013; RILEM Report 41, 2007; Bentur et al., 2001; Weber & Reinhardt, 1997).

In reference to the work of Jensen & Hansen (2001 & 2002), researchers have tested various types of SAP, and shown some has good ability to mitigate autogenous shrinkage in HPC (Mechtcherine et al., 2006; Ingarashi & Watanabe., 2006). Preference for SAP is based on the fact that they can be

engineered for special purpose of IC by designing the necessary particle size and shape, water absorption capacity and other properties. The application as IC-agent involves only a small amount of SAP with some additional water added directly as constituent materials of the concrete during the production process.

The effect of SAP on autogenous shrinkage can be treated on the concept of IC, targeted at mitigating volume reduction of hardening and hardened cement paste component of concrete. Considering the fact that shrinkage of concrete (autogenous or otherwise) is generally known to be smaller in comparison to that of cement paste. Two opposing issues highlighted by Mechtcherine & Reinhardt, (2012) of relevance on effect of SAP addition to cement paste versus concrete (or mortar) are: i) the distribution of SAP particles over the cement paste volume might be more homogenous in the concrete due to involvement of generally higher mixing intensity, and ii) the presence of aggregates and fibres in concrete may cause some additional mechanical loading on SAP in fresh concrete, which could lead to destruction of some unstable SAP particles.

Mechtcherine & Reinhardt (2012) present the works of previous researchers on effect of SAP on autogenous shrinkage of cement paste. Jensen & Hansen (2002) reports that SAP addition (0.3% and 0.6%  $b_{woc}$ ) led to a successful mitigation of autogenous shrinkage and some induced expansion. Ingarashi & Watanabe (2006) noted drastic reduction on autogenous shrinkage in a cement paste of 0.25 W/C through SAP addition (0.35%  $b_{woc}$ ) while autogenous shrinkage was completely prevented in the 0.33 W/C paste at higher SAP content. A further reduction of autogenous shrinkage to approximately one third was reported by the authors for a 0.25 W/C paste containing SF by the addition of 0.35% ( $b_{woc}$ ) SAP and corresponding amount of extra water. An increase in SAP content to 0.70% in the paste with SF still led to slight shrinkage at the early ages, a contrast to the corresponding SF-free cement paste, for which SAP completely prohibited autogenous shrinkage (Ingarashi & Watanabe, 2006).

Lura et al., (2006), in a study of the effect of SAP particle size and content reported that the size of expanded particles in the cement paste was 2-3 times greater due to pore fluid absorption. The authors reported that SAP pore absorption of approximately 12.5 g/g during the mixing of the cement paste.

They showed that at 0.3%  $b_{woc}$  SAP addition with extra water, contrary to the usually expected IC-efficiency enhancement due to better particle in the pastes with smaller-size SAP particles, the overall efficiency was somewhat lower than that of the mixes with larger particles. In the opinion of Lura et al (2006), the particle influence on the initial expansion mainly during the first day of measurement and that the small-sized SAP particles released IC-water less promptly at early ages, thus the bulk of the SAP acted as the main water reservoir. At the doubled level of SAP addition (0.6%  $b_{woc}$ ) and extra water sufficient for complete prevention of self-desiccation in the first two weeks, the effect of particle size became less pronounced (Lura et al., 2006). Esteves (2009) findings affirm that smaller particles reached saturation more rapidly but absorbed less water as compared to larger particles of the same chemical composition and production process.

The work of Geiker et al., (2004) is one of the few investigations of SAP effect on mortars. Their study showed that addition of small quantity of SAP (0.4%  $b_{woc}$ ) is as efficient in mitigating autogenous shrinkage as the replacement of a considerable amount (20%) of normal weight aggregate by LWA.

Research works on effect of SAP as IC-agent in concrete (specifically HPC and UHPC) on autogenous deformation mitigation has shown similar trends as found for cement pastes and mortar. Ingarashi & Watanabe (2006) studied a 0.25 W/C concrete containing 10% SF ( $b_{woc}$ ), river gravel of 10 mm maximum aggregate, natural river sand, a Polycarboxylate ether (PCE) superplasticiser with an acrylamide/acid copolymer SAP powder added as IC-agent (0.35%  $b_{woc}$ , IC water to cement ratio ( $W_{IC}/C$ ) of 0.05 which is sufficient enough to saturate the SAP particles). The authors reported that the moderate SAP addition led to reduction of autogenous shrinkage but doubling the amount of SAP resulted in the concrete exhibiting a small expansion during the initial 24 hours, which was maintained up to the 7 days age. Another concrete of higher W/B of 0.3 experienced a smaller autogenous shrinkage than the reference mixture (0.25 W/B), which was far larger than that of same 0.3 W/B concrete with SAP incorporated as IC-agent. Thus, the autogenous shrinkage reduction in concrete containing SAP was clearly shown to result from the effective IC with SAP and not from the

possible increase in effective W/C which could have been due to a smaller than the expected water absorption by SAP (Ingarashi & Watanabe, 2006).

Mechtcherine et al. (2006), working with self-compacting fibre reinforced high performance concrete (SFRHPC) and Dudziak & Mechtcherine (2008) with UHPC, further revealed that concrete mixtures containing SAP and extra water exhibit pronounced reduction shrinkage deformations which were particularly dramatic at very early age (i.e. the first 12 hours after final set). The results showed that the reduction was up to 64% for 0.3%  $b_{woc}$  SAP plus extra water ( $W_{IC}/C$  of 0.04 and 0.05, respectively) in the first day of measurement with increasing amounts of SAP and additional water (e.g. from 0.3%  $b_{woc}$  SAP,  $W_{IC}/C$  of 0.04 and 0.05 to 0.4%  $b_{woc}$  SAP,  $W_{IC}/C$  of 0.07; 1.0%  $b_{woc}$  SAP,  $W_{IC}/C$  of 0.16). More considerable reduction in autogenous shrinkage deformations as recorded in Mechtcherine et al., (2009) was observed making the autogenous shrinkage of the UHPC mixtures negligible. The degree of internal curing was adjudged as causing the changes in the development of the autogenous shrinkage over time beyond the first few days. The strain curves were noted to follow approximately the same trend at the beginning (one or two days) with or without SAP addition, while curing effect of the entrained water continued to work even at concrete ages higher than the mere first few days especially in mixes with smaller quantity of SAP plus additional water (Mechtcherine & Reinhardt, 2012).

#### **2.5.4.3 Drying shrinkage**

Drying Shrinkage is the progressive loss of gel water to the surrounding environment over a long time by concrete kept in drying conditions. The cement paste is known to shrink more than mortar and mortar shrinks more than concrete. Aggregate size also contributes to the extent of concrete shrinkage. Concrete made with smaller size aggregate shrinks more than concrete made with bigger size aggregate. Drying shrinkage is also a function of the gel fineness. Finer gel results in higher shrinkage ((Mechtcherine & Reinhardt, 2012).

Jensen & Hansen (2002) are among the few researchers that examined the effect of SAP as an IC-agent on both autogenous shrinkage and drying shrinkage of cement pastes. Working with 0.3 W/B

pastes exposed to drying (RH = 50%, T = 20°C), taking the specimens out of corrugated moulds at approximately 4.5 months, the authors showed that the drying shrinkage increased for SAP modified pastes, while autogenous shrinkage decreased drastically. The negative effect of IC on drying shrinkage was reported not to have significant influence on the total deformations, which decreased clearly with increasing SAP content and extra water in the mixtures (Jensen & Hansen, 2002).

Reinhardt & Mönnig (2006) studied the effect of IC on total shrinkage of concrete adopting two reference mixtures (0.36 W/C and 0.42 W/C). The 0.36 W/C concrete was modified with a suspension-polymerised particles of SAP (0.7%  $b_{woc}$ ) and extra water to arrive also at 0.42 W/C (i.e. 0.36 + 0.06), while pre-saturated LWA was used as IC in another mixture for comparative study. The authors reported decreased total shrinkage values in the SAP modified concrete when compared to the two reference mixtures. According to Reinhardt & Mönnig (2006), the shrinkage reducing effect of SAP on the shrinkage rate of concrete within the first week was a result of the densification of the paste and the binding of the water by the polymers.

Mechtcherine et al. (2009), from their study of effect of IC on total shrinkage of fine-grained UHPC observed an increase in total shrinkage in the SAP-modified mixtures. An increase in the amount of curing water resulted in an increase in total shrinkage. This according to the authors can be attributed significantly to higher drying shrinkage in the case of concretes containing IC-agents as caused by the presence of a larger amount of free water in the SAP-modified concretes. The reduction in autogenous shrinkage of the concretes containing SAP as IC-agents was more pronounced than the total shrinkage due to IC (Mechtcherine et al., 2009).

### **2.5.5 Effect of SAP on Mechanical Properties of Concrete**

Utilisation of SAP mainly as IC-agent in HSC/HPC aimed at mitigation of self-desiccation caused autogenous shrinkage has some accompanying effect of moderate strength reduction especially at the early ages because of higher porosity and moisture of the specimens (for those tested after sealed curing). According to the Mechtcherine & Reinhardt, (2012), SAP-enriched specimens tested at age of maturity sometimes indicate higher strength and elastic modulus than the mixtures without SAP.

The strength increase is possibly due to enhanced cement hydration caused by the IC, which compensate for strength reduction from the slightly higher porosity (Mechtcherine & reinhardt, 2012). Effect of IC by means of SAP on other mechanical properties of concrete such as tensile strength (uniaxial, bending and splitting) and elastic properties have been investigated and reported to some extent in literature while no record on studies on creep and fracture mechanics characteristics of concrete with SAP are known (Mechtcherine & Reinhardt, 2012).

Another possible application of SAP is as a water reducing agent (WR-agent). The fast water absorption of SAP within the first few minutes of mixing after contact with water results in decrease of the effective W/C in the cement matrix leading to a strength increase of the hardened concrete (Mechtcherine & Reinhardt, 2012). According to the report by RILEM TC 225 – SAP (Mechtcherine & Reinhardt, 2012), the tensile strength and elastic modulus of the concrete are expected to increase as well, but this is not always the case, especially in HPC mixtures. The available research results as compiled in the report and other literature on effect of SAP addition as IC-agent on mechanical properties of concrete are discussed in the following grouped sections.

#### ***2.5.5.1 SAP effect on compressive strength***

The outcome of the International RILEM Conference on Use of Superabsorbent Polymer and other New Additives in Concrete – PRO 74 presented diverse opinions by researchers on the effect of SAP on concrete. Although all affirmed that SAP is effective in mitigating autogenous shrinkage, the views on its effect on concrete strength differs; some argued that SAP incorporation leads to strength reduction and others were of the view that it enhance strength increase.

The view of the various researchers revealed that much remains to be done for a good understanding and utilisation of SAP in concrete construction. The beneficial contribution of SAP to mitigation of autogenous shrinkage in cement paste, mortar and concrete has been generally agreed on. Many researchers were however of the view that complete prevention was not always attained (Craeye et al., 2010; Ingarashi & Watanabe, 2006). In their study, Siramanont, et al. (2010) succinctly emphasise the need for an understanding of the SAP structure for a study of its impact on the IC mechanisms.

Mechtcherine & Reinhardt, (2012) states the resulting strength of concrete with SAP as generally depending on curing conditions, age and material composition. Jensen & Hansen (2002) reported a 19% compressive strength reduction due to SAP addition in mortar (0.6%  $b_{woc}$  SAP) when compared to the reference mixture (0.3 W/C), both specimen were subjected to 1 day sealed curing, followed by 27 days of water curing at 20°C. Bentz et al. (2002) obtained higher or equal later age strength in mortar with SAP (adding extra W/C of 0.046 for IC) compared to the reference mortar. Mönning (2005) conducted compressive strength tests on reference 0.55 W/C mortar with addition of different SAP types as part of an attempt to study freeze-thaw resistance of normal-strength mortar. The author concluded that there is no significant difference in the compressive strength development of mortars at different W/C using different SAP types. The W/C of the reference mortar mixture (0.55) is rather high and not typical for traditional SAP applications in high strength cement-based materials.

Craeye & De Schutter (2006) reported strength reduction of concrete containing SF (0.32 W/B) at different SAP contents (with an estimated SAP absorption capacity of 134 g/g). The strength reduction was noted to be very pronounced at higher SAP dosages and contents of entrained water ( $W_e$ ). Another experiment conducted in the same laboratory (Craeye et al., 2010) with another type of SAP (with estimated absorption capacity of 45 g/g) showed similarly significant reduction in the 28 days compressive strength. The authors of the two studies above were however believed to have overestimated the SAP absorption capacity and thus added too much water into the concrete leading inevitably to the strength reduction (Mechtcherine & Reinhardt, 2012; Hasholt et al., 2012).

Lam & Hooton (2005) in a study of IC effects adopting 0.35 W/C reference concrete with two SAP contents (0.3% and 0.6%  $b_{woc}$ ) to which the same amount of extra water ( $W_e/C = 0.10$ ) was provided reported that SAP introduction reduced the compressive strength. The mixture with 0.3%  $b_{woc}$  SAP addition has the lowest strength while the highest was obtained in the reference (0.35 W/C) mixture. The strength of the mix with 0.6% SAP ( $b_{woc}$ ) was found to be same (approximately) as that of the 0.45 W/C reference mixture, to which it can be said to have equivalent porosity and microstructure as characterised by the combination of capillary porosity and degree of hydration (Mechtcherine &

Reinhardt, 2012). According to Mechtcherine & Reinhardt (2012), it can be assumed that the negative effect of additional voids induced by SAP particles addition was compensated by the improved degree of hydration in the mix containing 0.6% SAP ( $b_{woc}$ ).

Studies on compressive strength of cement pastes and concrete (basic W/C of 0.25) with or without SAP was conducted by Ingarashi & Watanabe (2006) using mono-sized spherical particles (200  $\mu\text{m}$  diameter size) of acrylamide/acrylic acid copolymer having absorption capacity of about 13 g/g. The result showed that SAP introduction in the specimens (both paste and concrete) resulted in compressive strength decrease. The lower the W/C, the more sensitive the materials to the quantity of SAP added (Ingarashi & Watanabe, 2006). Piérard et al., (2006) measured compressive strength of 0.35 W/B concrete cubes containing SF and two SAP contents (0.3% and 0.6%  $b_{woc}$ ) cured at  $20\pm 2^\circ\text{C}$  temperature, 95% minimum RH for 2, 7 and 28 days curing ages. The results showed that SAP addition slowed down the early strength development (2-7 days) and a reduction of 7% and 13% for the 0.3% and 0.6% SAP-modified mixtures respectively at the 28 days curing (Piérard et al., 2006). According to the authors, strength losses can be attributed to the increased porosity of the concrete due to empty voids left behind by swollen SAP particles after desorption of the absorbed water. The SAP-enriched mixtures were viewed to have possibility of showing similar or higher strength, as the hydration proceeds at higher rate due to the higher RH maintained in the specimens (Piérard et al., 2006).

Lura et al., (2006) from the study of pastes mortars with or without silical fume, reported that SAP incorporation as an IC-agent had no significant influence on the compressive strength of high performance mortars (HPM), while the compressive strength of paste was reduced by 20% at the early age and 10% at later ages (up to 56 days). Largest aggregate size (resulting in largest defects), significantly larger than SAP particles was seen by the authors as responsible for the differences in effect of SAP addition. Lura et al., (2006) concluded that since aggregate or the ITZ and not cement paste, are the limiting factor for mortar strength, SAP's influence on strength of mortar and concrete should be negligible.

In the list of authors with report of reduction of compressive strength due to SAP addition as IC-agent in mortar and concrete are: Mechtcherine et al. (2006) – adopted 0.25 W/C reference mortar and concrete with 0.4%  $b_{woc}$  SAP (0.29 W/C total); Esteves et al. (2007) – mortar mixes of different W/C (0.25 – 0.35) under different curing conditions (30% to 100% RH at 20°C temperature and water curing); and Wang et al. (2009) – observed that higher SAP content or entrained water in concrete results to decreased compressive strength.

SAP containing UHPC (W/C 0.22) was reported by Mechtcherine et al. (2009) to show noticeable compressive strength decrease at the early ages (1 – 7 days), but exhibited only slight decrease in compressive strength at the 28 days for relatively small content of SAP (0.3%  $b_{woc}$ ) and extra water. Considerable decrease in compressive strength was observed at higher (0.6%  $b_{woc}$ ) SAP content.

In another study from the same laboratory, Dudziak & Mechtcherine (2008) reported that though SAP addition resulted in reduction of compressive strength of UHPC, the effect is not pronounced when the right quantity of extra water is added for IC purpose. Results of the experiments stated above (Mechtcherine et al., 2009; Dudziak & Mechtcherine, 2008), with noticeable decrease of compressive strength at early age, but only slight decrease at 28 days are consistent with the observed trend in mortar and concrete adopting other IC approach (use of LWA and IC-agents, other than SAP) as reported in RILEM Report 41 by TC-196 ICC (Kovler & Jensen (eds.), 2007). Internally cured concrete was reported to experience increased compressive (or flexural) strength, compared to reference mixes for concrete with LWA (Weber & Reinhardt, 1997; Lura, 2003; Zhutovsky et al., 2004).

Possible reason for compressive strength enhancement with age by SAP and other IC-agents offered in Mechtcherine & Reinhardt, (2012), is the improved degree of hydration of cement grains. Reinhardt et al. (2008) suggested that the cement hydration products grows at later ages inside the grain boundaries of swollen SAP particles, thus contributes to strength of the cement-based system at maturity.

Craeye et al., (2010) studied the mechanical and thermal properties of HPC using different degrees of IC and asserted in their conclusion that addition of SAP leads to a significant reduction of mechanical

strength and modulus of elasticity. Hasholt et al., (2012) in response to this argue that the conclusion of Craeye et al., (2010) is misleading. In their view, the additional water added to required mixing water to compensate for water absorbed by SAP in the concrete examined by Craeye et al., (2010) was in excess of the absorption capacity of SAP; hence the water in the concrete was in excess of what is required for complete hydration. This is said to be responsible for the significant reduction in strength as recorded by Craeye et al., (2010). The appropriate determination of SAP absorption in cement paste, mortar and concrete holds the key to good understanding of the influence of SAP addition on the compressive strength and other mechanical properties of the concrete.

Schrofl et al., (2012) examined the relationship between the molecular structure and efficiency of SAP in the mitigation of autogenous shrinkage in concrete. Working with different SAP types, they observed that the type of SAP and its water kinetics are relevant to mechanical properties of cement paste, mortar and concretes. The work inferred that SAP with higher anion concentration performs well in efficient mitigation of autogenous shrinkage and hence enhanced hydration leading to no or moderate decrease in strength. Most of the studies above however (except few, for instance the works of Hasholt, et al., (2010a & b) and Craeye, et al., (2011)) focussed on cement pastes and mortar.

Hasholt et al., (2010a & b) investigated the mechanical properties of concrete with emphasis on the compressive strength and elastic modulus using concrete specimens with W/B ranges of 0.35 - 0.50 varying the proportion of SAP between 0% and 0.06% cured in water up to 28 days. They modelled the effect of SAP on concrete strength and elastic modulus by combining Bolomey's formula and Powers' model and observed that the net effect of SAP (negative or positive) depends on the mix design and curing age (Hasholt et al, 2010a &b). They also concluded that SAP has little effect on hydration and hence leads to reduced strength when the W/B is high ( $> 0.45$ ) especially at early ages and large SAP additions. Concrete specimen with low W/B ratio and low SAP addition are said to experience compressive strength increase at later ages (Hasholt et al., 2010a).

### **2.5.5.2 SAP effect on tensile strength**

Tensile strength is considered a good indication of the crack resistance and depends majorly on the existing micro-cracks which often provoke formation of macro-cracks under tensile stresses. Tensile strength can be determined through different loading types – uniaxial, flexural (bending) and splitting. Mechtcherine & Reinhardt (2012) presents a review of studies on the effect of SAP on tensile strength of concrete, some extracts of which are as follows:

Many researchers reported reduction in the tensile strength similar to the compressive strength reported earlier (Section 2.5.5.1) despite difference of their specimen and test procedure (Mechtcherine et al., 2006; Ingarashi & Watanabe 2006; Dudziak & Mechtcherine, 2008). Mechtcherine et al. (2006) measured uniaxial tensile strength on special dog-bone shaped prism (40x24 mm cross section by 80 mm long) with non-rotatable loading plates. Flexural strength test was also conducted on beams (40x40 mm cross section by 160 mm long) using a 120 mm span. SAP addition was reported to result in decrease in tensile strength, similar to the trend observed for compressive strength. The uniaxial tensile strength was determined on oven-stored specimen for 0.25 W/C concrete at ages 7 and 28 days. Dudziak & Mechtcherine's (2008) work was on bending strength of low W/C UHPC cured internally by SAP addition with extra water.

Mortar mixes of different W/C (0.25 to 0.35) were tested under different curing condition (ranging from 30% to 100% RH at 20°C) by Esteves et al. (2007). Although the type of tensile strength conducted was not mentioned, an approximately 30% reduction in tensile strength was reported for the SAP-modified mortars in the study. The test results for mortar subjected to adverse curing conditions were more favourable for the SAP mixes, having some cases of higher tensile strength than the reference mixtures at the 28 days (Esteves et al., 2007). Result of the splitting tensile strength experiments conducted by Lam and Hooton (2005) on different IC materials showed a different trend from that obtained under compression. The specimen from 0.35 W/C reference concrete was better at ages 3 to 7 days, as in the compressive strength tests. The mixture made with 0.6%  $b_{woc}$  SAP content gave the best result for splitting tensile strength at the 28 days, far better than the reference mixture (0.3%  $b_{woc}$  SAP-containing mixture been argued as having too much entrained water). Based on this

finding, the highest tensile strength of the SAP-modified concrete at the 28 days was explained by Mechtcherine & Reinhardt (2012) as resulting from the fact that SAP, in parallel to shrinkage mitigation, successfully increase the tensile cracking resistance of the cement-based system. The review above shows that the technique adopted for conducting the tensile strength can influence the result obtained, as also the SAP contents and the amount of entrained water.

### **2.5.5.3 Effect of SAP on elastic properties**

Elastic moduli of internally cured ultra high performance mortars (UHPM) and concretes as reported by Dudziak and Mechtcherine (2010) showed no significant difference when compared with those of reference mixtures. The W/C in the reference mixtures were 0.22, while the additional water for IC was based on  $W/C = 0.04$  for the SAP-modified mixtures. The E-modulus values obtained by the authors for the respective mixtures are: UHPM – 48.8 GPa at 28 days, 0.3%  $b_{woc}$  SAP internally cured mixture – 46.8 GPa, steel reinforced fibre UHPC – 54.7 GPa and the SAP-enriched UHPC – 53.4 with a standard deviation of  $\leq 1.35$  GPa. This shows clearly that only a slight decrease of E-modulus was experienced by SAP addition.

Hasholt et al. (2010b) observed that though the outcome of their test on modulus of elasticity reflects that the theoretical models for mechanical properties work as well for concrete with SAP as for concrete without, there is need for further studies with more empirical models.

## **2.6 Mechanical Behaviour of HPC**

Mechanical behaviour of HPC refers to the characteristic quality, traits or distinctive features of HPC often determined by use of equipment to ascertain its meeting some of the basic performance requirements. In general the mechanical properties often examined for HPC are compressive strength, flexural strength (or modulus of rupture), splitting tensile strength and elastic modulus (Hueste, et al., 2004).

HPC application has been noted to be necessitated by some basic performance requirements which the NSC cannot offer as listed in Section 2.2.2. Amongst these are the strength and elastic modulus characteristics which are often placed as a demand in HPC mixes.

The strength properties of concrete can be said to comprise compressive and tensile strength, while tensile strength can be of three types; flexural, splitting and direct. This study shall investigate the compressive strength, elastic modulus, splitting tensile strength and fracture energy of HPC.

Studies on mechanical properties of HPC with SAP are scarce in literature. The works of Craeye & De Schutter (2006), Craeye et al., (2010) and Hasholt, et al., (2010a, b & 2012) are amongst the few that looks at SAP inclusion in actual concrete (not cement paste or mortar). Hasholt et al., (2012) however argued that the assumed swelling ratio of SAP used by Craeye et al., (2010) leads to excess additional mixing water used in their concrete that contains SAP hence their conclusion on SAP causing a decrease in strength is mis-leading.

The work of Hasholt et al., (2010a & b), is of particular interest to this study. Hasholt et al., (2010a & b) studied the mechanical properties of concrete with SAP with emphasis on compressive strength and elastic modulus and examined the compatibility of the results with the Powers' Model. The concrete samples studied were noted to be those with 0.35 to 0.50 W/B; this cannot actually be classified as HPC according to the definitions offered above, while the concern on autogenous shrinkage is basically to be an issue with concrete having low W/B (i.e. less than or equal to 0.35 W/B).

There is need for simulating the water absorption of SAP into the existing model (i.e. the Powers' Model) for strength and elastic properties of concrete and specifically the HPC with characteristic strength C55/67 – C100/115 as provided for in the EC2 which adoption in South Africa is currently being envisaged. The need for a good understanding of the effect of SAP addition on the micro-structure and molecular interaction of the constituent materials will be handy in explaining the mechanical behaviour of HPC of very low W/B (0.20 to 0.35). This study thereby is an attempt to fill the gap in literature with a focus on the effect of SAP incorporation on the mechanical behaviour of HPC with W/B values between 0.2 and 0.30, having a minimum 70 MPa, 28 day cube strength (C55/67 – C100/115) in both the fresh and hardened states.

## 2.7 Existing Models on Mechanical Properties of HPC

Mechanical properties of concrete can be influenced by many factors such the material constituents; cement/binder type; proportion of mixing water (W/B); porosity and the curing environment aside material handling and mixing as mentioned in Section 2.5. Previous works have emanated mathematical expressions relating mechanical properties of concrete to some of the factors highlighted above and this section presents a review of these models.

### 2.7.1 Powers' Model

Studies on mechanical behaviour of concrete are rooted in the work of Powers and Brownyard (1947) referred to as the Powers' Model. This states that the principal factors governing the ultimate degree of hydration regardless of the time required are the relative proportion of particles having mean diameters greater than about 50  $\mu\text{m}$  and the original water-cement ratio. It was further argued that cements having no particles larger than 50  $\mu\text{m}$  (or thereabout), becomes completely hydrated if W/C is not too low (i.e.  $W/C \geq 0.4$ ). Ultimate degree of hydration ( $\alpha_{\text{max}}$ ) is said to be inversely proportional to the 325-mesh residue (particles  $\geq 44 \mu\text{m}$ ). The work deduced that at a limiting average W/C value of about 0.44 ( $b_{\text{woc}}$ );  $\alpha_{\text{max}}$  is proportional to the water content of the paste in all cement pastes. Pastes with low W/C are said to experience lower rate of hydration except during the short initial period and hence require longer time for ultimate hydration (Powers & Brownyard, 2003a & b). Cement gel is composed of hydration products that contain all the principal oxides (CaO, SiO<sub>2</sub>, Al<sub>2</sub>O<sub>3</sub> and Fe<sub>2</sub>O<sub>3</sub>). The total surface area of the solid phases is related to the computed cement composition by:

$$V_m = 0.230(C_3S) + 0.320(C_2S) + 0.317(C_3A) + 0.368(C_4AF) \quad (2.3)$$

where:  $C_3S$  is a short hand notation for  $3CaO.SiO_2$  (i.e. Tricalcium silicate);  $C_2S$  is a short hand notation for  $2CaO.SiO_2$  (i.e. Dicalcium silicate);  $C_3A$  is a short hand notation for  $3CaO.Al_2O_3$  (i.e. Tricalcium aluminate) and  $C_4AF$  is a short hand notation for  $4CaO.Al_2O_3.Fe_2O_3$  (i.e. Tetracalcium aluminate).

Powers and Brownyard (1947) further identify relative vapour pressure and self-desiccation as other factors influencing the rate of hydration of cement pastes. A minimum vapour pressure of 0.85 kPa was adjudged in their work as the requirement for hydration below which hydration stops. Curing condition of concrete is thereby an important factor as sealed specimen may never reach full hydration (Powers & Brownyard, 2003a & b). The Powers' Model stands on the fact that strength of concrete at any W/B ratio depends on the degree of hydration of cement and its physical properties; the temperature at which the hydration takes place; the air content of the concrete; change in effective W/C ratio and cracks formation due to bleeding. The cement content in the mix and properties of aggregate-cement paste interface also play relevant role.

Powers' Model as developed in 1947 focussed on hydration of Portland cement in concrete having W/C within 0.45 to 0.70 (NSC) and was concluded not to be applicable for drawing conclusions on concrete of low W/C ratio (e.g. W/C = 0.25). The empirical study of 50 mm mortar cubes conducted by Powers and Brownyard (1947) resolved that compressive strength is proportional to the gel-space ratio and this is said to hold for all ages and for all cements low in Tricalcium aluminate ( $C_3A$ ) – low alkali cements. This compressive strength of 50 mm cement-pastes cubes as a function of the relative strength, ( $w_n/w$ ) in low alkali cement they presented is shown in Figure 2.2. It further gave an expression for cube compressive strength of the mortar pastes as:

$$f_{c,cube} = 240 \left( \frac{w_n}{w} - 0.11 \right) \quad (2.4)$$

where:  $w_n = non - evaporable water$  (i.e. the difference in mass measurement of the crushed paste after heated at 950 °C and 105 °C). The expression for determining the non – evaporable water content is given later in Chapter 3; and  $w = mixing water$ .

Brouwers (2004 and 2005) re-examined the works of Powers and Brownyard. The work highlighted the specific volume of  $w_n$  and the gel water in relation to degree of hydration as the most important features of the Powers' Model. It presented a detailed study of the chemistry involved in cement hydration as influenced by specific volume of  $w_n$  water and gel water with an intensive examination of reaction of the calcium silicate phases. The work revealed further that the minimum W/C ratio for

complete hydration in conventional cement (CEM I type) is around 0.39 which stands as the value accepted nowadays.

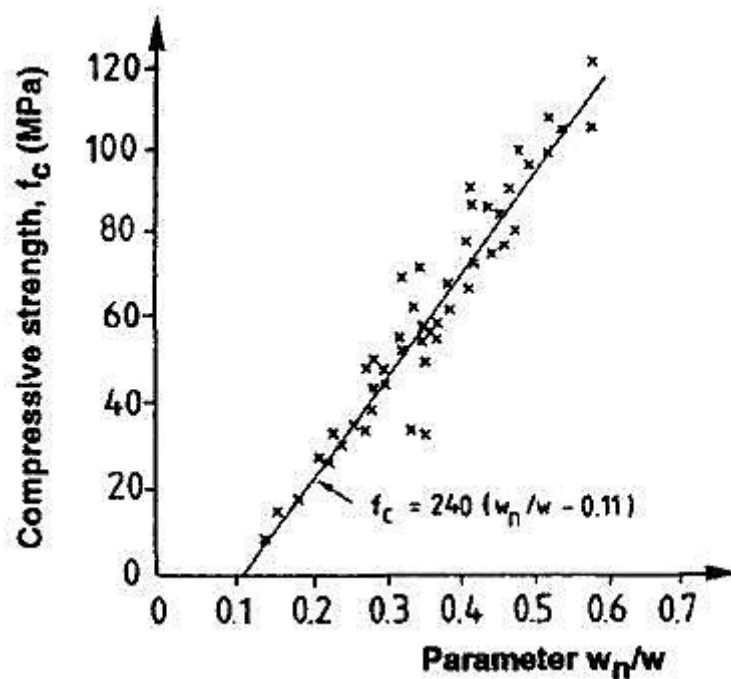
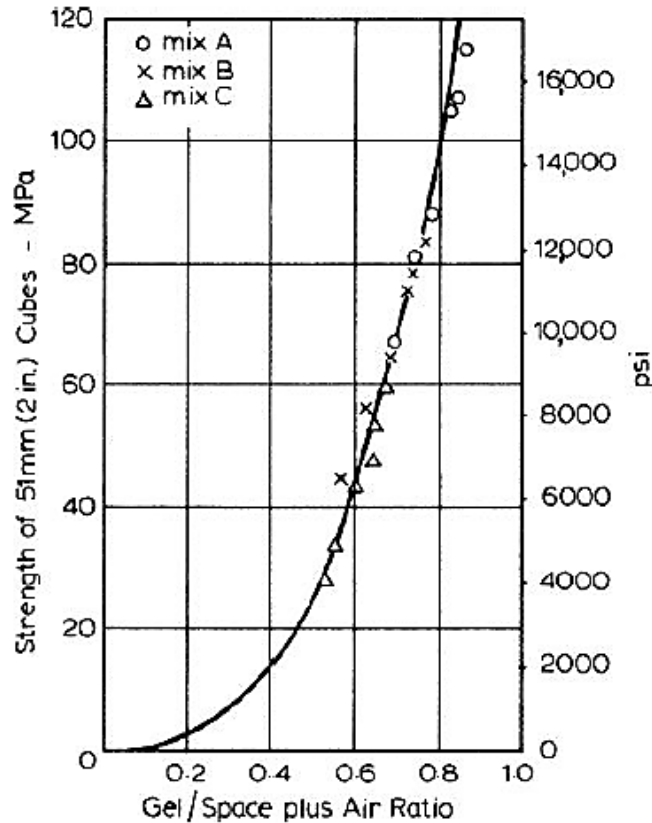


Figure 2-4 : Compressive strength,  $f_c$  of 50 mm cement-paste cubes as a function of relative strength ( $\frac{w_n}{w}$ ), Low-alkali cement (Persson, 1996)

The works of Hasholt et al., (2010a & b) examined SAP influence on the mechanical properties of concrete focussing on concrete of W/C ratio between 0.35 and 0.5. The study adopted the modified relation presented by Powers later for concrete (Powers, 1958). This gave the compressive strength of hardening cement paste in relation to the amount of gel and space available as an empirical power function (see figure 2.3 for illustration) as:

$$f_c = A.X^3, \quad X = \frac{\text{volume of gel}}{\text{volume of space}} \quad (2.5)$$

where A is a constant, X is the gel-space ratio. A is the intrinsic strength of the gel i.e. A is the strength when the gel-space ratio is unity (1).



**Figure 2-5: Compressive strength vs. gel-space ratio for cement-sand mortars**  
 $f_c$  = compressive strength (lbs. per in<sup>2</sup>); x = gel-space ratio (Powers, 1958)

The expression in equation 2.5 and figure 2.3 gives  $f_c = 234 x^3$  (MPa) (Neville, 2012) while some authors use a round up value of  $f_c = 240 x^3$  (MPa). The numerical value 234 MPa is referred to as the intrinsic strength of gel for the cement type and of specimen used (Neville, 2012 and Shetty, 2010).

This study with focus on HPC (W/B range 0.2 to 0.35) is concerned with W/C significantly lower than the limits within which complete hydration is possible and thereby examines recent improvements on this expression focussing on such concretes. Persson (1996) presents a study of the hydration and strength (compressive and split tensile) of HPC as influenced by the curing environment (water and air) over 450 days. The work states that unlike in NSC, hydration in HPC (containing SF) only proceeds to a final stage of  $w_n/c = 0.25$ ,  $w_n$  here refers to the non-evaporable water content of the concrete. The maximum degree of hydration  $\alpha_{max} = 1$  can only be achieved at a W/C ratio greater than 0.39. The maximum degree of hydration in concrete with W/C less than 0.39 is then linear, dependent on the W/C (Persson, 1996). Persson (1996) thereby postulates that:

$$(w_n/w)_{max} = 0.64 \quad (0 < W/C < 0.39) \quad (2.6)$$

and

$$(w_n/w)_{max} = 0.25 \times c/w \quad (W/C > 0.39) \quad (2.7)$$

Persson (1996) developed a modified relation between relative hydration and compressive cylinder strength of HPC (with or without SF) as:

$$f_{c,cyl} = 260 \times \left(\frac{w_n}{w} - 0.085\right) \quad (\text{No SF; } R^2 = 0.93) \quad (2.8)$$

and

$$f_{c,cyl} = 310 \times \left( \ln t \times \left( 0.030 - \left(\frac{w_n}{w} - 0.46\right)^2 \right) - 2.25 \times \left(\frac{w_n}{w} - 0.54\right)^2 + 0.31 \right) \quad (10\% \text{ SF; } R^2 = 0.97) \quad (2.9)$$

Where:  $w_n$  is the non-evaporable water content of concrete ( $\text{kg/m}^3$ ),  $w$  is the mixing water,  $c$  is the cement content of the concrete ( $\text{kg/m}^3$ ) and  $f_{c,cyl}$  is the cylinder strength of concrete.

### 2.7.2 Bolomey's Model

Bolomey's model is an expression which gives a relation between the water-cement ratios to compressive strength in normal weight concretes. The original expression postulated by Bolomey (1935) as shown in Equation 2.10 is basically a linear equation with little or no consideration for neither parameters relating to coarse aggregate nor the air content in the concrete.

$$f_c = A (1/W/C) + B \quad (2.10)$$

where: A & B are constants for given sets of materials; W/C is the water-cement ratio while  $f_c$  is the cylinder compressive strength of concrete.

There have however been variations of the Bolomey's Equation (2.10) in literature to suit particular types of concrete with the most common for practical grades of concrete (Brandt, 1995a & b) shown as:

$$f_c = A \left( (1/W/C) - 0.5 \right) \quad (2.11)$$

where: the value of B is taken as  $-0.5 * A$ .

The expressions in Equation 2.11 account for cement type and to some extent the properties of aggregate. It does not consider the quantity and quality/strength of aggregates in the concrete nor does it account for the air content. Hasholt et al., (2010a and b) in their works adopted a variant of the Bolomey's equation which incorporated the effect of air content for conventional normal weight concretes as follows:

$$f_c = K_{Bolomey} \left( (1/W/C) - 0.5 \right) \times (1 - B \times (a - a_0)) \quad (2.12)$$

where  $K_{Bolomey}$  (is the same as A in Equations 2.10 and 2.11) and  $B$  are constants,  $a$  is the actual air content (% relative to volume of concrete), and  $a_0$  is a reference air content. The expression

$(1 - B \times (a - a_0))$  is referred to as correction factor as related to air content.

The works of Kadri et al., (2012) introduced another variant of the Bolomey's equation specifically for concrete containing SF. The work postulates that at the early age between 1 ( $t_1$ ) and 10 days ( $t_d$ ), the compressive strength of SF-concrete ( $R$ ) increases according to the logarithm of time  $t$  given by

$$R = A + B \log \frac{t_d}{t_1} \quad (2.13)$$

where: A & B are constants. The coefficient B is referred to as the kinetics of the hydration reaction (Kadri, et al., 2012). This is said to be activated by the pozzolanic effect of SF in SF-concretes which starts before 2 days (Ollivier, et al., 1988; Sellevold & Radjy, 1983) as sited in Kadri et al., (2012).

Bolomey's equation for an estimation of compressive strength of NSC is presented as

$$f_{c28} = KR_{c28} \left( \frac{C}{E+V} - 0.5 \right) \quad (2.14)$$

where: C and E are mass of cement and water; V is the air volume; K = a coefficient dependent on aggregates characteristics;  $R_{c28}$  is the compressive strength of standard mortar after 28 days. Kadri et al., (2012) present a simple equation for SF-concretes as

$$f_{c28} = K \frac{1}{\rho_c} R_{c28} \frac{L}{(E+V)} \quad (2.15)$$

where:  $\rho_c$  is the relative density of the cementitious material and L is the effective cementitious content such that  $L = C + \alpha (sf/c) C$ . The function  $\alpha (sf/c)$  is referred to by Kadri et al., (2012) as the SF contribution in cement “equivalent” to compressive strength of concrete. The efficiency of SF is assumed to be linked to the presence of cement and only depends on  $sf/c$  ratio. The experimental work of Kadri et al., (2012) on compressive strength of standardised mortar thereby led to

$$\alpha (sf/c) = 0.36 - [2.1(sf/c) - 0.6]^2 \quad (2.16)$$

Substituting Equation 2.16 and  $V = y E$  (an account for air volume) into Equation 2.15 gives a generalised equation at any time as:

$$f_c(t) = KR_{c28} \frac{C}{(y+1)E} * \left\{ A(t) + 1.36 - \left[ 2.1 \left( \frac{sf}{c} \right)^2 - 0.6 \right]^2 \right\} \quad (2.17)$$

where: K depends on aggregates and is to be calculated from reference concrete strength without SF at 28 days;  $A(t)$  is a kinetic function determined from the reference concrete at a time t which ranges between 0 and 28 days; y is a coefficient dependent on concrete type having the following values: 0.13 for firm concrete, 0.10 for plastic concrete and 0.07 for very plastic or fluid concrete.

This modified model by Kadri et al., (2012) valid for W/C less than 0.4 thereby gave the compressive strength of SF-concrete at 28 day as

$$f_{c28} = \frac{KR_{c28}}{\left[ 1 + 3.1 \left( \frac{E}{C} \right) / \left( 1.4 - 0.4 \exp \left( -\frac{11sf}{c} \right) \right) \right]} \quad (2.18)$$

This study will examine the validity of this modified Bolomey’s equation for HPC (being a SF-concrete) as combined with the Powers’ Model for predicting the mechanical behaviour of HPC containing SAP as an IC-agent.

### 2.7.3 Constitutive Relations of Mechanical Properties of Concrete

The fib model code 2010 gives constitutive relations for the mechanical properties of concrete. The compressive strength as presented in Table 2.1, serves as the reference to which other properties of concrete are related. The highlights of the codes provisions can be presented as follows:

### 2.7.3.1 Tensile Strength and Fracture Properties

The relation between tensile and compressive strength of concrete is not proportional. An increase in compressive strength (especially in higher strength grade concrete) leads to a minor increase in tensile strength (Dehn, 2012). Hence, fib Model Code 2010 offers two different formulae for first estimate of mean value of tensile strength  $f_{ctm}$  (N/mm<sup>2</sup>) from characteristic compressive strength  $f_{ck}$  as:

$$f_{ctm} = 0.3(f_{ck})^{2/3} \quad \text{Concrete grades} \leq \text{C50/60} \quad (2.19)$$

$$f_{ctm} = 2.12 \ln(1 + 0.1 (f_{ck} + \Delta f)) \quad \text{Concrete grades} \geq \text{C50/60} \quad (2.20)$$

where:  $f_{ck}$  is the characteristic compressive strength according to Table 2.1.

$$\Delta f = 8 \text{ N/mm}^2$$

The fib MC 2010 thereby gave the lower and upper values of the characteristic tensile strength

$f_{ctk,min}$  and  $f_{ctk,max}$  respectively as:

$$f_{ctk,min} = 0.7 f_{ctm} \quad (2.21)$$

And

$$f_{ctk,max} = 1.3 f_{ctm} \quad (2.22)$$

When tensile strength is measured using splitting tensile strength  $f_{ct,sp}$  or flexural tensile strength  $f_{ct,fl}$ , fib MC 2010 further recommends a conversion factor for estimation of the mean axial strength  $f_{ctm}$  from the mean splitting tensile strength  $f_{ctm,sp}$  using Equations 2.23 and 2.24 from mean flexural tensile strength  $f_{ctm,fl}$ .

$$f_{ctm} = \alpha_{sp} f_{ctm,sp} \quad \text{for splitting tensile strength} \quad (2.23)$$

where:  $f_{ctm,sp}$  = mean splitting tensile strength

$$\alpha_{sp} = 1.0.$$

$$f_{ctm} = \alpha_{fl} f_{ctm,fl} \quad \text{for flexural tensile strength} \quad (2.24)$$

where:  $f_{ctm,fl}$  = mean flexural tensile strength

$$\alpha_{fl} = \frac{0.06 h_b^{0.7}}{1 + 0.06 h_b^{0.7}} \quad (2.25)$$

$h_b$  = the beam depth.

A smaller value than 0.06 is however required for HSC/HPC in  $\alpha_{fl}$  calculation from Expression 2.25. The fracture energy  $G_F$  (N/m), defined as energy required for propagating a tensile crack of unit area is recommended to be determined from related tests with axial tensile strength adjudged most appropriate (fib MC 2010). The MC 2010 offers that in the absence of experimental data, the fracture energy for normal weight concrete may be estimated by the relation

$$G_F = 73 f_{cm}^{0.18} \quad (2.26)$$

where:  $f_{cm}$  = mean cylinder compressive strength in MPa =  $f_{ck} + \Delta f$ ;  $\Delta f = 8$  MPa.

The factors influencing fracture energy ( $G_F$  - values) of NSC as highlighted in literature are W/C ratio; maximum aggregate size, age of concrete, curing condition, and size of structural members (Hu & Wittmann, 1990; Mechtcherine & Müller, 1997; Wittmann et al., 1987; fib MC 2010). The same factors' influence on fracture energy applies to HPC but at a smaller magnitude. Hansen, et al., (1996) argue that aggregate type and content seem to have the greatest influence on fracture energy of HPC as a phenomenon caused by transition from interfacial fracture to trans-aggregate fracture. High strength aggregates' utilisation (e.g. Basalt or Granites) is said to lead to increased  $G_F$  - values in HPC (International Federation for Structural Concrete (fib), 2008) - fib Bull42, 2008). This is said to impede crack propagation leading to concrete fracture such that breaking tougher aggregates, change in crack orientation and multiplication of cracks all resulting in higher energy dissipation.

Fracture energy estimation from the compressive strength is given in CEB-FIP MC 90 (as sited in fib Bull42 2008) as:

$$G_F = G_{FO} \left( \frac{f_{cm}}{f_{cmo}} \right)^{0.7} \quad (2.27)$$

where:  $G_F$  = fracture energy (N/mm)

$G_{FO}$  = base value of fracture energy which depends on maximum aggregate size  $d_{max}$  as provided by CEP FIP MC 90 (1993) sited in fib Bull42 (2008).

$f_{cm}$  = mean cylinder compressive strength (MPa)

$f_{cmo} = 10$  MPa

**Table 2-3: Effect of maximum aggregate size  $d_{max}$  on base value of fracture energy  $G_{FO}$  (CEP FIP MC 90)**

$d_{max}$	(mm)	8	16	32
$G_{FO}$	(N/mm)	0.025	0.03	0.058

Fracture energy determined using Equation 2.27 in comparison with experimental results was said (fib Bull42, 2008) to present an under-estimation (for concretes with 16 mm maximum aggregates) for all concrete grades except very high strength concretes ( $f_{cm} > 120$  MPa). In concretes with 32 mm maximum aggregates, over-estimation of fracture energy is said to be reported by the relation for concretes with mean compressive strength above 40 MPa (fib Bull42, 2008). Therefore many postulations of relations exist for estimating fracture energy on basis of type of aggregate or concrete class. The two relations offered by Fib Bull42, 2008 are as follows:

$$G_F = G_{FO} \left[ 1 - 0.77 \frac{f_{cmo}}{f_{cm}} \right] \quad (2.28)$$

where:  $G_{FO} = 0.18$  N/mm and  $f_{cmo} = 10$  MPa or

$$G_F = G_{FO} \left( \frac{f_{cm}}{f_{cmo}} \right)^{0.18} \quad (2.29)$$

where:  $G_{FO} = 0.11$  N/mm and  $f_{cmo} = 10$  MPa

These are however inconsistent with very low strength (below C12/15) and low strength concretes, but are adjudged to be suitable for C40 concrete grades and above. The Fib Bull42, 2008 states that Equation 2.28 provides a relatively better fit to experimental data than Equation 2.29.

### **2.7.3.2 Modulus of Elasticity and Poisson's Ratio**

Modulus of elasticity (E-modulus) is defined as the tangent modulus of elasticity at the origin of the stress-strain diagram (fib MC 2010). Equation (2.30) is given by the fib Model Code 2010 for an estimation of E-modulus from characteristic compressive strength of normal weight concrete made from sand and gravel.

$$E_{ci} = E_{co} \alpha_E \left[ \frac{f_{ck} + \Delta f}{10} \right]^{1/3} \quad (2.30)$$

where:  $E_{ci}$  is E-modulus (N/mm<sup>2</sup>) at concrete age of 28 days

$E_{co} = 21.5 \times 10^3$  N/mm<sup>2</sup>;  $f_{ck}$  and  $\Delta f$  as defined in Equation 2.19 and 2.20.

$\alpha_E = 1.0$  for quartzite aggregates.

Table 2.4 gives qualitative values  $\alpha_E$  for different aggregate types.

**Table 2-4: Effect of type aggregates on the modulus of elasticity  $E_{ci}$  (fib MC 2010)**

Types of aggregate	$\alpha_E$	$E_{co} \times \alpha_E$ [N/mm <sup>2</sup> ]
Basalt, dense limestone aggregates	1.2	25800
Quartzite aggregates	1.0	21500
Limestone aggregates	0.9	19400
Sandstone aggregates	0.7	15100

The following is given by the fib MC 2010 as an estimation of the E-modulus in situations where actual compressive strength ( $f_{cm}$ ) of the concrete at 28 day is known.

$$E_{ci} = E_{co} \alpha_E \left[ \frac{f_{cm}}{10} \right]^{1/3} \quad (2.31)$$

The fib MC 2010 however allows for use of a reduced E-modulus according to the following equation where only elastic analysis of concrete structure is to be carried out. According to Dehn (2012), this is to account for initial plastic strain, causing some irrecoverable deformations.

$$E_c = \alpha_i E_{ci} \quad (2.32)$$

$$\text{where: } \alpha_i = 0.8 + 0.2 \frac{f_{cm}}{10} \leq 1.0 \quad (2.33)$$

Values of tangent modulus ( $E_{ci}$ ) and reduced modulus ( $E_c$ ) for different grades of concrete as given in the Code (fib MC 2010) are presented in Table 2.5:

**Table 2-5: Tangent modulus and elastic modulus of elasticity (fib MC 2010)**

Concrete grade	C12	C16	C20	C25	C30	C35	C40	C45	C50
$E_{ci}$ [GPa]	27.1	28.8	30.3	32.0	33.6	35.0	36.3	37.5	38.6
$E_c$ [GPa]	22.9	24.6	26.2	28.0	29.7	31.4	33.0	34.5	36.0
$\alpha_i$	0.845	0.855	0.864	0.875	0.886	0.898	0.909	0.920	0.932
Concrete grade	C55	C60	C70	C80	C90	C100	C110	C120	
$E_{ci}$ [GPa]	39.7	40.7	42.6	44.4	46	47.5	48.9	50.3	
$E_c$ [GPa]	37.5	38.9	41.7	44.4	46	47.5	48.9	50.3	
$\alpha_i$	0.943	0.955	0.977	1.000	1.000	1.000	1.000	1.000	

It can be observed from Table 2.5 that concrete of very high grade (i.e. > C70) has same values for both tangent modulus and elastic modulus.

## 2.8 The modified Wedge Splitting Test Setup for Fracture Energy

The modified wedge splitting test setup (Figure 2.6) is an approach for obtaining nonlinear fracture mechanics parameters based on the RILEM recommendation AAC 13.1. Two wedges are pressed symmetrically between four roller bearings in order to split the specimen into two halves. The test setup is similar to the RILEM recommendation AAC 13.1. The only difference is that the specimen is placed on two line supports, not only one single line support in the middle of the specimen (Figure 2.7). The supports are placed directly under the mass concentration of each half specimen.

The advantage of this loading arrangement according to Trunk et al. (1999) is that a multiaxial stress distribution at the end of the crack may be avoided, thus preventing the crack being forced to propagate through the damage material. This single line support type of setup of the RILEM recommendation AAC 13.1 is known to result in the later damage type which often influences the measured fracture energy (Trunk et al., 1999).

The measurements taken during the test are the crack mouth opening displacement (CMOD) and the applied vertical load ( $F_v$ ). The measured CMOD is the mean of value of the readings of two linear variable displacement transducers (LVDT) placed both sides of the specimen, immediately under the loading points, while the vertical load is recorded directly from the testing equipment. The horizontal splitting force ( $F_{sp}$ ) is calculated from measured vertical load and the wedge angle. The test is normally run under the CMOD control at a specified rate.

The work of fracture ( $W_f$ ) is calculated from the area under the splitting force CMOD diagram while the specific fracture energy ( $G_f$ ) is the work of fracture divided by the ligament area ( $A_{lig}$ ). The  $A_{lig}$  is the projected area on a plane parallel to the ideal crack direction. That is the ligament height multiplied by the specimen thickness (i.e.  $F_{sp} = \frac{F_v}{2 \tan(\alpha)}$ ). Brühwiler (1998), recommend the use of a mean deflection diagram for determination of the nonlinear fracture mechanics parameters from the experimental results.

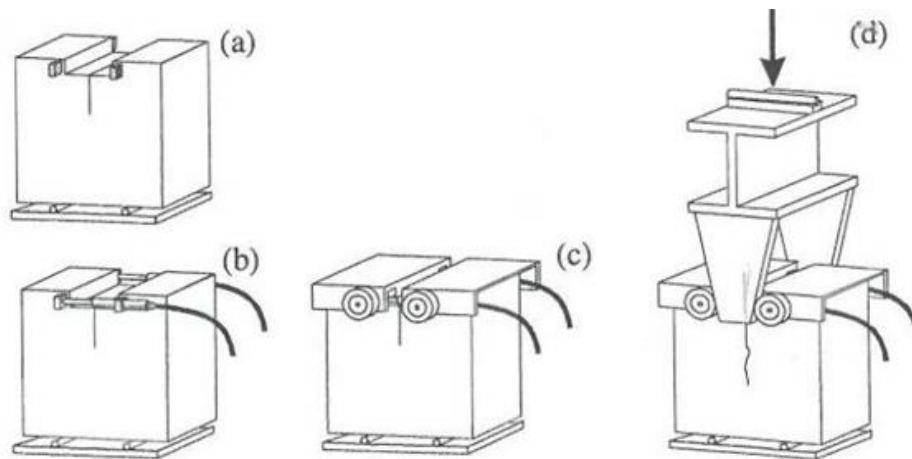


**Figure 2-6: Principle of wedge splitting test: (a) specimen on two linear supports, (b) LVDT on both sides of the specimen, (c) steel holding devices with roller bearings, (d) transversers with wedges**

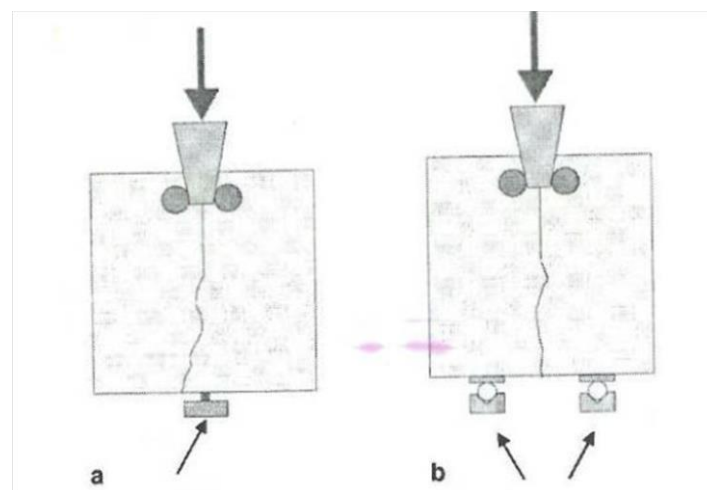


**Figure 2-7: Modified wedge splitting test setup according to RILEM: AAC 13.1. (a) One single line support at the end of the theoretical crack path. (b) Two line supports under the mass concentration points under each half specimen**

The wedge splitting test of RILEM recommendation AAC 13.1 and its modified test setup approach has been applied in many previous research on Autoclaved Aerated Concrete (AAC) (Brühwiler & Wittmann, 1990; Guofan et al., 1991; Gils et al., 1995; Trunk et al., 1999) and Fibre Reinforced Concrete (FRC) (Löfgren, 2005; Löfgren et al., 2004; NT BUILD 511, 2005) but no evidence of fracture energy parameters determination has been found in literature.

## 2.9 Summary

The use of HPC is gaining more attention in construction works while the issue of its susceptibility to self-desiccation and autogenous shrinkage has been addressed by introduction of IC-agents. SAP introduction as IC-agent is generally agreed as a possible way of mitigating autogenous shrinkage

but an in-depth understanding of SAP influence on the mechanical properties of HPC is still lacking. Reports on the influence of SAP on concrete are scarce in literature while the few experimental works in this regard are seen to have utilised mortar pastes or concrete having  $W/B \geq 0.35$  which does not fall within the real classification of HPC. A review of the existing body of knowledge has been presented and it is clear that a need exists for a thorough study of the influence of SAP on the behaviour of low  $W/B$  (0.2 – 0.35) concrete which are the real classification called HPC. Models exist giving constitutive relation between compressive strength and other mechanical properties of concrete. This work examines influence of SAP addition as IC-agent on the mechanical behaviour of HPC with efforts made to simulate the voids created by SAP into the existing mathematical models. The work is categorised into fresh and early age properties, mechanical properties and non-destructive tests for easy understanding.

# 3

## *Materials and Experimental Procedures*

A proper understanding of the mechanical behaviour of composite materials like HPC will be impossible without a detailed study of the physical and chemical properties of the constituent materials, the characteristics of the concrete mixtures in the fresh state, early age strength development trends and the response of the hardened HPC mixtures to the effect of applied force (in compression and tension), stiffness (i.e. elastic modulus) and fracture properties. These processes require specific material treatment, specimen preparation and handling to conform to the requirements of the requisite standards and available facilities. This section of the dissertation gives a detailed discussion on the properties of the materials used for the experiments, the general procedure for their handling, specimen sizes, sample preparation and respective treatment. It also includes experimental setup for the various tests (destructive and non-destructive) involved towards the achievement of the research objectives. Discussions in this chapter are therefore placed under three major groups: materials, experimental procedures and characterisation of constituent materials.

### **3.1 Materials**

SAP was introduced as an IC-agent in four reference HPC mixtures for an examination of the effect of SAP sizes, contents and binder types on the mechanical behaviour of the HPC mixtures at both short and long hydration periods. The materials used for this study are as discussed in the following sub-sections.

#### **3.1.1 Superabsorbent Polymers**

The type of SAP used in this study is a thermoset polymer specifically the covalently cross-linked polymers of acrylic acid and acrylamide, neutralised by alkali hydroxide produced by SNF Floerger in France. Two grain sizes of SAP (< 300µm with product label FLOSET CS 27 and < 600 µm, labelled

FLOSET CC 27) as specified by the manufacturer were used with the SAP contents varied (0%, 0.2%, 0.3%, and 0.4%) by weight of binder.

### 3.1.2 Binders

Cement CEM I 52.5 N supplied by PPC, Western Cape, South Africa conforming to BS EN 197-1-2000 and SANS 50197-1 served as the main binder while SF by SiliconSmelters of the FerroAltantica group; FA from AshResources and CS supplied by PPC; all in powdered form were used as supplementary cementitious materials (SCM) for the various HPC mixtures as required by the mix design. The blend of the binders are categorised into three types as follows:

Binder Type 1 is the combination of CEM I 52.5 N and SF which is also referred to as binary cement and adopted for reference HPC mixtures  $M_2$  (0.25 W/B) and  $M_3$  (0.30 W/B). Binder Type 2 is composed of CEM I 52.5 N, SF and FA used for  $M_{1F}$  (0.2 W/B) while Binder Type 3 is made of CEM I 52.5 N, SF and CS used for  $M_{1S}$  (0.2 W/B). Binder Types 2 and 3 are thereby referred to as ternary cements.

Tests were conducted on the CEM I 52.5 N and the SCM for first-hand information on their physical and chemical properties towards a better understanding of their possible influence on the cement hydration process and its products; microstructure; early-age and long term strength characteristics and the microstructure of various hardened HPC mixtures.

### 3.1.3 Aggregate

A natural sand with minimum particle size of 300  $\mu\text{m}$  (i.e. all the particles smaller than 300  $\mu\text{m}$  were removed using the sieving method), having physical property values (Fineness Modulus,  $FM = 2.79$ , coefficient of uniformity ( $C_u = 2.43$ ), coefficient of gradation ( $C_c = 1.02$ ) and dust content (0.3%)) of medium sand classification (Shetty, 2004) as observed in the preliminary sieve analysis reported in Section 3.3 below was used as fine aggregate. 13mm crushed greywacke stone served as coarse aggregate in compliance with typical HPC mixes found in literature (Beushausen & Dehn, 2009; Neville, 2012) and based on observations from the trial mixes carried out at the preliminary stage. The crushed stone were also washed and spread in open air for surface drying before measuring the

required quantity for particular reference HPC mixture production. This was to reduce the dust content of the coarse aggregate in order to achieve a low water demand for the HPC mixtures (especially) the  $M_{1F}$  and  $M_{1S}$  which are of extremely low W/B.

### 3.1.4 Water

Clean, potable water supplied by the local municipality was used for concrete mixing.

### 3.1.5 Admixtures

The choice of superplasticiser was governed by the required long slump retention period to allow for sieving out mortar from the fresh HPC mixtures to be used for setting times and rate of hydration tests in accordance to ASTM C403 – 08 and compatibility with the particular binder as pointed out in literatures (Aïtcin, 1998; Mehta & Monteiro, 2014; Neville, 2012). Trial tests made with available materials however favour the choice of Chryso fluid Premia 310 for this study. The water content of the superplasticiser was appropriately accounted for and deducted from the volume of mixing water to maintain the W/B designed for as recommended in the work of Aïtcin (1998).

### 3.1.6 HPC Mixtures

Table 3.1 presents the mix composition of the four references HPC mixtures designed for 28 day target cube strength of 70 MPa minimum (i.e. C55/67 – C100/115 HSC of EC2) used for this study. The Binder Type 1 (i.e. CEM I 52.5 N+ SF) was adopted for  $M_2$  and  $M_3$  – HPC mixtures with  $M_2$  being of 0.25 W/B while  $M_3$  is of 0.3 W/B. Binder Type 2 was adopted for  $M_{1F}$  – HPC mixture and the Binder Type 3 for  $M_{1S}$  – HPC mixture. These two ternary cements HPCs were however maintained as 0.2 W/B with FS and CS respectively as alternative additional SCM to achieve good workability in these extremely low W/B HPC mixtures while working within the limit of the manufacturer's optimum content specified for the water reducing admixtures chosen on basis of the findings of the preliminary tests.

SAP at varied contents (0%, 0.2%, 0.3%, and 0.4% by weight of binder) was then introduced as admixture with provision made for additional water on basis of the SAP absorbency determined via

the tea-bag test to produce other HPC containing SAP as specified in Section 3.1.1. Details of the specimen designations are attached in Appendix A1 while Tables 4.2 and 4.3 of Section 4.2.1 give the actual weight measurement and fresh properties of the various HPC mixtures.

**Table 3-1: Mix constituents of reference HPC mixtures**

Constituents	Reference Mixes (kg/m <sup>3</sup> )			
	M <sub>1F</sub>	M <sub>1S</sub>	M <sub>2</sub>	M <sub>3</sub>
Water	125	125	134	156
Cement (CEM I 52.5 N)	530	530	540	500
Coarse Aggregate, (13 mm maximum)	1050	1050	1050	1050
Sand (retained on 300 µm sieve)	590	602	710	700
FA	122.5	0	0	0
CS	0	122.5	0	0
SF	52.5	52.5	40	40
Superplasticiser (Chryso Premia 310)	21	21	16	5.4
Water/binder (W/B)*	0.2	0.2	0.25	0.3
Air content or Porosity* (%)	0.58	0.20	0.17	1.58

\*W/B = ((water + liquid content of superplasticiser)/(cement + SF + FA + CS))

\* Porosity = 100 x (Designed density – Demoulded density)/Designed density =  $(dd - dmd/dd) \times 100$

## 3.2 Experimental Procedures

Experimental procedures involved in this study are classified into four groups (preliminary tests, early-age strength developments, mechanical properties and non-destructive image analysis) with the discussions giving adequate attention to specific experiments.

### 3.2.1 Preliminary Tests

These are tests carried out to ascertain the properties of the constituent materials. These include the particle size distribution, pH determination of CPS of varied W/B, morphology and chemical analysis of various cementitious materials.

#### 3.2.1.1 Particle size distribution

The particle size distribution (PSD) analysis for the aggregates was determined through the sieving method in accordance to standards (BS EN 933-1 - 1997). The set of standard sieves used in descending order are 4.75 mm, 2.36 mm, 1.18 mm, 600 µm, 300 µm, 150 µm and 75 µm (for fine aggregates); while for coarse aggregates, 12.5 mm, 10 mm, 6.3 mm and 4.75 mm were used. The preliminary study examined the different types of fine aggregates available and the blends of them as

reported in Section 3.3 before the choice of the specific material conforming to the requirements of the HPC mixtures for this work.

The binders and SAP particles were however analysed for PSD using a Saturn DigiSizer 5200 V1.10 (5200 LSHU V2.01 S/N 216) high definition digital particle size analyser with a Mie model, while specific surface area in Nitrogen ( $N_2$ ) adsorptive medium using 3Flex (Version 1.02 and S/N 103) Surface Characterisation (both equipment made by Micrometrics Instruments Corporation). The laser diffraction particle size adopted a wet technique using Isopropanol (an ethanol non-absorbent liquid medium) at a Refractive Index (RI) of 1.376 with a Laser 658 nm light source and analysed particle range by specification was 0.1 to 1000  $\mu m$  up to a lower limit of 0.07  $\mu m$  on the instrument. The instrument is of 600 ml reservoir at a 1.2 litre/min pump speed.

The dry SAP particles were also examined using the computed tomography (CT) scanner as discussed in Chapter 6 to ascertain the grain sizes for a clear assessment of the absorption capacity of the SAP in HPC in a non-destructive test approach.

### **3.2.1.2 Tea-bag test**

The tea-bag test as standardised by EDANA (2002) reported in literature (Assmann et al., 2014; Mechtcherine & Reinhardt 2012; Schrofl et al., 2012), is the most popular method for determination of SAP absorption capacity. It is a differential weighing method used to characterize the sorption behavior of SAP or similar liquid absorbent materials in water or a particular liquid. The basic apparatus for this test are: 500 ml beaker; tea filters (available commercially, as oblong, with dimensions: approximately 185 mm x 85 mm), gloves, towel, analytical balance (precision: 0.0001 g) with glass Petri dish ( $d = 60$  mm), spatula, stopwatch, and a shallow bowl for weighing the test material (say about 4 mm x 4 mm).

The SAP particle as received in the original container from the manufacturer was used as the test substance. The test procedure involves immersing a tea filter (“tea-bag”) in a beaker containing about 300 ml of test fluid and completely moisturised. This was lifted out of the liquid within 10 seconds and placed between two fingers with light pressure to drain out excess liquid from the filter. The tea-

bag was then placed on a towel in another 10 seconds blotted from both sides with the flat surface of one's hand and rolled over. This was then placed on the weighing balance in a petri glass dish to measure the mass of moist tea-bag ( $m_{\text{TBT}, f}$ ).

About 0.2 g (equivalent to  $m_{\text{SAP}, t}$ ) of the test substance to be tested (dry SAP) is weighed accurately and placed in a dried tea bag with a uniform distribution of the particles at the bottom of the tea-bag ensured. This was immersed in the liquid and the stop watch made to start for time measurements. The substance in tea-bag was then brought out of the test fluid, drained and weighed at time intervals of 30 sec, 2 min, 5 min, 10 min, 15 min, 30 min, 60 min and 180 min following the same repeat process described above for the empty dried tea-bag. The test samples were brought out, weighed and returned back to the test fluids within 25 seconds in all and vessel containing the test fluid was sealed airtight specifically for longer test times (60 min and above). A test fluid was adopted for one test routine with new liquids prepared for every test.

Visual features such as depositions and precipitation were noted. Also recorded was such other information as test specimen, test liquid and date while the calculated mass of the wet weight of the tea-bag and the swollen SAP ( $m_{\text{TBT}, f} + m_{\text{SAP}, t}$ ) were recorded in tabular form for the respective time records.

The test liquids examined in the aspect of the study are water and five different mix of CPS - CPS (5.2, 6.5, 7.8, 9.1 and 10.4 W/C ratio) to stimulate expected CPS in HPC mixtures of different W/B (0.2, 0.25, 0.3, 0.35 and 0.4). SAP absorption was then calculated using the following.

$$m_{\text{Fabs}} = m_{\text{TBT}, f} + m_{\text{SAP}, t} - (m_{\text{TBT}, f} + m_{\text{SAP}, t}) \quad (3.1)$$

### **3.2.1.3 PH determination of CPS**

A determination of the pH-value of CPS was carried out for a study of the influence of the pore concentration on the absorbency of SAP in concrete. This was carried out using a Crison pH meter Basic 20+ (Crison, Barcelona, Spain). The pH meter was standardised using buffer solutions of pH  $9.02 \pm 0.01$ ,  $7.00 \pm 0.01$  and  $4.01 \pm 0.01$  at 20 °C.

Different concentration of CPS from cement and distilled water in same proportion as adopted for the tea-bag test to represent W/B values of 0.2; 0.25; 0.3; 0.35 and 0.4 were simulated for CEM 52.5 N, binary (CEM I 52.5 N and SF (7.5%  $b_{wob}$ )) and ternary (CEM I 52.5 N, SF (7.5%  $b_{wob}$ ) and FA or CS (at 12.5%  $b_{wob}$ ) cements respectively according to what is adopted for the tea-bag test above (5.2; 4.3; 3.7; 3.1 and 2.5 W/B). The CPS mixtures were kept agitated using the Crison pH meter probe through-out the test to ensure a uniform liquid before taken measurements of the pH-values and temperature of particular mixture with an average of three tests conducted to arrive at the values reported in this study.

#### **3.2.1.4 Microstructure and chemical analysis**

The microstructure (shape and morphology) and chemical composition of the material constituents of the various binders for the HPC and the dry SAP particles were also studied through a back scattered electronic (BSE) image analysis conducted at the Scanning Electron Microscopy (SEM) unit. The amorphous silica content of the cementitious materials were also analysed through a Fourier Transmission Infra-red Spectroscopy (FTIR).

The BSE image analysis involves pressing the particular cementitious material into pellets before taking the pellets to the SEM unit. This involves weighing a quantity (about 6 g) of the specific binder particles (CEM I 52.5 N; SF; FA and CS); grinding it properly in a mortar and pestle with a drop or two of mould-oil (MOVIOL) applied and then placed under a hand operated press with some pressure of about 600 kPa applied. The pressed pellets were then dried in the oven at 40 °C for 1 hour before being taken to the SEM unit for imaging and chemical analysis. The processes of SEM (BSE image analysis) are discussed in detail under the procedure for non-destructive tests as outlined for Section 3.2.5.2.

#### **3.2.2 Concrete Production**

The production process in HPC has an influence on the quality of the final product in meeting the requisite performance requirements. In addition to mix proportioning, materials handling, mixing and curing are observed to be factors that differentiate HPC from NSC (Addis & Goodman, 2009; Aïtcin,

1998; Mehta & Monteiro, 2014; Neville & Aitcin, 1998; Neville, 2012). This process attracted some attention in this work, with consideration given to the timing and sequence of the various operations involved in this important aspect of concrete production.

The fine aggregate was first poured into the 50 litres capacity pan-mixer, followed by the binders which had first been thoroughly hand-mixed to enhance even dispersion of the SF and the other cementitious materials (FA or CS as appropriate) and a uniform colour observed. After mixing for about 30 seconds, the dry SAP particles were then poured in and all the fine contents mixed for another 30 seconds. The coarse aggregate were then added and mixing continued for another 1 minute, before water already mixed with superplasticiser (Chryso fluid Premia 310 – a PCE) was added. The mixing was allowed to continue for another 3 minutes as recommended in literature (Aitcin, 1998, Neville, 2012; Mehta & Monteiro, 2014). Only about half of the mixer volume was the maximum volume of concrete produced per batch noting that for these low W/B concrete, the mix is very stiff and becomes difficult if 50% volume of mixer is exceeded.

Slump flow measurement was then carried out using the flow table test (as described in BS EN 12350 – 5:2009) as a measure of workability of the HPC mixture while both the room and concrete temperature were also measured using a digital pocket thermometer (Checktemp 1, Model No. H1-740024 by HANNA Instruments Incorporated). After ascertaining that the mixture met the required workability and cohesion for specified design mix, specimen for the various tests were then cast in two layers on a vibrating table into the already oiled moulds. These were thereafter covered in the Laboratory with thick polythene sheets and allowed to harden for 24 hours, before demoulding and curing in water bath at  $20 \pm 3$  °C till the required curing ages (7, 28, 56 and 90 days respectively) before testing in accordance to standards (BS EN 12390 – 1, 2, 3, 4, 6 & 7, 2009). Procedures and specimen preparation for the individual tests are discussed in detail in the following sections.

### **3.2.3 Early-age strength properties of HPC**

The tests carried out for investigation of the early age strength properties are the setting time tests, rate of hydration and early age compressive strength of the HPC with SAP.

### **3.2.3.1 Setting times tests**

The setting times (initial and final) of the HPC mixtures were determined using a penetration resistance method in accordance to ASTM C403 – 08. A standard 4.75 mm sieve was used to extract mortar samples from the fresh HPC mixtures which were cast in two layers into 150 mm cube moulds to about 10 mm below the height edge. The specimens were then kept in a climate control room set at  $21 \pm 2$  °C temperature and  $65 \pm 5\%$  humidity. A penetrometer Model C213, S/No – C213/AB/0010 (Matest S.P.A.) was then used to measure the resistance of the concrete to 25 mm depth penetration of respective needle heads beginning from the biggest as specified by the code at regular time intervals. This plot of penetration resistance (on ordinate axis) against time in minutes (abscissa axis) gives the initial (3.5 MPa resistance) and final setting (27.6 MPa resistance) times respectively using a direct fitting on a powers regression line.

### **3.2.3.2 Strength development and degree of hydration of HPC with SAP**

An assessment of early-age strength development and degree of hydration of HPC with SAP was conducted on sieved mortar samples of HPC mixtures obtained as explained in Section 3.2.3.1. The study adopted the same approach as reported by Hasholt et al., (2010a). The process is broken down into the following stages:

- i. Mortar samples (50 mm cube) were cast and crushed after different curing ages (i.e. immediately after demoulding (24 hrs); 48 hrs; 72 hrs and 7days) to assess the strength development trends of the HPC with SAP.
- ii. The remains of the sample in (i) above was then milled properly using the mould for Aggregate Crushing Value (ACV) Test and a 25 mm diameter bar (as shown in Figure 3.1) as mortar and pestle. The milled sample was then vacuum-dried for 1 hour to stop further hydration.
- iii. The sample was then sieved and from the particles passing the 300 µm standard sieve, a known weight of about 50 g was measured and oven dried for 24 hours at 105 °C and

weighed again (to determine the amount of evaporable water i.e. capillary water + gel water).

- iv. It was then heated and kept at 950 °C for 1 hour and weighed (this measurement is used for determination of amount of chemically bound water). All calculations were then made based on ignited weight basis to give the following:

Loss on ignition (LOI) of the binders (CEM I 52.5 N, SF, FA and CS) and hydrated mortar pastes calculated by

$$\text{LOI (\%)} = 100 \times (\text{as received weight} - \text{ignited weight}) / \text{as received weight} \quad (3.2)$$

$w_n$  (i.e. non-evaporable water) content of the hydrated mortar pastes were determined to evaluate the degree of hydration, as provided for in literature (Lam, et al., 2000; Neville, 2012). This is the difference in mass measurement of the crushed paste at 950 °C and 105 °C, to calculate the degree of hydration ( $\alpha$ ) on the basis that 1 g of anhydrous cement produces 0.23 g of  $w_n$ , hence the  $w_n$  is calculated by using the following formula

$$w_n \% = \frac{100 \times (\text{dried weight of paste} - \text{ignited weight of paste})}{(\text{Ignited weight of paste} - \text{loss of ignition of cement})} \quad (3.3)$$

The degree of hydration ( $\alpha$ ) is then:

$$\alpha = 100 \times \frac{w_n}{0.23} \quad (3.4)$$



**Figure 3-1: ACV mould used as mortar and pestle for milling hardened HPC mortars**

The degree of hydration in the binary ( $M_2$  and  $M_3$ ) and ternary ( $M_{1F}$  and  $M_{1S}$ ) cement pastes were however calculated with the LOI of the SCM and their proportion made to adjust for their  $w_n\%$  as appropriate.

The crushing force in (i) above recorded was used to determine the early-age compressive strength of HPC containing SAP as IC-agent while multiple regression was carried to assess the influence of SAP sizes and contents on the early-age strength development of the HPC mixtures.

### **3.2.4 Mechanical Properties Tests**

This is the core experimental work of the research. It involves establishing the mechanical behaviour of the HPC containing SAP as an IC-agent. The mechanical properties were therefore investigated at three levels and the tests and specimens sizes involved are:

- Compressive strength – 100 mm cubes.
- Splitting tensile and fracture energy (i.e. wedge splitting) test – 100 mm cubes.
- Elastic modulus test –  $\varnothing 100 \times 200$  mm cylinders.
- CT Scanning and SEM –  $\varnothing 50 \times 100$  mm cylinders.

#### **3.2.4.1 Compressive strength**

The compressive strength is a major property of concrete to which many of its characteristics are related (Neville, 2012). The design and material proportioning for concrete (be it normal, high strength or high performance) is mostly governed by this unique property. Investigation of compressive strength of HPC with SAP in this study was based on the following variables:

- Four reference mixtures of HPC for the 0.2 to 0.3 W/B as stated in Section 3.1.6
- Sizes of SAP - 2
- SAP content – four levels (0%; 0.2%; 0.3% and 0.4%  $b_{wob}$ )
- Curing age before testing - four levels (i.e. 7, 28, 56, and 90 days).
- Number of replicates – three

The tests setup are as shown in Figure 3.2 (a & b) in accordance to BS EN 12390 – Parts 1, 2 and 3 (2000) and RILEM Technical Recommendation TC14-CPC 4, 1975.

A total of 384 (100 mm) concrete cubes were tested using the digitised Contest Materials Testing machine (Grade A type, S/No – 3118 by Contest Instruments.) of 2000 kN maximum loading capacity ensuring the face in touch with the loading platens are not same as the cast face of the cube. Also determined were the demoulded density and total porosity % as discussed in Section 4.1.1.



**Figure 3-2: Compressive strength test setup**

### **3.2.4.2 Elastic modulus**

High elastic modulus (E-modulus) is one of the specific performance and required properties for which HPCs are normally designed hence it is important to investigate how addition of SAP in HPC influences its E-modulus. E-modulus is normally determined from the stress – strain relation during measurement of compressive strength. This relation is of relevance when the concrete has hardened and reached some level of strength development with E-modulus value after 28 days of curing common in specifications, although the value after 7 days curing might be necessitated by specific project requirements. The E-modulus was conducted for the various HPC mixtures in this study after 28, 56 and 90 days of concrete hydration for ease with result compilation and handling of the multiple numbers of variable inputs (curing age, SAP type, SAP contents, binder type and W/B). A total of 288 (Ø100 x 200 mm) concrete cylinders were cast and cured as explained in Section 3.2.2 for this particular test. The test was carried out with four cyclic loads in accordance to standards (ASTM C469 – 2010 and RILEM TC14-CPC 8, 1975) as setup in the Contest Materials Testing machine shown in Figure 3.3.

This comprise of a 2000 kN capacity load cell and three linear variable displacement transducers (LVDT) with a range of 10 mm each attached centrally to the concrete cylinders (Figure 3.3), which were connected to a HBM spider data acquisition system used for storage and analysis of the stress-strain relationship for computation of E-modulus of the HPC.

The variables in consideration for this test remain as outlined for compressive strength above except that the curing ages now becomes three (28, 56 and 90 days) giving a total 288 concrete cylinders tested for E-modulus.



**Figure 3-3: E-modulus test setup for HPC with SAP**

### **3.2.4.3 Splitting tensile strength and fracture energy**

Splitting tensile strength and fracture energy for the HPC mixtures were determined through the modified wedge splitting test approach as explained in Section 2.8 based on the works of Brühwiler & Wittmann (1990) and RILEM Recommendations AAC13.1 (TC51-ALC, 78-MCA, 1992). The specimen for the wedge splitting test was cast with a 30 mm x 20 mm groove introduced by insertion of a wooden block and cured in the water-bath as explained in Section 3.2.2. It was further notched to 50 mm depth from the cube specimen bottom (Figure 3.4 (b)) at the required curing ages (28, 56 and 90 days) and an epoxy glue was used to attach PVC clips (Figure 3.4 (a)) fabricated to hold LVDTs at the groove edge for a measurement of the CMOD during the test. The test setup developed as shown in Figure 3.4 (c) using a loading assembly (14 ° wedge plate welded to IPE 160 I-section (160 x 82 x 15.8 kg/m<sup>3</sup> I-section)) made to move within two Ø25 mm needle roller bearings (NKI 25/30) attached to the sides of fabricated steel frame (made of C-channels) for a transfer of the vertically applied load to horizontal loading on the cube specimen.

The cube was placed on a base plate with two 10 mm diameter bars welded to it (for stability) as observed in Zhao, et al. (2008) and Trunk et al.(1999) to induce crack opening from the notched

groove-end of the wedge splitting specimen instead of the single bar centrally placed specified in the recommendations above (Brühwiler & Wittmann, 1990; International Union of Testing and Research Laboratories for Materials and Structures (RILEM), 1994) - RILEM AAC13.1). This is to ensure stability of the cube specimen during testing. An interlayer of 4 mm thick hardboard of 8 mm width was placed on the 10 mm diameter bars on the base plate (as shown in Figure 3.4 (d)) to prevent direct transfer of axial force from the base when carrying out the wedge splitting test.

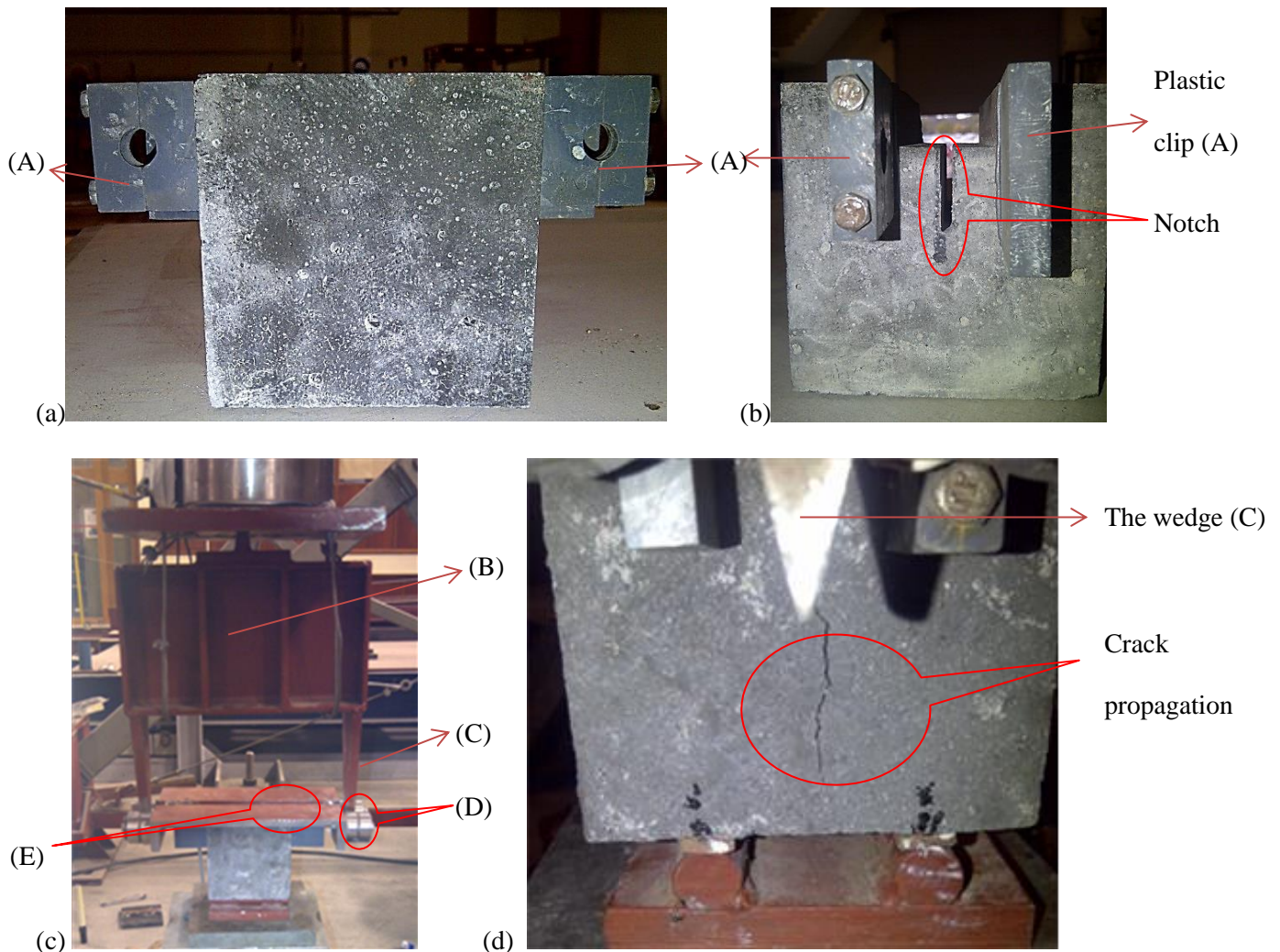


**Figure 3-4: Test setup for wedge splitting test – (a) shows the plastic clip (LVDT holder) glued to concrete specimen; (b) the groove (30mm x 20mm) and notch (20 mm deep); (c) the complete wedge splitting setup and (d) the crack propagation on the cube specimen.**

\*Note that the label (A) in Figure 3.4 above plastic clip; (B) is the IPE 160 I-section; (C) is the metal wedge; (D) is the two Ø25 mm needle roller bearings and (E) is the fabricated steel frame (made of C-channels).

The load was applied at a crack mouth opening rate of 0.1 mm/min in a closed loop servo control machine (Instron 50 kN actuator by Instron Ltd.) having maximum loading capacity of 50 kN (dynamic) / 62.5 kN (static).

The crack opening displacement (COD) was measured on the specimen with two LVDTs attached using the plastic holders (Figure 3.4 (a)) connected directly to the Instron machine ensuring crack opening control of the test set up and a direct data transfer to a dedicated computer. A total of 288 (100 mm) cube HPC samples were studied for splitting tensile strength and fracture energy. An average of the three tests per specific sample gave the values reported in this work.

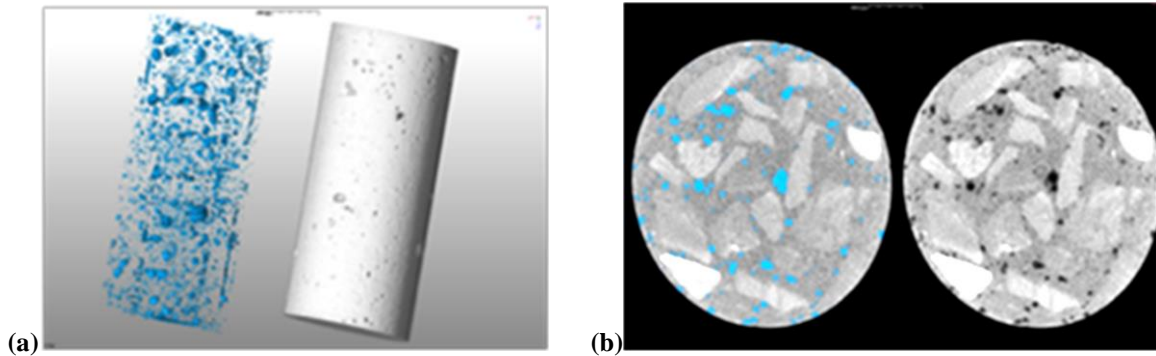
### **3.2.5 Non-destructive tests on HPC mixtures**

#### **3.2.5.1 X-ray CT scanning**

The hardened Ø50 x 100 mm cylinders cast and cured as explained in Section 3.2.2 were placed in the oven at 40 °C for 30 minutes after removal from the curing tank at the respective hydration period before taking it to the CT scanner for analysis. 3D X-ray images were examined and analysed in this study using Avizo Fire, version 8.0 by FEI Visualisation Science Group and VG Studio Max 2.2 by Volume Graphics to filter and classify the individual voids for determination of the sizes, distribution and volume analysis of voids created by SAP in the HPC with the respective influence of binder type, W/B, SAP content and curing age. The CT scanning was also used to affirm the grain sizes and distribution of the dry SAP particles.

The 3D X-ray images were obtained using a General Electric Phoenix VTomeX L240 X-ray micro computed tomography scanner (microCT), having mounted the concrete specimen on a less dense cardboard tube to reduce external influences on the samples during the scan. Reconstruction was performed with system supplied Datos Reconstruction software and analysis conducted. The voxel size was set to 100 µm with settings at 170 kV and 150 µA for x-ray generation and image acquisition settings was 500 ms per image. Figure 3.5a shows the 3D image of the HPC specimen while the 2D slice image of same is shown in Figure 3.5b.

The VGStudio Max 2.2 analysis involved selection of a surface to identify only the voids in the sample with a defect analysis performed on these voids to determine the sizes and abundance of the voids. The results from the analysis include size, abundance, sphericity and volume of the voids.



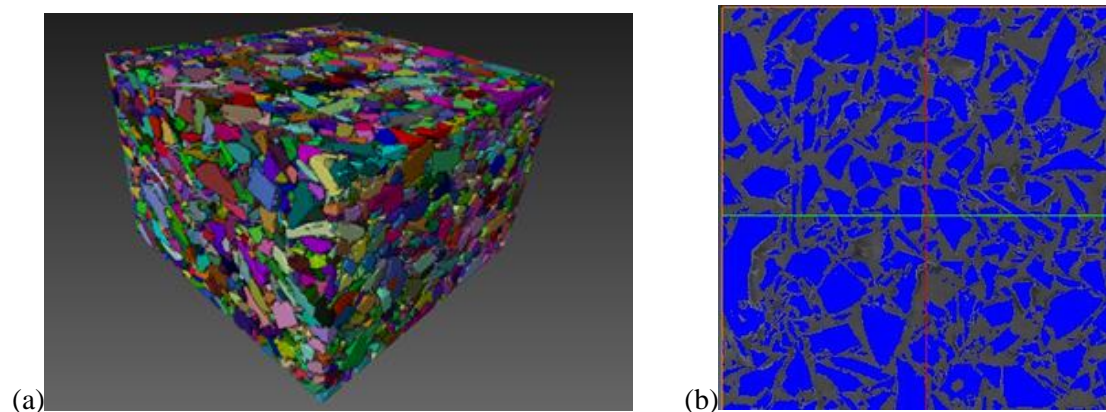
**Figure 3-5: 100 µm scan of HPC cylinder - (a) 3D visualisation and (b) thresholding applied to 2D image**

Image analysis using the Avizo Fire 8.0 involved the following steps:

- i. Loading in the reconstructed image data;
- ii. Volume rendering;
- iii. Thresholding the volume rendered;
- iv. Crop editing: Here the material region is cropped to remove external air. For this exercise, the same 3D image (25 mm x 25 mm x 50 mm) was maintained throughout the analysis for all HPC mixtures;
- v. Non-local means filtering - to smoothen the data;
- vi. Interactive thresholding - to colour the pores;
- vii. Separate objects - to separate touching pores;
- viii. Label analysis - volume render and data saved and
- ix. Sieve analysis.

All the various stages of this CT scanning and analysis have minimum human influence except the thresholding aspect. Details of the method adopted for the 3D volume analysis are as reported in studies by du Plessis, et al., (2014) and Maire & Withers (2014). The outcome of the analysis was then plotted using histogram charts for the respective HPC mixtures tested after different curing ages (28, 56 and 90 days).

Determination of the dry SAP particle size distribution using X-ray CT involves scanning the two SAP types separately in a transparent cylindrical container. Reconstruction was performed as explained above and analysis conducted with the Avizo Fire 8.0 following the steps stated previously. Scanning for the dry SAP particles was however done at 2  $\mu\text{m}$  voxel size to be able to capture the actual size of the particles while a crop of 80 mm x 40 mm x 40 mm was made centrally from the VGI file when loaded before thresholding. The analysis examined a complete particle distribution of the dry SAP samples rather than individual particle. The 3D image of separated SAP particles with different colours depicting various size categories is shown in Figure 3.6a below, while Figure 3b gives the 2D image of cropped dry SAP specimen being analysed with the separated SAP particles in blue colour with spaces in between them.



**Figure 3-6: 3D Image of separated dry SAP particles with colour indicating sizes classification (a) and (b) Centrally cropped CT image of dry SAP particles obtained from 3D VGI file**

### **3.2.5.2 Scanning electron microscopy**

In quality assurance of concrete, scanning electron microscopy can be used for important information on degree of hydration of cement, formation and distribution of hydration products, adhesion to aggregates and homogeneity of cement pastes and possible influence of admixtures on the products of hydration of cements in concrete (Winter, 2012). This section of the study examined the dry SAP particles (in powdered (as received) form); binders (in pressed pellets) and HPC samples (in thin sections). It covers imaging and analysis of the phase compositions of the samples using a Zeiss EVO® MA15 Scanning Electron Microscope.

Specimen preparation depends on the sample in consideration. The SEM machine accepts samples of very small thickness (around 3 mm maximum), hence for the binders the pressed pellets as prepared in Section 3.2.1 is adequate, while the HPC's requires cutting thin sections out from the 50 mm diameter x 100 mm concrete cylinders cast in Section 3.2.2 and cured for requisite hydration periods. The thin circular sections cut out from the central part of the concrete cylinder were then thoroughly surface-smoothened and well-polished before the Carbon-coating. The dry SAP particles requires no preparation, as they were only placed on the double sided tape and Carbon-coated appropriately. A Quorum QT150T was used for the Carbon-coating. The samples (dry SAP particles; pressed pellets or thin section of HPC's) were placed in the coating chamber, the carbon rods sharpened and placed appropriately before the coating process according to equipment guidelines was followed. The properly coated specimen was then loaded on the Zeiss EVO® MA15 Scanning Electron Microscope and Energy Dispersive X-ray Spectroscopy (EDX)/Wavelength Dispersive Spectroscopy (WDS) - SEM procedure followed as below:

- i. Load the FC (Faraday Cup) and the sample in the SEM.
- ii. Keep the chamber door flush and select pump under SEM status page.
- iii. When the vacuum status shows ready switch beam on under icon Beam.
- iv. Select under Detection/detectors/CENT for Backscatter detector.
- v. Leave the beam on for 5 minutes to stabilise.
- vi. Ensure the REMCON program is running – this is the communication port between SEM and EDS setups.
- vii. Beam current of 100  $\mu\text{m}$  (set by default); Accelerating Voltage of 20 kV to be maintained.
- viii. Put FC in the middle of beam, focus the edges as best as possible (not in the middle of the hole).
- ix. Place FC under the beam, select spot mode and when reading on the specimen current monitor was kept at -4.00 nA. This is controlled by changing the spot size in the SEM status/Gun dialog window (NB: Spot size varies according to FC reading).

- x. When the specimen current monitor reading on the FC ranges between -3.97 and -4.00 nA and it is stable for a minute/two, the sample was located and focussed on a small sharp object, before zooming in to 1000X magnification.
- xi. Left click on the WD bottom toolbar and note the reading. Type in 13 and use the little joystick (Z) to focus the sample. This is a crucial step as the WD needs to be within a 0.01 mm limit around 13 mm.
- xii. The focusing procedure is repeated if the focus changes during the SEM appointment.
- xiii. The spot mode is used when a smooth area (avoiding cracks/polishing marks/holes/cleavage planes) has been selected. No movement of the spot is done after the spot mode has been selected. The spot mode is always cancelled before another area is selected if the first is not satisfactory.

Following the procedures above, the samples were identified with BSE and /or secondary electron images and phase compositions were quantified by EDX analysis using an Oxford Instruments® X-Max 20 mm<sup>2</sup> detector and Oxford INCA software. Beam conditions were kept at 20 kV, a working distance (WD) of 8.5 mm maintained and approximate beam current of -20 nA used throughout the analyses. The counting time was 10 seconds live-time and Internal Astimex Scientific mineral standards were used for standardisation and verification of the analyses while the works of (Winter, 2012) serve as a guide for quantitative analyses in this study.

### **3.3 Characterisation of Constituent Materials**

A good knowledge of the physical properties of the constituent materials helps with the in-depth understanding of the mechanical behaviour of concrete. It is important to study the particle size distribution, shape, structure and surface area of the cementitious materials as this could be of relevance to what the products of hydration will be especially with an introduction of a new admixture for IC of low W/B concretes. Fine powders are known to exhibit different properties to the same material in coalesce form depending on magnitude of their surface area and nature of porosity, so also are they said to be more reactive (Mehta & Monteiro, 2014; Neville, 2012). The type, shape, size and

molecular structure of constituent materials of the HPC mixtures used in this study are thereby reported with an attempt made to discuss their effects on the mechanical behaviour of the concrete with SAP.

### 3.3.1 Results

Figure 3.7 presents the plot of the sieve analysis of the various available fine aggregates (and their blends) investigated in this study, while Table 3.2 on the other hand, gives the summary of the particle size distribution.

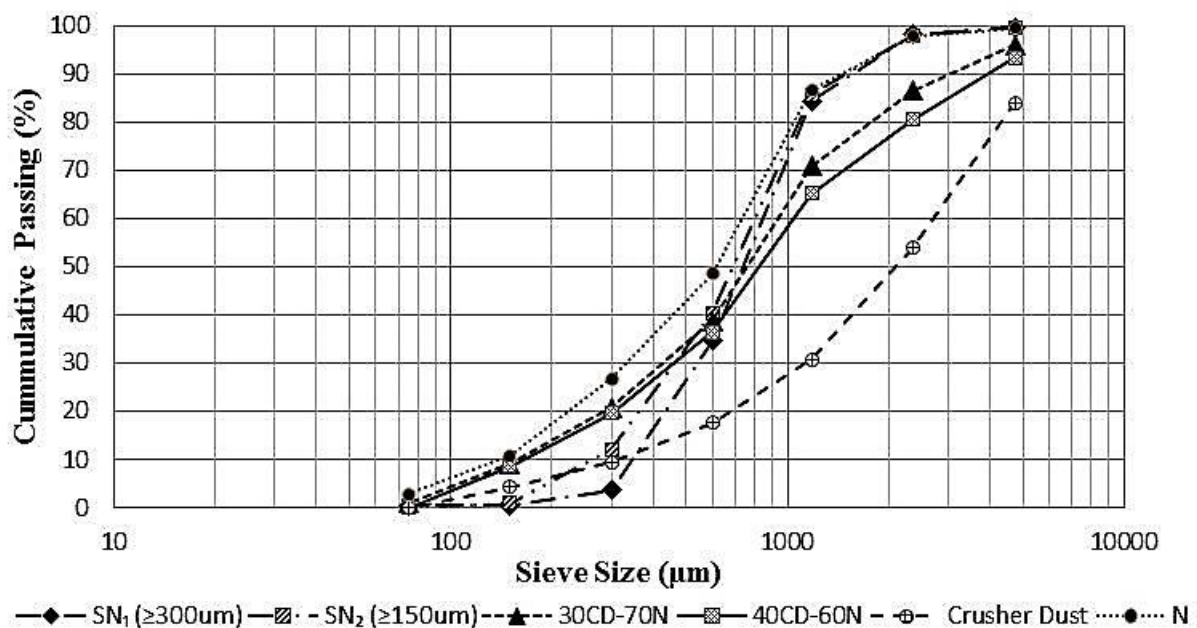


Figure 3-7: Plot of sieve analysis of available and blended fine aggregates

Table 3-2: Summary of particle size distribution of available fine aggregates

Available f/aggregate	SN <sub>1</sub> (≥300 µm)	SN <sub>2</sub> (≥150 µm)	30CD-70N	40CD-60N	CD	N*
D10	350	270	160	160	320	150
D30	550	450	420	450	1150	350
D60	850	800	950	1100	2050	740
Cu	2.43	2.96	5.94	6.88	6.41	4.93
Cc	1.02	0.94	1.16	1.15	2.02	1.10
FM	2.79	2.64	2.78	2.97	4.00	2.30
Dust content	0.31	0.27	5.22	6.32	12.52	5.69

NB: \*N – Natural sand; SN: Sieved natural sand; CD – Crusher Dust; 30CD-70N is 30% CD/70%N and 40CD- 60N is 40%CD/60%N.

This was the basis for the choice of the natural sand with minimum particle size of 300 µm (i.e. all the particles smaller than 300 µm removed using the sieving method) as discussed in Section 3.2.1.1.

13 mm crushed greywacke stone serve as coarse aggregate in compliance with typical HPC mixes observed in literature (Beushausen & Dehn, 2009; Neville, 2012) and based on observations from the trial mixes carried out at the preliminary stage.

The available natural sand (N) is well graded, belongs to fine sand category (FM of 2.3) of Shetty, (2004) and has dust content of 5.69% which makes it unsuitable for HPC mixtures as recommended in literature (Addis & Goodman, 2009; Aïtcin, 1998; Neville, 2012). The crusher dust (CD) on the other shows a gap-grading, very coarse (FM of 4.0) and also has very high dust content (12.52%). Blends of the natural sand and crusher dust (40CD – 60N and 30CD – 70N) were also unsuitable. An attempt made at sieving the natural sand with 300  $\mu\text{m}$  ( $\text{SN}_1$ ) and 150  $\mu\text{m}$  ( $\text{SN}_2$ ) sieves to reduce the dust content resulted in  $\text{SN}_1$  with FM of 2.79 and 0.31 dust content which conform well specified requirement in literature (Aïtcin, 1998; ACI 363.2R-98; Addis & Goodman, 2009) been adjudged the most suitable for workability and strength development of HPC mixtures.

A summary of the PSD and specific surface area of cementitious materials (CEM I 52.5 N, SF, FA and CS) and dry SAP particles ( $\text{SP}_1$  and  $\text{SP}_2$ ) carried out by laser diffraction particle size distribution method and Brunauer–Emmett–Teller (BET) nitrogen absorption technique analysis is presented in Table 3.3 and Figure 3.8 (PSD plot). The laser diffraction particle size analysis was repeated and similar result obtained with the particle size of SF seen as lower than other cementitious materials. The results show that the used binders are fine in nature with the CEM I 52.5 N, FA and CS having over 90% (D90) of the particles below 75  $\mu\text{m}$  size and 50% (D50) of the particles being lower than 25  $\mu\text{m}$  (CEM I 52.5 N) and 12  $\mu\text{m}$  in size (FA and CS) respectively. BET specific surface area of the CEM I 52.5 N, FA and CS were close in value (5.56, 5.13 and 3.22  $\text{m}^2/\text{g}$  respectively as shown in Table 3.3). SF surprisingly is reported from the laser diffraction PSD as the coarsest of all the cementitious materials. It has D50 of 43  $\mu\text{m}$  and D90 of 150  $\mu\text{m}$  but BET specific surface area is 19  $\text{m}^2/\text{g}$ . The BET method is recommended in literature (Silica Fume Association, 2005) as the best approach for determining the specific surface area of SF while laser or other PSD methods may be adopted for other SCMs, specific surface area for SF particles is often determined by the BET method. Neville (2012) is of the view that absolute measurement of specific surface can be obtained

by BET – nitrogen adsorption method as the internal area of the particles is also accessible to the nitrogen molecules. The measured value by BET is said to be considerably higher than that determined by the air permeability method (Neville, 2012). The BET specific surface area in this study for SF falls within the value  $13 \text{ m}^2/\text{g}$  to  $30 \text{ m}^2/\text{g}$  specified by Siddique & Khan (2011) and Silica Fume Association, (2005) as typical for SF in their work, a large surface area indicative of very fine particles. Zang (2015) in his work on UHPC argues that the size of SF determines the grading and hence the paste packing. Medium size SF having specific surface area of approximately  $12 \text{ m}^2/\text{g}$  was recommended as best for workability and compressive strength while the common SF with relatively high specific surface area between  $15 - 20 \text{ m}^2/\text{g}$  is said to lead to high water demand in UHPC (Wille et al., 2011; Habel et al., 2008 as cited in Zang 2015). The specific surface area of the SF available in South Africa is reported by Zang (2015) as  $23 \pm 3$ , a range to which the value  $19 \text{ m}^2/\text{g}$  obtained for the SF used in this study complied with, an indication that the BET result from this study is reliable. UHPC mix in the work of Zang (2015) was based on particle parking density concept which is more applicable when coarse aggregate are minimal or absent in the mix (Fennis et al., 2012). The concrete mix in this study has coarse aggregates incorporated while the natural sand used for the mix had been sieved as discussed in Section 3.1.3 to achieve a more flowable mix.

The BET specific surface area value for SF is higher than that of CEM I 52.5 N, FA and CS (Table 3.3), thereby affirming that SF is much finer than the other three materials. This appears to be a contradiction to the PSD result obtained from laser diffraction method. CS is slightly coarser than FA and CEM I 52.5 N. The higher specific surface according to literature (Silica Fume Association, 2005) contributes to the high reactivity of SF in concrete.

The laser diffraction PSD result for grain sizes of SF reported in Table 3.3 and Figure 3.8 (red colour in Table 3.3 and Figure 3.8) is thus wrong since the grains sizes in SF are expected to be much lower in value (about 100 to 150 times finer than CEM I 52.5 N), typically  $< 1 \mu\text{m}$ . Reports from literature (Siddique & Khan, 2011) gave an average particle size of 150 nm. The SF came out of the bag in the condensed form and effort made at grinding with mortar and pestle in the laboratory before the laser diffraction PSD test, possibly did not result in complete separation of the grains. This could explain

the error in the result of the laser diffraction PSD test on SF. The Laser diffraction method is reported by DiStefano, et al., (2010) and Kowalenko & Babuin, (2013) as having some inherent errors in determining particle sizes of very fine materials susceptible to particle aggregation.

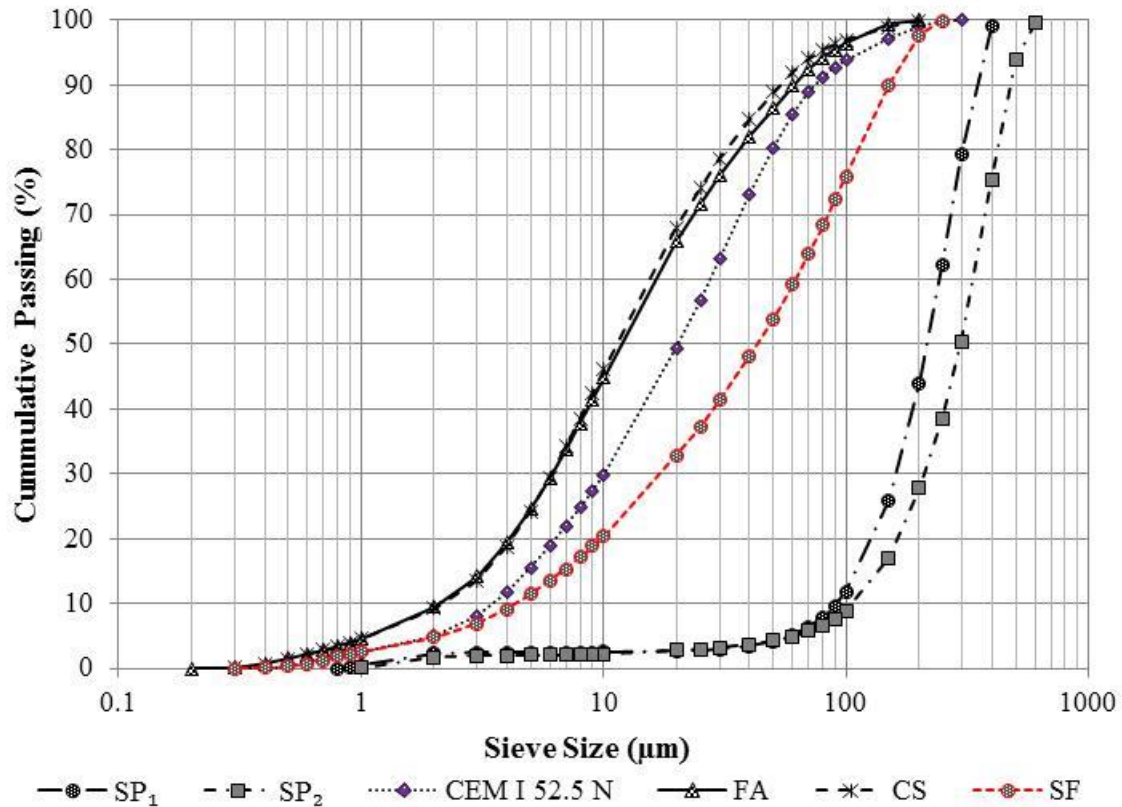


Figure 3-8: Particle size distribution of binders

Table 3-3: Summary of particle size distribution and BET surface area

Characteristics	diameter (µm)					
	SP <sub>1</sub>	SP <sub>2</sub>	CEM I 52.5N	SF	FA	CS
D90	337.799	472.36	73.669	150.264	60.256	53.179
D50	216.076	298.38	20.381	43.177	11.667	11.21
D10	91.825	108.05	3.541	4.381	2.11	2.182
Mean	214.9	293.8	32.93	61.47	23.04	21.62
Median	216.1	298.4	20.38	43.18	11.67	11.21
Model	300.4	400.5	30.04	112.9	11.29	11.29
BET surface area (m <sup>2</sup> /g)	3.82	4.45	5.56	19.16	5.13	3.22
Model	(1.43, 0.001), 1.376	(1.43, 0.001), 1.376	(1.72, 0.100), 1.376	(1.52, 0.100), 1.359	(1.45, 1.000), 1.376	(1.45, 1.000), 1.376

The dry SAP particles were however more coarse than the cementitious materials with SP<sub>2</sub> having grains ranging between 0 and 600 µm in size, D90 and D50 of 472.4 µm and 298.4 µm respectively

being the coarsest. SP<sub>1</sub> on the other hand has particle sizes between 0 and 400 µm sizes, D90 and D50 of 216 µm and 338 µm. BET specific surface area values - 3.82 m<sup>2</sup>/g (SP<sub>1</sub>) and 4.52 m<sup>2</sup>/g (SP<sub>2</sub>) respectively on the other hand are similar but a bit lower than that of CEM I 52.5 N, FA and CS. These BET values are considerably lower than the BET value of SF.

The X-ray CT scanning result of PSD on the dry SAP particles gave similar result as the laser diffraction method. SP<sub>1</sub> has particle sizes within 3 and 300 µm (i.e. < 300 µm), while SP<sub>2</sub> has particles ranging between 3 and 600 µm (i.e. < 600 µm) as presented in Figure 3.9.

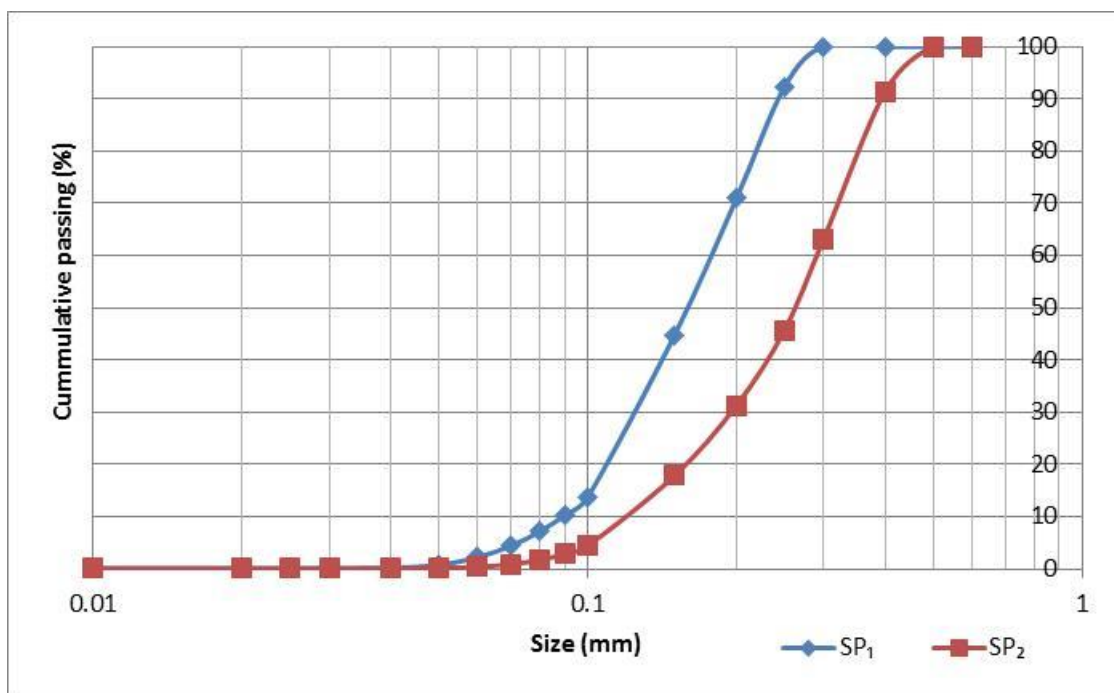


**Figure 3-9: Particle of SAP obtained from X-ray CT Scanning**

D10, D50, D90 values are 90 µm, 160 µm, 240 µm (SP<sub>1</sub>) and 110 µm, 260 µm, 390 µm (SP<sub>2</sub>) respectively. Minimum particle captured in the CT scanning is 2.481 µm since the scan was done at a 2 µm setting. The maximum particle sizes observed are 298.5 µm (SP<sub>1</sub>) and 451 µm (SP<sub>2</sub>). SAP particle size distribution from both the laser diffraction particle analysis and the X-ray CT scanning are in agreement and affirms the size specification of the manufacturer (SP<sub>1</sub> < 300 µm; SP<sub>2</sub> < 600 µm).

Note that Sphericity is a measure of the roundness of a shape. A sphere is the most compact solid, so the more compact an object is, the more closely it resembles a sphere. Sphericity is a ratio and therefore a dimensionless number. Sphericity  $\phi_s$  is defined as:

$$\phi_s = 6V_p/D_pA_p \quad (4.1)$$

Where  $V_p$  is the volume,  $A_p$  is its surface area, and  $D_p$  is the diameter of a sphere with the same volume ( $\pi D_p^3/6$ ).

The volume graphic image (VGI) obtained from the X-ray CT scanning also reflects that the dry SAP particles are irregular in shape (mostly angular) and that some of the SAP particles have voids within (Figure 3.10). Complete particles distribution of the dry SAP grains (Figure 3.10 - objects in blue colour) was possible as presented in this report without particle agglomeration due to improvement in non-local filter, interactive thresholding, separation of objects and label analysis functions available in Avizo Fire 8.0 software. The sphericity assessment revealed  $SP_1$  having values ranging between 0.16 and 1.61, while  $SP_2$  has sphericity values between 0.32 and 1.61. The upper limit value of 1.61 being above 1.0 expected for a perfect sphere is a confirmation of presence of empty hollow spaces within some SAP particles.

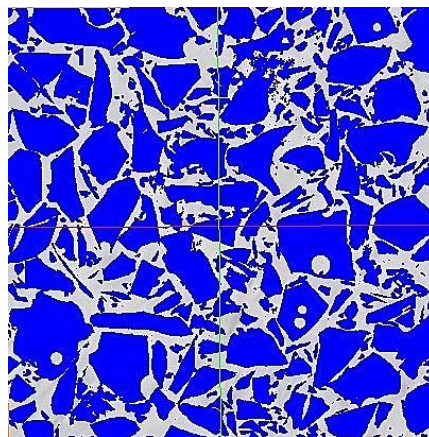


**Figure 3-10: Snapshot of filtered central portion of VGI file of dry SAP particles (blue) under analysis**

### 3.3.2 Inferences

The results and discussion in the previous sections on the constituent materials for this study reflect that:

- i. Choice of fine aggregate for this study was influenced by the demand for coarse sand as required in literature (Beushausen & Dehn, 2009; Neville, 2012) for HPC of low W/B, known to have a high fines (i.e. high cement, SF and other pozzolanic materials) content. The sieved natural sand - SN<sub>1</sub> with FM of 2.79 and dust content of 0.31 conforms to the specifications while the 13 mm greywacke stone used as coarse aggregate is appropriate for this concrete type.
- ii. The binders (CEM I 52.5 N, SF, FA and CS) were all of good fineness with the CEM I 52.5 N, FA and CS reported to be finer than the SF based on laser PSD analysis. This is however wrong as BET specific surface area analysis reported SF has having the largest surface area of all the fine constituent materials in the HPCs – an indication of the very fine nature of the grain sizes of SF. The error in result from laser diffraction was due to particle agglomeration of SF grains as reported in works of DiStefano et al., (2010) and Kowalenko & Babuin, (2013).
- iii. The CEM I 52.5 N is expected to result in good early strength development and also good ultimate strength since above 50% of the particles lies between 3 to 30 µm sizes according to Neville (2012). Same is observed for the particles of FA and CS.
- iv. The specific surface area obtained from BET analysis of the various binding materials including the SF were however noted to be of similar values reported in literature (Siddique & Khan, 2011) – an indication that the BET results from the study can be taken as reliable.
- v. The SF is thereby adjudged in this study as significantly finer than the other cementitious materials used and this is responsible for resulting sticky nature of the concrete produced with SF while FA and CR has additional cementitious materials enhances better workability of such concretes.

The SAP particles (SP<sub>1</sub> and SP<sub>2</sub>) on the other hand were observed as coarser than the binders. PSD result from the laser diffraction particle size analysis and the CT-Scanning are in agreement giving SP<sub>1</sub> grains as 0 to 300 µm and SP<sub>2</sub> as 0 to 600 µm, affirming the manufacture's classification of SP<sub>1</sub> (≤ 300 µm) and SP<sub>2</sub> (≤ 600 µm).

### **3.4 Summary**

Materials, experimental procedure and characterisation of constituent materials adopted for this study have been presented in this chapter. Properties of the constituent materials for the HPC mixtures and basis for their choice, the concrete production process and various test set up for preliminary tests, early age strength properties and the core mechanical properties of the HPC were discussed. Also included are the procedures for the non-destructive – SEM and CT scanning tests. Results and discussion of the experimental data for proper understanding of SAP influence on the mechanical behaviour of this low W/B concrete are presented in the next three chapters.

## 4

# *Fresh and Early - Age Strength Properties of HPC with SAP*

Results and discussion of fresh and early-age strength properties of the HPC containing SAP as IC-agent are presented in this chapter. Results of SAP absorption in water and the CPS conducted with the tea-bag test and the pH values of the CPS were first reported and discussed as this could explain the influence of SAP on the cement hydration and early-age strength development process of the HPC mixtures.

### **4.1 SAP Absorption and pH-value of CPS**

A major property for consideration in SAP utilisation is its absorption and desorption in CPS (CPS) as discussed in Section 2.4.1 and 2.4.2 with different values of SAP absorbency reported in literature (Assmann et al., 2014; Jensen & Hansen, 2002; Esteves, 2014; Hasholt et al., 2012, Lura et al., 2006; Schrofl et al., 2012). There was also an assumption in this study that the concentration of the CPS has an influence on SAP absorbency and desorption, hence the need to examine SAP absorbency in different CPS concentrations. Different CPS were simulated and their pH-values determined as explained in Section 3.2.1.3, just as SAP absorption in these CPS mixtures was determined.

#### **4.1.1 Results**

Tables 4.1 reports the results of the pH-value determination of various simulated CPS and the summary of SAP absorption after 10 minutes in various CPS mixtures. A detailed result of the SAP absorption for the entire test period (180 minutes) is however presented in Table A2.

The pH-values of all the CPS lies within 12.4 and 13.0 implying they are all of high alkaline nature as expected of concrete especially those made with Type II cement (usually CEM I blended with SCMs especially the ternary cements with  $\text{Al}_2\text{O}_3$  and  $\text{Fe}_2\text{O}_3$  (alkaline) content contribution from FA and CS) as pointed out in a recent study (Kakade, 2014).

**Table 4-1: pH-values of CPS**

Solution	Water	(W/C*)	(W/C)	(W/C)	(W/C)	(W/C)	$M_2$	$M_{IF}$	$M_{IS}$
		5.2	4.3	3.7	3.1	2.5			
pH-value	7.43	12.87	12.85	12.81	12.62	12.59	12.89	12.47	12.41
Temp °C	23.10	18.63	18.26	18.50	21.30	19.40	18.70	19.17	18.20
10 mins absorption ( $SP_1$ )	228.44	24.30	21.64	24.08	22.77	27.24	-	-	-
10 mins absorption ( $SP_2$ )	258.22	33.93	24.45	27.85	23.61	24.09	-	-	-

\*W/C on this table is the content of water to cement for the simulated pore solution extracted from cement pastes and concrete according to the standards for the teabag test. The W/C of 5.2 represent a CPS from a typical 0.42 W/C paste or concrete, while simulated pore were made for the 0.35 W/B (using W/C of 4.3); 0.3 W/B (W/C of 3.7); 0.25 W/B (W/C of 3.1) 0.2 W/B (W/C of 2.5) pastes/concrete respectively.

The pH-values decreases slightly as the water content in the CPS increases, while the CPS from binary cements (CEM I 52.5 N and SF) has similar value (12.8 to 12.9) as the CPS made from only CEM I 52.5 N simulated for concrete having W/B of 0.2 to 0.3. The CPS made from ternary cements (CEM I 52.5 N, SF and FA or CS) on the other hand have pH-values (12.47 ( $M_{IF}$ ) and 12.41 ( $M_{IS}$ )) which are slightly below 12.5 (the expected minimum value range for Type II cement). The value is however within the range for high alumina cement (Kakade, 2014). The pH test for distilled water gave a value of 7.43 which is within the level for a neutral solution, although this was conducted on a hot day as opposed to the remaining solutions.

The determination of SAP absorption was carried out on CPS made from CEM I 52.5 N only simulated for concrete of varying W/B (0.2; 0.25; 0.3; 0.35 and 0.4). The values obtained in the CPS at 10 minutes durations were generally within the same range (mostly around 24 g/g with one or two inconsistencies) while the observed slight differences is of no particular pattern. The round up average of 25 g/g was taken as the SAP absorption capacity in CPS and adopted for the HPC mixtures in this study. SAP absorption in water on the other hand is taken as 230 g/g.

### 4.1.2 Inferences

The outcome of the study on SAP absorption and pH-value above can be summarised as follows:

- i. The pH-values of all the CPS are within 12.4 and 13.0 implying they are all of high alkaline nature as expected of concrete especially those made with Type II cement as pointed out in Kakade, (2014).
- ii. The pH-values decrease slightly as the water content in the CPS increases, while the CPS from binary cements (CEM I 52.5 N and SF) have similar value (12.8 to 12.9) as the CPS made from only CEM I 52.5 N simulated for concrete having W/B of 0.2 to 0.3. The CPS made from ternary cements (CEM I 52.5 N, SF and FA or CS) on the other hand have pH-values (12.47 ( $M_{1F}$ ) and 12.41( $M_{1S}$ )) which are slightly below 12.5 (the expected minimum value range for Type II cement).
- iii. The round up average of 25 g/g (10 mins insertion in CPS) was thereby taken as the SAP absorption capacity in CPS and adopted for the HPC mixtures in this study while SAP absorption in water on the other hand is taken as 230 g/g ( $SP_1$ ) and 260 g/g ( $SP_2$ ).
- iv. There is no significant difference in influence of CPS concentration on the SAP absorption capacity. This is within the limit of CPS (5.2 to 10.4 W/C and the binary and ternary cements ( $M_2$ ,  $M_{1F}$  and  $M_{1S}$ )) concentration as tested for in this research.

## 4.2 Fresh Properties of HPC Mixtures

The rheology of fresh concrete is an indication of the possibilities of arriving at the intended strength and performance properties of the hardened concrete. In HPC, the slump flow as a measure of workability and consistency is a first measure of appropriateness of the chosen constituent materials and adequacy of the handling and mix proportioning. The properties examined at the fresh stage of the HPC mixtures for this study are slump flow, room and concrete temperatures and an assessment of the actual W/B with account taken of the additional water provided for SAP absorption and the liquid content of the superplasticiser.

## 4.2.1 Results of Tests on Fresh Properties

The results of test conducted for fresh properties of the HPC mixtures with SAP are presented in Tables 4.2 ( $M_2$  and  $M_3$  from binary cements) and 4.3 ( $M_{1F}$  and  $M_{1S}$  from ternary cements).

**Table 4-2: Mix constituents and fresh properties of HPC mixtures from binary cements**

Constituents (kg/m <sup>3</sup> )	M <sub>2</sub>							M <sub>3</sub>						
	Ref	SP <sub>1</sub>			SP <sub>2</sub>			Ref	SP <sub>1</sub>			SP <sub>2</sub>		
SAP contents%	0.0	0.2	0.3	0.4	0.2	0.3	0.4	0.0	0.2	0.3	0.4	0.2	0.3	0.4
Water	134	134	134	134	134	134	134	156	156	156	156	156	156	156
Cement	540	540	540	540	540	540	540	500	500	500	500	500	500	500
SF	40	40	40	40	40	40	40	40	40	40	40	40	40	40
FA	0.0	0.0	0.0	0.0	0.0	0.0	0.0	0.0	0.0	0.0	0.0	0.0	0.0	0.0
CS	0.0	0.0	0.0	0.0	0.0	0.0	0.0	0.0	0.0	0.0	0.0	0.0	0.0	0.0
C. Aggregate	1050	1050	1050	1050	1050	1050	1050	1050	1050	1050	1050	1050	1050	1050
F. Aggregate	710	710	710	710	710	710	710	700	700	700	700	700	700	700
SAP	0.00	1.16	1.74	2.32	1.16	1.74	2.32	0.00	1.08	1.62	2.16	1.08	1.62	2.16
S/plasticizer	16.0	16.0	16.0	16.0	16.0	16.0	16.0	5.4	5.4	5.4	5.4	5.4	5.4	5.4
Additional Water	0.00	29.00	43.50	58.00	29.00	43.50	58.00	0.00	27.00	40.50	54.00	27.00	40.50	54.00
Total W/B	0.25	0.30	0.33	0.35	0.30	0.33	0.35	0.30	0.35	0.37	0.40	0.35	0.37	0.40
Slump Flow	550	530	580	550	550	580	570	500	500	500	450	460	450	450
Room Temperature °C	19.0	17.0	17.0	16.0	14.0	16.5	16.1	18.0	19.5	19.5	19.5	18.0	16.0	16.0
Concrete Temperature °C	26.0	24.0	23.0	22.0	21.0	21.8	20.3	22.0	23.6	23.5	23.5	20.0	18.0	18.0
Designed Density*	2490	2520	2535	2550	2520	2535	2550	2451	2479	2494	2508	2479	2494	2508
Demoulded Density	2486	2457	2431	2407	2469	2429	2409	2413	2399	2344	2357	2382	2405	2394
Total Porosity %	0.17	2.52	4.13	5.61	2.03	4.21	5.53	1.58	3.25	6.00	6.00	3.92	3.56	4.54
air content - SAP voids %	0.17	1.36	2.39	3.29	0.87	2.47	3.21	1.58	2.17	4.38	3.84	2.84	1.94	2.38
(a-a <sub>0</sub> )	0.00	1.19	2.22	3.13	0.70	2.30	3.04	0.00	0.59	2.79	2.26	1.26	0.36	0.80
(1-B (a-a <sub>0</sub> ))	1.00	0.96	0.93	0.90	0.98	0.92	0.90	1.00	0.98	0.91	0.93	0.96	0.99	0.97

**Table 4-3: Mix constituent and fresh properties of HPC mixtures from ternary cements**

Constituents (kg/m <sup>3</sup> )	M <sub>1F</sub>							M <sub>1S</sub>						
	Ref	SP <sub>1</sub>			SP <sub>2</sub>			Ref	SP <sub>1</sub>			SP <sub>2</sub>		
SAP Contents%	0	0.2	0.3	0.4	0.2	0.3	0.4	0	0.2	0.3	0.4	0.2	0.3	0.4
Water	125	125	125	125	125	125	125	125	125	125	125	125	125	125
Cement	530	530	530	530	530	530	530	530	530	530	530	530	530	530
SF	52.5	52.5	52.5	52.5	52.5	52.5	52.5	52.5	52.5	52.5	52.5	52.5	52.5	52.5
FA	122.5	122.5	122.5	122.5	122.5	122.5	122.5	0.0	0.0	0.0	0.0	0.0	0.0	0.0
CS	0.0	0.0	0.0	0.0	0.0	0.0	0.0	122.5	122.5	122.5	122.5	122.5	122.5	122.5
C. Aggregate	1050	1050	1050	1050	1050	1050	1050	1050	1050	1050	1050	1050	1050	1050
F. Aggregate	590	590	590	590	590	590	590	590	590	590	590	590	590	590
SAP	0.00	1.41	2.12	2.82	1.41	2.12	2.82	0.00	1.41	2.12	2.82	1.41	2.12	2.82
S/plasticizer	21.0	21.0	21.0	21.0	21.0	21.0	21.0	21.0	21.0	21.0	21.0	21.0	21.0	21.0
Additional Water	0.00	35.25	52.88	70.50	35.25	52.88	70.50	0.00	35.25	52.88	70.50	35.25	52.88	70.50
Total w/b	0.20	0.25	0.28	0.30	0.25	0.28	0.30	0.20	0.25	0.28	0.30	0.25	0.28	0.30
Slump Flow	570	550	550	560	550	600	550	450	450	500	500	500	500	550
Room Temperature °C	16.0	16.0	16.0	16.5	16.5	16.0	16.0	11.5	11.0	15.0	14.0	15.0	14.0	15.0
Concrete Temperature °C	23.0	22.0	21.0	22.0	23.0	23.0	23.5	20.0	18.5	20.0	18.0	20.0	18.0	19.5
Designed Density *	2491	2528	2546	2564	2528	2546	2564	2503	2540	2558	2576	2540	2558	2576
Demoulded Density	2477	2417	2379	2394	2466	2402	2406	2498	2438	2444	2412	2450	2431	2412
Total Porosity %	0.58	4.39	6.56	6.66	2.43	5.67	6.17	0.20	3.99	4.47	6.38	3.52	4.96	6.39
air content - SAP voids %	0.58	2.98	4.44	3.84	1.02	3.56	3.35	0.20	2.58	2.35	3.56	2.11	2.84	3.57
(a-a <sub>0</sub> )	0.00	2.40	3.87	3.26	0.44	2.98	2.77	0.00	2.38	2.16	3.37	1.92	2.64	3.38
(1-B (a-a <sub>0</sub> ))	1.00	0.92	0.87	0.89	0.98	0.90	0.91	1.00	0.92	0.93	0.88	0.93	0.91	0.88

\*Note that the “design density” (dd) in Table 4.2 and 4.3 for HPC with SAP was arrived at by the addition of the weight of SAP and extra water added for SAP absorption to the initial calculated weight in kg/m<sup>3</sup> for the reference mixture, hence the increase. The “demoulded density” (dmd) was determined by dividing the direct weight of the demoulded concrete with the measured volume of individual concrete cube. The density value at a specific curing age was the average of three specimens for that age divided by the average of the demoulded densities for all the twelve specimens of an HPC mixture.

$$\text{Total porosity \%} = \frac{dd - dmd}{dd} \times 100 \quad (4.1)$$

It is evident from the results that the total W/B increases as the SAP content increases while the slump flow values on the other hand remain in the same range for all HPC mixtures (530 to 570 mm – M<sub>2</sub>; 450 to 500 mm – M<sub>3</sub>; 550 mm to 600 mm – M<sub>1F</sub> and 450 to 500 mm – M<sub>1S</sub>). M<sub>1F</sub> is however more flow-able than M<sub>1S</sub>, while M<sub>2</sub> is more flow-able than M<sub>3</sub>. The result (Tables 4.2 and 4.3), thereby reflecting that all the HPC mixtures are of similar workability (slump low range 450 mm – 600 mm) as expected from literature (Neville, 2012). SAP addition and extra water provided for SAP absorption did not result in higher slump flow values. The difference between room temperature (RTemp) and concrete temperature (CTemp) decreased gradually as the SAP content increased with reference mixes having the highest temperature difference values. Evolving high heat of hydration is typical of binders containing SF and this had always necessitated the introduction of water reducers especially the lignosulfate based to serve as set retarder by reducing the heat evolved (Silica Fume Association, 2005). The water-filled swollen SAP within the HPC during the vigorous mixing process possibly released some of water absorbed, or serves as means of reducing the temperature rise through conduction, from the agitated solid constituents into the absorbed water within the SAP particles. This lowers the internal concrete temperature.

All the HPC mixtures irrespective of SAP contents and mix composition were noted to be of slump flow values conforming to provisions of literature (Aïtcin, 1998; *ACI 363.2R* - 1998; Beushausen &

Dehn, 2009; Mehta & Monteiro, 2014; Neville, 2012). The mixtures were all of similar consistency even with SAP added and no segregation was observed.

### 4.2.2 Inferences

The results of tests carried out on fresh concrete as presented above offer the following inferences:

- i. SAP addition with extra water has no direct influence on the consistency of the HPC mixtures.
- ii. Although the total W/B increases as the SAP content increases (with extra water added for SAP absorption), the slump flow values remain in the same range for all HPC mixtures (530 to 570 mm – M<sub>2</sub>; 450 to 500 mm – M<sub>3</sub>; 550 mm to 600 mm – M<sub>1F</sub> and 450 to 500 mm – M<sub>1S</sub>).
- iii. The temperature difference between room temperature (RTemp) and concrete temperature (CTemp) decreased gradually as the SAP content increased with reference mixes having the highest temperature difference values.
- iv. All the HPC mixtures irrespective of SAP contents and mix composition were noted to be of slump flow values conforming to reports in literature (Aïtcin, 1998; ACI 363.2R - 1998; Beushausen & Dehn, 2009; Mehta & Monteiro, 2014; Neville, 2012). This implies that the water added for SAP absorption was effectively taken by the SAP particles in the mixtures and available for IC purposes when released by SAP as hydration progresses.

### 4.3 Setting Times and Early-Age Strength Development

Setting times and early-age strength development are properties of concrete which depict the hydration process of cement in the early ages of concrete. These properties are noted in literature (Mehta & Monteiro, 2014; Neville, 2012) to be influenced by physical and chemical properties of the composite materials of concrete, the mix composition and condition of the curing environment.

### 4.3.1 Results

The results and discussion for this aspect of the study are classified into three major sub-topics and are presented in the following sections.

#### 4.3.1.1 Setting times of HPC with SAP

Figures 4.1 to 4.4 present the results of setting time test using concrete penetrometer in accordance to ASTM C403 – 08. The fresh mortar extracted from HPC mixtures cast into 150 mm cube moulds were kept in a climate control room and readings were taken at intervals as discussed in Section 3.2.3.1. A plot of the penetration resistance (MPa) against the elapsed time (in minutes) as shown in Figure 4.1 for M<sub>2</sub> fitted on a power regression line gave the setting times with the expression:

$$Y = (2E - 21)X^{8.8671} ; \text{ having a strong correlation } (R^2 = 0.9851)$$

Y in the expression represents the penetration resistance (PR); X represents the elapsed time and the regression constants c (2E – 21) and d (8.8671) are in similarity to the code (ASTM 403 – 08) provisions. Plots for individual HPC mixtures summarised as shown in Appendix A4, gave similar expressions having strong correlations too.

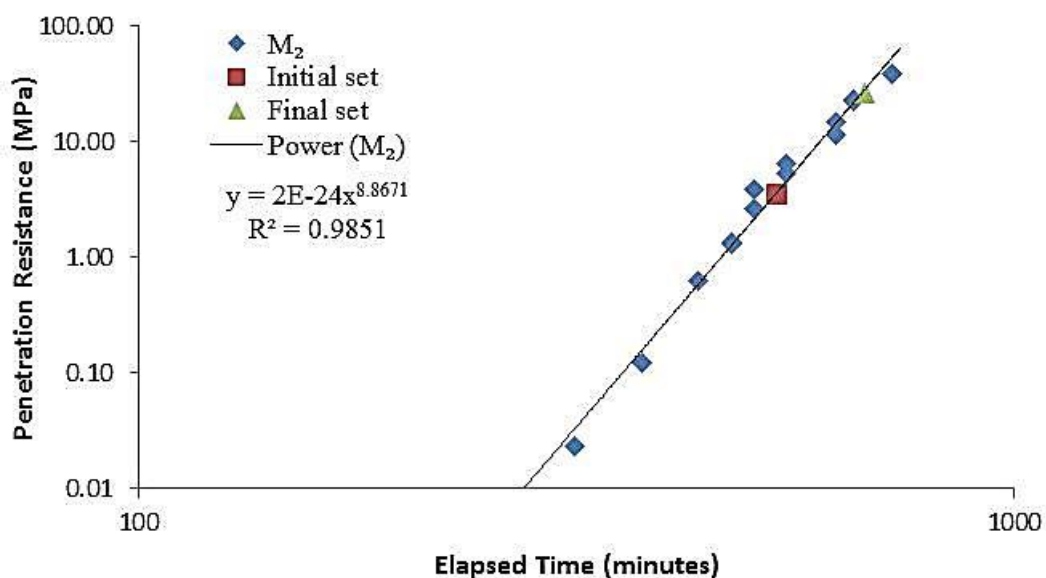
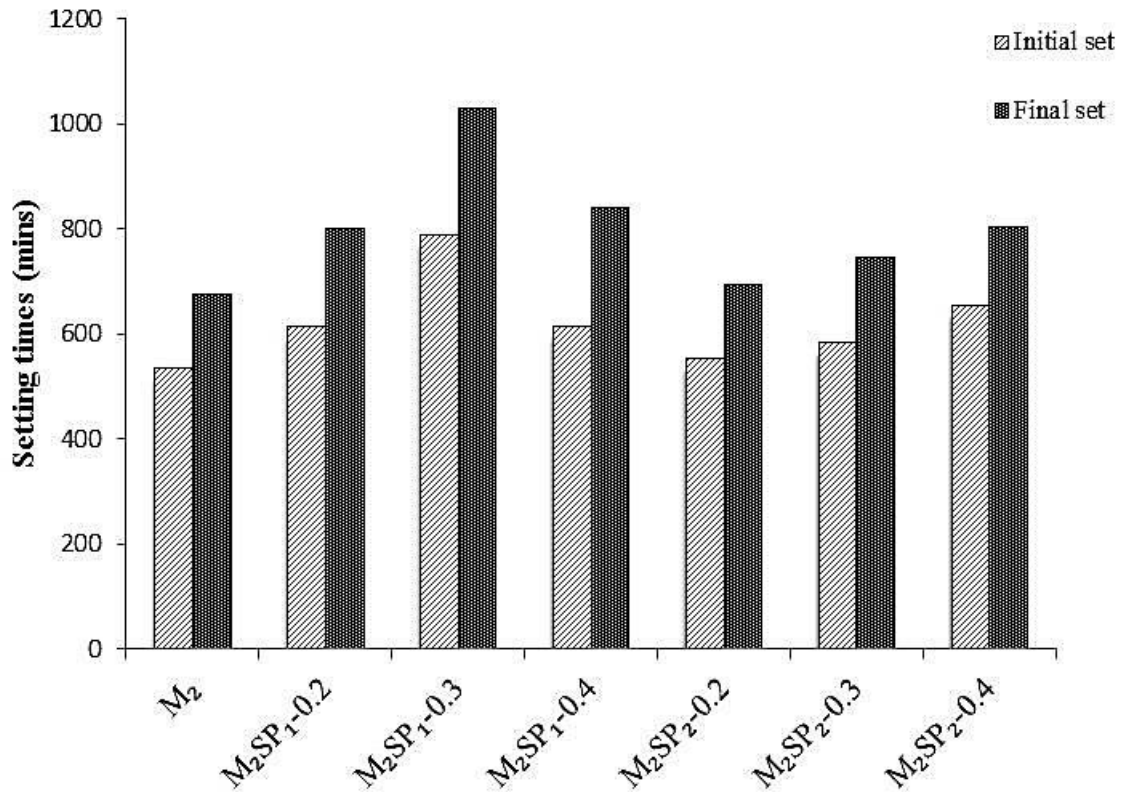


Figure 4-1: Setting times (initial and final) plot of M<sub>2</sub>-HPC mixture

Figure 4.2, on the other hand, is a plot of the setting times for various  $M_2$  – HPC mixtures (with or without SAP). It shows that the setting time increased as the SAP content increased up to 0.3%  $b_{wob}$ , implying SAP addition generally resulted in set retardation.



**Figure 4-2: Initial and Final setting times for  $M_2$ -HPC mixtures made from binary cements**

Figure 4.3 for  $M_{1S}$  – HPC mixtures (from ternary cements) show the same trend as in Figure 4.6 ( $M_2$  – HPC (from binary cements)) cases. In both cases of HPC from binary –  $M_2$  (Figure 4.6) and ternary –  $M_{1S}$  cements HPC (Figure 4.7) mixtures,  $SP_1$  addition resulted in a steady increase in both initial and final setting time of the concrete.  $SP_2$  addition on the other led to setting times (initial and final) increasing at a lower rate. Figure 4.8 shows all the HPC mixtures ( $M_{1F}$ ,  $M_{1S}$ ,  $M_2$  and  $M_3$ ) and influence of  $SP_1$  contents on their initial and final setting times. In general  $SP_1$  addition led to longer setting times in all the HPC mixtures.

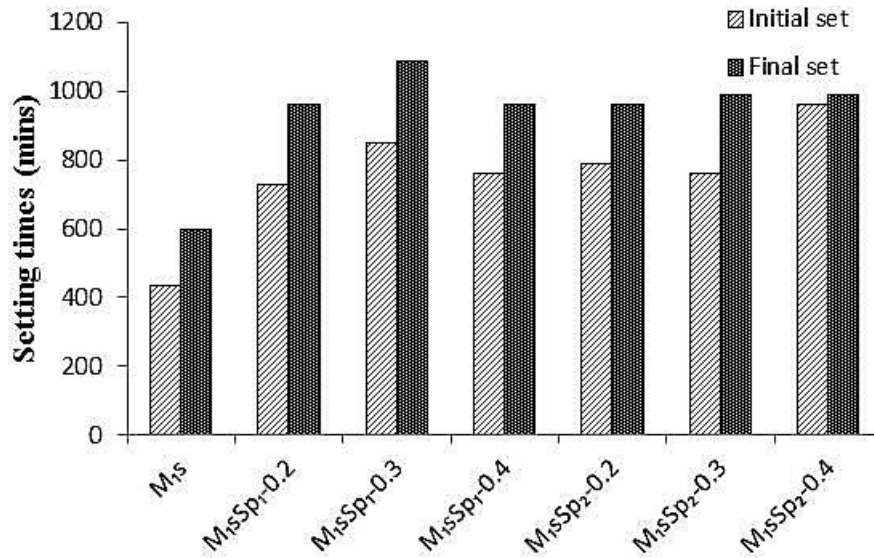


Figure 4-3: Initial and Final setting times of M<sub>1S</sub> - HPC mixtures made from ternary cements

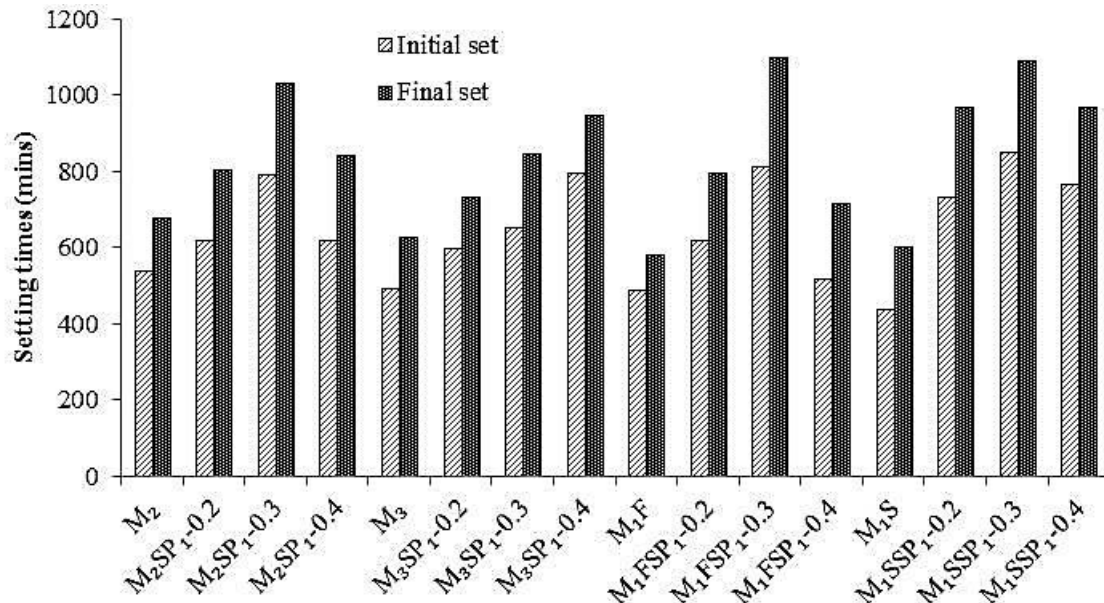


Figure 4-4: Initial and Final setting times of HPC mixtures with SAP1

The results for 0.4% SAP contents in both instances for SP<sub>1</sub> deviates slightly from this trend.

The findings of this study of generally retardation as caused by SAP addition is in agreement with the findings in previous studies as stated earlier in Section 2.4.3. Lura et al. (2012) reported higher  $w_n$  at 28 days in cement pastes with SAP compared to reference mixtures while Klemm (2009) observed significant influence due to SAP addition on the dormant period of the paste.

#### 4.3.1.2 Degree of hydration of HPC with SAP

Degree of hydration of the HPC with SAP is presented in Figures 4.9 and 4.10 for  $M_2$  – HPC mixtures (made from binary cements [CEM I 52.5 N+ SF]) and  $M_{1S}$  – HPC mixtures (made from ternary cement [CEM I 52.5 N+ SF + CS]), respectively. Table 4.6 gives a summary of results on degree of hydration for all the HPC mixtures studied.  $M_{1F}$  and  $M_3$  mixtures were only examined for  $SP_1$  while  $M_2$  and  $M_{1S}$  were studied for both  $SP_1$  and  $SP_2$  to investigate influence of SAP types on rate of hydration when different binder combination types are used.

The result shows that degree of hydration generally increases as the SAP content increases for all curing ages studied with an indication that  $SP_2$  resulted in higher degree of hydration than  $SP_1$  with few inconsistencies. Similarly, the higher the W/B, the higher the early age hydration ( $M_3$  – HPCs with the highest water content – 0.3 W/B recorded the highest degree of hydration). The relative rates of hydration called **RH<sub>7</sub>** factor (on basis of 7<sup>th</sup> day degree of hydration for reference mixtures) were highest for  $M_{1F}$  (the ternary cement HPC of 0.2 W/B containing FA).

Examining SAP type for both binder combination types (binary –  $M_2$  or ternary –  $M_{1S}$  cements) as shown in Figures 4.5 and 4.6, reveals that  $SP_2$  has hydration rate generally higher than  $SP_1$  especially for ages 3days to 7days. Generally, HPC mixtures from ternary cements ( $M_{1S}$ ) even though with lower W/B reflected higher degree of hydration at the initial 24 hrs (values for the reference mixes are: -  $M_{1S}$  = 31.3% and  $M_2$  = 25.0%); this however progressed at a slower rate than seen in the binary cements HPC mixtures ( $M_{1S}$  at 7<sup>th</sup> day = 39.2% while  $M_2$  = 53.9%). The same trend is maintained even as SAP addition increases in the HPC mixtures. The degree of hydration between day 3 and 7 is however highest in the binary cement HPC mixtures ( $M_2$  and  $M_3$ ) with the mixture having the higher W/B (0.3) –  $M_3$  HPC displaying highest degree of hydration at these ages up to 7days. The value by the 7<sup>th</sup> day was noted to be already above 60% for the specimen with highest  $SP_1$  content ( $M_3SP_1$ -0.4).

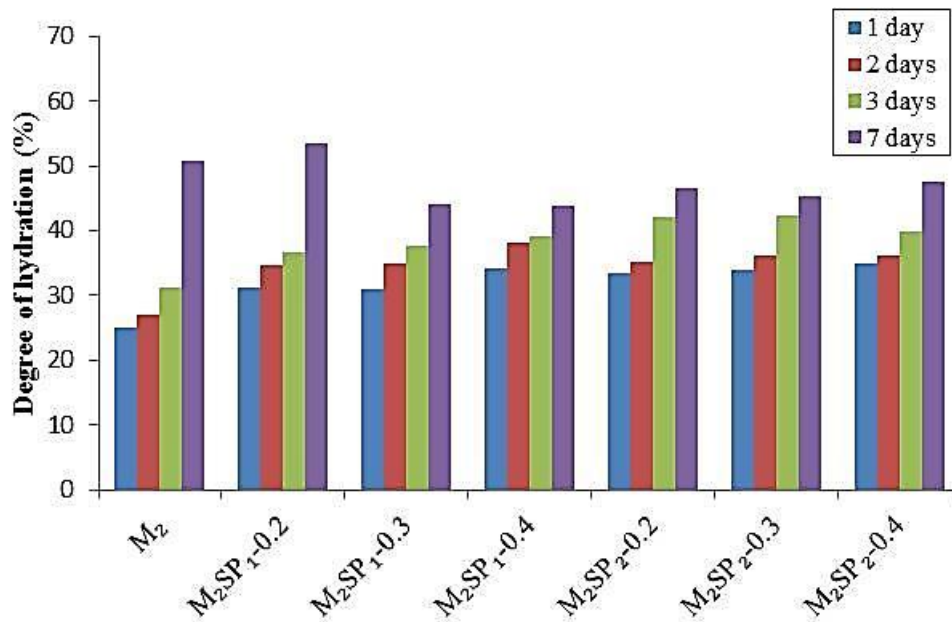


Figure 4-5: Degree of hydration of M<sub>2</sub>-HPC (binary cements) with SAP

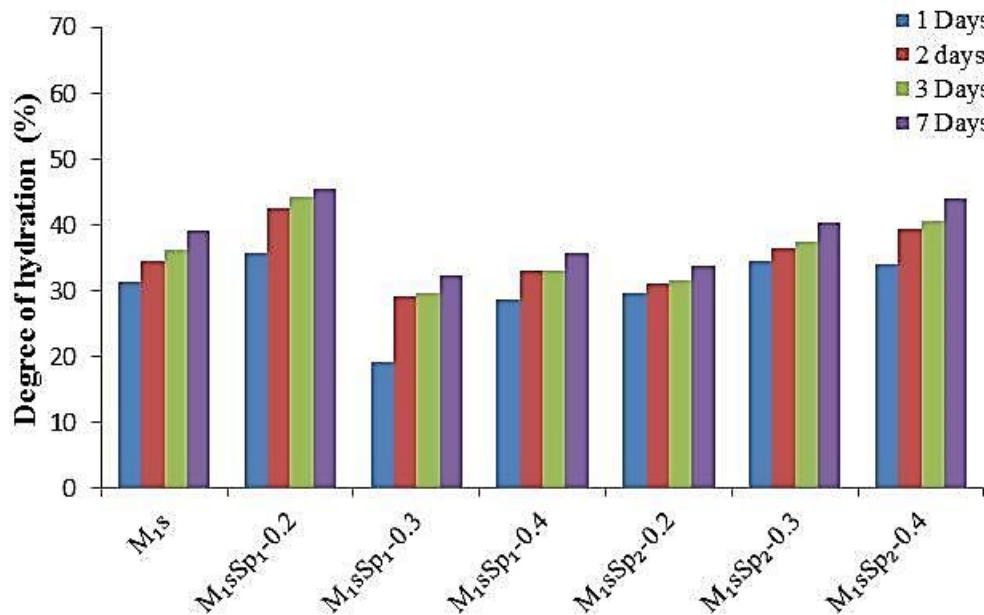


Figure 4-6: Degree of hydration of M<sub>1S</sub>-HPC (ternary cements) with SAP

An examination of the two HPC mixtures from binary cements (M<sub>2</sub> and M<sub>3</sub>) shows the mixtures with higher W/B (M<sub>3</sub>) exhibiting higher initial degree of hydration which however progressed at a decreasing rate as the SAP contents and curing age increased. The higher the SAP content and W/B for all mixtures, the higher the chemically bounded water ( $w_n$ ) and this increases as the hydration

period increases. The  $RH_7$  factor for the HPC mixtures containing SAP shows that hydration increased as the SAP contents increases for all concrete W/B at the respective ages of curing.

The  $M_{1S}SP_1-0.3$  – HPC mixture does not conform to the observed trend of the experimental work in this aspect as the values obtained for these specimens (green highlights on Table 4.4) generally deviates from the trend observed. 0.2%  $b_{wob}$  for  $SP_1$  content was however noted to give similar or even higher values as reference mixes in all cases and at all ages. The mixing water provided in the mix proportioning as a function of W/B can be adjudged as a major influence on hydration in general in these low W/B concretes at the early ages as all mixtures studied had the same SF content. FA and CS addition in  $M_{1F}$  and  $M_{1S}$  retard the hydration process for the first two days; their inclusion however also improved workability and slump retention capacity for the extreme low W/B concretes.

**Table 4-4: Influence of SAP and binder type on degree of hydration of HPC**

Specimen	Degree of Hydration (%)				$RH_7$ Factor			
	1 day	2 days	3 days	7 days	1	2	3	7
$M_2$	25.0	26.3	30.2	53.9	0.46	0.49	0.56	1.00
$M_2SP_1-0.2$	31.2	32.9	34.4	54.0	0.58	0.61	0.64	1.00
$M_2SP_1-0.3$	31.1	39.9	57.9	62.6	0.58	0.74	1.08	1.16
$M_2SP_1-0.4$	34.2	38.1	63.2	65.5	0.63	0.71	1.17	1.21
$M_2SP_2-0.2$	33.4	35.3	42.0	42.7	0.62	0.65	0.78	0.79
$M_2SP_2-0.3$	33.4	36.2	42.5	48.8	0.62	0.67	0.79	0.91
$M_2SP_2-0.4$	31.1	32.9	40.0	47.6	0.58	0.61	0.74	0.88
$M_{1S}$	31.3	34.6	36.2	39.2	0.80	0.88	0.93	1.00
$M_{1S} SP_1-0.2$	35.7	42.6	44.4	45.5	0.91	1.09	1.13	1.16
$M_{1S} SP_1-0.3$	19.3	29.2	29.7	32.3	0.49	0.74	0.76	0.82
$M_{1S} SP_1-0.4$	28.8	33.0	33.2	35.7	0.73	0.84	0.85	0.91
$M_{1S} SP_2-0.2$	29.7	31.2	31.7	33.9	0.76	0.80	0.81	0.87
$M_{1S} SP_2-0.3$	34.5	36.4	37.5	40.4	0.88	0.93	0.96	1.03
$M_{1S} SP_2-0.4$	34.1	39.3	40.7	44.2	0.87	1.00	1.04	1.13
$M_{1F}$	36.3	39.4	41.1	45.9	0.79	0.86	0.90	1.00
$M_{1F} SP_1-0.2$	39.9	45.2	46.9	48.6	0.87	0.98	1.02	1.06
$M_{1F} SP_1-0.3$	37.6	43.1	50.2	55.6	0.82	0.94	1.09	1.21
$M_{1F} SP_1-0.4$	45.1	50.0	53.7	59.5	0.98	1.09	1.17	1.30
$M_3$	43.8	47.9	50.6	57.1	0.77	0.84	0.89	1.00
$M_3SP_1-0.2$	47.6	50.6	52.0	58.6	0.83	0.89	0.91	1.03
$M_3SP_1-0.3$	52.6	55.1	55.1	62.0	0.92	0.97	0.97	1.09
$M_3SP_1-0.4$	53.9	56.6	57.8	65.1	0.94	0.99	1.01	1.14

#### 4.3.1.3 Early-age strength development of HPC with SAP

The early-age strength development plot for the reference mixes (Figure 4.7) shows a conformance with the relationship postulated for SF- concrete at one to ten days ( $t_1 - t_{10}$ ) of hydration by Kadri et al (2012) as presented in Equation 2.13. The compressive strength increased linearly according to

logarithm of time  $t$  ( $R = A + B \log \frac{t}{t_1}$ ), the coefficient  $A$  being the intercept on the compressive strength axis while  $B$  is the kinetic of the hydration reaction. The coefficient  $B$  in this particular test increased slightly as the  $W/B$  increased. Since the  $SF$  content was kept constant for all mixes while two of the HPC mixtures contain additional pozzolanic materials (FA and CS) to achieve the extremely low  $W/B$  concretes ( $M_{1F}$  and  $M_{1S}$ ). Further influence of these other pozzolanic materials is however noted on the kinetics of the hydration reaction. The results shows a higher value of the  $B$  coefficient for the HPC made from ternary cements having CS as an addition ( $M_{1S}$ ) than the one in which FA was added. This implies that CS addition enhances an improved early-age strength development than FA. The CS boosted reference HPC mixture ( $M_{1S}$ ) exhibited the highest compressive strength value of 115 MPa at the 7 day moving from initial one day strength of 44 MPa. The FA boosted HPC mixture ( $M_{1F}$ ) on the other hand had a 7 day compressive strength of 100 MPa moving from one day strength of 39 MPa. The binary cement HPC mixtures ( $M_2$  and  $M_3$ ) however present similar values for the kinetic of the hydration reaction. The 1 and 7 days compressive strength value of  $M_2$  can however be considered non-conforming and the reason for the slight drop in the  $R^2$  value of the regression (best fit trend-line) equation for this particular HPC mixture.

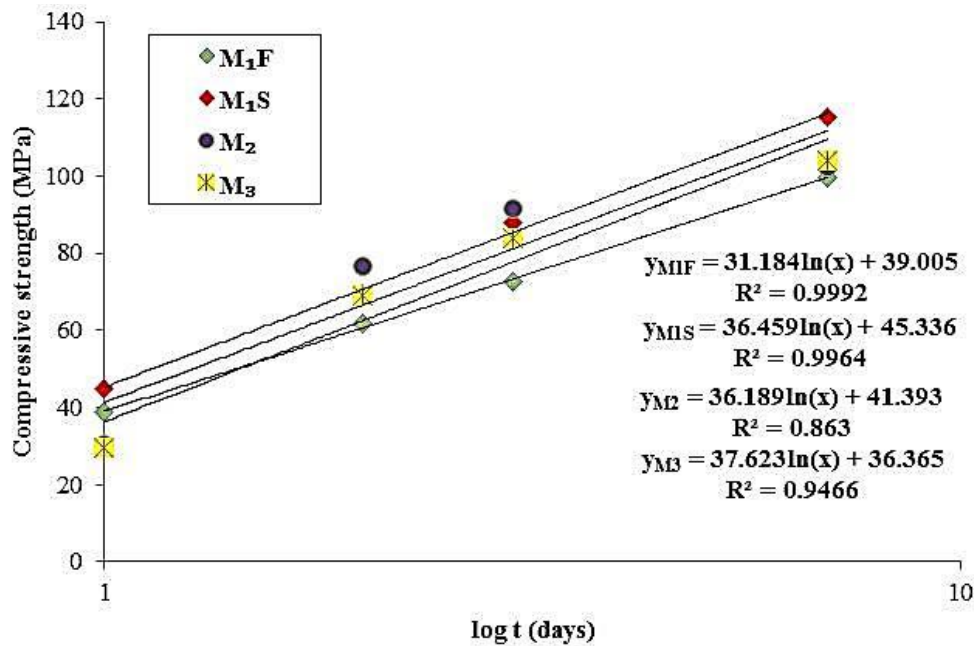


Figure 4-7: Early-age strength development of control HPC mixes

Figures 4.8 to 4.12 present the plot of SAP influence on the early-age strength development of the respective HPC mixtures. The respective reference mixes were studied with SAP Type 1 (SP<sub>1</sub>) while only M<sub>1S</sub> had mixtures produced for this particular experiment using both SAP types (SP<sub>1</sub> and SP<sub>2</sub>). The results show that compressive strength value at this early age decreases as the SAP content increases for all HPC mixtures. There is a progressive increase in strength as the hydration period increases for all HPC mixtures. There is a progressive increase in strength as the hydration period increases for all samples studied.

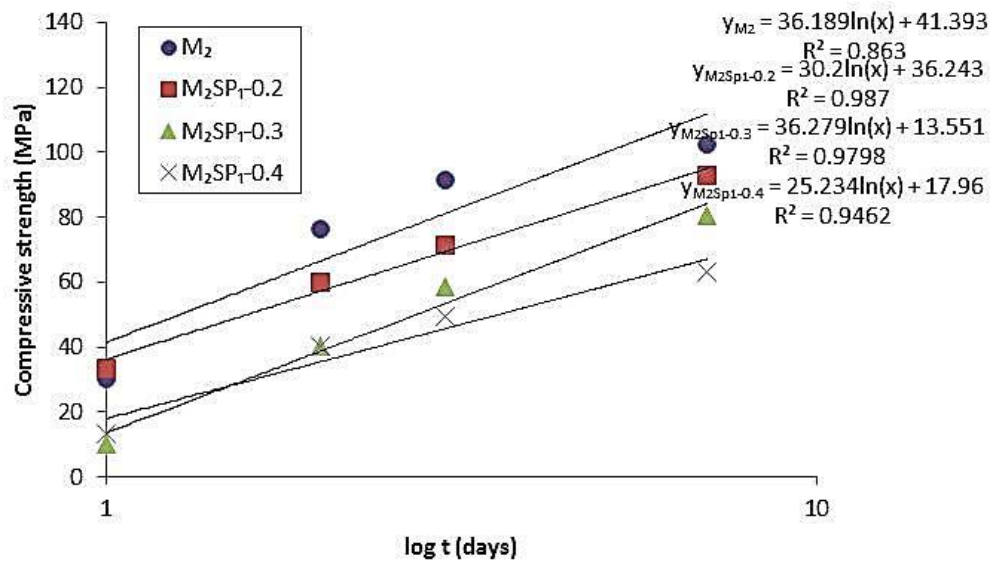


Figure 4-8: SP<sub>1</sub> influence on early-age strength development of M<sub>2</sub>- HPC

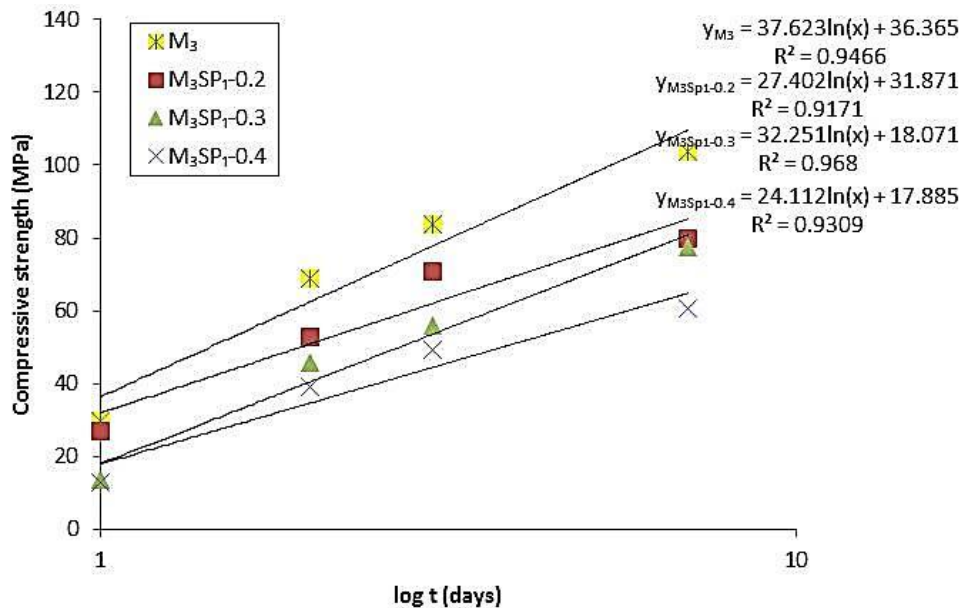


Figure 4-9: SP<sub>1</sub> influence on early-age strength of M<sub>3</sub>-HPC

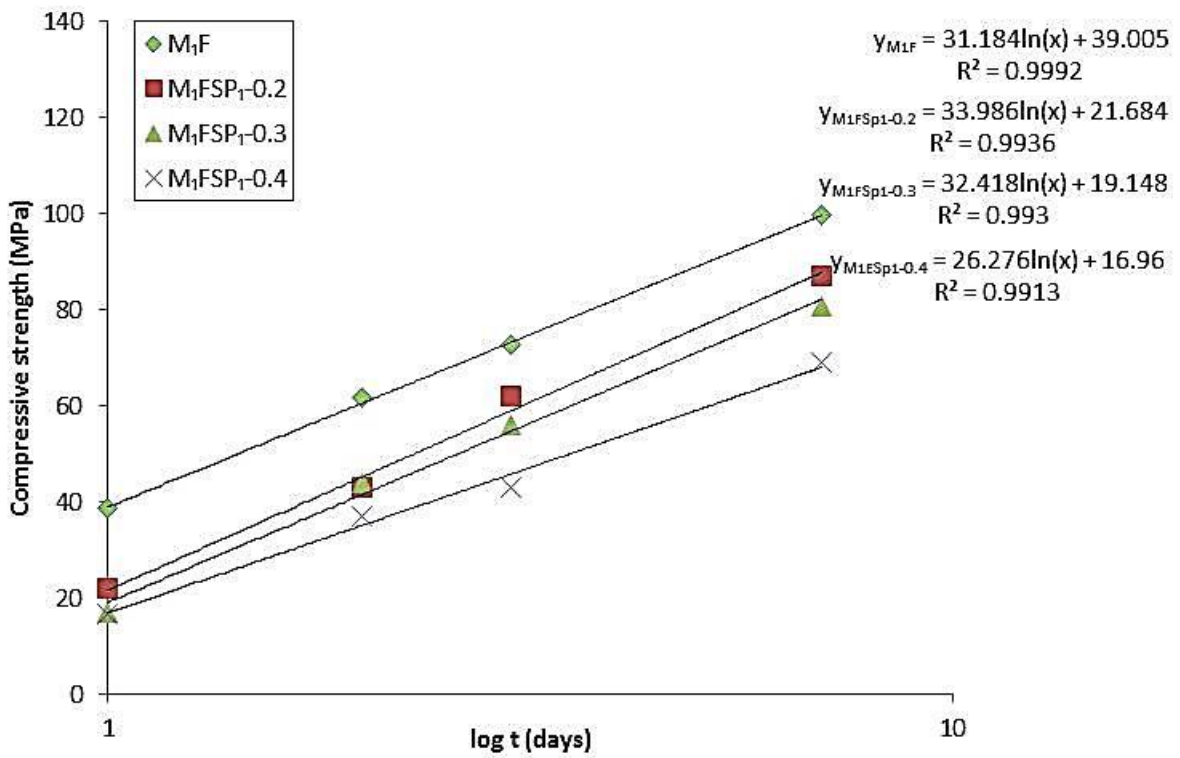


Figure 4-10: SP<sub>1</sub> influence on early-age strength of M<sub>1F</sub>-HPC

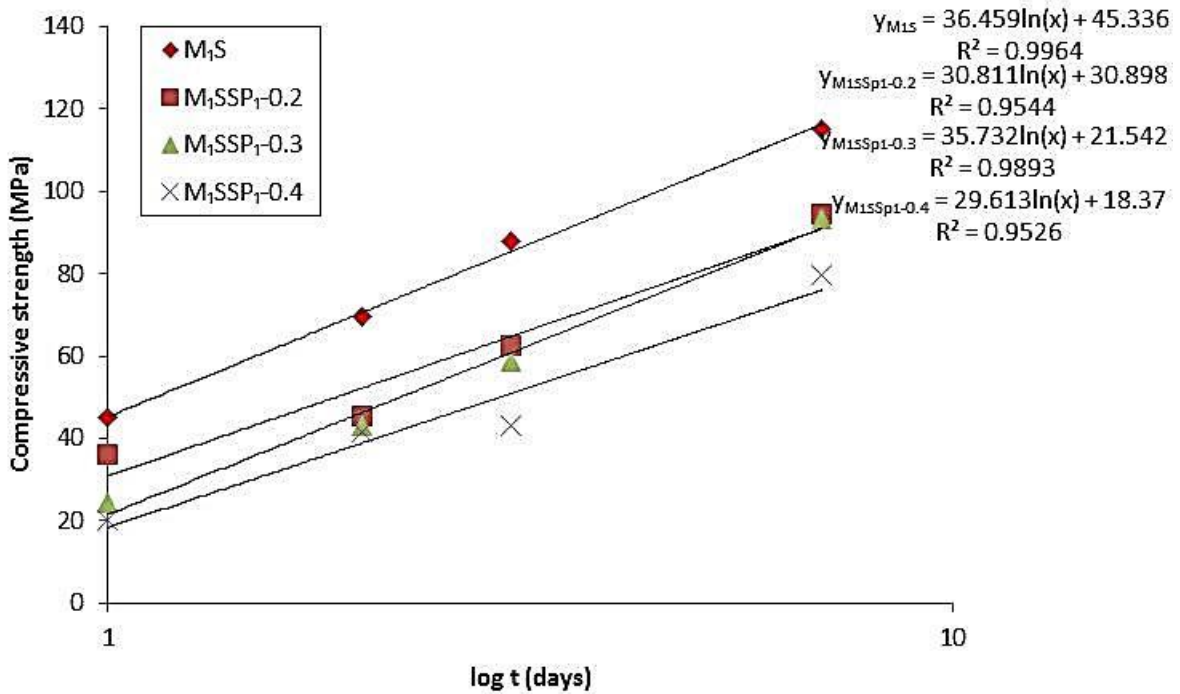


Figure 4-11: SP<sub>1</sub> influence on early-age strength of M<sub>1S</sub>-HPC

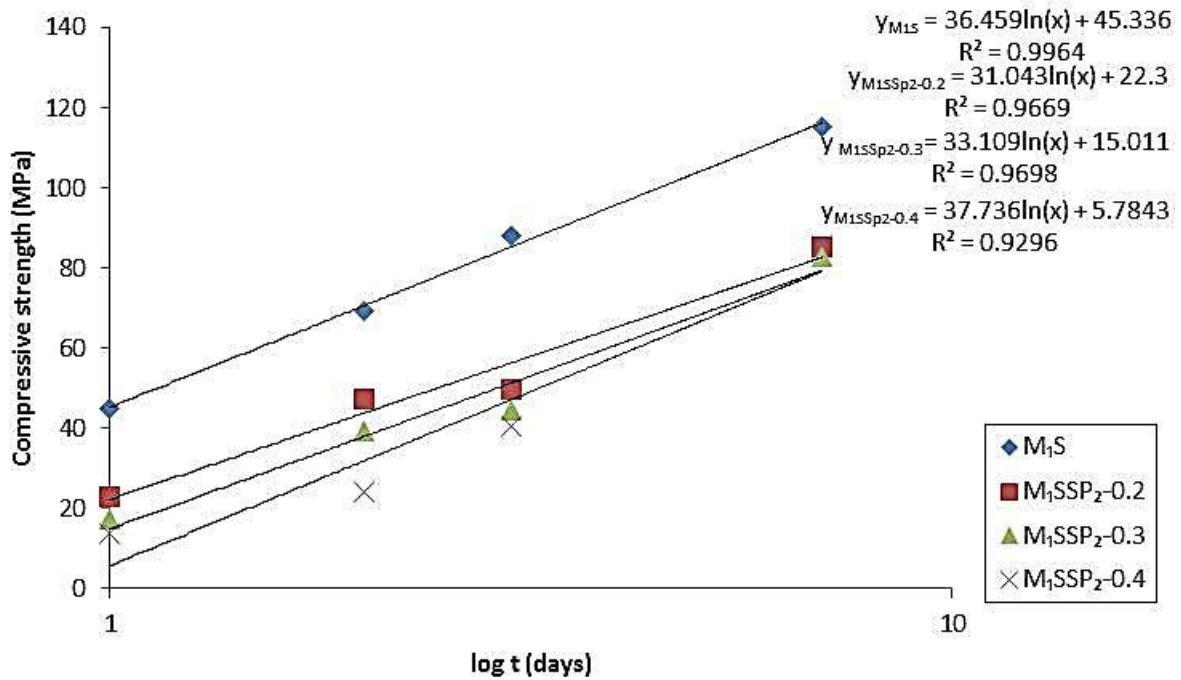


Figure 4-12: SP<sub>2</sub> influence on early-age strength of M<sub>1</sub>S–HPC

The compressive strength increase linearly according to logarithm of time  $t$  for all the HPC's containing SAP as IC-agent also conforming to the Kadri et al., (2012) expression of:

$$R = A + B \log \frac{t_d}{t_1} \quad (2.13).$$

All the HPC mixtures (Figure 4.8 to 4.12) show similar values for coefficient  $B$  (kinetic of hydration reaction) at a good correlation for all levels of SAP addition.

### 4.3.2 Inferences

The findings of the experiments in this sub-section can thereby be summarised as follows:

- i. SAP addition in general resulted in longer setting times (both the initial and final) in all HPC mixtures. Setting time is observed to increase as SAP content increased up to a limit of 0.3%, hence SAP addition can be said to result in some level of set retardation. This is in agreement with the observation of Klemm (2009) that SAP addition led to longer dormant period as mentioned earlier in Section 2.4.3.
- ii. This is of advantage in this low W/B concrete types which are known to be susceptible to rapid self-desiccation-caused autogenous shrinkage deformation on exposure to

atmosphere especially with very fine cement used (Neville, 2012). SAP addition will enhance the slump retention time and hence longer time to work with the concrete in the production process. It might however be a disadvantage in early concrete de-moulding on site. A slower concrete setting with SAP addition in cement coupled with pozzolanic materials (FA and CS) addition can also be a way of mitigating strong reaction with alkali-reactive aggregates in finer cements (Neville, 2012).

- iii.  $SP_1$  –HPC displayed longer initial and final setting time than the  $SP_2$  -HPC. The better distribution of the smaller water reservoirs ( $SP_1$ ) in these mixtures can be adduced to have made the water available for longer period and better distributed within the concrete phases, hence longer water retention.
- iv. Addition of both FA and CS resulted in similar setting times (initial and final) for all SAP contents.
- v. The degree of hydration of the HPC mixtures increases as the SAP content increases with an indication that  $SP_2$  results in higher degree of hydration than  $SP_1$  in both binder combination types (binary –  $M_2$  or ternary –  $M_{1S}$  cements). This is because the larger  $SP_2$  grains resulted in bigger swollen SAP and hence higher water desorption at the early age for cement hydration. This finding agrees well with the postulation made by Mönning (2009).
- vi. The binary cement with highest W/B ( $M_3$ ) reflected good early age degree of hydration but progressed at a lower rate as the age increased. The degree of hydration after 1 day is 43.8% and still remains at 57.1% after 7 days.
- vii. The influence of SAP addition on rate of hydration is noted to be highest in the HPC mixtures containing FA ( $M_{1F}$  mixtures) and increased at similar rate as HPC mixtures containing CS ( $M_{1S}$  mixtures). The  $RH_7$  factor for  $M_{1F}$  specimen is 0.79 after 1 day, while the specimen with highest SAP content –  $M_{1F}SP_1-0.4$  already has a  $RH_7$  factor of 1.30 after 7 days.
- viii. The higher the SAP content and W/B for all mixtures, the higher the chemically bounded water ( $w_n$ ) at specific times and this increased as the hydration period increased.

## 4.4 Microstructure and Chemical Composition

The results presented in the following sections are the SEM image, BSE/WDS analysis and FTIR (for amorphous silica content) of the binders.

### 4.4.1 SEM images of the binders and SAP particles

#### 4.4.1.1 SEM Images of binders

The SEM images of the various materials combined as binder (CEM I 52.5 N, SF, FA and CS) are shown in Figures 4.13 to 4.16. The SEM images reveal that CEM I 52.5 N used in this study when viewed at 50 X magnification (Figure 4.13 a) and 500 X magnification (Figure 4.13 b) settings is irregular if not angular in shape, it is also interlinked but has some micro-air spaces (dark/black spots (C) on Figure 4.13 b) separating the grains, thereby making the individual grains to be easily identified. The SF (Figure 4.14) is more closely packed (sticky) than the CEM I 52.5 N with no or little air spaces within the particles. Some large particles sizes can however be viewed in the pressed pellet of the SF (Figure 4.14 b). The CEM I 52.5 N SEM image revealed two grey scale levels for the particles (i.e. light grey (A) and dark grey (B) in Figure 4.13 b representing alite and belite respectively). The SEM image for SF show only one sticky grey colour (B) of Figure 4.14 b as background particles with some scattered white substance (D) all around, while the dark spots (C) were scanty too. The white substance should indicate presence of some ferrite or aluminate and the grey should be majorly silica.

The SEM images of CS and FA (Figures 4.15 and 4.16) show two distinct features despite their similarity by physical visualisation. CS particles are majorly angular while the FA particles are spherical in shape. CS particles are similar in shape to the CEM I 52.5 N; they inter-connect too with micro-air spaces (C) within the grains. The CS particles (Figure 4.15 b) are also dominantly of one grey colour (B) with some white substance (D) within. This also indicates the presence of ferrite or aluminate in a supposed majorly calcium and silicon composition. The FA particles (Figure 4.16) being spherical can be identified clearly as individual particles and has many large pieces with hollow

spheres (C) within which according to Ramezani-pour (2014) contain smaller particles. They are of one grey colour scale (B) and show presence of dispersed white substances (D) too.

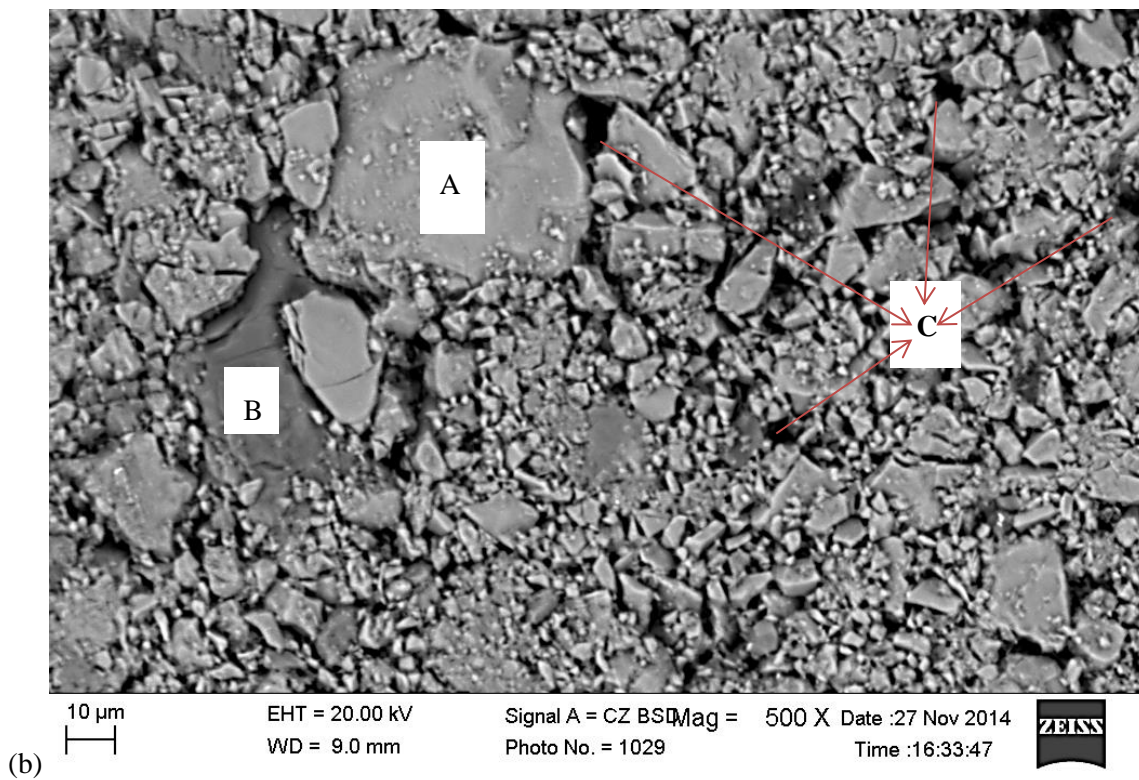
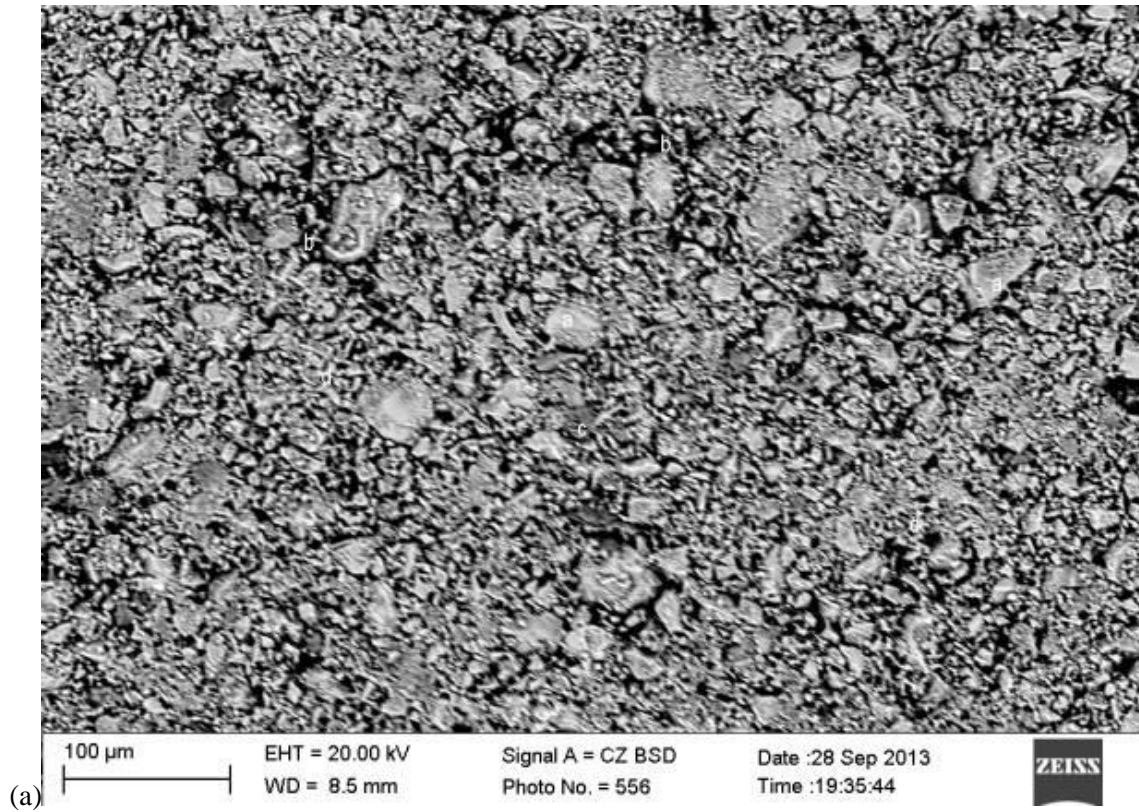


Figure 4-13: SEM image of microstructure of CEM I 52.5 N (a) 50 X and (b) 500 X magnifications

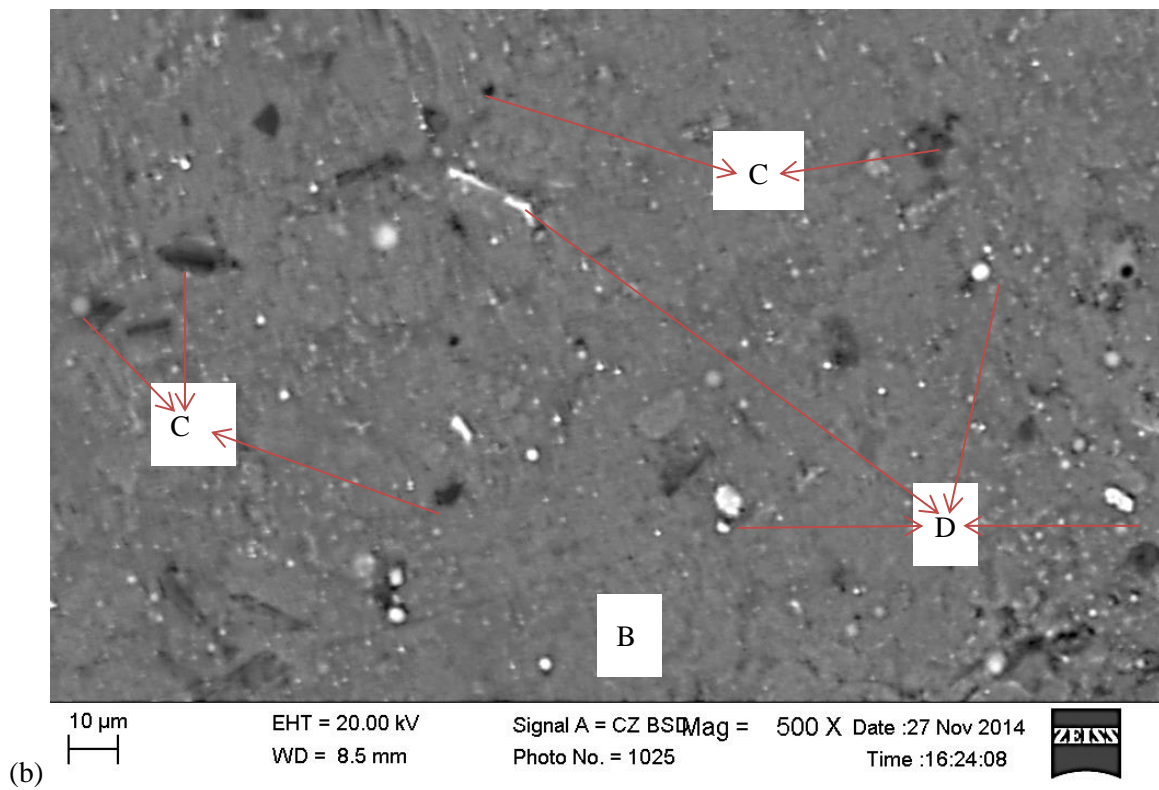
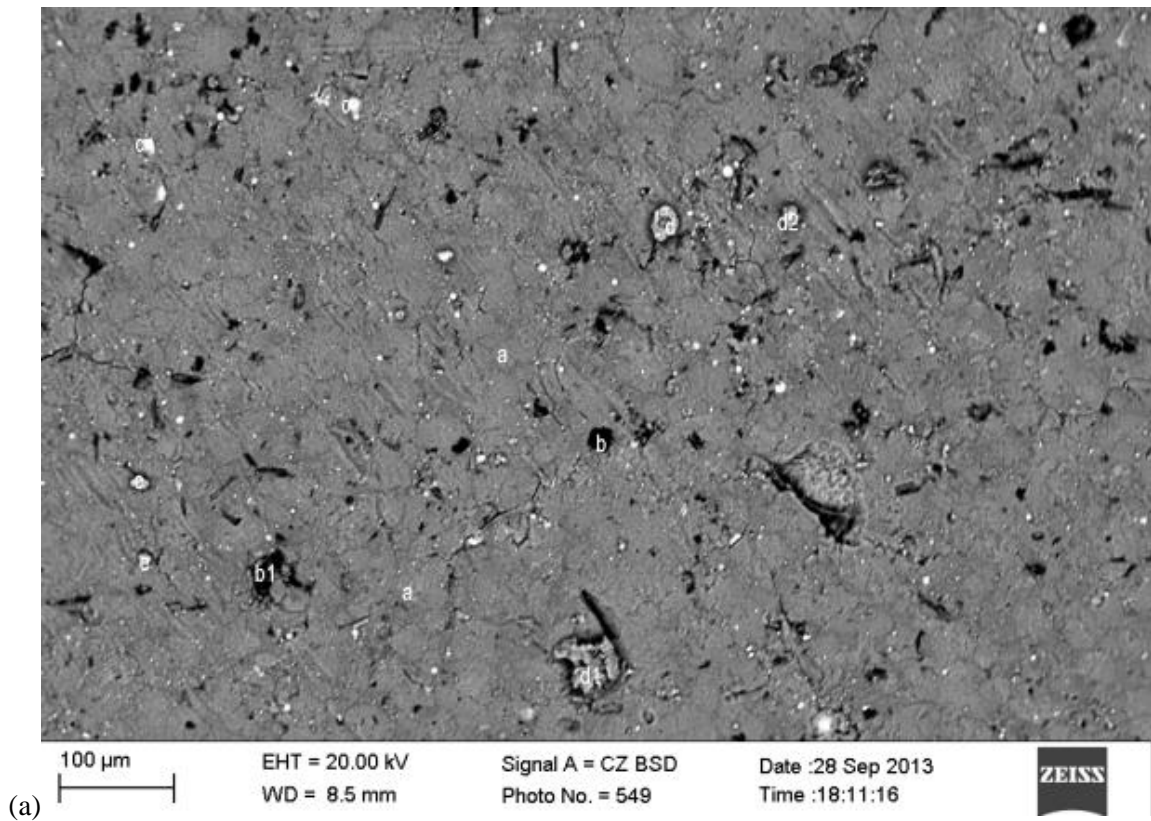


Figure 4-14: SEM image of microstructure of SF (a) 50 X and (b) 500 X magnifications

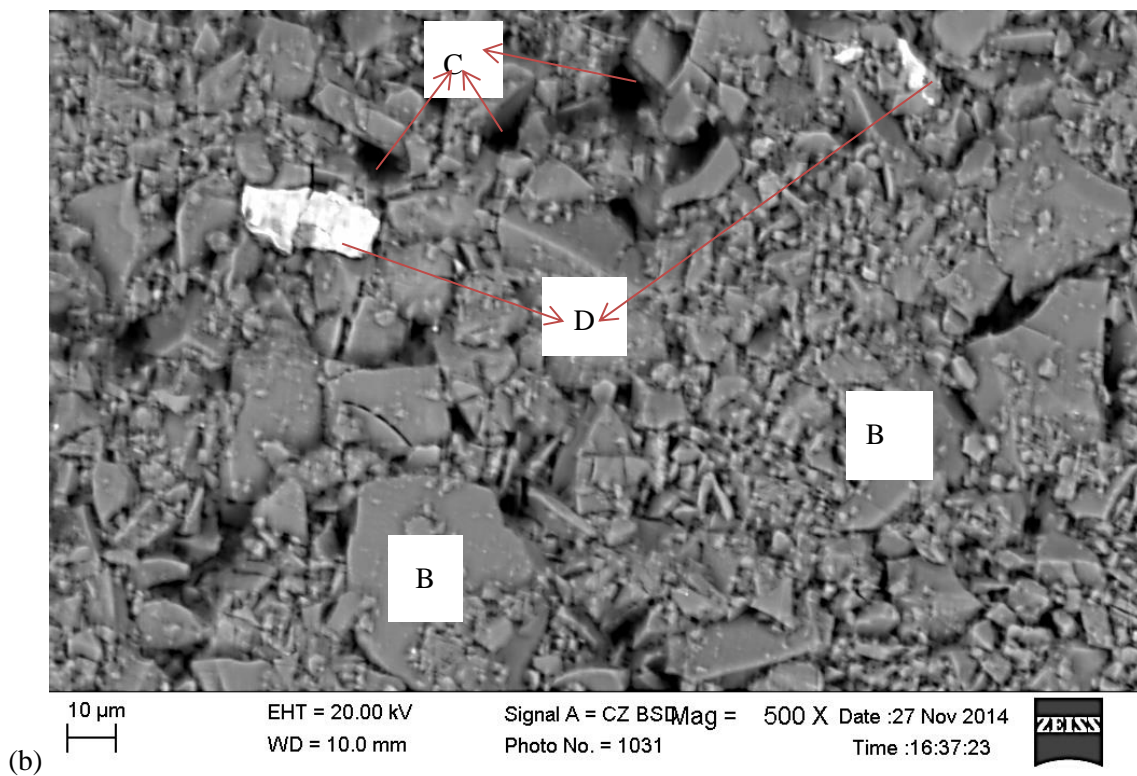
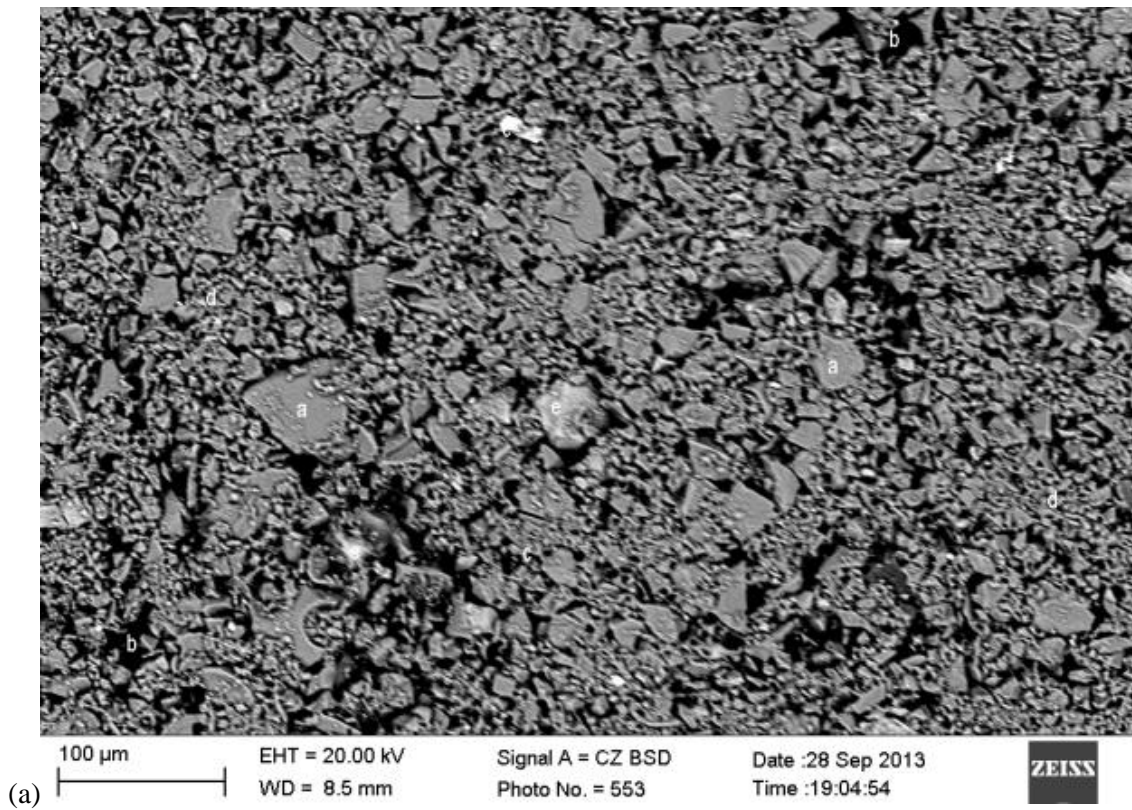
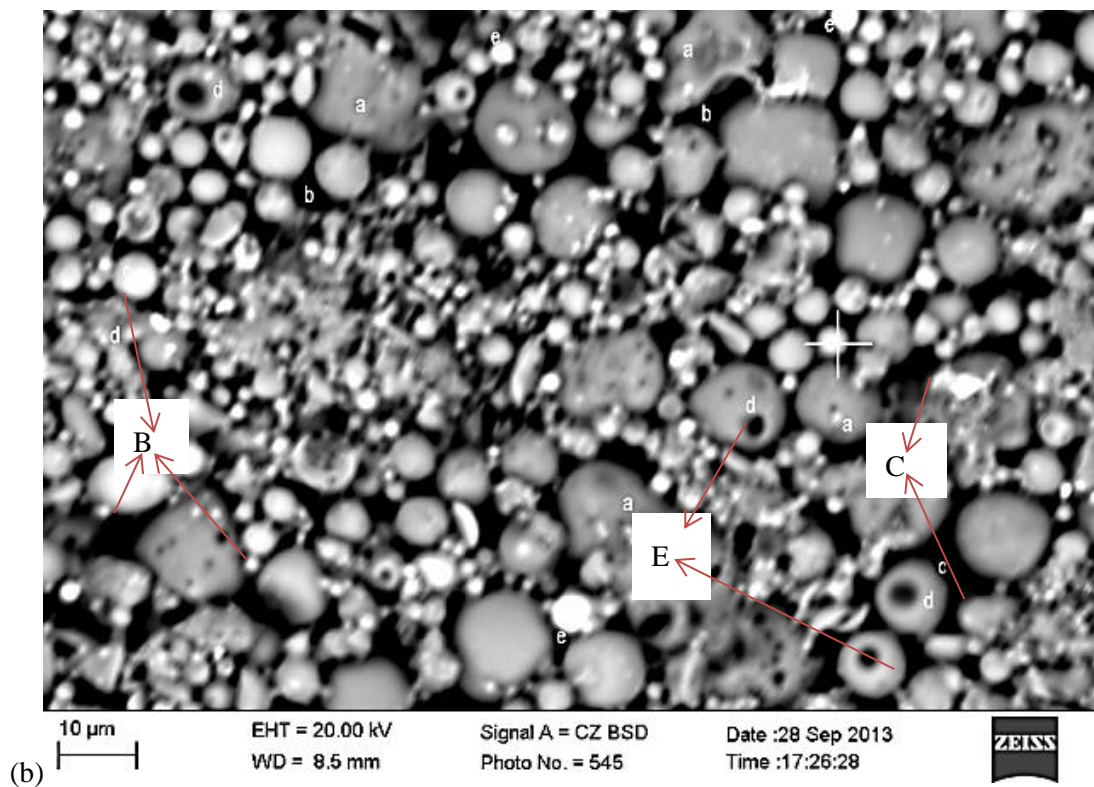
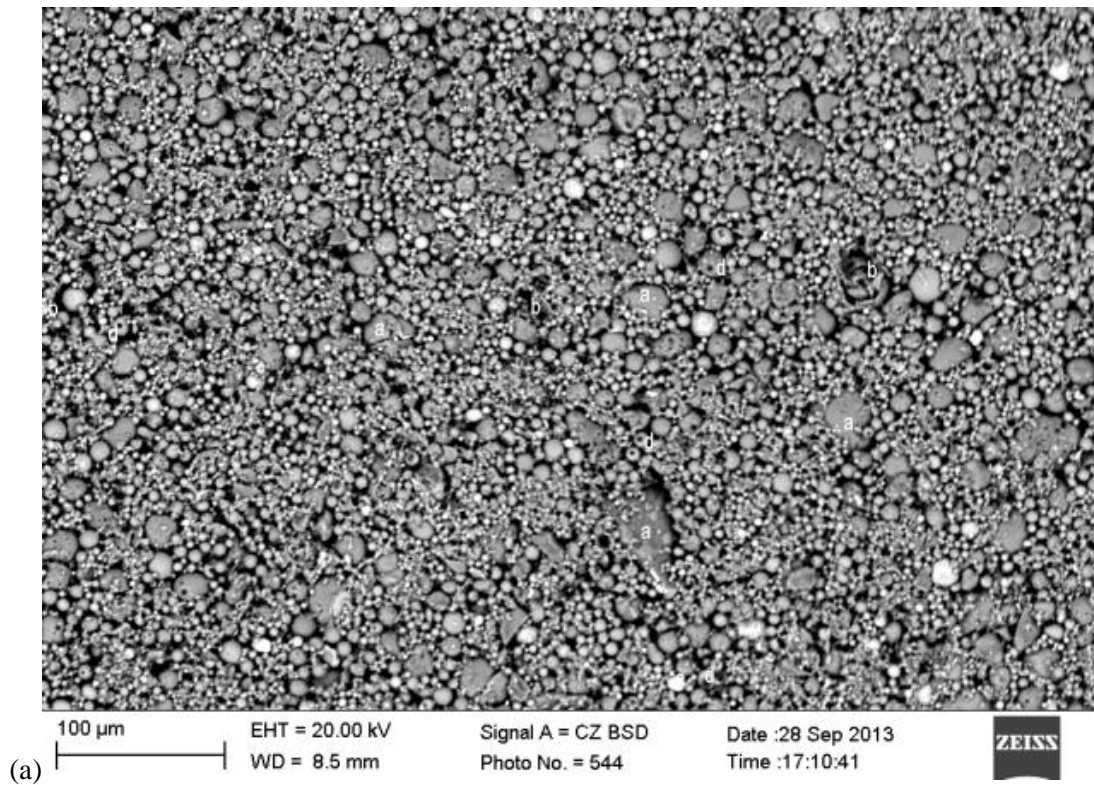


Figure 4-15: SEM image of microstructure of CS (a) 50 X and (b) 500 X magnifications



**Figure 4-16: SEM image of FA (a) 50 X and (b) 500 X magnifications**

The FA being spherical and having more inter-grain spaces could possibly explain their low water demand in concrete than the SF and the ability to enhance better workability in concrete.

The dry SAP particles were however observed under the SEM (Figure 4.17) as irregular (mostly angular) in shape with SP<sub>1</sub> been about 300 µm maximum diametric size (Figure 4.17a) while SP<sub>2</sub> is slightly above 400 µm in size (Figure 4.17b).

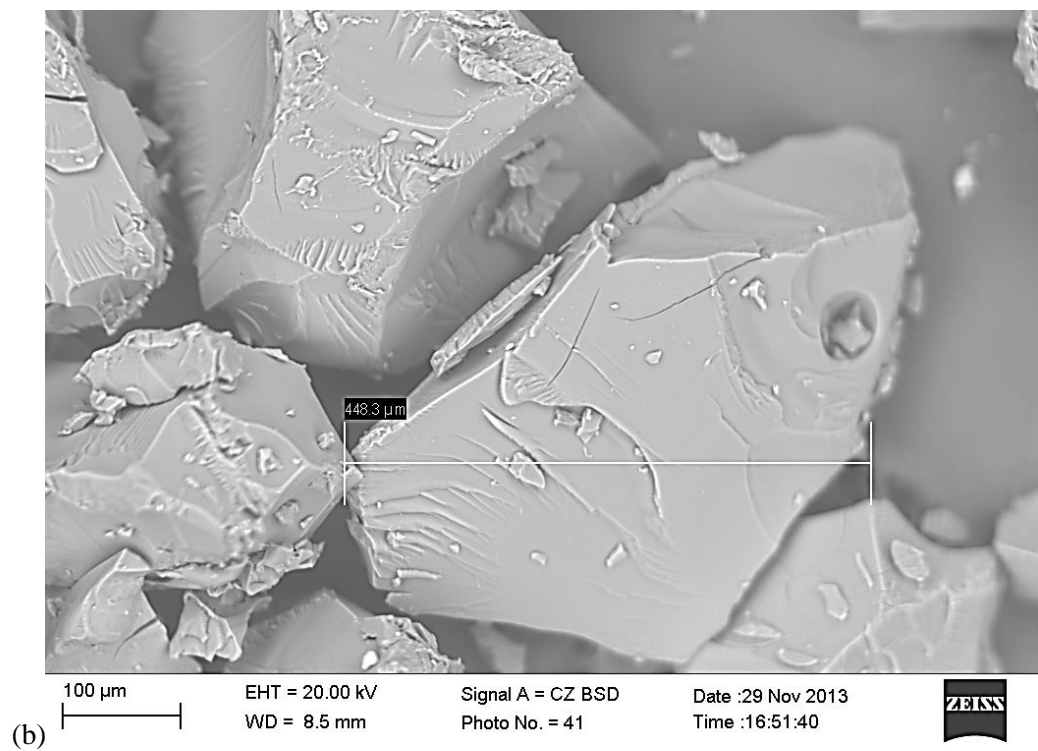
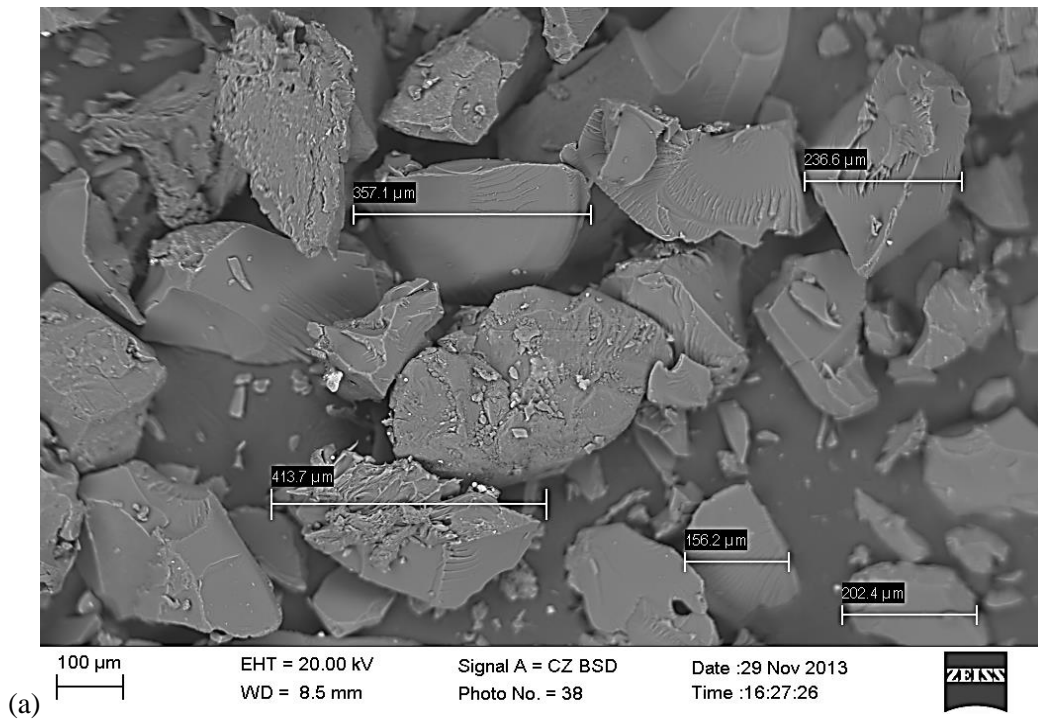


**Figure 4-17: SEM image SAP particles (a) SP<sub>1</sub> and (b) SP<sub>2</sub>**

#### 4.4.1.2 SEM/WDS composition analysis

EDX/WDS carried out for area analysis of each pellet gives an indication of the chemical composition of the various binder constituents (CEM I 52.5 N, SF, FA and CS) used in this study. It further helps to ascertain their possible effect on strength development of the HPC mixtures both at the early age and long term.

A typical spectra image of SEM/WDS area analysis is shown in Figure 4.18 while Table 4.5 presents the results of SEM/BSE analysis of the binders in compound (oxide)% composition.

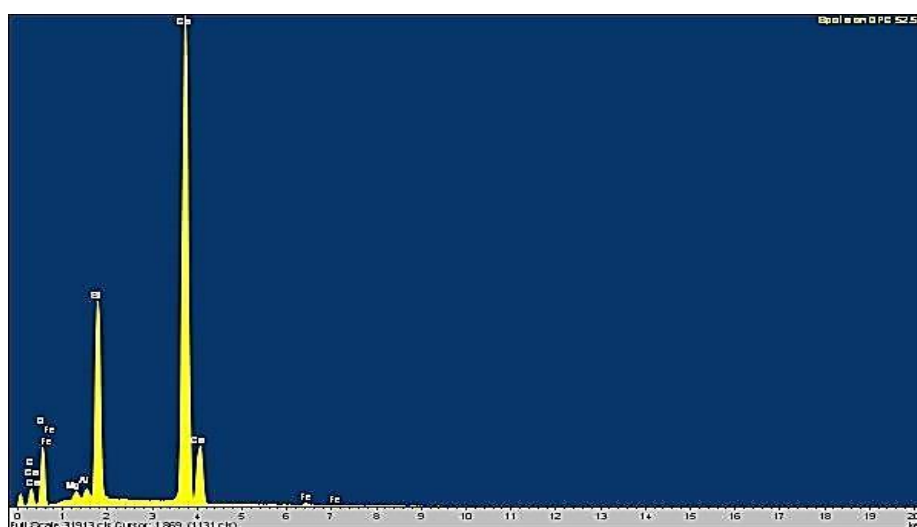


Figure 4-18: Typical spectra image of SEM/WDS analysis of Binders (CEM I 52.5 N52.5 N)

Table 4-5: Oxides composition of the binders obtained through SEM/BSE

Oxide (%)	Binder			
	CEM I 52.5N	SF	CS	FA
Na <sub>2</sub> O	0.45	1.78	0.00	0.40
MgO	0.97	1.67	9.52	0.97
Al <sub>2</sub> O <sub>3</sub>	3.18	0.53	12.37	29.93
SiO <sub>2</sub>	17.53	77.90	27.61	52.07
P <sub>2</sub> O <sub>5</sub>	0.00	0.00	0.00	0.57
SO <sub>3</sub>	4.73	5.66	3.37	2.26
K <sub>2</sub> O	1.96	7.78	0.50	0.99
CaO	68.57	2.00	45.56	7.17
TiO <sub>2</sub>	0.00	0.00	0.43	0.00
Fe <sub>2</sub> O <sub>3</sub> *	2.60	1.98	0.63	3.81
Others	0.00	0.70	0.00	1.84
SiO <sub>2</sub> +Al <sub>2</sub> O <sub>3</sub> +Fe <sub>2</sub> O <sub>3</sub>		80.41	40.62	85.81
CaO+(SiO <sub>2</sub> +Al <sub>2</sub> O <sub>3</sub> +Fe <sub>2</sub> O <sub>3</sub> )	91.88	82.41	86.17	92.97
Total	100.00	100.00	100.00	100.00

\*Fe<sub>2</sub>O<sub>3</sub> as shown here represents total Iron Oxides (Fe<sub>2</sub>O<sub>3</sub>; Fe<sub>3</sub>O<sub>4</sub> and FeO) composition as the variant of these oxides of Iron cannot be separated in such analyses as a SEM. Hence the “sameness” specification for mill scale as provided in literature (TWG117) is adopted.

#### 4.4.2 Chemical composition of constituent materials and HPC mortar

Figure 4.19 presents the result of FTIR analysis carried out to determine the amorphous silica content of the various cementitious material. The SF was noted to be dominantly silica with all the constituents' being amorphous. This agrees well with reports in literature (Siddique & Khan, 2011). The SF can therefore be taken as a standard for all the binders examined. CS and FA reflect typically equal contents of amorphous silica (about 35% of SF) as shown in Figure 4.19 at the 1000 wavelength scale of absorbance. The CEM I 52.5 N on the other hand has very low content of amorphous silica (about 15%). CEM I 52.5 N however shows also high amounts of other light compounds (at 1500 wavelength) which is possibly believed to be Calcium oxide. The FTIR spectra agree well with the SEM BSE/WDS image analysis of Table 4.5.

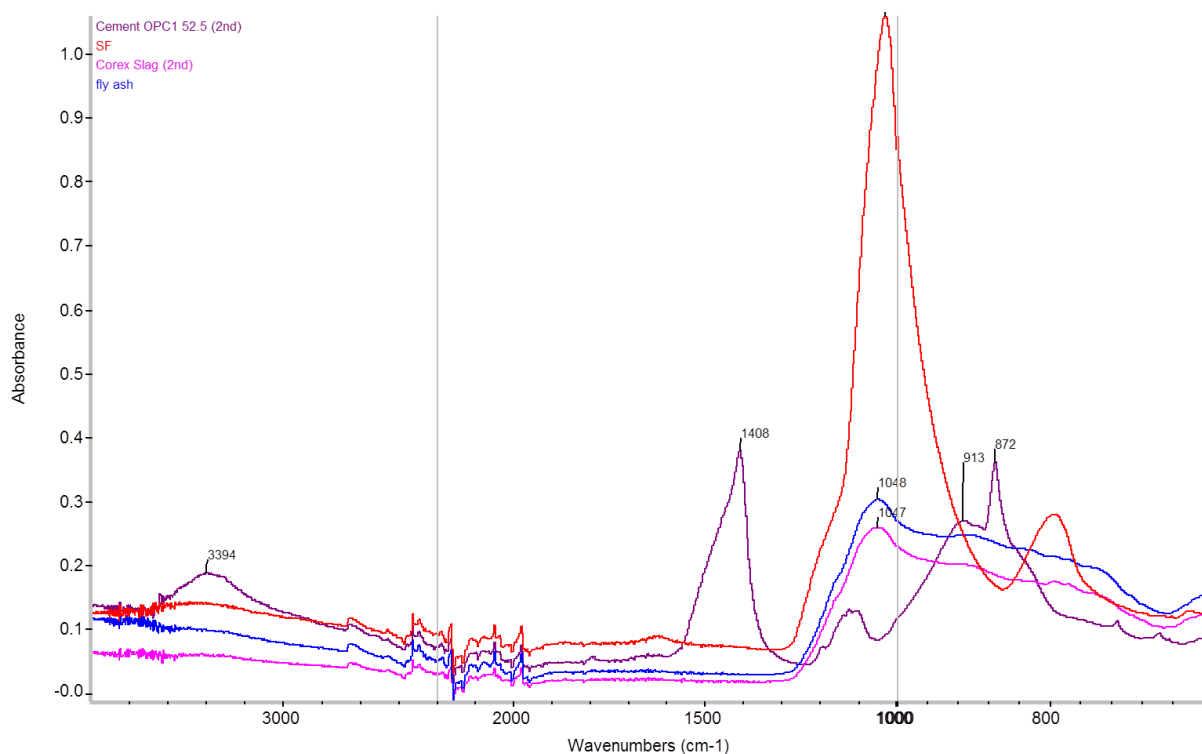


**Figure 4-19: Fourier Infra-Red (FTIR) spectroscopy spectra of the binders (CEM I 52.5, SF, FA and CS)**

The SAP particles according to these results serve purely as internal water reservoirs within the concrete samples.

## 4.5 Discussion

Using a statistical package SPSS to plot all the early-age compressive strength values of the HPC against curing age as shown in Figure 4.20 reflects that a positive correlation exists between the early-age compressive strength and the curing age and also the SAP content.

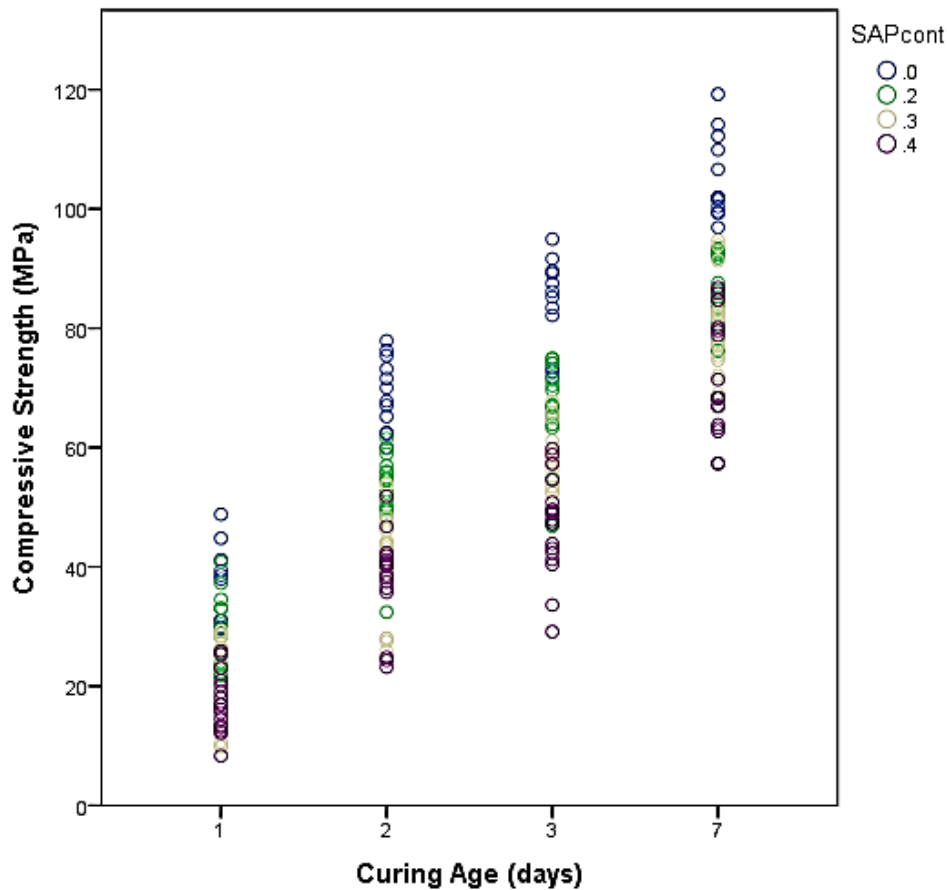


**Figure 4-20: Early-age compressive strength of all HPC mixtures**

The influence of W/B, SAP type, SAP contents, binder types and curing age (called independent variables) were examined on the early-age compressive strength and density (dependent variables) of the HPC mixtures as reported above using statistics (general linear model - multivariate) and presented in Table 4.8. This is to examine which of the independent variables had a significant effect on compressive strength and density of the HPC mixtures. The statistical analysis indicated that all the independent factors when considered individually had significant effect on both the compressive strength and density of the HPC at 95% confidence level ( $\alpha = 0.05$ ) except SAP type (asterisks (\*<sup>1</sup>) in Table 4.6) which was observed not to be significant on density.

**Table 4-6: Test between Subject Effects**

Source	Dependent Variable	Type III Sum of Squares	df*	Mean Square*	F*	Sig*.
Corrected Model	Density	851676.317 <sup>a</sup>	87	9789.383	15.952	.000
	CompStr*	163965.516 <sup>b</sup>	87	1884.661	145.939	.000
Intercept	Density	1.231E9	1	1.231E9	2.006E6	.000
	CompStr	746067.635	1	746067.635	5.777E4	.000
Single Factor Analysis						
W/B	Density	45187.574	1	45187.574	73.633	.000
	CompStr	155.821	1	155.821	12.066	.001
SAP content	Density	130580.880	2	65290.440	106.391	.000
	CompStr	5888.988	2	2944.494	228.008	.000
SAP type	Density	929.742	1	929.742	1.515	.220* <sup>1</sup>
	CompStr	168.627	1	168.627	13.058	.000
Binder type	Density	4404.767	1	4404.767	7.178	.008
	CompStr	1065.361	1	1065.361	82.497	.000
Curing Age	Density	12149.593	3	4049.864	6.599	.000
	CompStr	112201.203	3	37400.401	2.896E3	.000
Two Factor Analysis						
W/B * SAP content	Density	3954.613	2	1977.307	3.222	.042
	CompStr	133.905	2	66.952	5.184	.006
W/B * Curing Age	Density	10661.544	3	3553.848	5.791	.001
	CompStr	33.890	3	11.297	.875	.455* <sup>2</sup>
SAP content * SAP type	Density	3529.390	2	1764.695	2.876	.059* <sup>3</sup>
	CompStr	643.170	2	321.585	24.902	.000
SAP content * Binder type	Density	3423.694	2	1711.847	2.789	.064* <sup>3</sup>
	CompStr	15.174	2	7.587	.588	.557* <sup>2</sup>
SAP content * Curing Age	Density	6867.958	6	1144.660	1.865	.089* <sup>3</sup>
	CompStr	421.462	6	70.244	5.439	.000
SAP type * Curing Age	Density	5553.567	3	1851.189	3.017	.031
	CompStr	115.925	3	38.642	2.992	.032
Binder type * Curing Age	Density	3707.632	3	1235.877	2.014	.114
	CompStr	350.027	3	116.676	9.035	.000
Three Factor Analysis						
W/B * SAP content * Curing Age	Density	4143.662	6	690.610	1.125	.349* <sup>4</sup>
	CompStr	172.780	6	28.797	2.230	.042
SAP content * SAP type * Curing Age	Density	3523.855	6	587.309	.957	.456* <sup>4</sup>
	CompStr	838.667	6	139.778	10.824	.000
SAP content * Binder type * Curing Age	Density	2985.501	6	497.584	.811	.563* <sup>4</sup>
	CompStr	227.861	6	37.977	2.941	.009
Error	Density	108008.820	176	613.686		
	CompStr	2272.865	176	12.914		
Total	Density	1.371E9	264			
	CompStr	955301.926	264			
Corrected Total	Density	959685.137	263			
	CompStr	166238.382	263			

a. R Squared = .887 (Adjusted R Squared = .832)

b. R Squared = .986 (Adjusted R Squared = .980)

\*CompStr = Compressive strength, df = degrees of freedom, F = F-ratio, Sig. = exact significance level.

This implies that whenever any of the factors (W/B, SAP type, SAP contents, binder types and curing age) vary, the compressive strength and density also changes except for SAP type. The degree of variation is proportional to the magnitude of the change. The coefficient of determination (adjusted R-Square value) obtained from the analysis was 0.986 (98.6%) for early-age compressive strength and 0.887 (88.7%) for density. This suggests strong statistical association between each independent variable and the dependent variables. The independent variables were estimated to account for 98.6% of the variance in the compressive strength of the concrete. The coefficient of correlation was obtained as  $R = 0.98$ . This implies strong correlation or linear relationship existing between the two sets of variables being considered.

An examination of influence of the interaction between two and three independent variables on early-age compressive strength (referred to as two and three factor analysis) reveals that all – except two scenarios (combined effect of W/B with curing age & SAP content with binder type as shown with asterisks (\*<sup>2</sup>), Table 4.6) – are all significant. It can therefore be inferred that all the fixed factors individually and combined had significant effect on early-age compressive strength while only SAP type as an independent variable does not have significant effect on the density of HPC. Two factor analysis of density reflects a shared situation of three sets of combination significant (asterisks (\*<sup>3</sup>)) and the other three not significant while the three factor analysis on density shows all (asterisk (\*<sup>4</sup>)) the respective combinations as not significant.

The Duncan's multiple range post-hoc test (Tables 4.7 to 4.11) – which is a multiple comparison procedure in statistics used to examine set of means – was also conducted for comparison of the sets of means amongst the independent variables (W/B, binder type, SAP contents, SAP types, and curing age) and their effect on the early age compressive strength of HPCs. The test reveals that the mean early-age compressive strength does not show any significant difference for the various groupings (whether on basis of W/B, SAP content, SAP type, or curing age).

**Table 4-7: Duncan's multiple range test (W/B effect on Early-age Compressive Strength)**

W/B	N	Subset	
		1	2
0.2	132	5.408176E1	
0.3	48	5.471719E1	5.471719E1
0.25	84		5.556938E1
Sig.		.282	.150

**Table 4-8: Duncan's multiple range test (Binder type effect on Early-age Compressive Strength)**

Binder type	N	Subset	
		1	2
2	48	5.375941E1	
3	84	5.426595E1	5.426595E1
1	132		5.525949E1
Sig.		.391	.093

**Table 4-9: Duncan's multiple range test (SAP contents effect on Early-age Compressive Strength)**

SAP content	N	Subset			
		1	2	3	4
0.4	72	4.328406E1			
0.3	72		5.050547E1		
0.2	72			5.762353E1	
0	48				7.356882E1
Sig.		1.000	1.000	1.000	1.000

**Table 4-10: Duncan's multiple range test (SAP type effect on Early-age Compressive Strength)**

SAP type	N	Subset	
		1	2
2	72	5.010426E1	
1	144	5.065440E1	
0	48		7.356882E1
Sig.		.360	1.000

**Table 4-11: Duncan's multiple range test (Curing Age effect on Early-age Compressive Strength)**

Curing Age	N	Subset			
		1	2	3	4
1	66	2.427844E1			
2	66		4.869777E1		
3	66			6.166292E1	
7	66				8.404336E1
Sig.		1.000	1.000	1.000	1.000

Means for groups in homogeneous subsets are displayed based on observed means.  
The error term is Mean Square (Error) = 12.914.

The result of the microstructure and chemical composition as shown in Section 4.5 revealed that the finer particles of CEM I 52.5 N, FA and CS contribute to the high strength development in the HPC. The FA and CS introduction in the ternary cements HPC ( $M_{1S}$  and  $M_{1F}$ ) led to low W/B of 0.2 without this it would have been impossible to achieve this particular mixture. SF presence in the HPC mixtures was responsible for the sticky nature always experienced in HPC mixtures. The microstructure of the SF revealing very sticky nature (composing grains of very high fineness) with difficulty in identifying individual particles affirms the nature of this admixture and its effect in concrete. This is also in agreement with the BET specific surface area analysis which shows higher surface area for SF particles than the other cementitious materials – indicative of its very fine grain sizes. The result obtained from the laser diffraction PSD analysis can therefore not be relied upon for SF as literature states some inherent limiting factors on use of laser diffraction for PSD in samples of some particle sizes especially below 1  $\mu\text{m}$  (Kowalenko and Babuin, 2013; Di Stefano et al., 2010). The chemical composition of SF shows high amorphous silica content and thereby explains its ability at resulting in higher early strength especially in the first two days. The early strength can also be attributed to the higher fineness of the SF particles. The high amorphous  $\text{SiO}_2$  content effectively reacts fast with the excess lime ( $\text{CaOH}$ ) liberated from the CEM I 52.5 N while the FA and CS (known to be of latent hydraulic reaction) take a longer time for the pozzolanic reaction. The spherical nature of the FA contributed to the air spaces within the individual particles while CS larger particle grains also enhance good workability of concrete containing CS and enhance its contribution to lower water demand than SF. The CS and FA were noted to be very different in chemical composition. While FA used in this study is majorly  $\text{SiO}_2$  (52.1%) and  $\text{Al}_2\text{O}_3$  (29.9%), the CS is mainly  $\text{CaO}$  (45.6%) and  $\text{SiO}_2$  (27.1%). The ternary cements-HPC made from CS had higher initial strength and similar rate of early age cement hydration as the FA based ternary cement-HPC. It will be of interest to assess how this transfer to the final strength development at concrete maturity. The Kinetic of hydration (B) for all the HPC mixtures however remains within the same range at this early age and conforms to the relationship as reported in literature for this class of concrete (i.e. SF-concretes).

# 5

## *Mechanical Properties of HPC with SAP*

This chapter reports the outcome of the experimental work carried out on the mechanical properties of HPC containing SAP as IC-agents. The respective major tests are presented as sub-sections with proper discussion made while efforts were also made to curve-fit the results with a view at assessing the influence of SAP on the mechanical properties of the HPC.

### **5.1 Compressive Strength of HPC with SAP**

Results and discussion of compressive strength conducted are presented in the following sections.

#### **5.1.1 Results**

Tables 5.1 and 5.2 present the density of binary and ternary cements – HPCs (respectively) as influenced by SAP addition with the SAP porosity factor calculated in comparison with the average demoulded density of the twelve specimens for the respective reference mixtures. It is observed that there is a general trend of slight decrease in the density of the HPCs as the SAP contents increase. This is seen as a reflection that SAP addition led to increased porosity in the HPC as calculated for in Table 4.1 of Section 4.3.1. The observed porosity increase is in agreement with the expectation of literature for SAP-modified concrete (Mehtcherine & Reinhardt, 2012).

Results of compressive strength development over the hydration periods (7, 28, 56 and 90 days) studied for the various HPC mixtures with SAP (SP<sub>1</sub> and SP<sub>2</sub>) added as IC-agent are presented in Figures 5.1 to 5.4 while Tables 5.3 (binary cement HPC) and 5.4 (ternary cement HPC) gives the comparative compressive strength (i.e. the strength factor) values with references to the 28 day strength of control mixtures in parentheses under the compressive strength values.

**Table 5-1: Density of Binary cements - HPC with SAP**

Curing Age	Density (kg/m <sup>3</sup> )				SAP Porosity factor (%)*			
	7 days	28 days	56 days	90 days	7 days	28 days	56 days	90 days
M <sub>2</sub>	2504	2495	2494	2494	100.7	100.4	100.3	100.3
M <sub>2</sub> SP <sub>1</sub> -0.2	2472	2461	2468	2473	99.4	99.0	99.3	99.5
M <sub>2</sub> SP <sub>1</sub> -0.3	2431	2436	2441	2460	97.8	98.0	98.2	99.0
M <sub>2</sub> SP <sub>1</sub> -0.4	2413	2404	2422	2418	97.1	96.7	97.4	97.3
M <sub>2</sub> SP <sub>2</sub> -0.2	2477	2478	2488	2475	99.6	99.7	100.1	99.6
M <sub>2</sub> SP <sub>2</sub> -0.3	2431	2428	2434	2428	97.8	97.7	97.9	97.7
M <sub>2</sub> SP <sub>2</sub> -0.4	2424	2429	2417	2425	97.5	97.7	97.2	97.6
M <sub>3</sub>	2432	2431	2434	2423	100.8	100.7	100.9	100.4
M <sub>3</sub> SP <sub>1</sub> -0.2	2406	2416	2414	2421	99.7	100.2	100.0	100.4
M <sub>3</sub> SP <sub>1</sub> -0.3	2358	2341	2362	2372	97.8	97.0	97.9	98.3
M <sub>3</sub> SP <sub>1</sub> -0.4	2366	2366	2381	2377	98.1	98.1	98.7	98.5
M <sub>3</sub> SP <sub>2</sub> -0.2	2402	2412	2386	2398	99.6	100.0	98.9	99.4
M <sub>3</sub> SP <sub>2</sub> -0.3	2409	2408	2393	2409	99.9	99.8	99.2	99.9
M <sub>3</sub> SP <sub>2</sub> -0.4	2357	2360	2326	2340	97.7	97.8	96.4	97.0

\*SAP porosity factor is calculated as a percentage in relation to average of Demoulded density of the twelve specimens of references HPC mixtures. SAP porosity is therefore 1 - SAP porosity factor.

**Table 5-2: Density of Ternary cements - HPC with SAP**

Curing Age	Density (kg/m <sup>3</sup> )				SAP Porosity factor (%)*			
	7 days	28 days	56 days	90 days	7 days	28 days	56 days	90 days
M <sub>1S</sub>	2486	2510	2503	2521	99.5	100.5	100.2	100.9
M <sub>1S</sub> SP <sub>1</sub> -0.2	2440	2449	2440	2453	97.7	98.0	97.7	98.2
M <sub>1S</sub> SP <sub>1</sub> -0.3	2437	2458	2473	2435	97.6	98.4	99.0	97.5
M <sub>1S</sub> SP <sub>1</sub> -0.4	2420	2432	2448	2451	96.9	97.4	98.0	98.1
M <sub>1S</sub> SP <sub>2</sub> -0.2	2471	2468	2397	2426	98.9	98.8	96.0	97.1
M <sub>1S</sub> SP <sub>2</sub> -0.3	2486	2438	2448	2445	99.5	97.6	98.0	97.9
M <sub>1S</sub> SP <sub>2</sub> -0.4	2436	2437	2416	2413	97.5	97.6	96.7	96.6
M <sub>1F</sub>	2494	2487	2488	2498	100.7	100.4	100.5	100.9
M <sub>1F</sub> SP <sub>1</sub> -0.2	2422	2440	2422	2445	97.8	98.5	97.8	98.7
M <sub>1F</sub> SP <sub>1</sub> -0.3	2394	2397	2395	2389	96.7	96.8	96.7	96.5
M <sub>1F</sub> SP <sub>1</sub> -0.4	2405	2412	2401	2402	97.1	97.4	97.0	97.0
M <sub>1F</sub> SP <sub>2</sub> -0.2	2456	2439	2419	2435	99.2	98.5	97.7	98.3
M <sub>1F</sub> SP <sub>2</sub> -0.3	2406	2406	2410	2412	97.2	97.2	97.3	97.4
M <sub>1F</sub> SP <sub>2</sub> -0.4	2407	2420	2416	2414	97.2	97.7	97.5	97.5

\*SAP porosity factor is calculated as a percentage in relation to average of demoulded density of the twelve specimens of references HPC mixtures. SAP porosity is therefore 1 - SAP porosity factor.

The result shows that compressive strength increases as the hydration rate increases at a decreasing rate for all the HPC mixtures. The strength however decreases as the SAP content increases for both SAP types. The strength factor indicates that for binary cement – HPCs (M<sub>2</sub> and M<sub>3</sub>), similar values as the 28-day strength of control specimen were attained for HPC containing SAP at the 90-day of curing up to 0.3% b<sub>wob</sub> SAP addition for both SAP types while the ternary cements – HPCs (M<sub>1F</sub> and M<sub>1S</sub>) attained similar and above the 28-day strength values for all mixtures (and all SAP contents studied) at the 90<sup>th</sup> day. Tables 5.3 and 5.4 (yellow highlights) show the various inconsistencies of the results as M<sub>3</sub>Sp<sub>1</sub>-03 (90 days), M<sub>3</sub>Sp<sub>2</sub>-0.3 (56 and 90 days) and M<sub>1F</sub>Sp<sub>1</sub>-0.2 (7days).

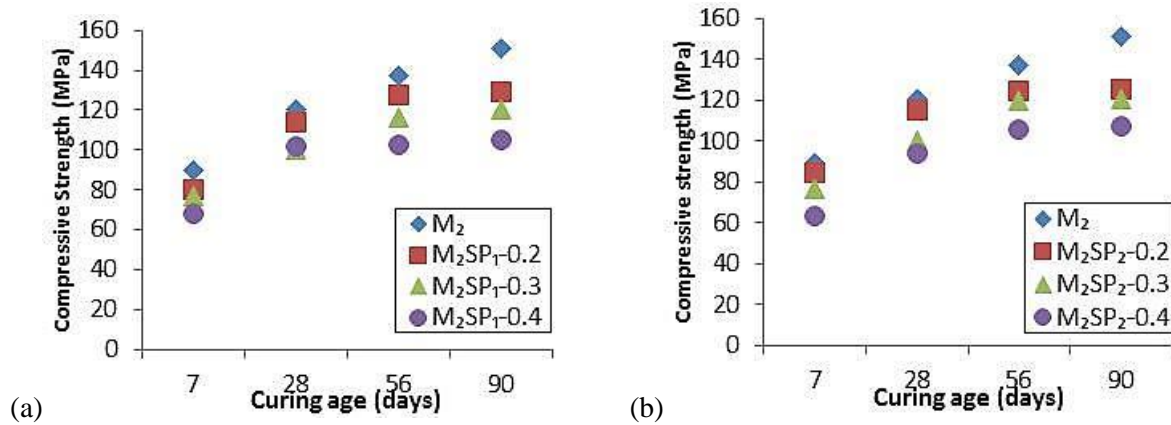
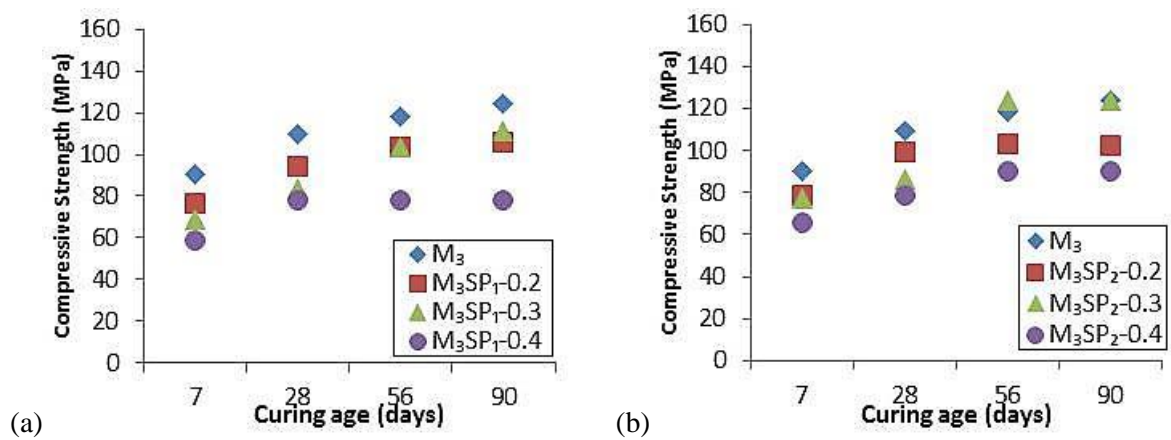

 Figure 5-1: Compressive Strength of M<sub>2</sub> - HPC (a) with SP<sub>1</sub> and (b) with SP<sub>2</sub>

 Figure 5-2: Compressive Strength of M<sub>3</sub> - HPC (a) with SP<sub>1</sub> and (b) with SP<sub>2</sub>

Table 5-3: Compressive Strength of Binary cements - HPC with SAP

Curing age	M <sub>2</sub> (Binder Type 1 (CEM I 52.5 N+ SF), 0.25 W/B)							
	Specimen	M <sub>2</sub>	M <sub>2</sub> SP <sub>1-0.2</sub>	M <sub>2</sub> SP <sub>1-0.3</sub>	M <sub>2</sub> SP <sub>1-0.4</sub>	M <sub>2</sub> SP <sub>2-0.2</sub>	M <sub>2</sub> SP <sub>2-0.3</sub>	M <sub>2</sub> SP <sub>2-0.4</sub>
7 Days	CompStr* (MPa)	89.46	79.94	76.70	68.01	84.66	76.70	63.18
	StrFac* (%)	74.26	66.36	63.67	56.45	70.27	63.66	52.45
	CoV* (%)	0.36	3.79	1.67	0.43	0.67	1.67	3.31
28Days	CompStr (MPa)	120.47	114.45	100.49	101.71	115.23	100.16	93.94
	StrFac (%)	100.00	95.00	83.41	84.43	95.65	83.14	77.98
	CoV (%)	2.92	2.64	2.54	3.80	3.03	2.70	7.31
56 days	CompStr (MPa)	136.97	127.25	116.27	102.50	124.37	120.12	105.54
	StrFac (%)	113.70	105.63	96.51	85.08	103.24	99.71	87.61
	CoV (%)	2.04	4.64	7.05	3.02	1.64	3.49	0.78
90 Days	CompStr (MPa)	151.19	129.41	119.95	104.86	125.08	120.82	107.07
	StrFac (%)	125.50	107.42	99.57	87.04	103.83	100.29	88.88
	CoV (%)	1.72	5.87	5.71	1.63	3.24	2.89	1.51
Curing age	M <sub>3</sub> (Binder Type 1 (CEM I 52.5 N+ SF), 0.3 W/B)							
	Specimen	M <sub>3</sub>	M <sub>3</sub> SP <sub>1-0.2</sub>	M <sub>3</sub> SP <sub>1-0.3</sub>	M <sub>3</sub> SP <sub>1-0.4</sub>	M <sub>3</sub> SP <sub>2-0.2</sub>	M <sub>3</sub> SP <sub>2-0.3</sub>	M <sub>3</sub> SP <sub>2-0.4</sub>
7 Days	CompStr (MPa)	90.3	76.8	68.9	58.9	78.9	77.3	65.7
	StrFac (%)	82.5	70.1	63.0	53.8	72.1	70.6	60.0
	CoV (%)	4.01	3.99	3.33	4.11	1.63	1.43	2.97
28Days	CompStr (MPa)	109.5	94.3	83.7	77.7	99.3	86.3	78.5
	StrFac (%)	100.0	86.1	76.5	71.0	90.7	78.8	71.7
	CoV (%)	6.51	8.11	1.16	3.93	1.61	1.94	1.93
56 days	CompStr (MPa)	118.3	103.3	103.8	78.1	103.5	123.6	90.0
	StrFac (%)	108.1	94.3	94.8	71.4	94.5	112.9	82.2
	CoV (%)	1.99	0.95	7.84	0.30	2.36	8.19	1.53
90 Days	CompStr (MPa)	124.0	106.0	111.3	78.4	102.8	123.7	90.4
	StrFac (%)	113.2	96.8	101.7	71.6	93.9	113.0	82.5
	CoV (%)	2.14	2.85	2.63	0.31	1.98	8.67	1.14

\*CompStr = Compressive Strength; StrFac = Strength factor i.e. relative compressive strength compare to 28 days strength; CoV = Coefficient of variation

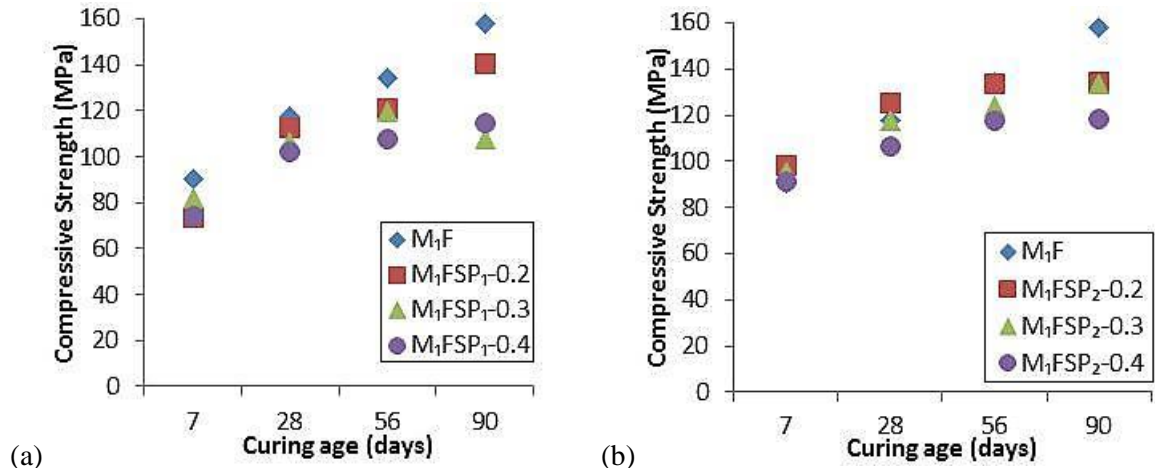


Figure 5-3: Compressive Strength of M<sub>1F</sub> – HPC (a) with SP<sub>1</sub> and (b) with SP<sub>2</sub>

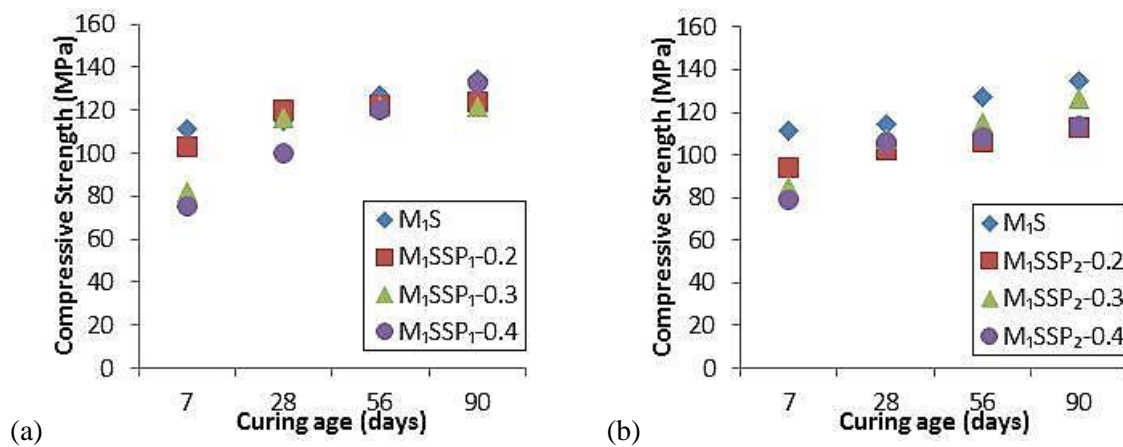


Figure 5-4: Compressive Strength of M<sub>1S</sub> – HPC (a) with SP<sub>1</sub> and (b) with SP<sub>2</sub>

Table 5-4: Compressive Strength of Ternary cements – HPC with SAP

Curing age	M <sub>1F</sub> (Binder Type 2 (CEM I 52.5 N+ SF + FA), 0.2 W/B)								
	Specimen	M <sub>1F</sub>	M <sub>1F</sub> SP <sub>1</sub> -0.2	M <sub>1F</sub> SP <sub>1</sub> -0.3	M <sub>1F</sub> SP <sub>1</sub> -0.4	M <sub>1F</sub> SP <sub>2</sub> -0.2	M <sub>1F</sub> SP <sub>2</sub> -0.3	M <sub>1F</sub> SP <sub>2</sub> -0.4	
7 Days	CompStr (MPa)	90.3	73.5	82.0	74.5	97.9	95.6	91.4	
	StrFac (%)	76.7	62.4	69.6	63.3	83.1	81.2	77.6	
	CoV (%)	2.35	1.65	3.42	1.96	2.06	4.08	1.21	
28Days	CompStr (MPa)	117.7	112.8	106.6	102.0	125.0	117.6	106.2	
	StrFac (%)	100.0	95.8	90.6	86.7	106.2	99.8	90.2	
	CoV (%)	8.74	4.96	4.36	3.50	5.06	1.26	2.02	
56 days	CompStr (MPa)	134.2	121.3	119.8	107.5	133.3	123.6	117.7	
	StrFac (%)	114.0	103.0	101.8	91.3	113.2	105.0	100.0	
	CoV (%)	0.56	0.56	2.91	0.19	2.44	1.86	3.00	
90 Days	CompStr (MPa)	157.8	140.6	121.2	114.8	134.6	133.3	118.5	
	StrFac (%)	134.0	119.4	103.0	97.5	114.3	113.2	100.6	
	CoV (%)	1.98	2.77	0.41	0.88	1.66	0.99	5.48	
Curing age	M <sub>1S</sub> (Binder Type 3 (CEM I 52.5 N+ SF + CS), 0.2 W/B)								
	Specimen	M <sub>1S</sub>	M <sub>1S</sub> SP <sub>1</sub> -0.2	M <sub>1S</sub> SP <sub>1</sub> -0.3	M <sub>1S</sub> SP <sub>1</sub> -0.4	M <sub>1S</sub> SP <sub>2</sub> -0.2	M <sub>1S</sub> SP <sub>2</sub> -0.3	M <sub>1S</sub> SP <sub>2</sub> -0.4	
7 Days	CompStr (MPa)	111.2	102.8	82.0	75.4	94.3	85.2	79.0	
	StrFac (%)	97.1	89.7	71.5	65.8	82.3	74.3	69.0	
	CoV (%)	2.42	1.93	2.27	0.39	2.23	0.39	2.38	
28Days	CompStr (MPa)	114.6	120.5	116.2	100.3	102.1	107.9	105.9	
	StrFac (%)	100.0	105.1	101.4	87.5	89.0	94.2	92.4	
	CoV (%)	1.10	0.98	0.73	6.47	1.20	3.15	2.06	
56 days	CompStr (MPa)	127.2	122.1	121.6	120.0	105.8	115.2	108.5	
	StrFac (%)	111.0	106.6	106.1	104.7	92.3	100.5	94.7	
	CoV (%)	3.61	1.57	2.79	4.43	2.62	2.54	3.02	
90 Days	CompStr (MPa)	134.7	123.9	121.8	133.1	112.9	126.2	113.5	
	StrFac (%)	117.5	108.1	106.3	116.1	98.5	110.1	99.1	
	CoV (%)	3.90	0.80	1.88	4.21	2.68	1.76	0.94	

\*CompStr = Compressive Strength; StrFac = Strength factor i.e. relative compressive strength compare to 28 days strength; CoV = Coefficient of variation

The coefficient of variation (CoV) of the compressive strength values was found to be below (8.67) with one of the non-conforming values ( $M_3SP_20.3$ ) having the highest CoV value. The trend of the results of compressive strength is in agreement with the findings of previous researchers (Mechtcherine et al., 2009; Dudziak & Mechtcherine, 2008; Hasholt et al., 2012) for moderate SAP application and extra water provided for SAP absorption.

### 5.1.2 Discussion

Examining the results obtained from the experiment (Table 5.1 and 5.2) reveals that density of this concrete type just like the compressive strength is influenced by the SAP contents. Though the density can be taken as stable over the curing ages, it decreases at relatively small proportion to the increase in SAP content, an indication that SAP addition also contributes to the air content in the concrete. Although the density for all the HPCs containing SAP studied were observed as still within the weight classification of normal weight concrete (as found in Dehn, (2012)). The density values fall within the  $2300 \text{ kg/m}^3$  to  $2500 \text{ kg/m}^3$  range as shown in Figure 5.5 with an indication of negative correlation between the density and SAP contents of the HPCs.

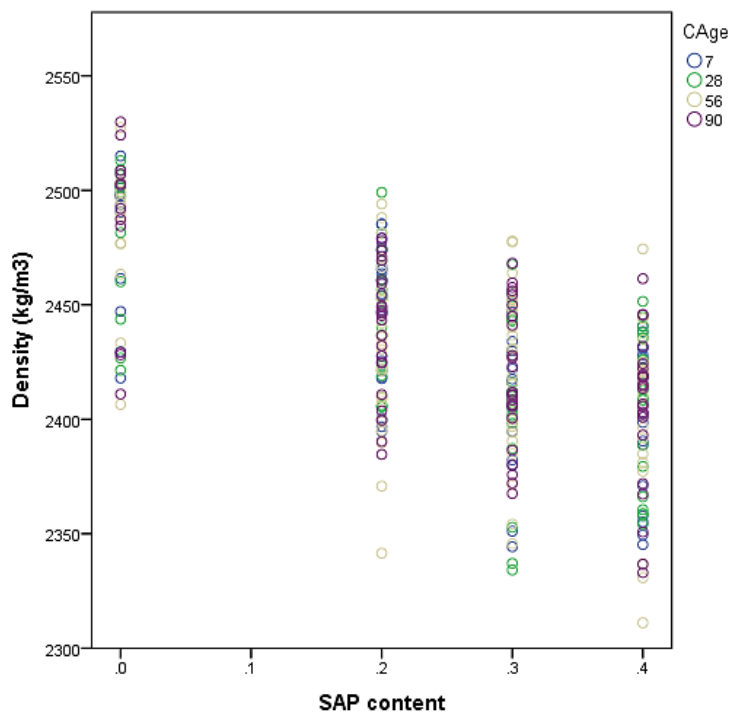


Figure 5-5: Influence of SAP contents on the density of HPC

General linear model – univariate analysis for each dependent variable reveal that three individual variables (W/B, SAP contents and binder type) had significant effect on the density of the HPCs while effects of two individual variable (SAP type and curing age) on density are observed to be insignificant (yellow highlights on Table 5.5).

**Table 5-5: Between Effect Test for Density**

Source	Type III Sum of Squares	df	Mean Square	F	Sig.
Corrected Model	502803.308 <sup>a</sup>	111	4529.760	22.609	.000
Intercept	1.822E9	1	1.822E9	9.094E6	.000
Single Factor Analysis					
W/B	146476.640	1	146476.640	731.084	.000
SAP content	59022.443	2	29511.221	147.294	.000
SAP type	215.991	1	215.991	1.078	.300
Binder type	19107.362	1	19107.362	95.367	.000
Curing Age	916.722	3	305.574	1.525	.209
Two Factor Analysis					
W/B * SAP content	784.656	2	392.328	1.958	.144
W/B * SAP type	30.963	1	30.963	.155	.695
W/B * Curing Age	281.134	3	93.711	.468	.705
SAP content * SAP type	3264.746	2	1632.373	8.147	.000
SAP content * Binder type	8684.169	2	4342.084	21.672	.000
SAP content * Curing Age	3949.016	6	658.169	3.285	.004
SAP type * Binder type	2811.571	1	2811.571	14.033	.000
SAP type * Curing Age	6440.944	3	2146.981	10.716	.000
Binder type * Curing Age	414.293	3	138.098	.689	.559
Three Factor Analysis					
W/B * SAP content * SAP type	16390.177	2	8195.088	40.903	.000
W/B * SAP content * Curing Age	596.292	6	99.382	.496	.811
W/B * SAP type * Curing Age	1218.247	3	406.082	2.027	.111
SAP content * SAP type * Binder type	284.560	2	142.280	.710	.493
SAP content * SAP type * Curing Age	1342.967	6	223.828	1.117	.353
SAP content * Binder type * Curing Age	1544.681	6	257.447	1.285	.265
SAP type * Binder type * Curing Age	2812.523	3	937.508	4.679	.003
Four Factor Analysis					
W/B * SAP content * SAP type * Curing Age	579.354	6	96.559	.482	.821
SAP content * SAP type * Binder type * Curing Age	1443.414	6	240.569	1.201	.307
Error	44879.590	224	200.355		
Total	1.983E9	336			
Corrected Total	547682.897	335			

a. R Squared = .918 (Adjusted R Squared = .877)

Two factor analyses show the combined effect of W/B with other three variables (SAP content, SAP type and curing age) not to be significant on density, so also is the combined effect of binder type and

curing age (Table 5.5 – light blue highlight). The combination with least significance here been W/B combined with curing age. Three and four variable combinations effects on density were mostly not significant (Table 5.5 - green highlights) with only two cases as an exception. Variables of great influence on the density of HPCs in this study can therefore be seen as SAP content and binder type, because individually and their combined effects with other variables resulted in significant influence on the outcome of density of HPCs.

The general linear model – univariate analysis (Table 5.6) shows each dependent variable to be of significant effect on the compressive strength individually and also at the two variable interaction level. The three factor analysis however indicates that two combination (grey colour highlights of Table 5.6) situations (W/B \* SAP type \* Curing Age and SAP type \* Binder type \* Curing Age) are of no significant effect on compressive strength while all other three factor combination types are significant. The four factor analysis reveals that binder type in combination with SAP type, SAP content and curing age had significant effect on the compressive strength, while W/B combination with the same set of factors (i.e. purple highlight on Table 5.6) is of no significant influence on the compressive strength. This implies that the binder type is of more importance in the outcome of the compressive strength than the W/B within the limits of the W/B examined in the study and the three binder types tested. Although all the independent variables - (W/B, SAP type, SAP contents, binder type and curing age) individually and at two factor combination - are of significant effect on the compressive strength, the binder type is of greater impact when the combined effects of all the variables are under consideration. It is however important here that the supposed influence of binder type on strength has some influence of W/B incorporated since HPCs made with Binder Type 1 ( $M_2$  and  $M_3$ ) comprise of two W/B (0.25 and 0.3) respectively. Figure 5.6 reveals that the ternary cements (Binder Types 2 ( $M_{1F}$ ) and 3 ( $M_{1S}$ )) had higher strength values after 7 days than the binary cements and continued with similar improved hydration. Binder Type 2 (CEM I 52.5 N+ SF + FA) – HPC reports better long term (90 days) strength development trend than Binder Type 3 (CEM I 52.5 N+ SF).

**Table 5-6: Between Effect Test on Compressive Strength**

Source	Type III Sum of Squares	df	Mean Square	F	Sig.
Corrected Model	136734.418 <sup>a</sup>	111	1231.842	59.748	.000
Intercept	3551504.067	1	3551504.067	1.723E5	.000
Single Factor Analysis					
W/B	6882.841	1	6882.841	333.841	.000
SAP content	10730.354	2	5365.177	260.229	.000
SAP type	364.150	1	364.150	17.662	.000
Binder type	374.165	1	374.165	18.148	.000
Curing Age	71010.544	3	23670.181	1.148E3	.000
Two Factor Analysis					
W/B * SAP content	794.488	2	397.244	19.268	.000
W/B * SAP type	440.036	1	440.036	21.343	.000
W/B * Curing Age	1524.933	3	508.311	24.655	.000
SAP content * SAP type	378.426	2	189.213	9.177	.000
SAP content * Binder type	313.387	2	156.693	7.600	.001
SAP content * Curing Age	838.172	6	139.695	6.776	.000
SAP type * Binder type	2526.068	1	2526.068	122.523	.000
SAP type * Curing Age	354.791	3	118.264	5.736	.001
Binder type * Curing Age	1218.394	3	406.131	19.699	.000
Three Factor Analysis					
W/B * SAP content * SAP type	136.252	2	68.126	3.304	.039
W/B * SAP content * Curing Age	552.093	6	92.016	4.463	.000
W/B * SAP type * Curing Age	20.655	3	6.885	.334	.801
SAP content * SAP type * Binder type	259.746	2	129.873	6.299	.002
SAP content * SAP type * Curing Age	344.189	6	57.365	2.782	.013
SAP content * Binder type * Curing Age	1832.835	6	305.472	14.816	.000
SAP type * Binder type * Curing Age	87.218	3	29.073	1.410	.241
Four Factor Analysis					
W/B * SAP content * SAP type * Curing Age	70.805	6	11.801	.572	.752
SAP content * SAP type * Binder type * Curing Age	630.489	6	105.081	5.097	.000
Error	4618.240	224	20.617		
Total	3892976.130	336			
Corrected Total	141352.658	335			

a. R Squared = .967 (Adjusted R Squared = .951)

Figure 5.7 shows that a negative correlation exists between W/B and the compressive strength of HPCs. The compressive strength decreases as the W/B increases. HPCs from Binder Types 2 and 3, referred to as ternary cement – HPCs ( $M_{1F}$  and  $M_{1S}$ ) having 0.2 W/B had similar values of compressive strength as the Binder Type 1 (binary cement – HPCs ( $M_2$ )) of 0.25 W/B while  $M_3$  – HPCs of 0.3 W/B (also from Binder Type 1) had the lowest values of compressive strength. The HPCs from Binder Type 2 (having FA as an additional SCM) however had slightly higher

compressive strength values after 90 days than the Binder Type 3 – HPCs (having CS as additional SCM) despite both being of the same W/B.

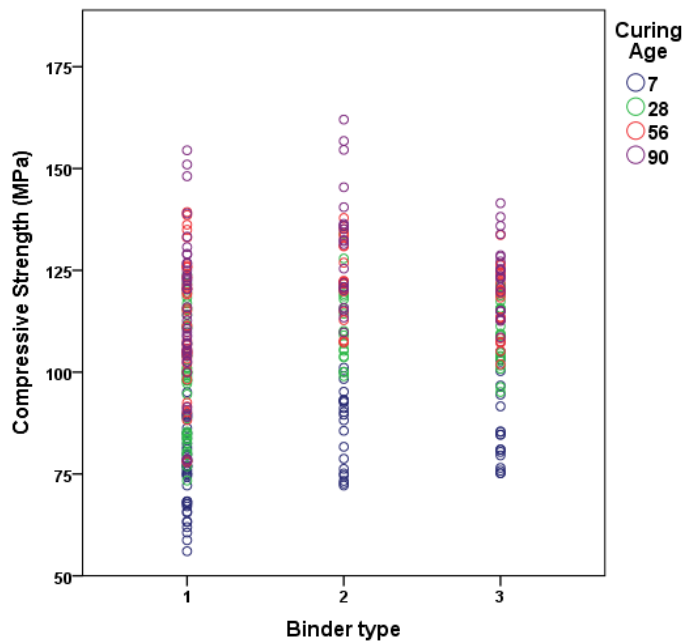


Figure 5-6: Compressive strength of HPC versus binder type as influenced by curing age

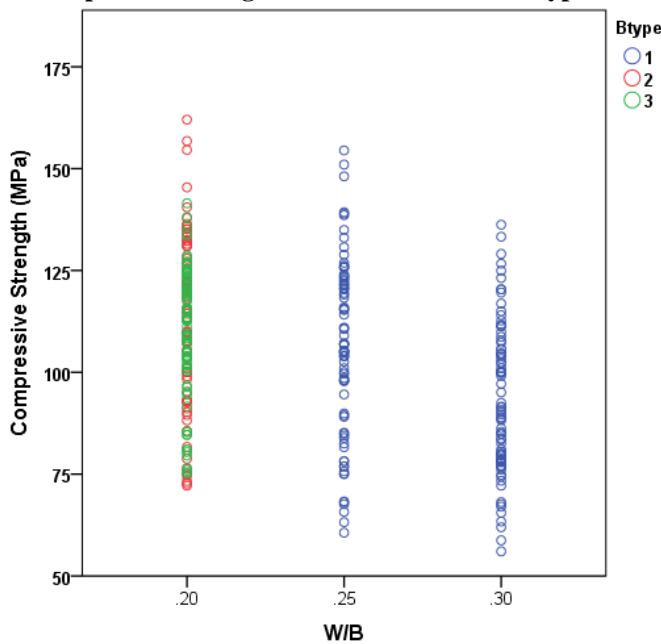
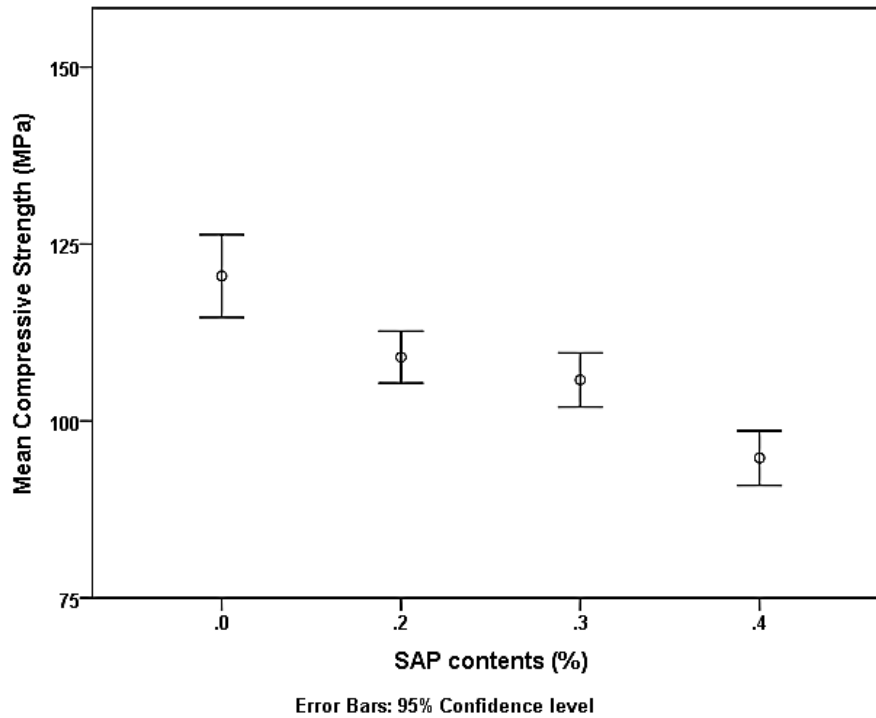


Figure 5-7: Compressive strength versus binder type as influenced by W/B

The higher SiO<sub>2</sub> content in FA continues to react with excess lime (CaOH) liberated by CEM I 52.5 N and results in better long term strength than the CS based ternary cement- HPC with high CaO content. Considering the fact that all the HPCs contains the same proportion of SF (7.5% b<sub>wob</sub>), the lower compressive strength result from the HPCs with highest W/B (M<sub>3</sub>-

HPC) within the same binder type (Type 1 for  $M_2$  and  $M_3$ ) is in agreement with expectation since higher water content in same binder content leads to lower strength in concrete.

Figure 5.8 on the other hand shows that mean compressive strength generally decreases as the SAP content increases. The mean compressive strength value was however still above 100 MPa for SAP addition up to 0.3%  $b_{wob}$ .



**Figure 5-8: Mean compressive strength of HPC against SAP contents**

The Duncan's multiple range test results as presented in Appendix B1.1 to B1.5 reveal that there is no significant difference in the observed means for the various groupings of the effect of independent variables on the compressive strength of HPCs.

The plot of compressive strength of reference HPCs on logarithmic time scale is presented in Figure 5.9 while influence of SAP addition on these references mixtures is shown in Appendix B2. The summary of the equations for respective trend-lines (i.e. lines of best fit) is presented in Table 5.7. It is observed that compressive strength increases linearly according to logarithm of time for all the HPCs studied at a good correlation for all levels of SAP addition. The long term compressive strength is observed to also conform to Equation 2.13 as proposed by Kadri et al., (2012).

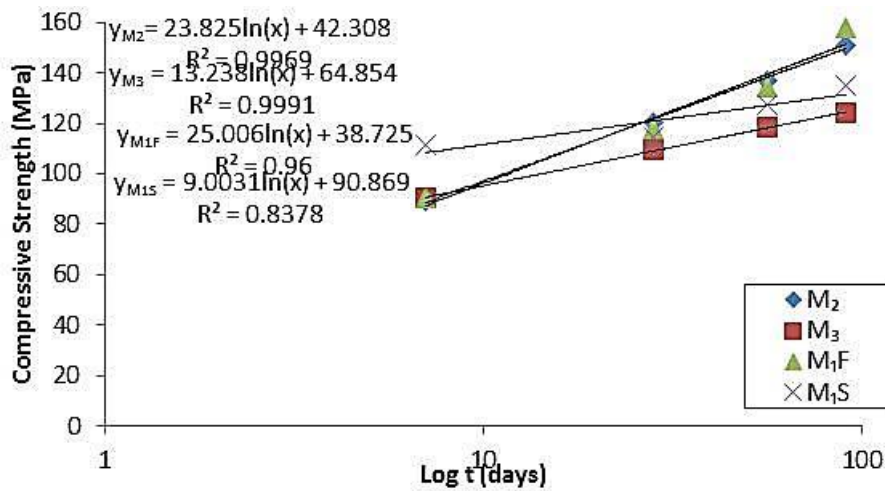


Figure 5-9: Compressive strength of reference mixtures - HPCs on log time scale

Table 5-7: Summary of Trend Line ( $A + B \log \frac{t_d}{t_1}$ ) for Compressive Strength of HPCs with SAP

Binary Cement - HPCs							
Specimen	A	B	R <sup>2</sup>	Specimen	A	B	R <sup>2</sup>
M <sub>2</sub>	42.31	23.825	0.997	M <sub>3</sub>	64.85	13.238	0.999
M <sub>2</sub> Sp <sub>1</sub> -0.2	42.93	20.221	0.968	M <sub>3</sub> Sp <sub>1</sub> -0.2	54.33	11.808	0.991
M <sub>2</sub> Sp <sub>1</sub> -0.3	42.62	17.599	0.990	M <sub>3</sub> Sp <sub>1</sub> -0.3	33.58	16.919	0.954
M <sub>2</sub> Sp <sub>1</sub> -0.4	43.59	14.686	0.805	M <sub>3</sub> Sp <sub>1</sub> -0.4	46.03	7.990	0.838
M <sub>2</sub> Sp <sub>2</sub> -0.2	55.08	16.604	0.945	M <sub>3</sub> Sp <sub>2</sub> -0.2	61.98	9.899	0.898
M <sub>2</sub> Sp <sub>2</sub> -0.3	40.77	18.452	0.970	M <sub>3</sub> Sp <sub>2</sub> -0.3	33.63	20.018	0.829
M <sub>2</sub> Sp <sub>2</sub> -0.4	30.35	17.990	0.965	M <sub>3</sub> Sp <sub>2</sub> -0.4	45.49	10.332	0.968
Ternary Cement - HPCs							
M <sub>1F</sub>	37.33	25.006	0.960	M <sub>1S</sub>	90.87	9.003	0.837
M <sub>1F</sub> Sp <sub>1</sub> -0.2	25.39	25.113	0.981	M <sub>1S</sub> Sp <sub>1</sub> -0.2	88.31	8.411	0.911
M <sub>1F</sub> Sp <sub>1</sub> -0.3	61.60	12.288	0.743	M <sub>1S</sub> Sp <sub>1</sub> -0.3	54.17	16.294	0.899
M <sub>1F</sub> Sp <sub>1</sub> -0.4	45.80	15.630	0.975	M <sub>1S</sub> Sp <sub>1</sub> -0.4	29.82	22.425	0.986
M <sub>1F</sub> Sp <sub>2</sub> -0.2	70.92	15.003	0.954	M <sub>1S</sub> Sp <sub>2</sub> -0.2	80.33	6.787	0.952
M <sub>1F</sub> Sp <sub>2</sub> -0.3	68.19	14.291	0.989	M <sub>1S</sub> Sp <sub>2</sub> -0.3	50.01	15.537	0.990
M <sub>1F</sub> Sp <sub>2</sub> -0.4	69.63	11.249	0.975	M <sub>1S</sub> Sp <sub>2</sub> -0.4	55.27	13.469	0.937

An increase in the W/B in the binary cement – HPC (M<sub>2</sub> and M<sub>3</sub>) mixtures leads generally to a decrease in the B coefficients (kinetic of hydration in Table 5.7), so does the increase SAP contents except in a few cases that can be referred to as non-conforming. The B coefficient (the kinetic of the hydration reaction as defined in Section 2.6.2 and 4.4.1) in ternary cement HPCs containing FA (M<sub>1F</sub> series) also decreases generally as the SAP content increases while the M<sub>1S</sub> series (containing CS) reflect a different pattern. The M<sub>1S</sub> – HPC which was observed to exhibit a high value of the A coefficient (i.e. the value at  $t_d = t_1$ ) representing the initial 24 hrs strength were however observed to display lower values of hydration kinetic for the long term strength development.

CS can then be seen to portray similar early age strength development in HPC than FA, but the FA inclusion in ternary cement HPC however had higher kinetic of hydration value on the long term – indicative of higher long term pozzolanic reaction than CS.

### 5.1.3 Curve – Fitting and Modelling

The curve fitting and modelling is based on the concepts as highlighted by Hasholt et al., (2010a).

These are:

- i. Concrete compressive strength is proportional to the compressive strength of the paste phase.
- ii. Paste compressive strength depends on gel space ratio, as suggested by Powers (1947).
- iii. The influence of air voids created by SAP on compressive strength can be accounted for by Bolomey's formula provision for air content in concrete (Hasholt et al., 2010a).

The experimental data on the direct weight measure of demoulded of concrete in this study showed that air content (excluding SAP voids) vary from 0.0 to 3.87% as influenced by the varied HPC mixture contents (Tables 4.4 and 4.5, Section 4.3). To study the pure effect of SAP, the measured cube compressive strength for both the early-age and long term were corrected for the air content on line with Equation 2.12.

The air content was determined on basis of density by the formula  $(dd - dmd/dd)$  for reference HPCs (excluding effect of SAP) varying from 0.17 to 1.58% as shown in Table 3.1. All values of compressive strength were thereby corrected with respective correction factors.

Using the Bolomey's Equation (2.12):

$K_{Bolomey}$  remains constant and of the same value for all mixtures (since all the HPCs are made from the same aggregate),  $a$  is the actual air content (% relative to volume of concrete), and  $a_0$  is a reference air content. The value of constant  $B$  of Equation 2.12 according to Hasholt et al., (2010a), as a rule of thumb equals 0.04, when the paste phase occupies 25% of the concrete volume. Hence from Table 3.1, the reference HPCs have paste contents (volume of binder + water) as 29% ( $M_{1F}$  and  $M_{1S}$ ); 31% ( $M_2$ ) and 32% ( $M_3$ ) respectively. The constant  $B$  for the compressive strength in line with Equation 2.12 is thereby calculated as shown in Table 5.8.

**Table 5-8: Correction factor for Reference HPCs**

HPC type		Paste content	constant $B$
Ternary cements HPCs	$M_{1F}$ and $M_{1S}$	0.29	0.034
Binary cements - HPCs	$M_2$	0.31	0.032
	$M_3$	0.32	0.031

The 28 day compressive strength of the HPC – mortar cubes were calculated by interpolation using the values obtained from the compressive strength tests conducted on the HPC mixtures with coarse aggregates from which the mortars were extracted as reported in Section 5.1. The 28 day strength of mortar cubes were not available from test results because the test on strength development and degree of hydration as explained in Section 3.2.3 were limited to 7 days due to difficulty of milling the mortar cubes manually adopting the ACV mould. The compressive strength of HPC mortar cubes (corrected for air and SAP voids) with age is hereby shown in Figures 5.10 (for HPC containing  $SP_2$ ) and 5.11 (for HPC containing  $SP_1$ ).

The outcome gave a good trend reflecting that when the compressive strength of the HPC mortars are corrected for air and SAP voids using the Bolomey's formula, there exists some differences in the compressive strength of the HPC - mortar cubes. The HPC containing SAP generally had lower strength than the reference mixtures. The strength development trend up to 28 days fit into a logarithmic curve with the trendline cutting across the 0.2% and 0.3% SAP contents ( $b_{wob}$ ) in most instances.

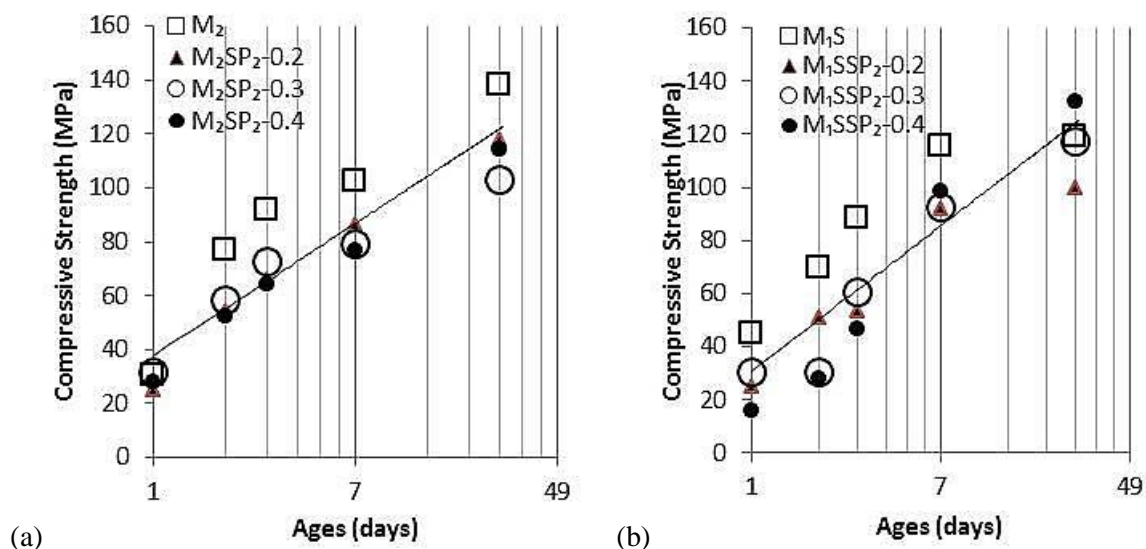


**Figure 5-10: Compressive strength of HPC – mortars cubes corrected for both air and  $SP_2$  voids**  
(a)  $M_2$  - HPC; (b)  $M_{1S}$  – HPC

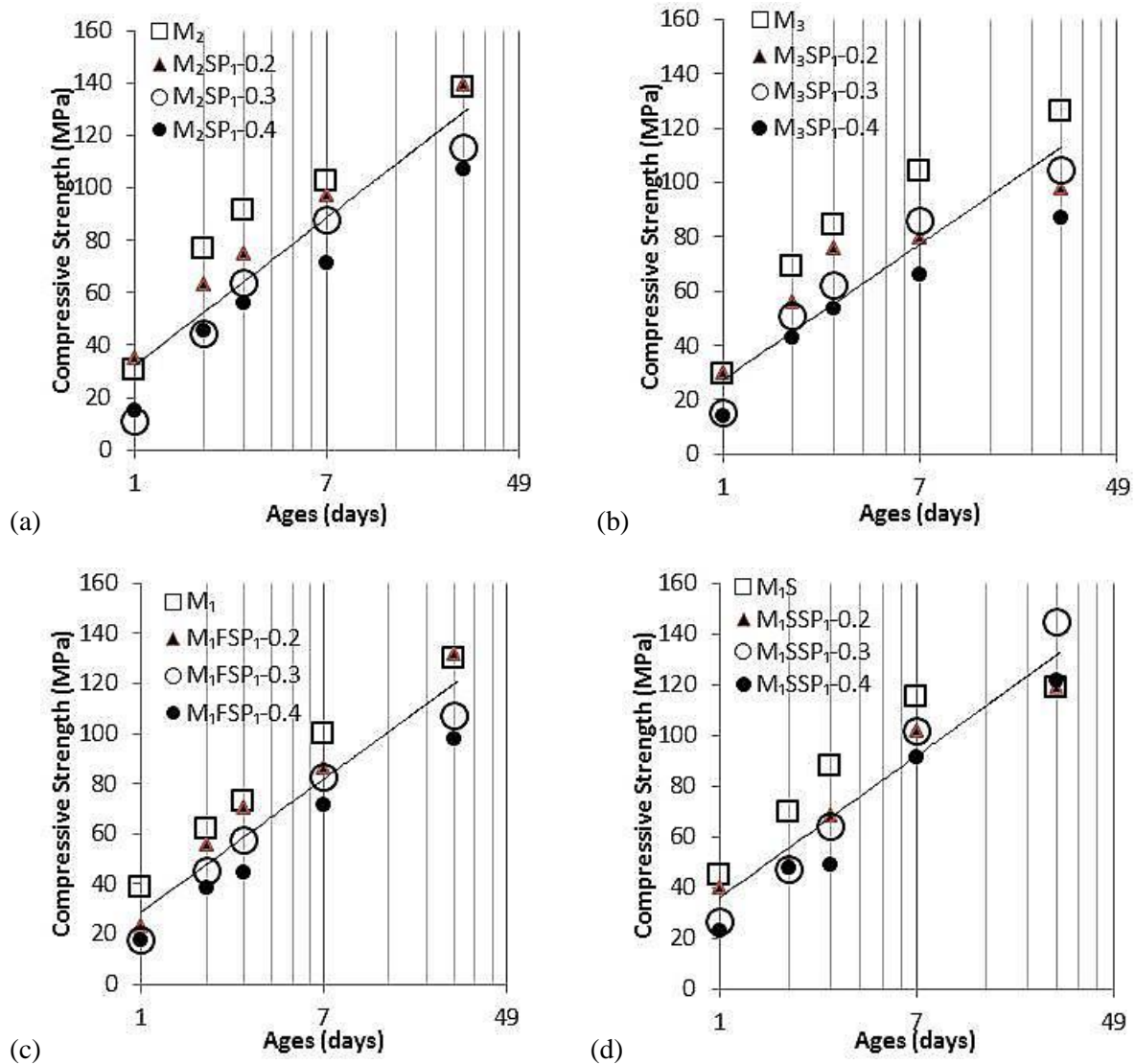


**Figure 5-11: Compressive strength of HPC mortar cubes corrected for both air and SP<sub>1</sub> voids**  
 (a) M<sub>2</sub> – HPC; (b) M<sub>3</sub> – HPC; (c) M<sub>1S</sub> – HPC and (d) M<sub>1F</sub> – HPC

The gel space ratio is defined by Neville (2012) as the ratio of the volumes of the hydrated cement to the sum of the volumes of the hydrated cement and of the capillary pores. Hence we have the expression for gel space ratio for CEM I 52.5 N given as:

$$X = \frac{2.06 v_c \alpha_c}{v_c \alpha_c + \frac{w}{c}} \quad (5.1)$$

where X is the gel space ratio of the HPC mortar paste;  $v_c$  is the specific volume of anhydrous binder (i.e. binary or ternary),  $\alpha_c$  is the degree of hydration of binder and W/C is the original water to binder ratio (Neville, 2012).

The gel space ratio for respective HPC mixtures ( $M_{1F}$ ,  $M_{1S}$ ,  $M_2$  and  $M_3$ ) were thereby calculated and plotted against the compressive strength of the various mortar cubes HPC mortar cubes as presented in Figure 5.12. These include results for all ages.

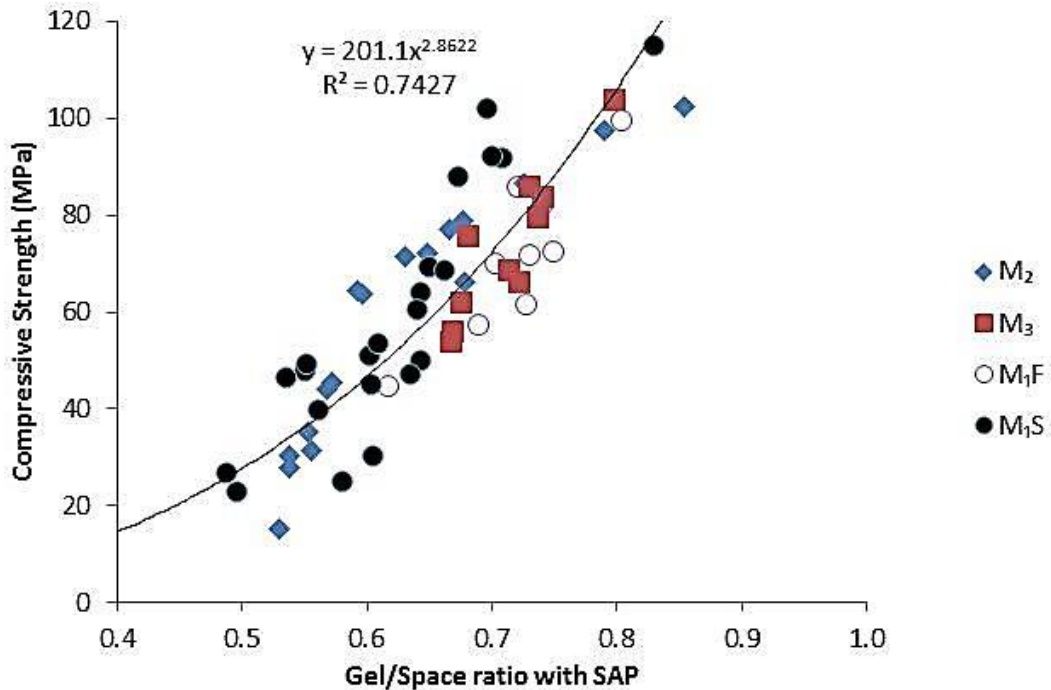


Figure 5-12: Compressive strength against the gel / space ratio for HPC mortar cubes

The plot in Figure 5.12 shows that for these low W/B HPC mixtures, a general relationship for the compressive strength of mortars cubes (with or without SAP addition) against the gel space ratio has a trend similar to that propounded by the Powers Model when Bolomey's formula had been used to account for the influence of air and SAP voids on the compressive strength up to the 7 days to which this study was able to determine the degree of hydration. The relationship deduced from the results in Figure 5.12 can be expressed as:

$$f_c = 201 X^{2.86} \quad (5.3)$$

This is similar to the expression adopted in the works of Hasholt et al., (2010a and b) from the modified relation presented by (Powers, 1958) stated as Equation 2.4 in Section 2.6.1.

$$f_c = A.X^3, \quad X = \frac{\text{volume of gel}}{\text{volume of space}} \quad (2.4)$$

The trendline power value of 2.86 is approximately 3 (when rounded up to whole number) has proposed in the Powers' Model while the constant is 201. It is however noted that the  $R^2$  is 0.74 because of the many variables (binder types; W/B and SAP types and contents) combined in the plots. Hasholt et al., (2010a) reported similar result of 2.88 power value and 299 as constant at an  $R^2$  of 0.97. The power value in Equation 2.4 according to literature (Neville, 2012; Shetty, 2004) is expected to be approximately 3 while the value arrived at for the constant could vary as influenced by the binder type.

The results from this study reveal that SAP addition leads to reduction in compressive strength of the low W/B HPC while correction made for void volume (SAP and air) using the Bolomey's formula and Powers gel-space ratio enhanced a good fit into the Powers' Model. This makes it possible to predict the SAP effect on the compressive strength of HPC.

## 5.2 Elastic Modulus

The outcome of the experimental work performed in this study on E-modulus is presented in under the sub-headings as follows:

### 5.2.1 Results

Results of E-modulus tests of the various HPC mixtures are presented in Tables 5.9 and 5.10 giving average result of triplicate samples for respective specimen at the various curing ages (28, 56 and 90 days). The CoV of the E-modulus values are generally below 6.0% except for some few specimens having values relatively high CoV (6.55 to 9.59% - yellow highlight in the Tables). This however is still below acceptable limit of 10.0%.

Figures 5.13 and 5.14 for binary ( $M_2$  and  $M_3$ ) and ternary ( $M_{1F}$  and  $M_{1S}$ ) cements HPCs gives the graphical representation of the E-modulus values. The results show that E-modulus for the HPCs with or without SAP remains generally within the same range but significantly lower at longer curing ages (56 and 90 days).

**Table 5-9: E-modulus of Binary cements - HPC with SAP**

Curing age	28 days		56 days		90 days	
	E-mod (GPa)	CoV (%)	E-mod (GPa)	CoV (%)	E-mod (GPa)	CoV (%)
M <sub>2</sub>	59.49	0.75	63.19	1.32	49.14	3.67
M <sub>2</sub> Sp <sub>1</sub> -0.2	53.32	1.36	55.85	1.97	47.75	0.99
M <sub>2</sub> Sp <sub>1</sub> -0.3	57.26	1.03	46.95	1.61	46.24	0.73
M <sub>2</sub> Sp <sub>1</sub> -0.4	56.61	4.25	42.42	3.52	46.31	2.12
M <sub>2</sub> Sp <sub>2</sub> -0.2	58.78	1.58	51.01	1.68	49.96	0.08
M <sub>2</sub> Sp <sub>2</sub> -0.3	65.50	8.10	57.76	2.19	48.46	1.48
M <sub>2</sub> Sp <sub>2</sub> -0.4	67.75	0.63	57.35	0.39	47.25	1.99
M <sub>3</sub>	55.09	3.35	48.75	2.54	49.16	3.35
M <sub>3</sub> Sp <sub>1</sub> -0.2	51.79	1.26	44.48	6.72	45.80	2.00
M <sub>3</sub> Sp <sub>1</sub> -0.3	51.61	5.83	43.33	0.36	43.09	4.41
M <sub>3</sub> Sp <sub>1</sub> -0.4	52.20	3.61	41.33	0.13	44.20	2.24
M <sub>3</sub> Sp <sub>2</sub> -0.2	51.14	5.36	44.35	1.19	44.66	0.10
M <sub>3</sub> Sp <sub>2</sub> -0.3	51.06	1.62	44.07	1.04	44.67	1.31
M <sub>3</sub> Sp <sub>2</sub> -0.4	45.91	4.14	42.31	3.63	43.09	1.27

**Table 5-10: E-modulus of Ternary cements - HPC with SAP**

Curing age	28 days		56 days		90 days	
	E-mod	CoV	E-mod	CoV	E-mod	CoV
M <sub>1</sub> F	61.82	3.31	51.94	2.00	52.42	0.98
M <sub>1</sub> FSp <sub>1</sub> -0.2	67.29	1.37	48.32	4.06	48.77	2.10
M <sub>1</sub> FSp <sub>1</sub> -0.3	63.19	9.59	44.68	0.88	45.09	1.82
M <sub>1</sub> FSp <sub>1</sub> -0.4	67.93	0.96	43.69	1.64	44.31	6.55
M <sub>1</sub> FSp <sub>2</sub> -0.2	69.82	0.69	39.90	0.96	48.13	1.64
M <sub>1</sub> FSp <sub>2</sub> -0.3	59.72	6.55	45.43	2.18	48.09	2.11
M <sub>1</sub> FSp <sub>2</sub> -0.4	57.82	0.54	43.89	4.62	46.07	2.33
M <sub>1</sub> S	44.89	0.44	47.69	4.27	50.03	0.49
M <sub>1</sub> SSp <sub>1</sub> -0.2	51.32	0.11	47.70	2.35	49.32	0.80
M <sub>1</sub> SSp <sub>1</sub> -0.3	49.38	1.15	49.66	0.95	49.15	1.80
M <sub>1</sub> SSp <sub>1</sub> -0.4	48.50	0.57	47.51	2.02	46.71	6.70
M <sub>1</sub> SSp <sub>2</sub> -0.2	45.14	2.12	48.70	1.66	45.15	2.48
M <sub>1</sub> SSp <sub>2</sub> -0.3	48.49	0.08	50.49	3.00	50.96	0.85
M <sub>1</sub> SSp <sub>2</sub> -0.4	47.85	0.81	47.29	2.02	47.22	1.90

The  $E_{ci}$  values (E-modulus at 28 days) generally falls within the expectations (42.6 to 50.3 GPa) as specified in the MC 2010 for concretes with strength range (C70 – C120) with some inconsistencies of slightly higher values.

The E-modulus decreases slightly in the binary cements HPCs (M<sub>2</sub> and M<sub>3</sub>, Figure 5.13) as the SAP contents increases and also as the curing age increases. This is agrees well with the report of Dudziak & Mechtcherine (2010) of observed slight decrease on elastic moduli of internally cured UHPM and concretes due to SAP addition.

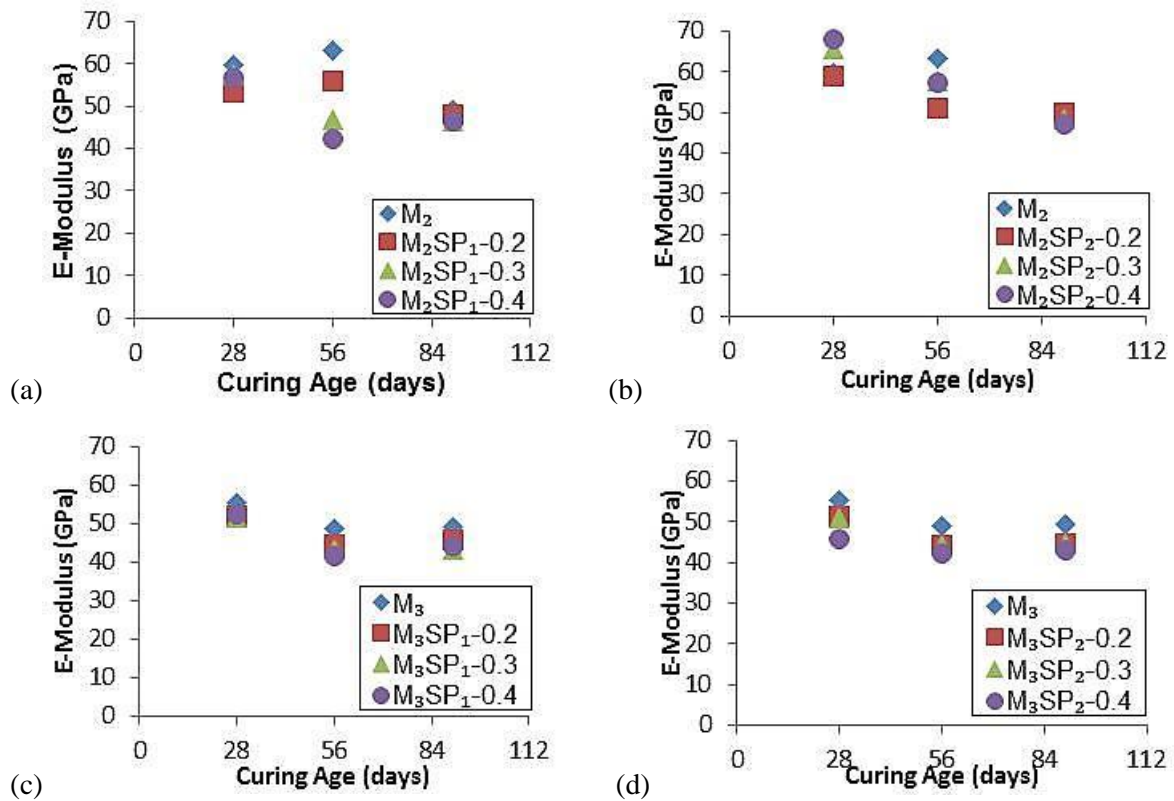


Figure 5-13: E-modulus of binary cements HPC against curing age; (a)  $M_2$ SP<sub>1</sub> - HPC; (b)  $M_2$ SP<sub>2</sub> - HPC; (c)  $M_3$ SP<sub>1</sub> - HPC and (d)  $M_3$ SP<sub>2</sub> - HPC.

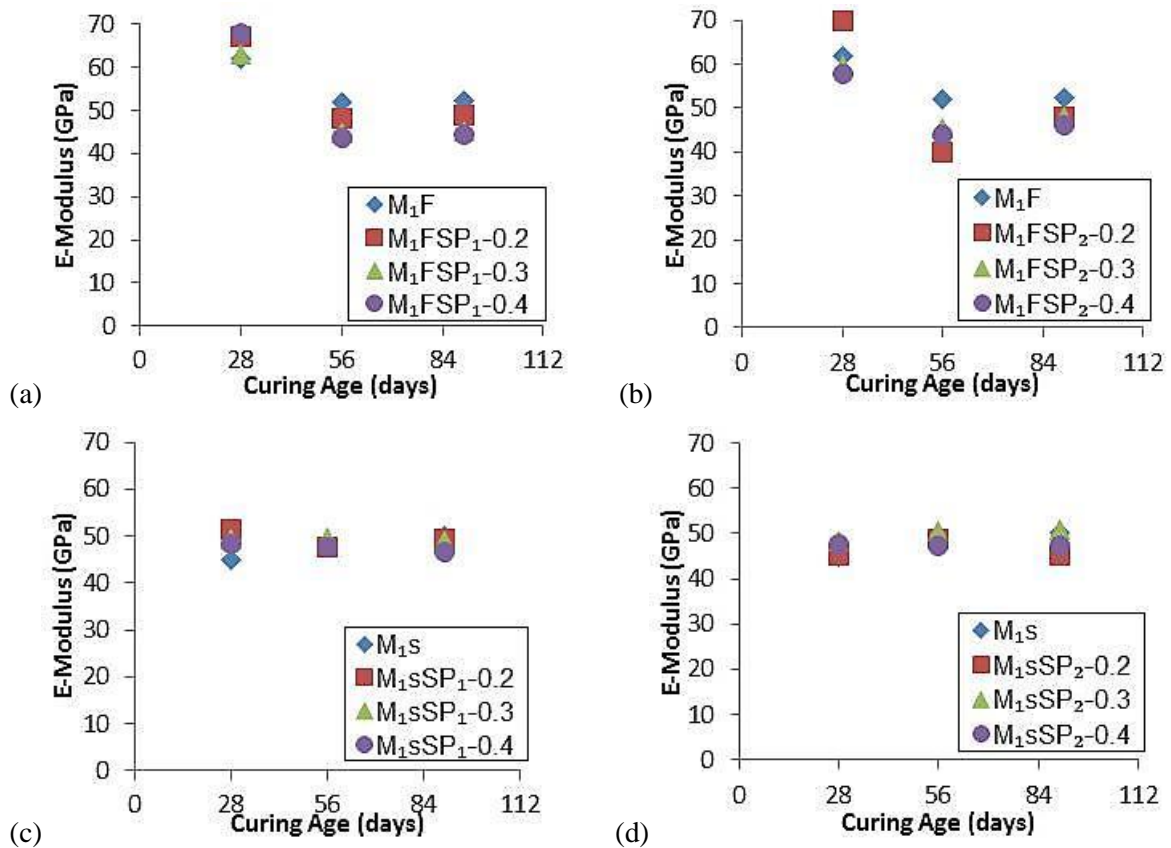
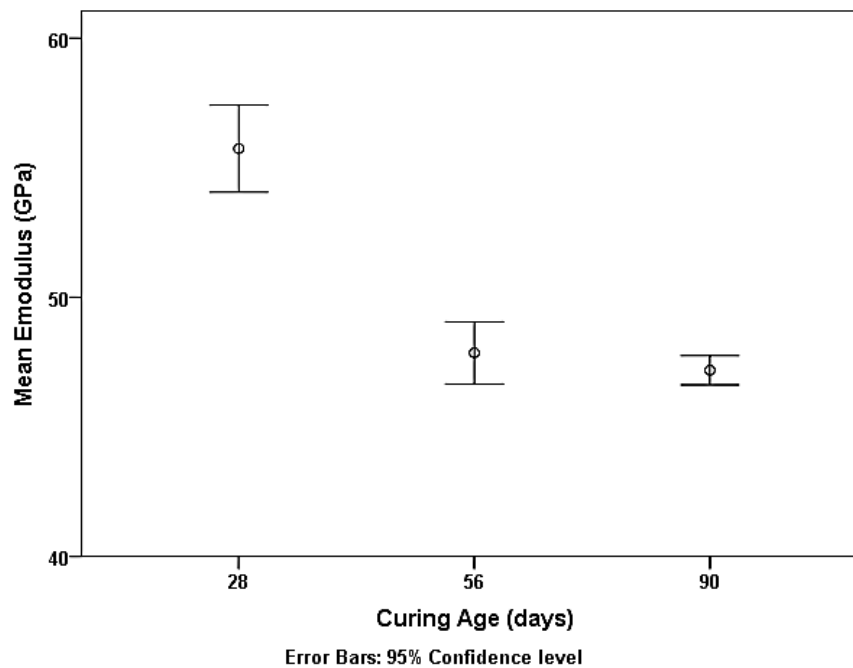


Figure 5-14: E-modulus of binary cements HPC against curing age; (a)  $M_{1F}$ SP<sub>1</sub>-HPC; (b)  $M_{1F}$ SP<sub>2</sub>-HPC; (c)  $M_{1S}$ SP<sub>1</sub>-HPC and (d)  $M_{1S}$ SP<sub>2</sub>-HPC

However, in the ternary cement HPCs (Figure 5.14), a difference was observed. While the  $M_{IF}$  series shows a trend of E-modulus decreasing as the curing age increases but having relatively similar values with or without SAP, the  $M_{IS}$  series maintains similar E-modulus values irrespective of the variations in the SAP contents and curing age studied. This implies that the E-modulus of  $M_{IS}$  is not influenced by the increase in SAP contents or the curing age of the concrete.

## 5.2.2 Discussion

An examination of the mean E-modulus results for the HPCs mixtures shows that the mean 28 days E - modulus is higher than the 56 and 90 days which gave similar values with higher variance in 56 days as reflected by the error bars (Figure 5.15). Error bars here refers to the spread of the measure of the data set which is taken as  $\pm 1$  standard deviation. This implies that the least variation in the result for the E-modulus of the HPCs is observed after 90 days curing. E-modulus specifically is often reported after 90 days for this type of concrete – HPC (Aïtcin, 1998; Mehta & Monteiro, 2014).



**Figure 5-15: Mean E-modulus of HPCs against curing age**

\*Note that the 95% CI shown in the figure is an indication that the analysis was performed at 95% confidence level.

The result of the experiment is an indication that the concrete stiffness is high at the 28 days possibly due to presence of some moisture still retained within the inter-phase while at the longer curing age almost all the moisture within the concrete had been used up by the hydration process of cement. Recent work of Liu, et al. (2014), reports that moisture content of concrete has an influence on its mechanical behaviour and that higher moisture content, results in higher modulus of elasticity for concrete of same compressive strength range. It can therefore be argued that E-modulus value after 90 days is better adopted for specification in performance-based design of HPCs especially when other admixtures and IC-agents are incorporated in the mix. The CoV as calculated in Tables 5.9 and 5.10 shows the two E-modulus values with widest variance from the its mean was found in the specimen tested at 28 days curing. Similar picture is seen at Figure 5.15 for the generalised mean E-modulus plot against curing age showing the 28 days value having a wider variance from its mean. This study will thereby want to align with the postulations of Liu et al. (2014) on higher moisture presence at the 28 days age resulting in the higher E-modulus values with wider variation.

The E-modulus values plotted against SAP contents (Figure 5.16a) and SAP type (Figure 5.16b) for the HPCs reveals further that SAP introduction at the concentrations studied in this work has little or no influence on the mean E-modulus of this low W/B concrete. The E-modulus plot against binder type (Figure 5.17a) shows some influence on the mean value of the E-modulus with binder Type 2 ( $M_{1F}$ ) giving the highest E-modulus value, followed by Type 1 ( $M_2$  and  $M_3$ ) while Type 3 ( $M_{1S}$ ) has the least value of mean E-modulus. Some influence of W/B on mean E-modulus of HPC with SAP is presented in Figure 5.17b. The ternary cements HPCs ( $M_{1F}$  and  $M_{1S}$  series), though been of lower W/B than  $M_2$  series is of lower E-modulus, while  $M_3$  which is of the lowest W/B has also the lowest E-modulus. The influence of  $M_3$  series was the reason for the E-modulus plot against binder type showing  $M_{1F}$  (binder type 2) as the best performed of the binder types since  $M_2$  and  $M_3$  are combined as binder Type 1. The binder type and W/B can therefore be adjudged as of major influence on E-modulus of HPC with SAP as IC-agent.

General linear model – univariate analysis using SPSS carried out on the results of E-modulus of this study as presented in Table 5.11 reveals that all the factors individually had significant effect on the

E-modulus of HPC. The two variable interaction effects analysis also show most variable combinations to be of significant effect with exception only three combination cases (asterisks (\*<sup>1</sup>)) Table 5.12 - (SAP content\* Curing age; SAP type \* Binder type and SAP type \* Curing Age)).

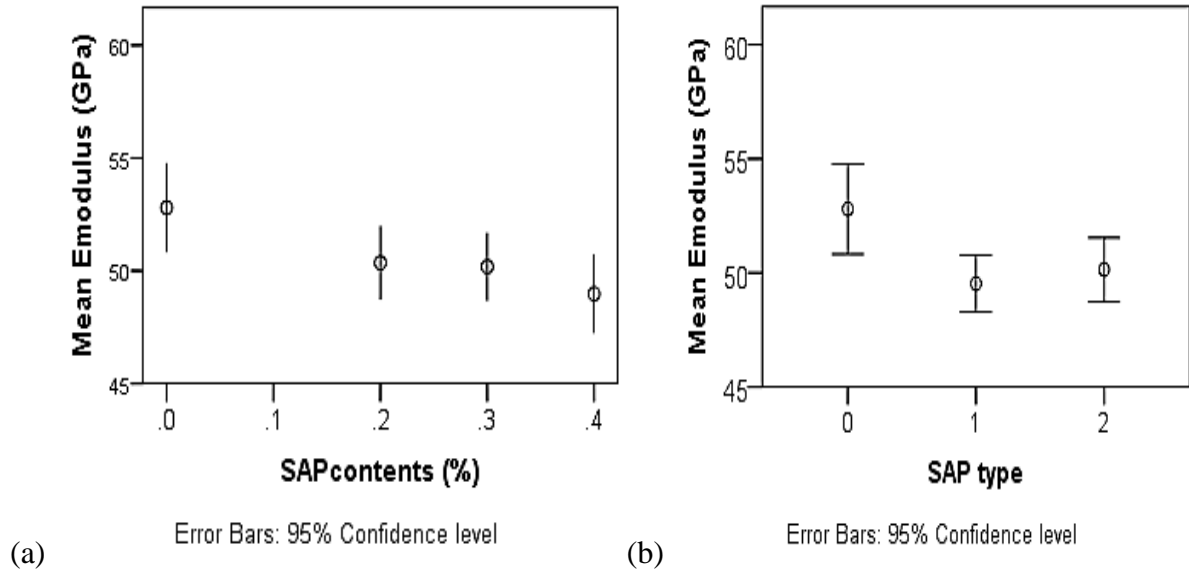


**Figure 5-16: Mean E-modulus of HPCs (a) against SAP contents (b) against SAP type**

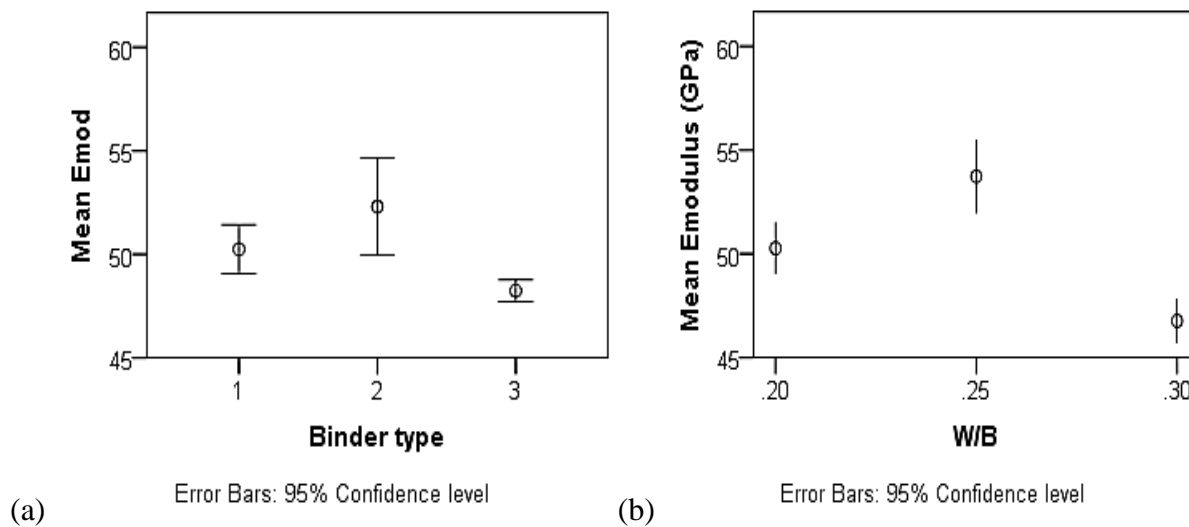


**Figure 5-17: Mean E-modulus of HPCs (a) against binder type (b) against W/B**

Three and four factor combination effects were generally observed to be significant too but only a combination series in three factor analysis (asterisks (\*<sup>2</sup>) - SAP content \* SAP type \* Binder type) is not significant. SAP content is noted to be of the least significant level as single factor of all the dependent variables and the most insignificant effect of the two factor analysis is noted to be with combination of SAP type and Binder type. The combination of W/B with other factors (be it at two,

three or four factor analysis) was significant in all situations, thereby signifying that W/B has the highest influence on the outcome of E-modulus. The  $R^2$  value 0.944 shows a strong correlation exists between the fixed factors (i.e. independent variables) and the dependent variable (E-modulus).

**Table 5-11: Between Test Effects on E-modulus**

Source	Type III Sum of Squares	df	Mean Square	F	Sig.
Corrected Model	11191.330 <sup>a</sup>	83	134.835	34.275	.000
Intercept	589388.334	1	589388.334	1.498E5	.000
W/B	1361.535	1	1361.535	346.098	.000
SAP content	80.439	2	40.220	10.224	.000
SAP type	20.539	1	20.539	5.221	.024
Binder type	590.941	1	590.941	150.215	.000
Curing Age	3037.730	2	1518.865	386.091	.000
Two Factor Analysis					
W/B * SAP content	26.501	2	13.251	3.368	.037
W/B * SAP type	277.363	1	277.363	70.505	.000
W/B * Curing Age	288.684	2	144.342	36.691	.000
SAP content * SAP type	104.420	2	52.210	13.272	.000
SAP content * Binder type	91.308	2	45.654	11.605	.000
SAP content * Curing Age	25.462	4	6.365	1.618	.172* <sup>1</sup>
SAP type * Binder type	3.459	1	3.459	.879	.350* <sup>1</sup>
SAP type * Curing Age	20.325	2	10.162	2.583	.079* <sup>1</sup>
Binder type * Curing Age	1947.695	2	973.847	247.549	.000
Three Factor Analysis					
W/B * SAP content * SAP type	102.871	2	51.436	13.075	.000
W/B * SAP content * Curing Age	87.554	4	21.888	5.564	.000
W/B * SAP type * Curing Age	86.349	2	43.175	10.975	.000
SAP content * SAP type * Binder type	14.248	2	7.124	1.811	.167* <sup>2</sup>
SAP content * SAP type * Curing Age	124.218	4	31.055	7.894	.000
SAP content * Binder type * Curing Age	42.759	4	10.690	2.717	.032
SAP type * Binder type * Curing Age	28.893	2	14.447	3.672	.027
Four Factor Analysis					
W/B * SAP content * SAP type * Curing Age	97.967	4	24.492	6.226	.000
SAP content * SAP type * Binder type * Curing Age	160.689	4	40.172	10.212	.000
Error	660.904	168	3.934		
Total	648425.636	252			
Corrected Total	11852.235	251			

a. R Squared = .944 (Adjusted R Squared = .917)

The Duncan's multiple range test results as presented in Appendix B3 reveal that there is no significant difference in the observed means for the various groupings of the effect of independent variables on the E-modulus of the HPCs. The grouping 1 of observed means for SAP type (for SP<sub>1</sub>) however has a value of significant level slightly above the 95% confidence level (Table B3.3 at a significant value of 0.079), being the least of the significant levels observed. This is followed by the

groupings 2 for means of SAP contents (i.e. 0.2 SAP contents) with a significant value of 0.641 as observed in Table B3.1 to B3.5 (Page 211).

### 5.3 Splitting Tensile Strength and Fracture Energy

Results and discussions of the splitting tensile strength and fracture energy tests conducted using the wedge splitting tests according to RILEM Recommendations AAC13.1 (TC51-ALC, 78-MCA, 1992) as explained in Section 3.2.4 are presented in the following sub-sections:

#### 5.3.1 Results

Results of the Wedge Splitting test carried out to determine the splitting strength and fracture energy are presented in this section. The results extracted from the test setup as explained earlier was the splitting force ( $F_{sp}$  in kN) against the crack mouth opening displacement (CMOD in mm). Figure 5.18 below shows a typical set of results for triplicate specimen (for  $M_{1S}SP_1-0.4$  after 28 days curing).

The data obtained was then computed for each sample for calculation of the work of fracture ( $W_f$ ) which is the area under the  $F_{sp}$  - CMOD curve using the trapezoidal rule in accordance to Brühwiler (1990) recommendations and hence the calculation of the fracture energy ( $G_f$ ) as discussed earlier in Section 2.8.

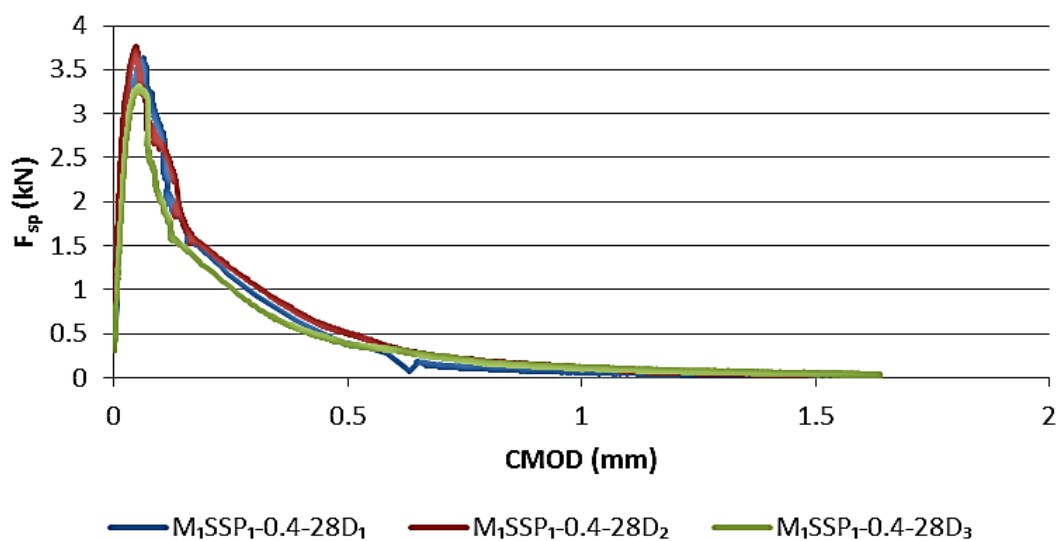


Figure 5-18: Typical plot of data extracted from Wedge Splitting Test for  $W_f$  and  $G_f$  Calculation

Tables 5.13 for  $M_{1F}$  and  $M_{1S}$  (i.e. ternary cements) and 5.14 for  $M_2$  and  $M_3$  (i.e. binary cements) present the fracture energy results for the respective HPCs as required by the RILEM Recommendation with values of the cube compressive strength ( $f_{c,cube}$ ), E-modulus ( $E_c$ ) and the Splitting force ( $F_{sp}$ ) provided.

**Table 5-12: Summary of Fracture Energy Results for Ternary Cement HPCs**

Specimen	28 days				56 days				90 days			
	$f_{c,cube}$ (kN)	$E_c$ (GPa)	$F_{sp}$ (kN)	$G_F$ (N/m)	$f_{c,cube}$ (kN)	$E_c$ (GPa)	$F_{sp}$ (kN)	$G_F$ (N/m)	$f_{c,cube}$ (kN)	$E_c$ (GPa)	$F_{sp}$ (kN)	$G_F$ (N/m)
Binder Type 2 (0.2 W/B)												
$M_{1F}$	117.8	61.8	5.11	162.9	134.2	51.9	4.59	137.1	157.8	52.4	4.48	131.5
$M_{1F}SP_1-0.2$	112.8	67.3	3.59	130.2	121.3	48.3	4.71	183.9	140.6	48.8	4.35	116.6
$M_{1F}SP_1-0.3$	106.6	63.2	4.19	175.1	119.8	44.7	3.46	140.4	107.5	45.1	3.65	142.8
$M_{1F}SP_1-0.4$	102.0	67.9	3.75	147.7	107.5	43.7	3.23	184.9	114.8	44.3	3.76	140.9
$M_{1F}SP_2-0.2$	125.0	69.8	4.07	100.4	133.3	39.9	4.08	123.0	134.6	48.1	4.63	150.2
$M_{1F}SP_2-0.3$	117.6	59.7	3.99	165.8	123.6	45.4	4.0	137.3	133.3	48.1	4.48	145.3
$M_{1F}SP_2-0.4$	106.2	57.8	3.50	139.1	117.7	43.9	3.95	159.9	118.5	46.1	4.00	121.2
Binder Type 3 (0.2 W/B)												
$M_{1S}$	114.6	44.9	4.48	152.8	127.2	47.7	4.63	155.1	134.7	50.0	5.38	177.0
$M_{1S}SP_1-0.2$	120.5	51.3	5.04	145.8	122.1	47.7	4.14	146.3	123.9	49.3	4.78	153.3
$M_{1S}SP_1-0.3$	116.2	49.4	4.61	148.0	121.6	49.7	4.53	175.1	121.8	49.1	3.96	169.4
$M_{1S}SP_1-0.4$	100.3	48.5	5.23	179.9	120.0	47.5	5.30	193.5	133.1	46.7	4.05	154.8
$M_{1S}SP_2-0.2$	102.1	45.1			105.8	48.7	3.59	172.5	112.9	45.2	3.45	136.9
$M_{1S}SP_2-0.3$	107.9	48.5	2.90	112.8	115.2	50.5	3.77	163.5	126.2	51.0	3.47	169.2
$M_{1S}SP_2-0.4$	105.9	47.9	3.58	143.7	108.5	47.3	3.90	150.5	113.5	47.2	3.63	184.8

**Table 5-13: Summary of Fracture Energy Results for Binary Cements HPCs**

Specimen	28 days				56 days				90 days			
	$f_{c,cube}$ (kN)	$E_c$ (GPa)	$F_{sp}$ (kN)	$G_F$ (N/m)	$f_{c,cube}$ (kN)	$E_c$ (GPa)	$F_{sp}$ (kN)	$G_F$ (N/m)	$f_{c,cube}$ (kN)	$E_c$ (GPa)	$F_{sp}$ (kN)	$G_F$ (N/m)
Binder Type 1 (0.25 W/B)												
$M_2$	120.5	59.5	4.59	120.1	137.0	63.2	4.67	155.6	151.2	49.1	4.71	166.7
$M_2SP_1-0.2$	114.3	53.3	3.94	185.0	127.3	55.9	3.69	155.1	129.4	47.7	4.36	146.5
$M_2SP_1-0.3$	100.5	57.3	4.09	151.4	116.3	46.9	4.55	179.0	120.0	46.2	4.38	155.6
$M_2SP_1-0.4$	101.7	56.6	3.57	157.7	102.5	42.4	4.16	138.3	104.9	46.3	3.91	152.1
$M_2SP_2-0.2$	115.2	58.8	4.27	120.2	124.4	51.0	4.31	143.4	125.1	50.0	3.89	145.7
$M_2SP_2-0.3$	100.2	65.5	3.64	101.1	120.1	57.8	3.76	129.5	120.8	48.5	3.98	180.9
$M_2SP_2-0.4$	93.9	67.7	4.04	156.5	105.5	57.3	3.61	160.1	107.1	47.3	3.91	181.6
Binder Type 1 (0.3 W/B)												
$M_3$	109.5	55.1	3.42	149.2	118.3	48.7	4.21	155.1	124.0	49.2	4.23	177.0
$M_3SP_1-0.2$	94.3	51.8	3.54	178.6	103.3	44.5	3.42	146.3	106.0	45.8	3.65	153.3
$M_3SP_1-0.3$	83.8	51.6	3.14	167.6	103.9	43.3	3.05	175.1	111.3	43.1	3.20	169.4
$M_3SP_1-0.4$	77.7	52.2	4.15	166.3	78.1	41.3	3.09	193.5	78.4	44.2	2.93	154.8
$M_3SP_2-0.2$	99.3	51.1	3.17	154.5	103.5	44.4	3.59	172.5	102.8	44.7	3.45	136.9
$M_3SP_2-0.3$	86.3	51.1	3.02	152.1	123.6	44.1	3.04	163.5	123.7	44.7	3.35	136.9
$M_3SP_2-0.4$	78.6	45.9	3.11	166.5	90.0	42.3	2.95	150.5	90.4	43.1	3.35	184.8

\* $f_{c,cube}$  = cube compressive strength,  $E_c$  = E-modulus,  $F_{sp}$  = splitting force,  $G_F$  = fracture energy

An assessment of the results reveals no particular trend on influence of SAP addition on the splitting tensile strength and fracture energy of the HPCs. The works of Lam & Hooton (2005) reported similar or higher splitting tensile strength for SAP modified concretes on the 28 days. The explanation offered the better splitting tensile strength at 28 days in SAP modified concrete by Mechtcherine & Reinhardt (2012) is that SAP, in parallel to shrinkage mitigation, successfully increased the tensile cracking resistance of the cement-based system. This explanation is applicable in this test too as the reason for no significant reduction in tensile splitting strength of the SAP modified HPC.

The fracture energy values are generally within the same range of 130 N/m to 185 N/m for all specimens with or without SAP addition except in a few instances (as highlighted in green in Tables 5.17 and 5.18 which deviates from the range). The  $G_F$  value obtained is within the expected range for concrete of this strength range made from maximum aggregate size of 13 mm (fib MC 2010). A check of the  $G_F$  in line with MC 2010 provision on basis of maximum aggregate size ( $G_F = a \cdot \Theta^n$ ) as 183.15 N/m while a second check using a characteristic compressive strength of 90 N/mm<sup>2</sup> (using  $G_f = 72 \cdot f_{cu}^{0.18}$ ) gives a value of 161.85 N/m. Both checks therefore show that  $G_f$  values obtained are similar to the MC 2010 provisions. The result for the 28 day test for  $M_{1S}SP_2-0.2$  sample (yellow highlight on Table 5.17) was however lost as the samples failed suddenly during testing due to poor closed loop control.

Figures 5.19 to 5.22 further show that curing age influence on the  $G_F$  values cannot also be placed into any particular trend too. The splitting force was also observed to generally maintain a value range of 3.0 kN to 5.0 kN for all the HPCs examined except two cases of inconsistencies (blue highlight of Table 5.10). There was however cases of observed reduction in the value of  $G_f$  with decrease in age (Figure 5.19,  $M_{1F}$  and  $M_{1F}SP_1-0.2$ )

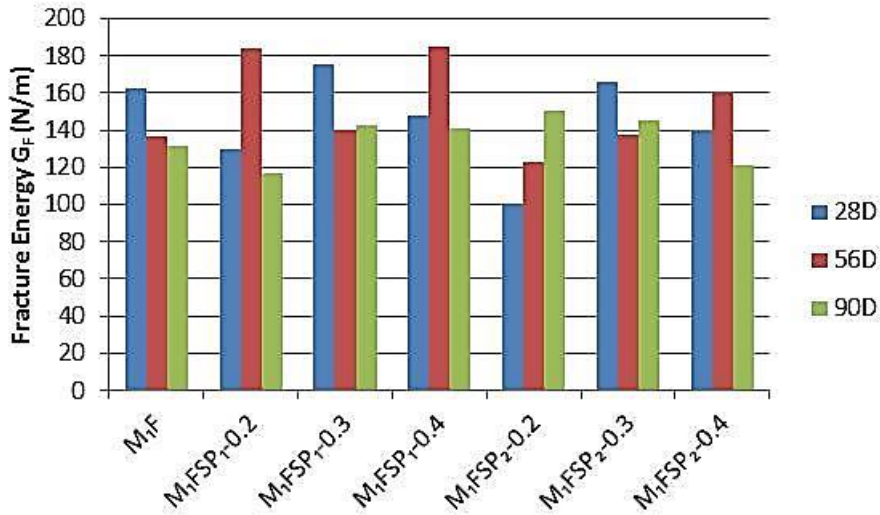


Figure 5-19: Fracture Energy ( $G_F$ ) of  $M_{1F}$  - HPC

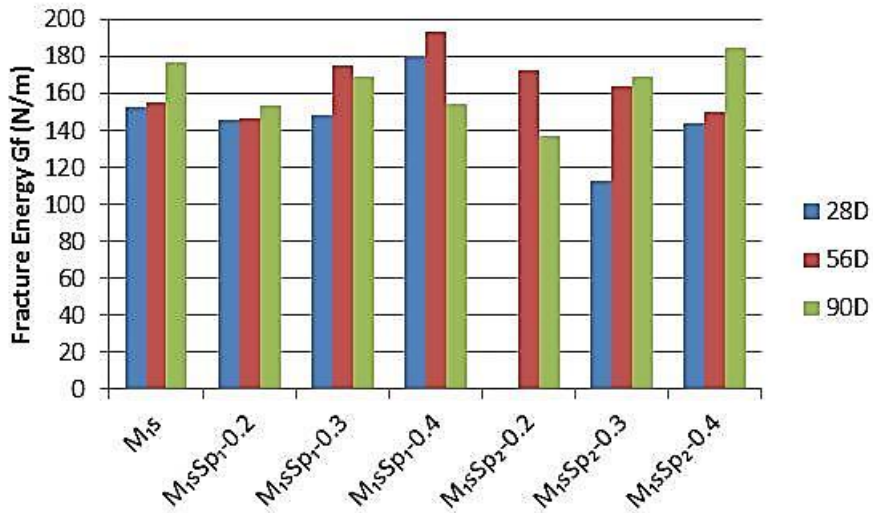


Figure 5-20: Fracture Energy ( $G_F$ ) of  $M_{1S}$  - HPC

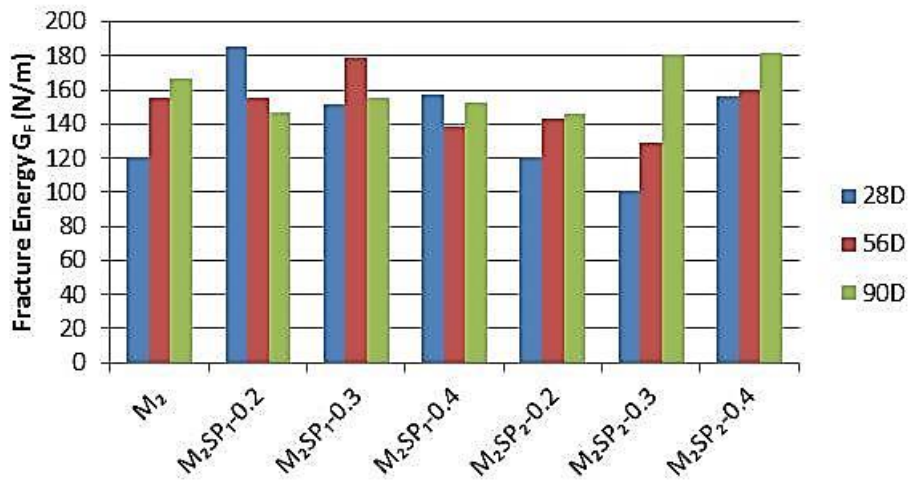


Figure 5-21: Fracture Energy ( $G_F$ ) of  $M_2$  - HPC

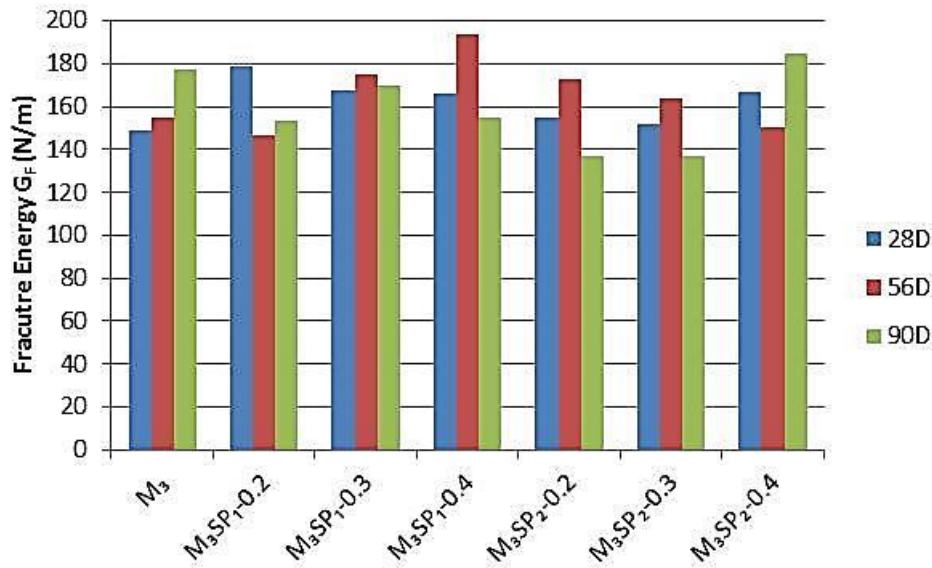


Figure 5-22: Fracture Energy ( $G_F$ ) of  $M_3$  – HPC

### 5.3.2 Discussion

Table 5.15 presents the results of the general linear model – univariate analysis for the splitting force of the HPC with SAP.

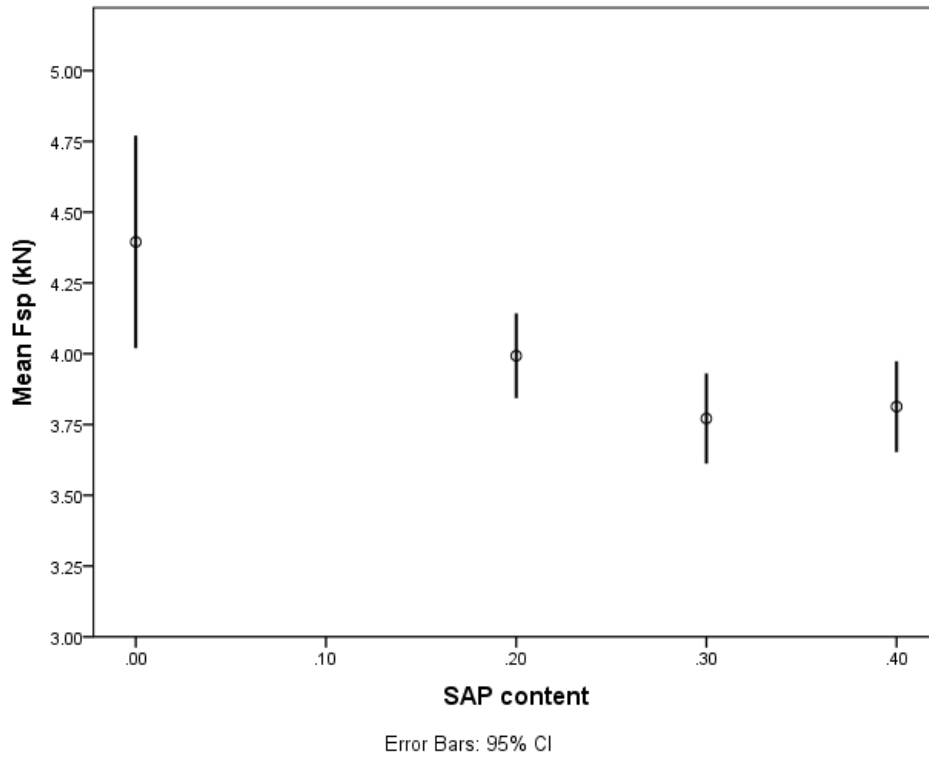
It is observed that three variables (W/B, SAP type and SAP content – asterisks' (\*<sup>1</sup>), Table 5.12) in that order had significant effect individually on the force of splitting. W/B showing the highest influence is as expected, since higher W/B in concrete should infer lower force required to split the concrete specimen. The two variable interactions further affirm the influence of SAP content and SAP type when combined with binder type on the splitting force of the HPC containing SAP.

Figure 5.23 show that the mean splitting force (from the statistical analysis) has a negative correlation with SAP content. The splitting force (and hence the splitting strength) decreases as the SAP content increases. The widest scatter of splitting force value was noted to be in the reference mixtures, an indication of the greater influence of W/B on the varied splitting force obtained for reference HPC mixtures. Figure 5.24 further shows that  $SP_2$  inclusion in HPC resulted in lower splitting force than  $SP_1$ . The splitting force of HPC containing  $SP_1$  was similar to that of the reference mixtures.

**Table 5-14: Tests of Between-Subjects Effects for Splitting Force ( $F_{sp}$ )**

Source	Type III Sum of Squares	df	Mean Square	F	Sig.
Corrected Model	69.768 <sup>a</sup>	82	.851	3.401	.000
Intercept	2794.699	1	2794.699	11171.046	.000
Single factor Analysis					
W/B	11.774	1	11.774	47.064	.000* <sup>1</sup>
SAP content	1.642	2	.821	3.281	.041* <sup>1</sup>
SAP type	2.314	1	2.314	9.250	.003* <sup>1</sup>
Binder type	.015	1	.015	.058	.810
Curing Age	.791	2	.395	1.580	.210
Two Factor Analysis					
W/B * SAP content	.616	2	.308	1.230	.296
W/B * SAP type	.028	1	.028	.110	.740
W/B * Curing Age	.018	2	.009	.036	.964
SAP content * SAP type	.097	2	.048	.193	.824
SAP content * Binder type	1.929	2	.964	3.855	.024* <sup>1</sup>
SAP content * Curing Age	.497	4	.124	.496	.739
SAP type * Binder type	5.658	1	5.658	22.617	.000* <sup>1</sup>
SAP type * Curing Age	.621	2	.310	1.241	.293
Binder type * Curing Age	.235	2	.118	.470	.626
Three Factor Analysis					
W/B * SAP content * SAP type	.670	2	.335	1.339	.266
W/B * SAP content * Curing Age	.420	4	.105	.420	.794
W/B * SAP type * Curing Age	.912	2	.456	1.822	.166
SAP content * SAP type * Binder type	.268	2	.134	.536	.586
SAP content * SAP type * Curing Age	1.621	4	.405	1.620	.174
SAP content * Binder type * Curing Age	2.024	4	.506	2.022	.095
SAP type * Binder type * Curing Age	.043	2	.021	.085	.918
Four Factor Analysis					
W/B * SAP content * SAP type * Curing Age	.966	4	.241	.965	.429
SAP content * SAP type * Binder type * Curing Age	1.307	3	.436	1.741	.162
Error	30.521	122	.250		
Total	3271.795	205			
Corrected Total	100.289	204			

a. R Squared = .696 (Adjusted R Squared = .491)



**Figure 5-23: Mean Splitting Force ( $F_{sp}$ ) against SAP content**

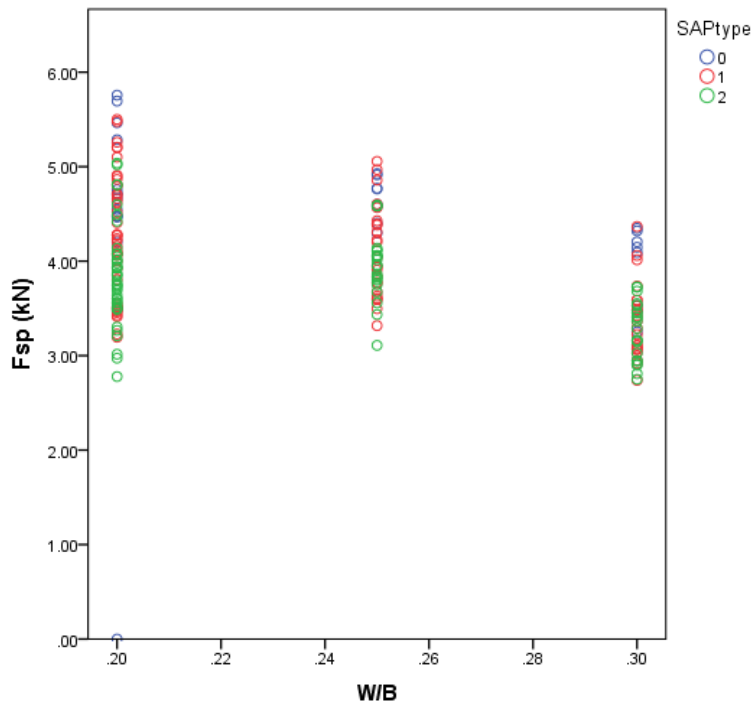


**Figure 5-24: Splitting Force ( $F_{sp}$ ) vs. W/B as influenced by SAP type**

The results of general linear – univariate analysis (using SPSS 22) of fracture energy of the HPC with SAP as presented in Table 5.16 reflect that binder type, SAP type and SAP content

(asterisks (\*<sup>1</sup>), in this decreasing order) has significant individual effect on the outcome of fracture energy, while the effect of W/B is not significant as a single factor.

**Table 5-15: Tests of Between-Subjects Effects for Fracture Energy**

Source	Type III Sum of Squares	df	Mean Square	F	Sig.
Corrected Model	86050.548 <sup>a</sup>	82	1049.397	2.620	.000
Intercept	3867589.069	1	3867589.069	9654.943	.000
Single Factor Analysis					
W/B	220.069	1	220.069	.549	.460
SAP content	3812.275	2	1906.137	4.758	.010* <sup>1</sup>
SAP type	2914.238	1	2914.238	7.275	.008* <sup>1</sup>
Binder type	3139.936	1	3139.936	7.838	.006* <sup>1</sup>
Curing Age	963.080	2	481.540	1.202	.304
Two Factor Analysis					
W/B * SAP content	607.826	2	303.913	.759	.471
W/B * SAP type	1199.360	1	1199.360	2.994	.086
W/B * Curing Age	5085.954	2	2542.977	6.348	.002* <sup>2</sup>
SAP content * SAP type	402.668	2	201.334	.503	.606
SAP content * Binder type	392.120	2	196.060	.489	.614
SAP content * Curing Age	1779.739	4	444.935	1.111	.355
SAP type * Binder type	68.479	1	68.479	.171	.680
SAP type * Curing Age	11191.428	2	5595.714	13.969	.000* <sup>2</sup>
Binder type * Curing Age	4629.895	2	2314.947	5.779	.004* <sup>2</sup>
Three Factor Analysis					
W/B * SAP content * SAP type	3315.301	2	1657.650	4.138	.018* <sup>3</sup>
W/B * SAP content * Curing Age	1863.591	4	465.898	1.163	.331
W/B * SAP type * Curing Age	604.438	2	302.219	.754	.472
SAP content * SAP type * Binder type	536.823	2	268.411	.670	.514
SAP content * SAP type * Curing Age	1111.548	4	277.887	.694	.598
SAP content * Binder type * Curing Age	4928.443	4	1232.111	3.076	.019* <sup>3</sup>
SAP type * Binder type * Curing Age	931.425	2	465.713	1.163	.316
Four Factor Analysis					
W/B * SAP content * SAP type * Curing Age	1432.025	4	358.006	.894	.470
SAP content * SAP type * Binder type * Curing Age	5918.920	3	1972.973	4.925	.003* <sup>4</sup>
Error	48069.747	120	400.581		
Total	4857480.375	203			
Corrected Total	134120.295	202			

a. R Squared = .642 (Adjusted R Squared = .397)

At two variable combinations level, SAP type combined with binder type has the least significant effect. Influence of combinations of W/B\*curing age, SAP type\*curing age and binder type\*curing age (asterisks (\*<sup>2</sup>)) are noted to be very significant at the two factor analysis level. Three and four factor analysis however affirmed the postulation that binder type is the more influential factor than the W/B in combination with the three other variables (SAP content, SAP type and curing age).

Figure 5.25 shows a plot of the fracture energy of the HPC mixtures against SAP contents as influenced also by the binder type. The figure shows that the fracture energy of the HPCs increases slightly with increasing SAP contents. The HPCs with the highest SAP content has the highest mean fracture energy, followed closely by the reference mixtures.

This implies that although the splitting force was higher at lower SAP content, the ductility of the HPC increases as the SAP contents increase. The ternary binders (Type 2 and Type 3) were generally observed to show better scatter than the binary binders (Type 1).

The compressive strength vs. fracture energy plots (Figure 5.26 – SAP contents influence and Figure 5.27 – W/B influence) also reflect that observed decrease in compressive strength with W/B and SAP contents increase does not translate to same change order in fracture energy.

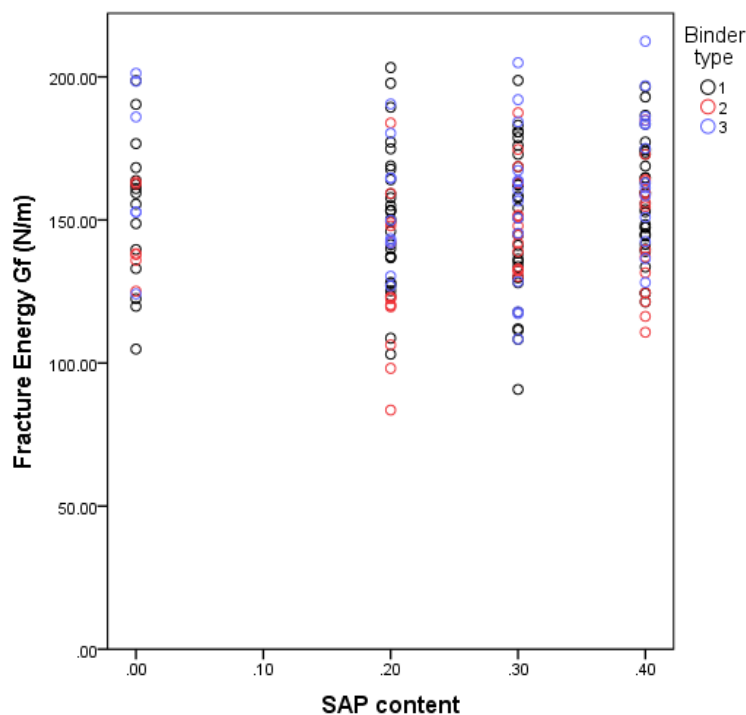


**Figure 5-25: Fracture Energy vs. SAP contents as influenced by binder type**

The Duncan's multiple range test results as presented in Tables B4.1 to B4.5 of Appendix B shows that the groupings of means for the fracture energy as influenced by W/B, SAP contents, SAP type, binder type, and curing age are all of significant influence. The groupings of means on SAP contents influence is the closest to the 95% level which serves as the bench-mark for assessing the significant level of influence for respective factors. It is therefore seen that the splitting tensile strength and

fracture energy of the HPCs are not directly affected by SAP addition neither by the SAP type nor SAP contents.

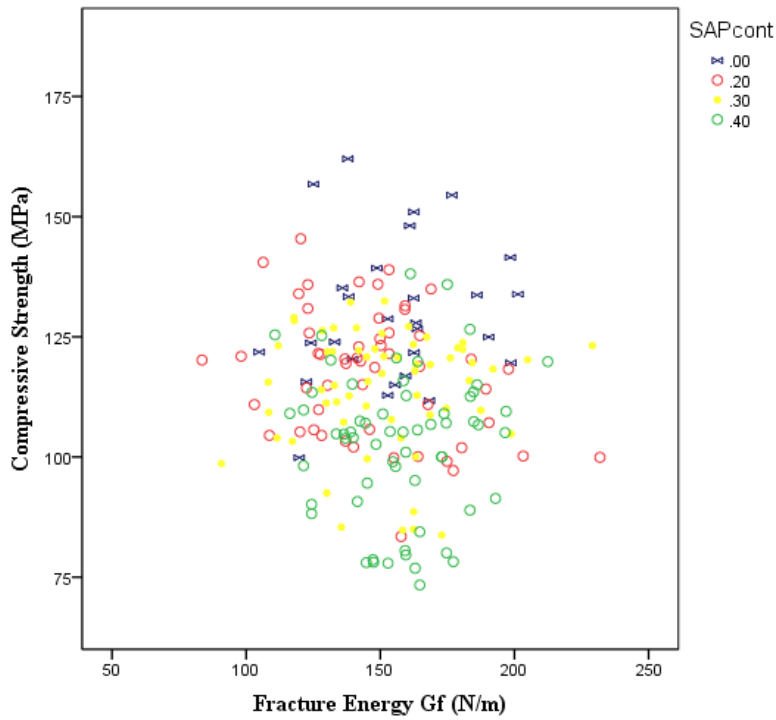


Figure 5-26: Compressive Strength vs. Fracture Energy as influenced by SAP contents

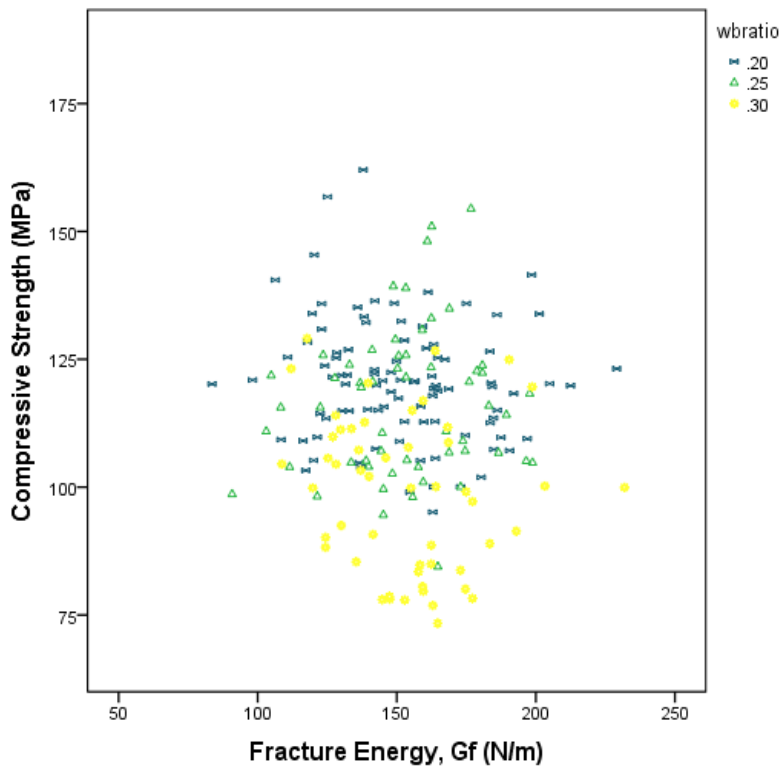


Figure 5-27: Compressive Strength vs. Fracture Energy as influenced by W/B

The Duncan's multiple range test results as presented in Tables B4.1 to B4.5 of Appendix B shows that the groupings of means for the fracture energy as influenced by W/B, SAP contents, SAP type, binder type, and curing age are all of significant influence. The groupings of means on SAP contents influence is the closest to the 95% level which serves as the bench-mark for assessing the significant level of influence for respective factors. It is therefore seen that the splitting tensile strength and fracture energy of the HPCs are not directly affected by SAP addition neither by the SAP type nor SAP contents.

## 5.4 Summary

The outcome of the various experimental works carried out on the mechanical properties of HPC with SAP introduced as IC-agents can be summarised as follows:

- i. SAP addition to HPCs contribute to the air content in the concrete as the density of the HPCs decreased at relatively small rate as the SAP content in the concrete increases.
- ii. Compressive strength of low W/B HPCs decreases slightly as SAP contents increases.
- iii. A combination of void volume correction by the Bolomey's formula and the Powers gel - space ratio is a good model for predicting effect of SAP addition on the compressive strength of the low W/B HPCs.
- iv. SAP addition within the limits of the contents used in this study (0.2 to 0.4%  $b_{wob}$ ) in low W/B HPCs has no significant influence on the elastic and fracture properties of the concrete.

SAP addition leads to reduction in compressive strength of HPC, correction made for void volume (SAP and air) using the Bolomey's formula and Powers' gel-space ratio enhanced a good fit into the Powers' Model and hence makes it possible to predict the SAP effect on the compressive strength of HPC. SAP addition within the limits of 0.2% to 0.4%  $b_{wob}$  did not lead to significant decrease in  $G_F$  of the low W/B HPCs.

# 6

## *Non Destructive Tests on HPC with SAP*

This chapter presents results and discussion on the non-destructive tests carried out on HPC mixtures with SAP towards examining the influence of SAP on the porosity, pore distribution, micro-morphology of the HPC and the crystalline structure of the solid phases of the hydration products in the various HPC mixtures. The results are classified and discussed in Sections 6.1 and 6.2.

### **6.1 X-ray CT Scanning**

This test involves two stages of investigations namely:

- i. X-ray CT scanning of single specimens for all the varied mixtures ( $M_{1F}$ ,  $M_{1S}$ ,  $M_2$  and  $M_3$ ) with varied SAP contents (0%, 0.2%, 0.3% and 0.4%) and sizes ( $SP_1$  – 0/300 um;  $SP_2$  – 0/600 um) cured in water bath at different ages (28, 56 and 90 days) – total of 84 (50 mm  $\varnothing$  x 100 mm) concrete cylinders; and
- ii. X-ray CT scanning of triplicate specimens of HPC mixtures ( $M_{1F}$ ,  $M_2$  and  $M_3$ ) studied after 7 and 28 days curing in water. Triplicates of  $M_2$  specimen were studied with both sizes of SAP ( $SP_1$  and  $SP_2$ ) – 42 concrete cylinders; while  $M_{1F}$  and  $M_3$  triplicates were studied for  $SP_1$  only – also 42 concrete cylinders.

The Stage II (triplicate specimen) analysis was conducted to verify the reason for variation in the results reported in Stage I.

While casting the triplicate HPC specimens (Stage II), effort was made to keep the fresh concrete on the vibration table for a longer time (10 mins instead of the 5 mins of Stage I) to ensure that entrapped air voids are minimised in the HPC mixtures.

The CT scanning analysis enhanced an in-depth view of the internal structure of the HPCs with the objective of examining the pore spaces within the cement paste matrix and a classification of the air

voids created by the swollen SAP after desorption of the absorbed water. Figure 6.1 presents a snapshot of the centrally cropped (air threshold) HPC specimen with air voids in blue colour within the cement paste matrix. The observed air voids were well distributed and of varying sizes and shapes.

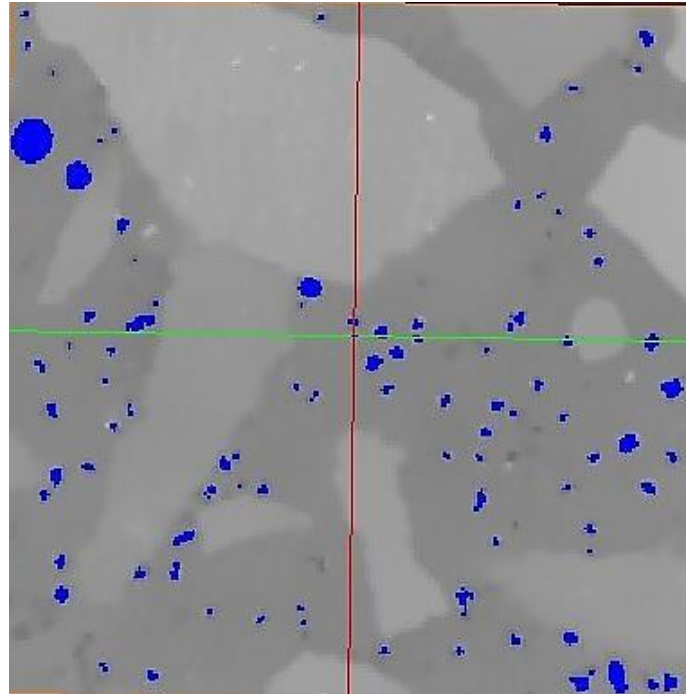


**Figure 6-1: Centrally cropped - 25 mm x 25 mm (air-threshold) HPC with air voids in blue colour**

Histogram plots for the single specimen test (i.e. Stage 1 test) of the various HPC mixtures after 28 days of curing is presented in Figures 6.2 to 6.5. This reveals all the HPC mixtures irrespective of SAP contents as having micro-air voids presents. The peak of the histograms were within 225  $\mu\text{m}$  to 300  $\mu\text{m}$  diameter air voids (i.e. 0.006 to 0.0141  $\text{mm}^3$  pore volume sizes) while a reference HPC mixture ( $M_{1S}$ ) only has a peak at 375  $\mu\text{m}$  diameter. The air void distribution in HPC mixtures containing SAP as IC-agent had more air voids and the air voids sizes have wider distribution than the reference mixtures. The discussion in the following sections on air voids thereby adopts the use of some terms with the meanings as follows:

SAP voids – these refer to the air voids created by SAP in the HPCs. Hence for SAP Type I ( $SP_1$ ), the air voids sizes of 0 – 900  $\mu\text{m}$  diameter applies while the void sizes of 0 – 1500  $\mu\text{m}$  diameter are implied for SAP Type II ( $SP_2$ ). The reference mixtures do not have SAP included and hence have no SAP voids.

SAP voids range – this refers generally to all air voids present in the HPC within the SAP voids sizes (i.e. 0 – 1500  $\mu\text{m}$ ) for all HPCs. Large voids however refers to air voids > 1500  $\mu\text{m}$  in diameter.

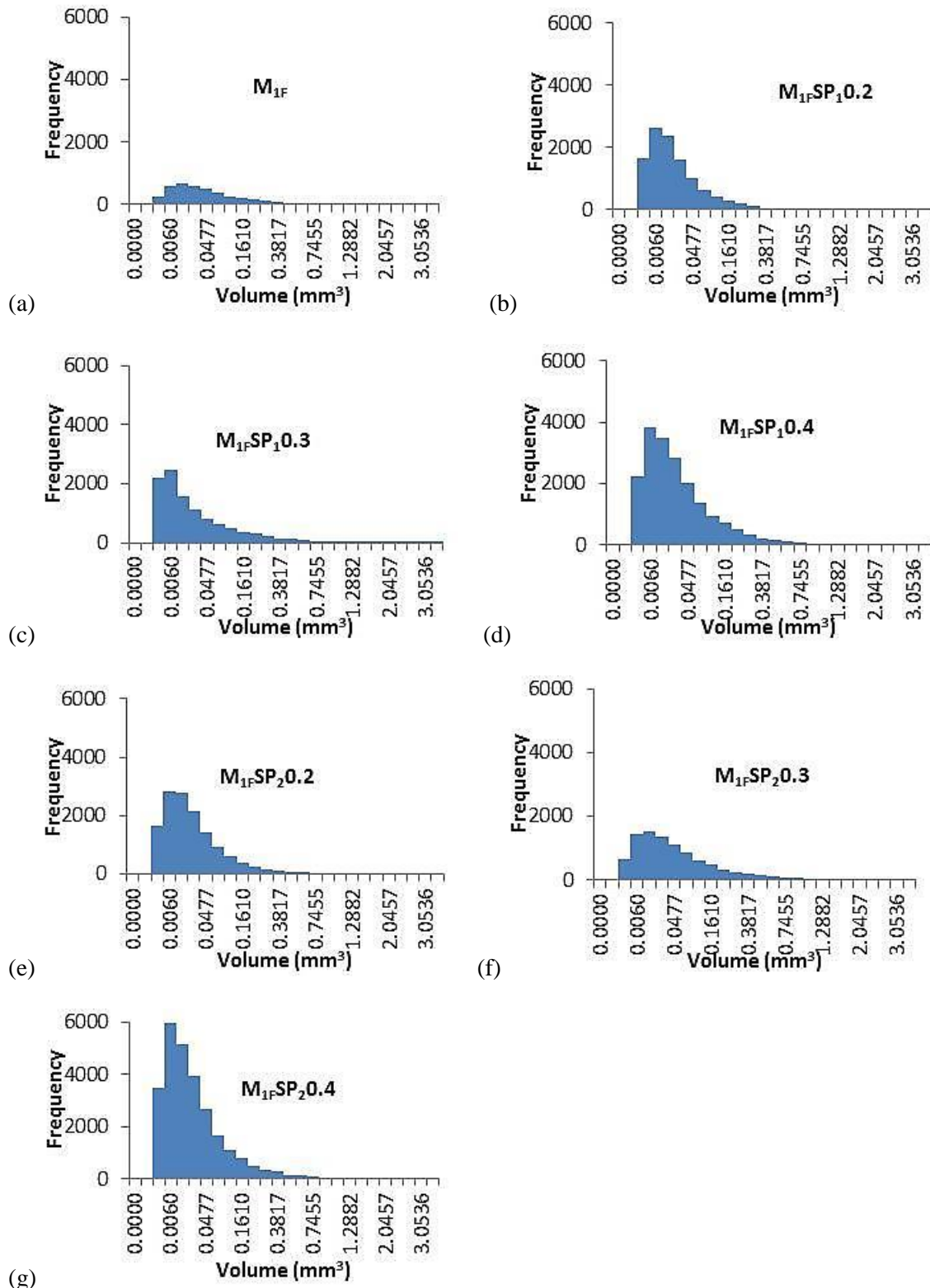


Figure 6-2: Histogram Plot of Air Void Distribution of (25 x 25 x 50 mm<sup>3</sup>)  $M_{1F}$  – HPC Samples

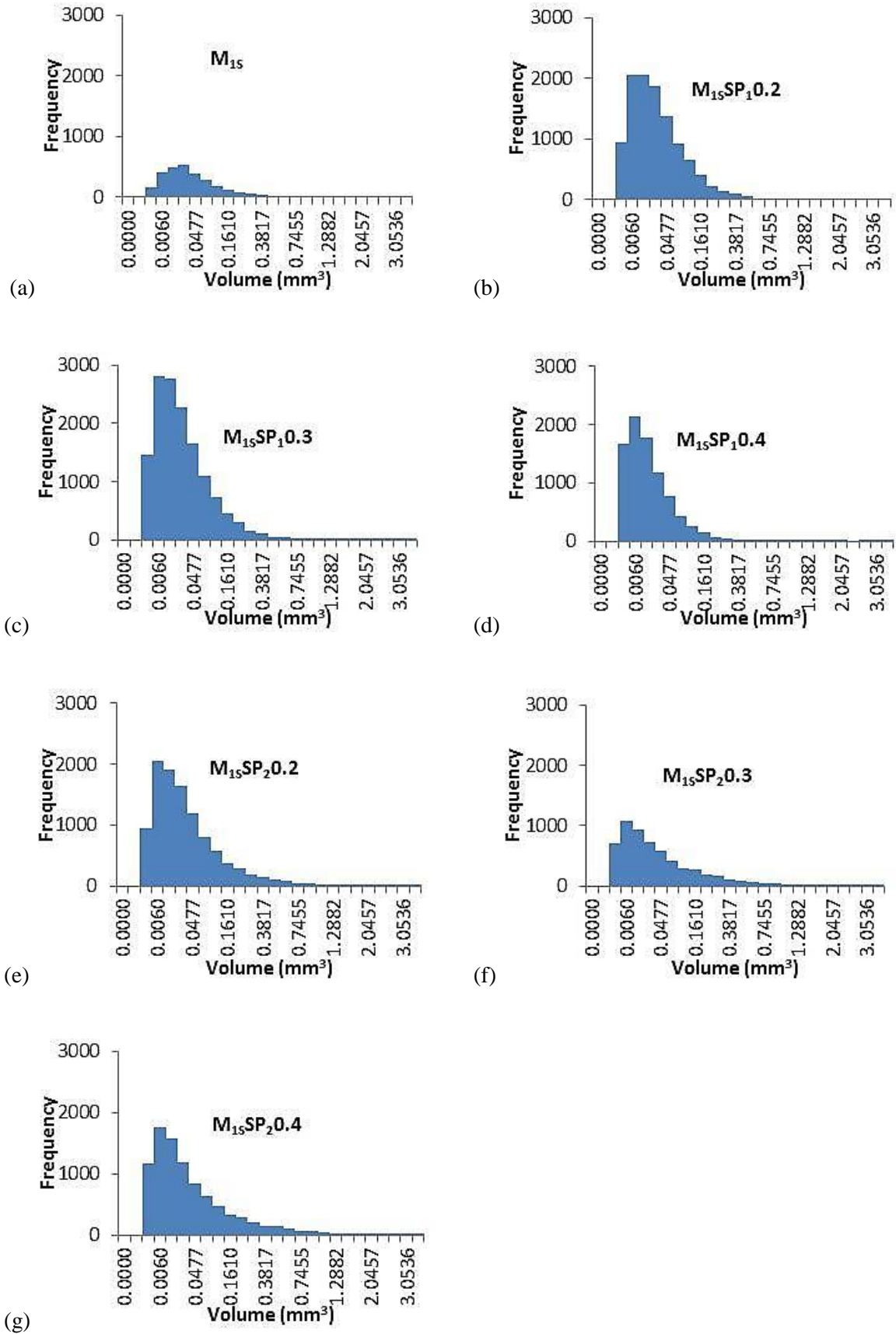


Figure 6-3: Histogram Plot of Air Void Distribution of (25 x 25 x 50 mm<sup>3</sup>)  $M_{15}$  – HPC Samples

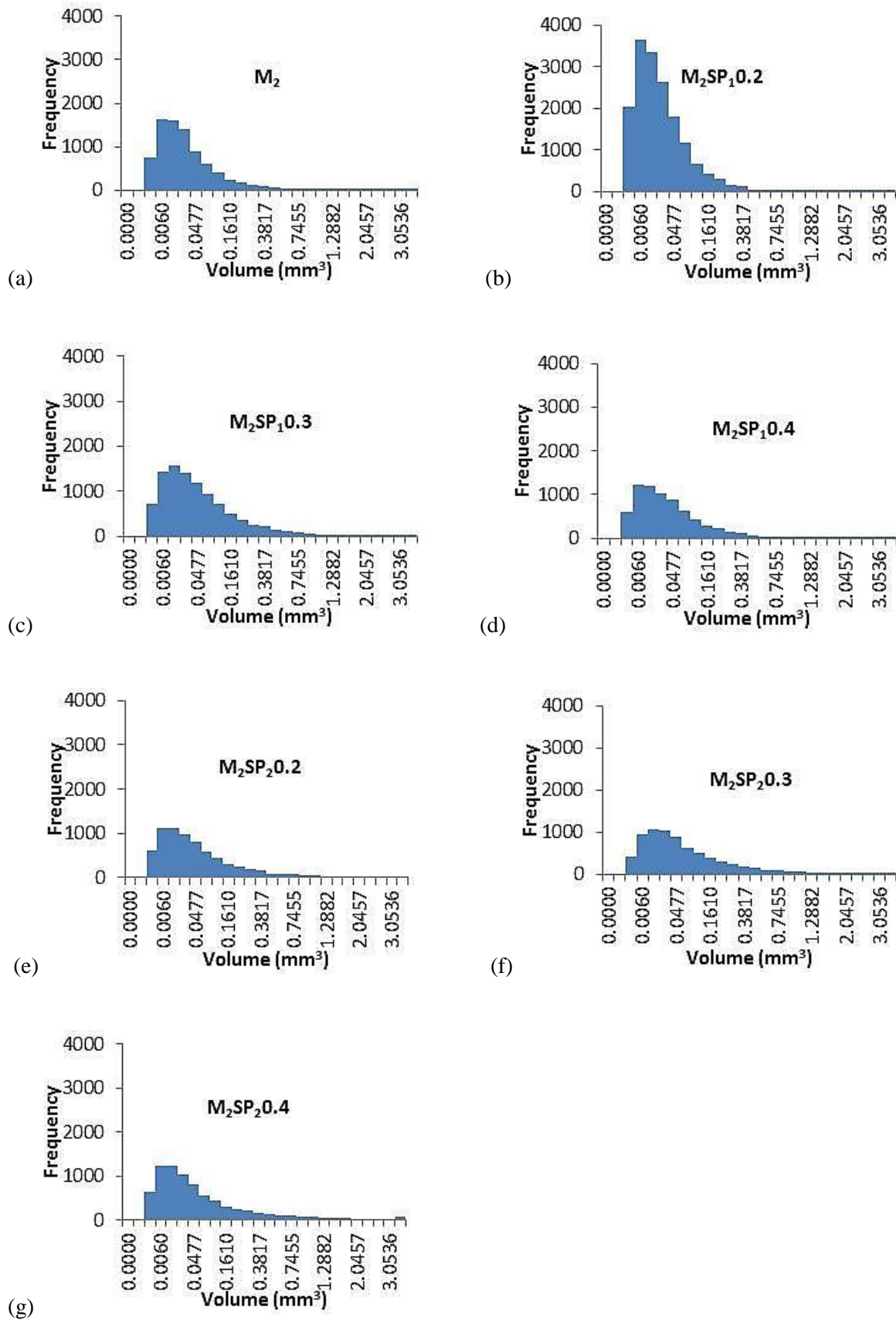


Figure 6-4: Histogram Plot of Air Void Distribution of (25 x 25 x 50 mm<sup>3</sup>) M<sub>2</sub> – HPC Samples

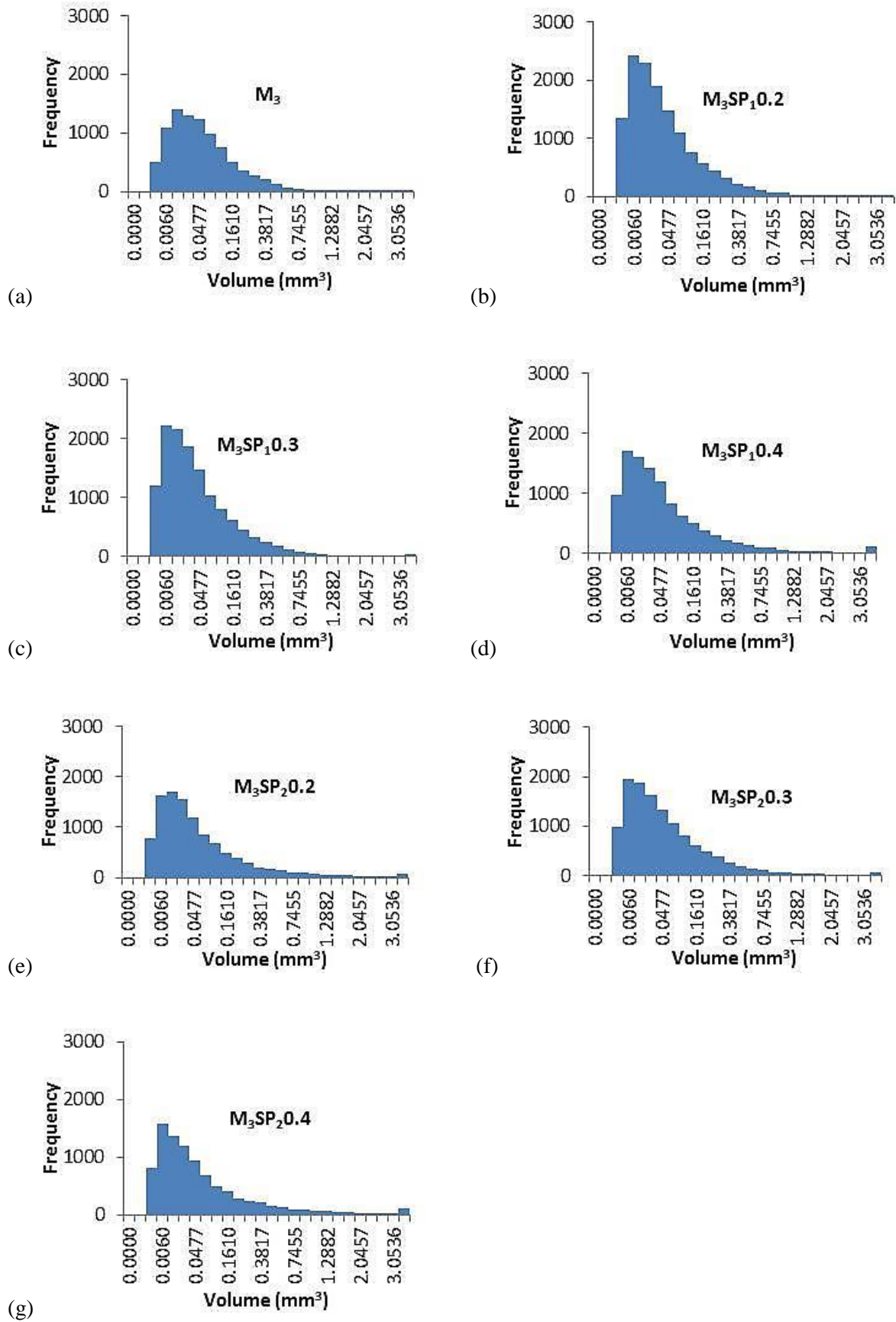


Figure 6-5: Histogram Plot of Air Void Distribution of (25 x 25 x 50 mm<sup>3</sup>)  $M_3$  – HPC Samples

### 6.1.1 Influence of SAP Contents on Air Void Distribution

The trend in general (Figure 6.2 to 6.5) is that SAP void% (i.e. SP<sub>1</sub> (0 – 900 μm) and SP<sub>2</sub> (0 – 1500 μm) as defined in Section 6.1) and total void% (i.e. percentage porosity) increases as the SAP contents and W/B increases with some inconsistencies present. These results are further summarised and presented in Tables 6.1 to 6.4 for proper discussion and understanding.

**Table 6-1: Summary of Influence of SAP contents and curing age on void distribution for M<sub>IF</sub> – HPC**

Curing Age Influence	Ref	SAP1			SAP2		
M <sub>IF</sub> -28 days series	M <sub>IF</sub>	M <sub>IF</sub> SP <sub>1</sub> -0.2	M <sub>IF</sub> SP <sub>1</sub> -0.3	M <sub>IF</sub> SP <sub>1</sub> -0.4	M <sub>IF</sub> SP <sub>2</sub> -0.2	M <sub>IF</sub> SP <sub>2</sub> -0.3	M <sub>IF</sub> SP <sub>2</sub> -0.4
SAP pore expected% <sup>+</sup>	0.00	3.40	5.01	6.56	3.40	5.01	6.56
Demoulded Porosity% <sup>++</sup>	0.58	4.39	6.56	6.66	2.43	5.67	6.17
No of voids >1500 μm	35	45	48	52	35	57	70
SAP voids%	0.00	1.25	1.51	2.77	2.19	3.05	4.40
Total Porosity%	1.47	2.03	2.91	4.42	2.53	3.53	5.06
Max. void size (mm <sup>3</sup> )	57.8053	23.1448	65.5331	49.5119	14.7461	11.2816	55.9819
Av. void size (mm <sup>3</sup> )	0.1535	0.0585	0.0878	0.0707	0.0554	0.1070	0.0556
M <sub>IF</sub> -56 days series	M <sub>IF</sub>	M <sub>IF</sub> SP <sub>1</sub> -0.2	M <sub>IF</sub> SP <sub>1</sub> -0.3	M <sub>IF</sub> SP <sub>1</sub> -0.4	M <sub>IF</sub> SP <sub>2</sub> -0.2	M <sub>IF</sub> SP <sub>2</sub> -0.3	M <sub>IF</sub> SP <sub>2</sub> -0.4
No of voids >1500 μm	37	37	37	64	42	67	36
SAP voids%	0.00	1.30	1.87	2.60	1.68	3.91	2.23
Total Porosity%	1.68	2.22	2.68	4.02	2.07	4.49	2.56
Max. void size (mm <sup>3</sup> )	55.0342	25.5845	57.4526	15.7617	46.9377	32.8651	121.8050
Av. void size (mm <sup>3</sup> )	0.0287	0.1079	0.0656	0.0570	0.0637	0.1161	0.0604
M <sub>IF</sub> -90 days series	M <sub>IF</sub>	M <sub>IF</sub> SP <sub>1</sub> -0.2	M <sub>IF</sub> SP <sub>1</sub> -0.3	M <sub>IF</sub> SP <sub>1</sub> -0.4	M <sub>IF</sub> SP <sub>2</sub> -0.2	M <sub>IF</sub> SP <sub>2</sub> -0.3	M <sub>IF</sub> SP <sub>2</sub> -0.4
No of voids >1500 μm	29	45	53	55	39	152	51
SAP voids%	0.00	1.35	2.21	2.57	1.63	3.88	2.69
Total Porosity%	1.48	2.21	3.31	4.40	2.00	5.31	3.17
Max. void size (mm <sup>3</sup> )	60.6563	77.9447	55.6584	38.8080	30.2217	31.2426	61.0476
Av. void size (mm <sup>3</sup> )	0.0861	0.0794	0.0888	0.0878	0.0534	0.1664	0.0560

+Expected pore content by volume based on the 25 g/g pore absorption used for provision of additional water calculated taking the swollen SAP as a spherical substance.

\*\*Porosity calculated volumetrically using Demoulded density in comparison to designed density

**Table 6-2: Summary of Influence of SAP contents and curing age on void distribution for M<sub>IS</sub> – HPC**

Curing Age Influence	Ref	SAP1			SAP2		
M <sub>IS</sub> -28 days series	M <sub>IS</sub>	M <sub>IS</sub> SP <sub>1</sub> -0.2	M <sub>IS</sub> SP <sub>1</sub> -0.3	M <sub>IS</sub> SP <sub>1</sub> -0.4	M <sub>IS</sub> SP <sub>2</sub> -0.2	M <sub>IS</sub> SP <sub>2</sub> -0.3	M <sub>IS</sub> SP <sub>2</sub> -0.4
SAP pore expected% <sup>+</sup>	0.00	3.40	5.01	6.56	3.40	5.01	6.56
Demoulded Porosity% <sup>++</sup>	0.20	3.99	4.47	6.38	3.52	4.96	6.39
No of voids >1500 μm	13	32	26	17	39	29	45
SAP voids%	0.00	1.60	1.92	0.73	2.71	1.70	2.65
Total Porosity%	0.82	2.31	2.60	1.08	3.05	1.98	3.03
Max. void size (mm <sup>3</sup> )	39.4069	41.7455	17.2391	26.4097	22.1718	23.4150	14.5798
Av. void size (mm <sup>3</sup> )	0.1085	0.0656	0.0517	0.0391	0.0815	0.1003	0.0934
M <sub>IS</sub> -56 days series	M <sub>IS</sub>	M <sub>IS</sub> SP <sub>1</sub> -0.2	M <sub>IS</sub> SP <sub>1</sub> -0.3	M <sub>IS</sub> SP <sub>1</sub> -0.4	M <sub>IS</sub> SP <sub>2</sub> -0.2	M <sub>IS</sub> SP <sub>2</sub> -0.3	M <sub>IS</sub> SP <sub>2</sub> -0.4
No of voids >1500 μm	25	21	25	32	21	154	21
SAP voids%	0.00	0.64	1.18	1.89	1.73	3.46	1.47
Total Porosity%	1.32	1.03	1.62	2.77	1.91	4.92	1.68
Max. void size (mm <sup>3</sup> )	39.5014	42.2539	66.9719	31.1374	13.1822	67.1117	31.0256
Av. void size (mm <sup>3</sup> )	0.0695	0.0752	0.0716	0.0602	0.0818	0.1977	0.0957
M <sub>IS</sub> -90 days series	M <sub>IS</sub>	M <sub>IS</sub> SP <sub>1</sub> -0.2	M <sub>IS</sub> SP <sub>1</sub> -0.3	M <sub>IS</sub> SP <sub>1</sub> -0.4	M <sub>IS</sub> SP <sub>2</sub> -0.2	M <sub>IS</sub> SP <sub>2</sub> -0.3	M <sub>IS</sub> SP <sub>2</sub> -0.4
No of voids >1500 μm	27	29	45	22	47	22	26
SAP voids%	0.00	1.55	1.73	1.86	2.15	2.40	2.45
Total Porosity%	0.86	2.29	2.65	2.63	2.55	2.61	2.69
Max. void size (mm <sup>3</sup> )	28.2159	15.2320	35.8571	21.9362	23.8276	17.2884	15.4103
Av. void size (mm <sup>3</sup> )	0.1477	0.0608	0.0817	0.0593	0.0641	0.0784	0.1051

+Expected pore content by volume based on the 25 g/g pore absorption used for provision of additional water calculated taking the swollen SAP as a spherical substance.

\*\*Porosity calculated volumetrically using Demoulded density in comparison to designed density.

**Table 6-3: Summary of Influence of SAP contents and curing age on void distribution for M<sub>2</sub> – HPC**

Curing Age Influence	Ref	SAP1			SAP2		
M <sub>2</sub> -28 days series	M <sub>2</sub>	M <sub>2</sub> SP <sub>1</sub> -0.2	M <sub>2</sub> SP <sub>1</sub> -0.3	M <sub>2</sub> SP <sub>1</sub> -0.4	M <sub>2</sub> SP <sub>2</sub> -0.2	M <sub>2</sub> SP <sub>2</sub> -0.3	M <sub>2</sub> SP <sub>2</sub> -0.4
SAP pore expected% <sup>+</sup>	0.00	2.85	4.21	5.53	2.85	4.21	5.53
Demoulded Porosity% <sup>++</sup>	0.17	2.37	3.98	5.47	1.88	4.06	5.38
No of voids >1500 µm	63	50	63	47	98	118	157
SAP voids%	0.00	2.01	1.91	1.19	2.51	3.12	3.12
Total Porosity%	2.33	3.05	3.65	2.22	3.39	4.19	4.65
Max. void size (mm <sup>3</sup> )	122.1950	101.0430	52.7768	87.1312	43.9629	87.0767	53.5381
Av. void size (mm <sup>3</sup> )	0.1247	0.0640	0.1244	0.1199	0.1469	0.1907	0.2474
M <sub>2</sub> -56 days series	M <sub>2</sub>	M <sub>2</sub> SP <sub>1</sub> -0.2	M <sub>2</sub> SP <sub>1</sub> -0.3	M <sub>2</sub> SP <sub>1</sub> -0.4	M <sub>2</sub> SP <sub>2</sub> -0.2	M <sub>2</sub> SP <sub>2</sub> -0.3	M <sub>2</sub> SP <sub>2</sub> -0.4
No of voids >1500 µm	49	50	70	44	43	36	195
SAP voids%	0.00	0.93	1.37	1.14	1.86	2.00	2.84
Total Porosity%	2.29	1.71	3.02	2.03	2.23	2.35	4.72
Max. void size (mm <sup>3</sup> )	28.6351	93.9300	84.8632	34.1548	52.4560	49.9551	72.2334
Av. void size (mm <sup>3</sup> )	0.0770	0.0707	0.1161	0.0881	0.1293	0.0909	0.3734
M <sub>2</sub> -90 days series	M <sub>2</sub>	M <sub>2</sub> SP <sub>1</sub> -0.2	M <sub>2</sub> SP <sub>1</sub> -0.3	M <sub>2</sub> SP <sub>1</sub> -0.4	M <sub>2</sub> SP <sub>2</sub> -0.2	M <sub>2</sub> SP <sub>2</sub> -0.3	M <sub>2</sub> SP <sub>2</sub> -0.4
No of voids >1500 µm	33	47	36	67	85	40	107
SAP voids%	0.00	1.44	1.77	2.05	2.19	1.98	2.89
Total Porosity%	1.78	2.44	2.60	3.19	2.95	2.37	3.88
Max. void size (mm <sup>3</sup> )	78.9696	46.8672	41.0228	14.3176	24.7034	34.7591	28.5593
Av. void size (mm <sup>3</sup> )	0.0913	0.0680	0.0648	0.0733	0.2126	0.1029	0.1779

+Expected pore content by volume based on the 25 g/g pore absorption used for provision of additional water calculated taking the swollen SAP as a spherical substance.

++Porosity calculated volumetrically using Demoulded density in comparison to designed density.

**Table 6-4: Summary of Influence of SAP contents and curing age on void distribution for M<sub>3</sub> – HPC**

Curing Age Influence	Ref	SAP1			SAP2		
M <sub>3</sub> -28 days series	M <sub>3</sub>	M <sub>3</sub> SP <sub>1</sub> -0.2	M <sub>3</sub> SP <sub>1</sub> -0.3	M <sub>3</sub> SP <sub>1</sub> -0.4	M <sub>3</sub> SP <sub>2</sub> -0.2	M <sub>3</sub> SP <sub>2</sub> -0.3	M <sub>3</sub> SP <sub>2</sub> -0.4
SAP pore expected% <sup>+</sup>	0.00	2.64	3.91	5.14	2.64	3.91	5.14
Demoulded Porosity% <sup>++</sup>	1.58	3.25	6.00	6.00	3.92	3.56	4.54
No of voids >1500 µm	65	50	57	191	171	119	199
SAP voids%	0.00	2.27	2.32	1.94	4.04	4.09	3.33
Total Porosity%	3.54	3.85	4.12	5.73	5.63	5.26	5.23
Max. void size (mm <sup>3</sup> )	50.0416	14.2617	20.4162	103.9910	86.8118	53.2107	48.4244
Av. void size (mm <sup>3</sup> )	0.1156	0.0821	0.0930	0.2443	0.1742	0.1576	0.2170
M <sub>3</sub> -56 days series	M <sub>3</sub>	M <sub>3</sub> SP <sub>1</sub> -0.2	M <sub>3</sub> SP <sub>1</sub> -0.3	M <sub>3</sub> SP <sub>1</sub> -0.4	M <sub>3</sub> SP <sub>2</sub> -0.2	M <sub>3</sub> SP <sub>2</sub> -0.3	M <sub>3</sub> SP <sub>2</sub> -0.4
No of voids >1500 µm	53	43	42	196	84	149	113
SAP voids%	0.00	1.75	1.39	2.23	3.05	3.34	3.75
Total Porosity%	2.10	2.84	2.33	6.05	3.86	4.71	4.83
Max. void size (mm <sup>3</sup> )	22.0547	38.5817	46.5664	39.6771	55.8621	60.3435	25.2584
Av. void size (mm <sup>3</sup> )	0.1185	0.0779	0.0915	0.1973	0.1859	0.1790	0.1508
M <sub>3</sub> -90 days series	M <sub>3</sub>	M <sub>3</sub> SP <sub>1</sub> -0.2	M <sub>3</sub> SP <sub>1</sub> -0.3	M <sub>3</sub> SP <sub>1</sub> -0.4	M <sub>3</sub> SP <sub>2</sub> -0.2	M <sub>3</sub> SP <sub>2</sub> -0.3	M <sub>3</sub> SP <sub>2</sub> -0.4
No of voids >1500 µm	34	35	64	70	51	52	104
SAP voids%	0.00	1.04	1.98	2.06	2.44	2.44	3.19
Total Porosity%	1.98	2.41	3.49	3.85	2.95	2.92	4.15
Max. void size (mm <sup>3</sup> )	31.7151	28.7177	12.1826	71.1845	45.9914	100.9750	26.2220
Av. void size (mm <sup>3</sup> )	0.0679	0.1026	0.1134	0.1008	0.1533	0.1634	0.1465

+Expected pore content by volume based on the 25 g/g pore absorption used for provision of additional water calculated taking the swollen SAP as a spherical substance.

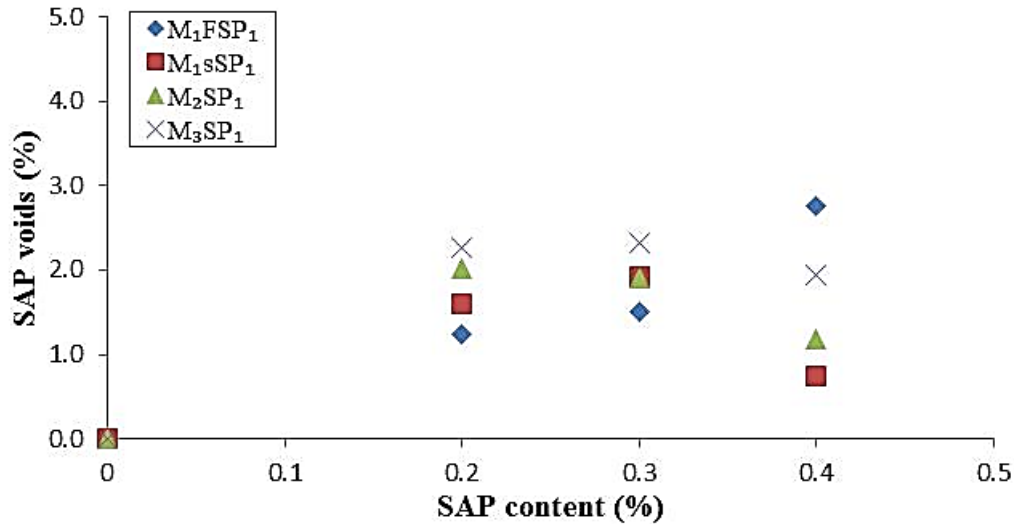
++Porosity calculated volumetrically using Demoulded density in comparison to designed density.

An examination of the maximum void sizes in the HPC mixtures (Tables 6.1 to 6.4) reveals neither a particular trend nor consistency which is expected as the maximum pore would depend on statistical probability and the sample size. The reference mixtures after 28 days of curing give maximum void sizes amongst the largest in most instances ( $M_{1F}$  (57.80 mm<sup>3</sup>);  $M_{1S}$  (39.41 mm<sup>3</sup>);  $M_2$  (122.2 mm<sup>3</sup>) and  $M_3$  (50.04 mm<sup>3</sup>) - Tables 6.1 to 6.4) while very high numbers (80 – 200) of large voids (> 1500 µm) are seen in many of the single specimen analysed (pink colour highlights in Tables 6.1 – 6.4). The study also observed the existence of a high number of air voids larger than SAP created voids (> 900 µm for  $SP_1$  ( $\leq 300$  µm) and > 1500 µm for  $SP_2$  ( $\leq 300$  µm)); arbitrary extremes (very small and large) air voids volumes (blue colour highlights in Tables 6.1 – 6.4) were noted too and these definitely contributed to the value obtained for total porosity as calculated from the X-ray CT scanning analysis. Average pore (i.e. air void) sizes in the HPCs varied between 0.02 mm<sup>3</sup> and 0.40 mm<sup>3</sup> without following a particular trend (Tables 6.1 to 6.4) in the single specimen analysis.

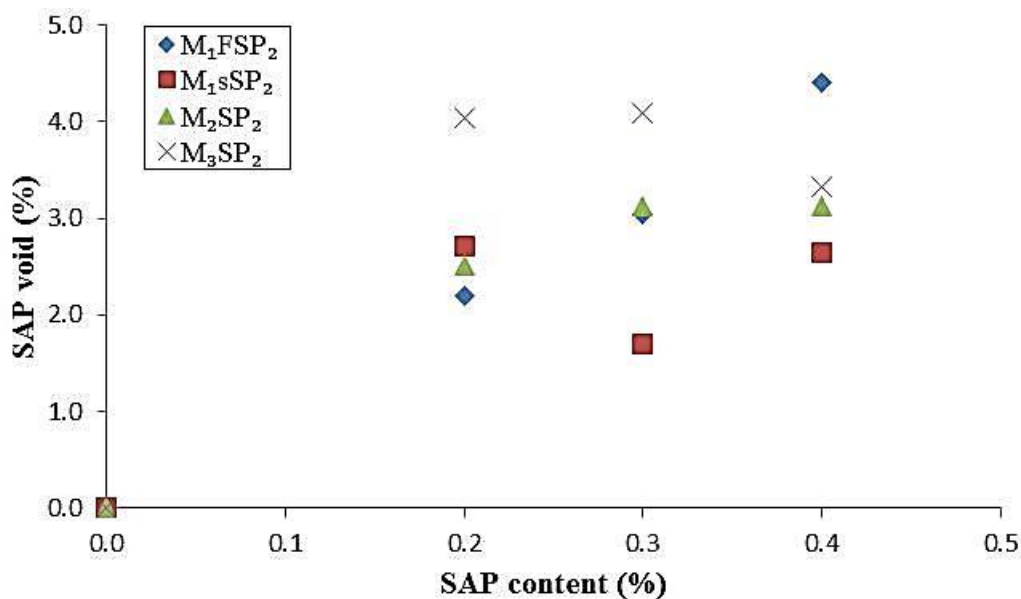
The porosity created by SAP in the HPC (SAP voids porosity) were generally about halve the value of porosity expected using the 25 g/g SAP absorption capacity determined via the tea-bag test as discussed and reported in Sections 3.2.1 and 4.1.2. The demoulded porosity however gave similar values to the calculated porosity expected (Table 6.1 to 6.4), although a bit higher. The total porosity from X-ray CT scanning analysis on the other hand is even lower than the demoulded porosity. This implies that porosity in the HPC generally decreased with cement hydration over time. An indication that the initial volume occupied by the swollen SAP in the fresh concrete observed as SAP voids reduces in size and hence volume with increased concrete age as cement hydration products occupy the spaces created by the swollen SAP. It follows that maintaining the water added to the mixing water for SAP absorption in concrete mixtures at 12.5 g/g (i.e. halve the 25 g/g used in this study), similar value to that suggested in previous studies (Esteves, 2014; Hasholt et al., 2012), will reduce occurrence of SAP created air voids in these HPCs and hence avert the strength reduction effect of SAP addition observed.

Figure 6.6 shows that for the single specimen analysis, the SAP voids ( $SP_1$  (0 -900 µm);  $SP_2$  (0 – 1500 µm)) increased with increase in SAP contents for all HPC mixtures irrespective of the SAP size

(except for the non-conforming – green colour highlights in Tables 6.1 to 6.4). The higher the binder (i.e. fines) contents also, the lower the porosity and hence the better the HPC produced.



(a). SP<sub>1</sub> void series after 28 days curing



(b). SP<sub>2</sub> void series after 28 days curing

**Figure 6-6: SAP void% against SAP content% (a) SP<sub>1</sub>; (b) SP<sub>2</sub>**

Figure 6.7 to 6.10 present the plot of cumulative SAP voids range% (< 1500 μm for all HPCs as defined in Section 6.1) against the curing age for Stage I (single specimen) analysis. This is observed to be with some inconsistencies while a triplicate test (Stage II) conducted for clarification is presented on page 172 for M<sub>2</sub> (Figure 6.11, Table 6.5) and pages 174 for M<sub>3</sub> and M<sub>IF</sub> specimens (Table 6.6 and Figure 6.12)

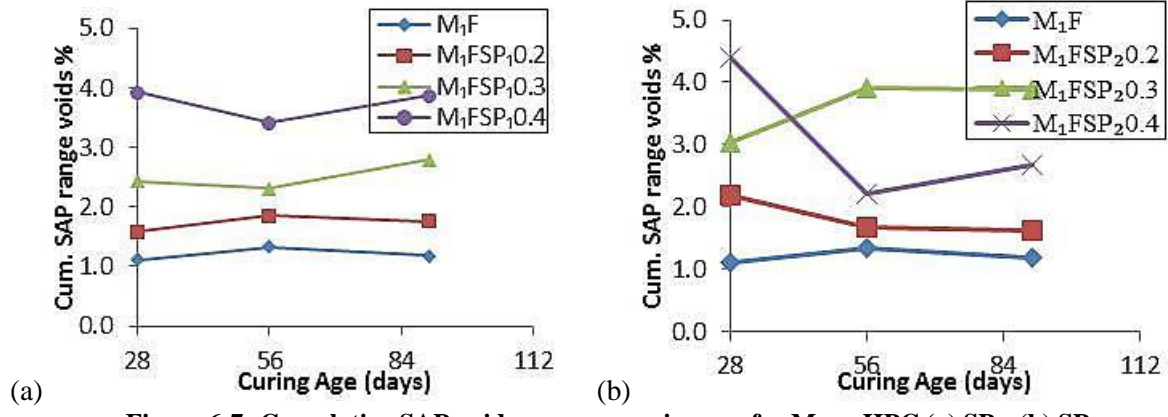


Figure 6-7: Cumulative SAP voids range vs curing age for M<sub>1F</sub> – HPC (a) SP<sub>1</sub>; (b) SP<sub>2</sub>

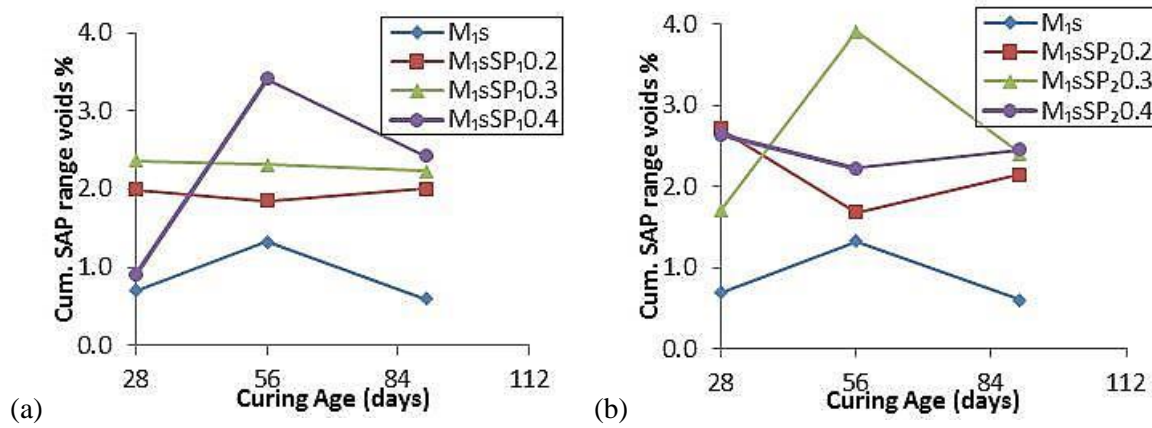


Figure 6-8: Cumulative SAP voids range vs curing age for M<sub>1S</sub> – HPC (a) SP<sub>1</sub>; (b) SP<sub>2</sub>

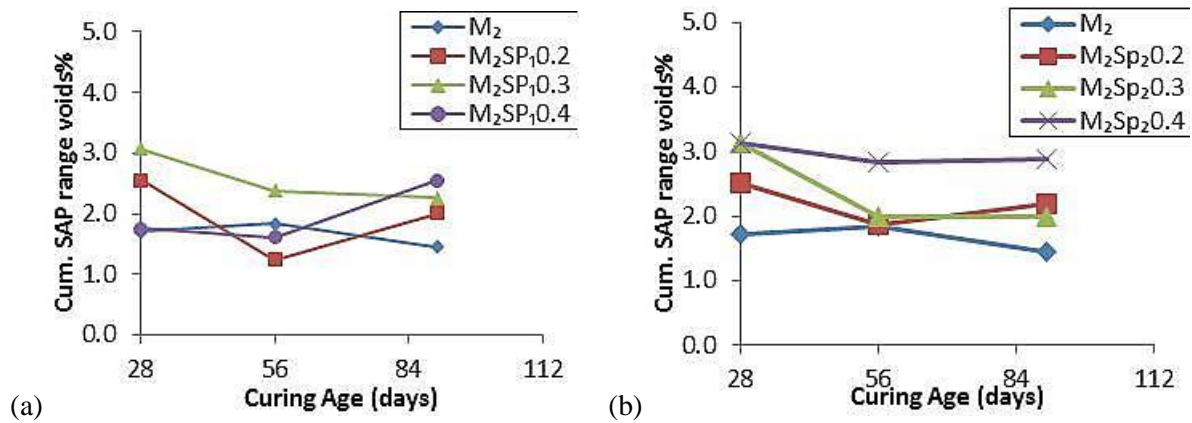


Figure 6-9: Cumulative SAP voids range vs curing age for M<sub>2</sub> – HPC (a) SP<sub>1</sub>; (b) SP<sub>2</sub>

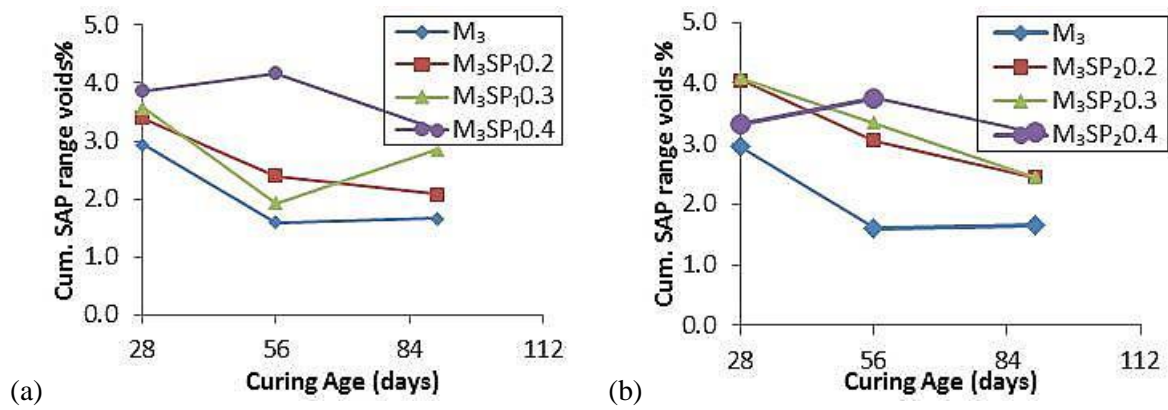


Figure 6-10: Cumulative SAP voids range vs curing age for M<sub>3</sub> – HPC (a) SP<sub>1</sub>; (b) SP<sub>2</sub>

This gives an indication that although a general decrease in cumulative SAP voids range% as the curing age increase occurs; there are inconsistencies in the trends of results for this Stage I analysis. While some specimens show decrease in cumulative SAP voids range%, others exhibit sudden value jump between the 28 and 56 days of curing. It was however observed that in about 50% of the specimens, the cumulative SAP range voids% after 56 and 90 days curing had similar values. This is because there is not significant cement hydration increase between these two ages.

The Stage II (triplicate specimen) analysis conducted to verify the reason for variation in the results reported in stage I further affirms that SAP voids and total voids percentages increase as the SAP size and contents increases (Table 6.5 for M<sub>2</sub> – HPC mixtures). Figure 6.11 further shows a plot of the cumulative SAP voids range% against the curing age for Stage II analysis of the M<sub>2</sub> – HPC mixture.

The use of triplicate HPC specimen however reveals no variation in the trend of the progressive increase of SAP voids and total porosity in the HPC as the SAP size and contents increase. The cumulative SAP range void% (i.e. < 1500 µm as defined in Section 6.1) clearly decreases as curing age increases with no ambiguity using the triplicate samples (Figure 6.11).

**Table 6-5: Summary of void distribution in triplicate HPC - M<sub>2</sub> with both SAP types**

Curing Age Influence	Ref	SAP1			SAP2		
M <sub>2</sub> -7 days series	M <sub>2</sub>	M <sub>2</sub> SP <sub>1</sub> -0.2	M <sub>2</sub> SP <sub>1</sub> -0.3	M <sub>2</sub> SP <sub>1</sub> -0.4	M <sub>2</sub> SP <sub>2</sub> -0.2	M <sub>2</sub> SP <sub>2</sub> -0.3	M <sub>2</sub> SP <sub>2</sub> -0.4
SAP pore expected	0	3.4	5.01	6.56	3.4	5.01	6.56
No of voids >1500 µm	25	25	25	25	29	36	46
SAP voids%	0.00	0.95	1.16	1.30	1.00	1.71	1.91
Total Porosity%	0.81	1.42	1.68	1.84	1.27	2.04	2.32
Small voids%	0.58	1.19	1.42	1.60	1.00	1.71	1.91
Max. void size (mm <sup>3</sup> )	23.716	35.789	17.927	34.185	21.598	34.045	50.996
Av. void diameter (mm)	0.658	0.501	0.470	0.457	0.616	0.570	0.594
M <sub>2</sub> -28 days series	M <sub>2</sub>	M <sub>2</sub> SP <sub>1</sub> -0.2	M <sub>2</sub> SP <sub>1</sub> -0.3	M <sub>2</sub> SP <sub>1</sub> -0.4	M <sub>2</sub> SP <sub>2</sub> -0.2	M <sub>2</sub> SP <sub>2</sub> -0.3	M <sub>2</sub> SP <sub>2</sub> -0.4
No of voids >1500 µm	18	16	23	22	14	36	30
SAP voids%	0.00	0.60	1.02	1.20	0.90	1.19	1.46
Total Porosity%	0.72	0.94	1.47	1.74	1.04	1.53	1.74
Small voids%	0.55	0.79	1.25	1.52	0.90	1.19	1.46
Max. void size (mm <sup>3</sup> )	25.260	42.208	56.197	60.147	21.837	38.206	18.764
Av. void diameter (mm)	0.542	0.525	0.429	0.464	0.549	0.576	0.550

+Expected pore content by volume based on the 25 g/g pore absorption used for provision of additional water calculated taking the swollen SAP as a spherical substance.

\*\*Porosity calculated volumetrically using Demoulded density in comparison to designed density.

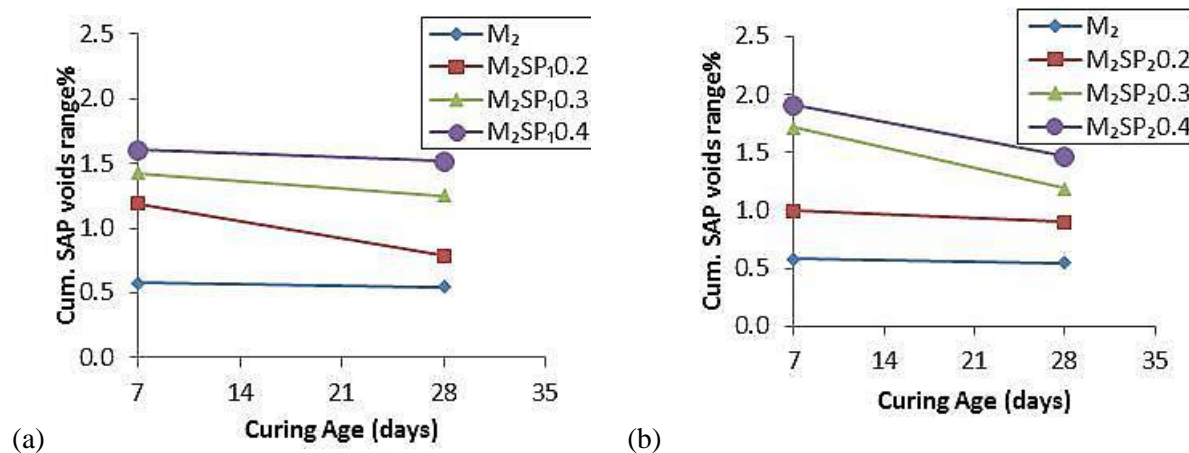


**Figure 6-11: Cumulative SAP voids range vs curing age for triplicate M<sub>2</sub> – HPCs (a) SP<sub>1</sub>; (b) SP<sub>2</sub>**

The maximum void sizes were also observed to be within similar value range (20 – 60 mm<sup>3</sup>) for both SAP sizes (Table 6.5 for M<sub>2</sub> – HPC mixtures). The total air void% in the mixtures and average void volumes were noted to be lower than the earlier values obtained for single specimen analyses. The longer time of vibration (10 minutes) of the HPCs as against the 5 minutes used for Stage I during concrete casting can therefore be seen to result in better compaction and reduction of trapped air voids within the concrete. The number of large voids (> 1500 μm) is observed to be of a uniform range (25 for reference and SP<sub>1</sub> mixtures and 29 – 46 for SP<sub>2</sub>) at 7 days of hydration and at 28 days of hydration (15 – 30 for both SAP sizes) for M<sub>2</sub> – HPC mixtures. The average pore diameter determined (taking the voids as sphere) were seen to be more uniform for both SAP sizes and at both hydration periods (0.5 to 0.6 mm) in the triplicate specimen analyses. The number of large voids, SAP porosity and total porosity decreased as the curing age increases for both SAP types in triplicate specimen analysis of M<sub>2</sub> – HPC mixtures.

Results for the triplicate specimen of M<sub>1F</sub> and M<sub>3</sub> examined for only SAP Type 1 (SP<sub>1</sub>) are presented in Table 6.6 and Figure 6.12 and properly discussed with M<sub>2</sub> triplicate specimens for SP<sub>1</sub> in Section 6.1.2 to study influence of W/B, binder type and curing age on air voids distribution of HPCs.

### 6.1.2 Influence of W/B, Binder Type and Curing on Air Void Distribution

Tables 6.1 to 6.4 present a summary of results on influence of curing age, W/B and binder type on air void distribution for single specimen (Stage I) analyses of the various HPC mixtures examined in this

study while Table 6.6 presents results summary for triplicate specimen (Stage II) for same using SP<sub>1</sub>. Graphical presentation of influence of W/B, binder type and curing age on the cumulative SAP voids range (< 1500 µm) for the respective HPC mixtures is also shown in Figures 6.7 to 6.12.

The result in Figures 6.7 and 6.8 reveal that for single specimen in the ternary cements HPCs (M<sub>1F</sub> and M<sub>1S</sub>, W/B = 0.2 reference mixtures) the cumulative SAP voids range% decreased as the hydration period increased with some inconsistencies too. The SAP voids were observed to increase as the SAP size and contents increases at all the respective hydration periods for both HPC mixtures. The number of air voids larger than 1500 µm (diameter) gave consistent range of value, 30 – 70 with some few inconsistencies (pink colour highlights in the Tables 6.1 to 6.4) while the maximum void sizes were also observed to be in a similar range, 20 – 70 mm<sup>3</sup> but for two extremes - 11 mm<sup>3</sup> and 121 mm<sup>3</sup> (blue colour highlights in Tables 6.1 to 6.4). The pattern of the cumulative SAP voids range% present in the respective HPC (Figures 6.7 – 6.10) also gave similar trends with deviation observed in some specimens (e.g. M<sub>1F</sub>SP<sub>2</sub>0.3-56D in Figure 6.7 (d); M<sub>1S</sub>SP<sub>1</sub>0.4-56D and M<sub>1S</sub>SP<sub>2</sub>0.4 -56D in Figure 6.8 (c & d)). Effect of large air voids (> 1500 µm) was also seen to be glaring in the total void calculated for these samples. The HPC with CS as SCM (M<sub>1S</sub>) was observed to exhibit the lowest number of large air voids present for all hydration periods.

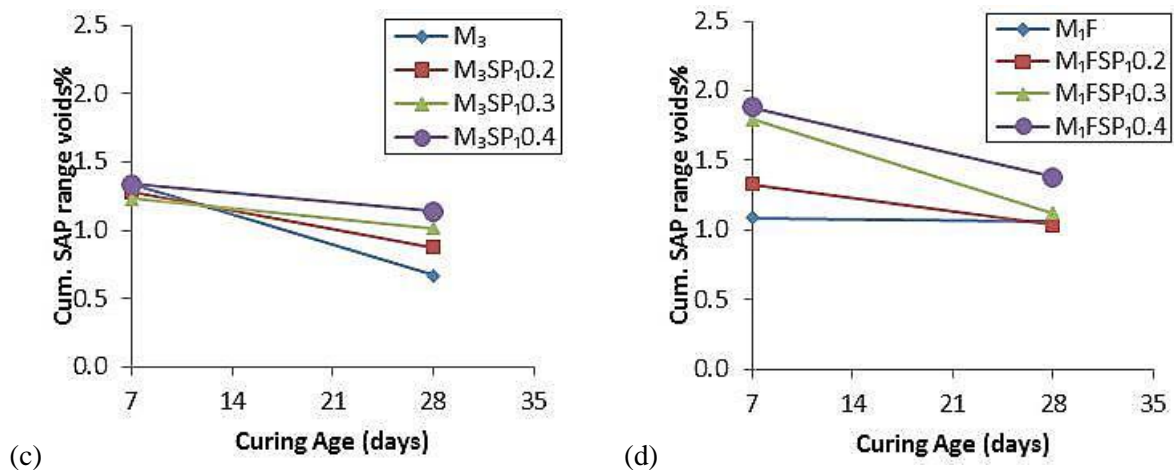
A similar trend is observed for the binary cements HPC (M<sub>2</sub> and M<sub>3</sub>, W/B = 0.25 and 0.3 reference mixtures) as presented in Figures 6.9 and 6.10 but with large numbers of void sizes above 1500 µm (i.e. large air voids) and great variation in the value of maximum void size present in these HPC mixtures (pink and blue colour highlights of Tables 6.3 and 6.4). Volumes of void above 70 mm<sup>3</sup> were observed to be more in these HPC samples at hydration period of 28 days, while some reference mixes also contain very large air void such as 122 mm<sup>3</sup> in volume (M<sub>2</sub> -28D in Table 6.5). The numbers of large voids were consistently very high (80 – 200) in the M<sub>3</sub> mixtures.

The Stage II analysis using triplicate specimen with SP<sub>1</sub> is as presented in Table 6.6 showing summary of influence of curing age and W/B on air void distribution for three HPC mixtures (M<sub>1F</sub>, M<sub>2</sub> and M<sub>3</sub>), while the influence of curing age and SAP sizes for M<sub>2</sub>-HPC mixtures is as earlier presented in Table 6.5.

**Table 6-6: Summary of curing age influence and W/B on void distribution using triplicate specimens**

Curing Age Influence	7 Days				28 Days			
M <sub>1F</sub> -Series	M <sub>1F</sub>	M <sub>1F</sub> SP <sub>1</sub> -0.2	M <sub>1F</sub> SP <sub>1</sub> -0.3	M <sub>1F</sub> SP <sub>1</sub> -0.4	M <sub>1F</sub>	M <sub>1F</sub> SP <sub>1</sub> -0.2	M <sub>1F</sub> SP <sub>1</sub> -0.3	M <sub>1F</sub> SP <sub>1</sub> -0.4
No of voids >1500 μm	32	26	30	23	16	39	31	32
SAP voids%	0.00	1.08	1.43	1.54	0.00	0.68	0.85	1.07
Total Porosity%	1.39	1.58	2.09	2.10	1.20	1.40	1.41	1.68
Total small voids%	1.09	1.33	1.80	1.88	1.06	1.03	1.12	1.38
Max. void size (mm <sup>3</sup> )	75.487	31.194	55.396	27.652	26.329	42.09	29.902	35.399
Av. void diameter (mm)	0.525	0.388	0.460	0.424	0.394	0.633	0.515	0.501
M <sub>2</sub> -Series	M <sub>2</sub>	M <sub>2</sub> SP <sub>1</sub> -0.2	M <sub>2</sub> SP <sub>1</sub> -0.3	M <sub>2</sub> SP <sub>1</sub> -0.4	M <sub>2</sub>	M <sub>2</sub> SP <sub>2</sub> -0.2	M <sub>2</sub> SP <sub>2</sub> -0.3	M <sub>2</sub> SP <sub>2</sub> -0.4
No of voids >1500 μm	25	25	25	25	18	16	23	22
SAP voids%	0.00	0.95	1.16	1.30	0.00	0.60	1.02	1.20
Total Porosity%	0.81	1.42	1.68	1.84	0.72	0.94	1.47	1.74
Total small voids%	0.58	1.19	1.42	1.60	0.55	0.79	1.25	1.52
Max. void size (mm <sup>3</sup> )	23.716	35.789	17.927	34.185	25.260	42.208	56.197	60.147
Av. void diameter (mm)	0.658	0.501	0.470	0.457	0.542	0.525	0.429	0.464
M <sub>3</sub> -Series	M <sub>3</sub>	M <sub>3</sub> SP <sub>1</sub> -0.2	M <sub>3</sub> SP <sub>1</sub> -0.3	M <sub>3</sub> SP <sub>1</sub> -0.4	M <sub>3</sub>	M <sub>3</sub> SP <sub>1</sub> -0.2	M <sub>3</sub> SP <sub>1</sub> -0.3	M <sub>3</sub> SP <sub>1</sub> -0.4
No of voids >1500 μm	36	35	26	21	18	12	27	26
SAP voids%	0.00	0.82	0.85	1.03	0.00	0.66	0.72	0.79
Total Porosity%	1.67	1.61	1.48	1.53	0.84	0.99	1.28	1.38
Total small voids%	1.34	1.28	1.23	1.34	0.67	0.88	1.02	1.14
Max. void size (mm <sup>3</sup> )	61.863	18.602	29.805	57.332	21.941	22.042	55.997	32.302
Av. void diameter (mm)	0.451	0.528	0.502	0.494	0.544	0.510	0.608	0.536

Figure 6.12 further shows a plot of cumulative SAP voids range% (i.e. all voids below 1500 μm diameter size as defined in Section 6.1 above) against the curing ages examined (7 and 28 days) for the triplicate samples of M<sub>3</sub> and M<sub>1F</sub> HPC series.


**Figure 6-12: Cumulative SAP voids range vs curing age (triplicates specimen) for (a) M<sub>3</sub> (b) M<sub>1F</sub>**

The result shows that in the triplicate specimens' analyses, the SAP voids% and total voids% increases as the SAP contents increases while cumulative SAP voids range% decreased as the curing age increases for all the HPC mixtures studied. The reference HPC with 0.25 W/B (M<sub>2</sub> – binary

cement binder) has the lowest porosity values followed by  $M_{1F}$  – ternary cement (0.2 W/B with FA as admixture), while  $M_3$  – binary cement (0.3 W/B) has the highest porosity value.

The maximum void size in the triplicate specimen analyses were seen to be in a similar range (20 – 75  $\text{mm}^3$ ) for the HPC mixtures studied with only one variation observed in  $M_3$ . The average pore size (0.40 – 0.65 mm, in diameter) determined taking the void volumes as spheres was consistent for all HPC mixtures studied. There were no excessively large voids present nor were there variations in the number of large voids (i.e. > 1500  $\mu\text{m}$ ) for the three HPC mixtures examined.

### 6.1.3 Inferences

The following can therefore be inferred from the CT Scanning analysis

- i. An increase in SAP content and also the W/B of the HPCs lead to increase in SAP voids (< 900  $\mu\text{m}$  ( $SP_1$ ); < 1500  $\mu\text{m}$  ( $SP_2$ ) as defined in Section 6.1) and the total air voids.
- ii. The porosity created by SAP in the HPC was generally about half the calculated value using the 25 g/g SAP absorption capacity determined via the tea-bag test. An indication that the initial SAP created voids in fresh concrete reduces in size and hence volume with increased concrete age as cement hydration products occupied the air spaces created by the swollen SAP. It follows that maintaining the water added to the mixing water for SAP absorption in concrete mixtures at 12.5 g/g (i.e. half the 25 g/g used in this study), a similar value to that suggested in previous studies (12.5 g/g by Hasholt et al., 2012 and Lura et al., 2006; and 13.8 ml/g by Esteves, 2014), will reduce occurrence of SAP created air voids in these HPCs and hence avert the strength reduction effect of SAP addition observed.
- iii. The cumulative SAP voids range% and total air voids% decreased as the hydration period increased while SAP voids increased as the SAP size and contents increased for all the curing ages.

- iv. There exists large air voids greater than SAP voids in all the HPCs (especially the single specimen) analysis, an indication that proper vibration is important in concrete especially HPC to avert presence of excessively large air voids.
- v. The presence of CS as SCM ( $M_{1S}$ ) in HPC resulted in a lower number of large air voids present for all hydration periods. This implies that CS enhances a better dispersion of the CEM I 52.5 N and hence proper compaction of the concrete than the FA in the ternary cements HPCs.
- vi. Porosity value amongst reference HPC mixtures were in the following order; lowest being  $M_2$  binary cement HPC, followed by  $M_{1F}$  ternary cement HPC and the highest porosity being in  $M_3$  binary cement HPC. This shows that aside from W/B increase, the binder type also has an influence on the porosity of HPC.

It can be concluded that though SAP addition increases the air voids content in HPC, the influence will be minimal when the additional water for SAP absorption is maintained within 12.5g/g (i.e. half the 25g/g obtained in the teabag test).

## 6.2 Scanning Electron Microscopy of HPC

This section presents the micro-morphology and crystalline structure of the solid phases of the products of hydration in the various HPC mixtures with a bid to study the effect of SAP (sizes and contents). The study examines the HPC samples after the 90 days hydration period.

### 6.2.1 Micro-morphology and crystalline structure

A typical scanning electron microscopy (SEM) image of HPC is as presented in Figure 6.13 showing the general morphology and crystalline structure of the internal surface of the HPC. The grey scale is normally used to identify and analyse individual items for definite assessment of the chemical composition. As shown in the SEM image taken at 50 X magnification, the item labelled number 1 represents the coarse aggregate which is dark grey in colour, large, of irregular shape and often has small number of almost black spots within. It is observed to be dominantly quartz as the quantitative

analysis (Section 6.2.2) reflects. It is often composed of a mixture of silica, feldspar and other materials.

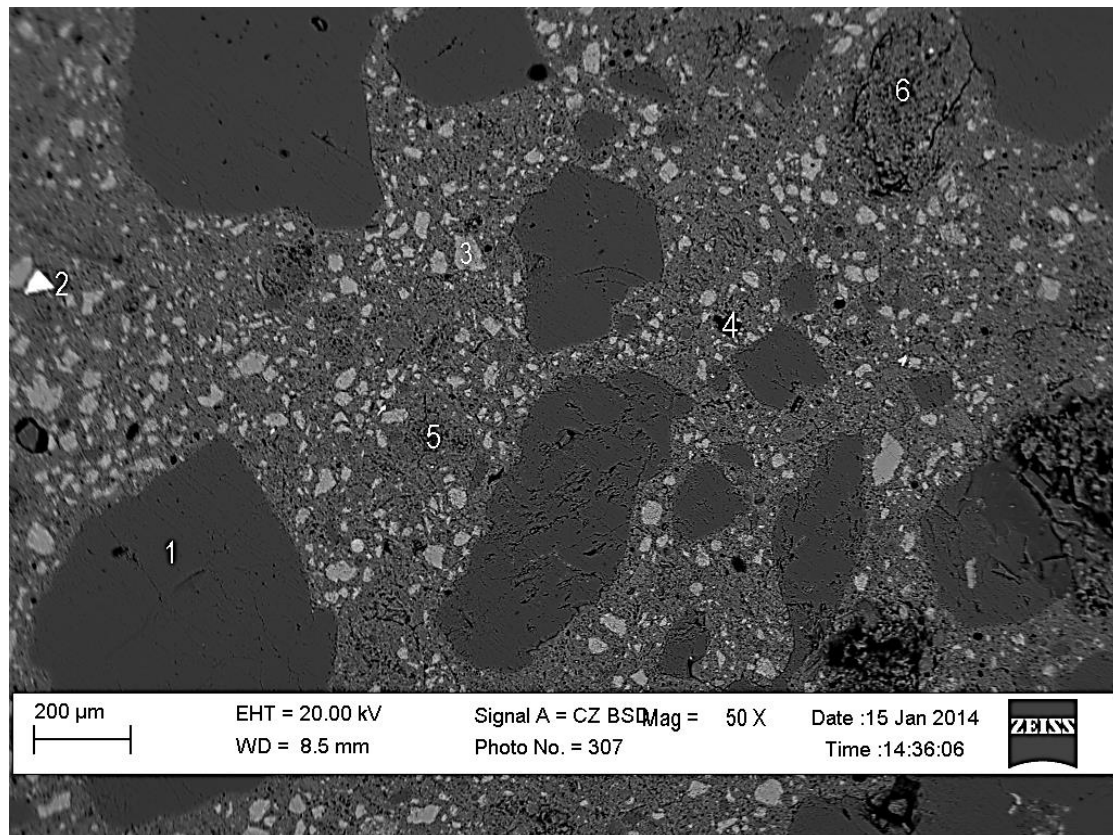


**Figure 6-13: General morphology and crystalline structure of the HPCs ( $M_{1F}$  as a sample)**

The cement paste matrix comprises of patterned mixture of grey background with the light grey portion (labelled 3) being spread all over and some white particles (labelled 2) which could be un-hydrated cement grains. This paste matrix is of major interest in this study since SAP addition (type and contents) i.e. amount of IC provided by the SAP absorbed water is expected to be of direct influence on the composition. The item labelled 4 shows air voids within the concrete which always appear as small black features (filled with epoxy resin) in the SEM images while the 5 label depicts other shades of grey within the cement paste which also require inspection to affirm their composition and what they represent. Item label 6 is likely a coarse aggregate which had been exposed by the sample preparation. A quantitative analysis of the SEM image will provide clear details on its composition.

Three sets of HPC mixtures ( $M_{IF}$ ,  $M_2$  and  $M_3$ ) with the respective SAP contents (0.0%, 0.2%, 0.3% and 0.4%) were examined individually by SEM as explained in Section 3.2.5 while the quantitative analysis of their paste portion enhances an understanding of SAP influence on the products of hydration after 90 days of curing.

## 6.2.2 Quantitative Analysis of HPCs and cement pastes

A typical SEM image analysis of the HPC as presented in Figure 6.13 classify into six different objects as mentioned in Section 6.2.1. Each component was examined using spot analysis and spectrum obtained analysed quantitatively using the INCA software. The quantitative analysis for the various identified phases as shown in Figure 6.13 for  $M_{IF}$  – HPC reference mixture is presented in Table 6.7

**Table 6-7: Quantitative Analysis of Typical concrete Polished Section ( $M_{IF}$  as Sample)**

Spectrum*	Binder Type 2 (0.2 W/B) HPC					
	1	2	3	4	5	6
Mg	0.00	0.00	0.95	0.00	0.95	0.50
Al	0.00	0.00	2.47	0.00	7.04	5.22
Si	46.74	0.33	41.92	46.74	37.77	40.59
Ti	0.00	0.00	0.47	0.00	0.51	0.28
Mn	0.00	0.41	0.00	0.00	0.00	0.00
Fe	0.00	76.77	2.56	0.00	2.70	1.57
Zn	0.00	0.00	0.00	0.00	0.00	0.00
O	53.26	22.49	51.63	53.26	51.03	51.85
Total	100.00	100.00	100.00	100.00	100.00	100.00
Oxide Composition in Weight%						
MgO	0.00	0.00	1.57	0.00	1.58	0.82
Al <sub>2</sub> O <sub>3</sub>	0.00	0.00	4.66	0.00	13.31	9.86
SiO <sub>2</sub>	100.00	0.71	89.68	100.00	80.80	86.83
TiO <sub>2</sub>	0.00	0.00	0.79	0.00	0.84	0.47
MnO	0.00	0.52	0.00	0.00	0.00	0.00
FeO	0.00	98.77	3.30	0.00	3.47	2.02
ZnO	0.00	0.00	0.00	0.00	0.00	0.00
Total	100.00	100.00	100.00	100.00	100.00	100.00

\*The Spectrum numbers in the Table represents the items labelling in the SEM image as presented in Figure 6.13.

Column 1 (yellow colour highlight of Table 6.7) is the coarse aggregate spectrum quantitative analysis of the  $M_{IF}$  – HPC polished surface.

### Coarse Aggregates (Spectrum 1)

Figure 6.14 shows the spectrum obtained in the object number 1 (coarse aggregates) in all the HPC mixtures while Table 6.8 shows the quantitative analysis of spectrum 1 in the  $M_{1F}$  – HPCs for various SAP contents.

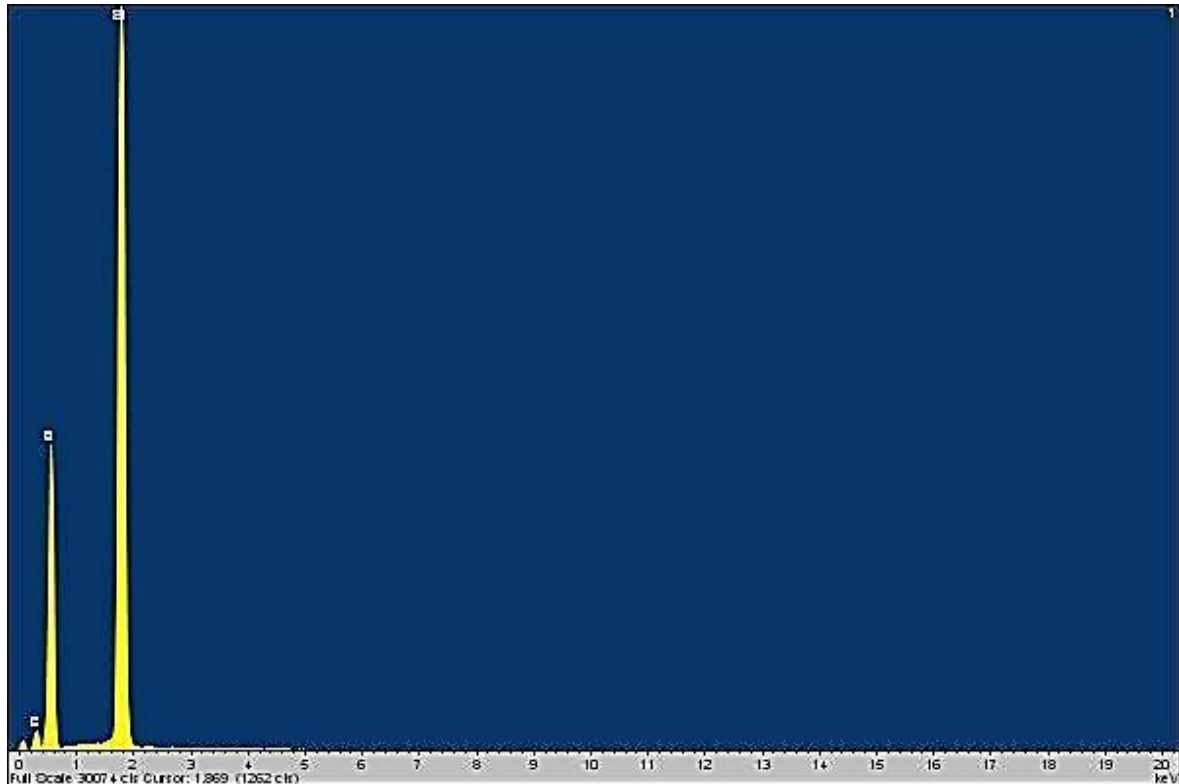


**Figure 6-14: Spectrum of Quantitative Analysis for Coarse Aggregates in  $M_{1F}$  – HPC**

The scale shown under the Spectrum image as obtained in the image is not of any particular importance as the INCA software generates the exact quantitative values for the respective elements or oxide as imputed. The peaks of the Spectrum image are used for identifying the specific element present in the specimen being analysed.

The results show that the coarse aggregates as examined in this study for  $M_{1F}$  with or without SAP is 100% silica ( $SiO_2$ ) as an oxide compound, individual element weight% composition by each constituent gave 47% silicon and 53% oxygen (Table 6.7). Similar composition is observed for the item labelled 6 with an indication of little iron ( $Fe = 1.57\%$ ), aluminium ( $Al = 5.22\%$ ) and magnesium ( $Mg = 0.5\%$ ) content - implying a mixture of silica, feldspar and other materials.

**Table 6-8: SEM Quantitative Analysis of Aggregates in M<sub>1F</sub> – HPCs by Weight%**

Element by Weight%	Binder Type 2 (0.2 W/B) HPC						
	M <sub>1F</sub>	M <sub>1F</sub> Sp <sub>1</sub> -0.2	M <sub>1F</sub> Sp <sub>1</sub> -0.3	M <sub>1F</sub> Sp <sub>1</sub> -0.3	M <sub>1F</sub> Sp <sub>2</sub> -0.2	M <sub>1F</sub> Sp <sub>2</sub> -0.3	M <sub>1F</sub> Sp <sub>2</sub> -0.4
Mg	0.00	0.00	0.00	0.00	0.00	0.00	0.00
Al	0.00	0.00	0.00	0.00	0.00	0.00	0.00
Si	46.74	46.74	46.74	46.74	46.74	46.74	46.47
Ti	0.00	0.00	0.00	0.00	0.00	0.00	0.00
Mn	0.00	0.00	0.00	0.00	0.00	0.00	0.00
Fe	0.00	0.00	0.00	0.00	0.00	0.00	0.00
Zn	0.00	0.00	0.00	0.00	0.00	0.00	0.00
O	53.26	53.26	53.26	53.26	53.26	53.26	53.53
Total	100.00	100.00	100.00	100.00	100.00	100.00	100.00
Oxide Composition in Weight%							
SiO <sub>2</sub>	100.00	100.00	100.00	100.00	100.00	100.00	100.00

Note that the total composition as presented in Tables 6.7 and 6.8 has been normalised to 100% for discussion in this work. The weight% (total) as obtained from BSE/WDS is normally between 50% and 80% as mentioned in Winter (2012)

### Cement Paste components

Figure 6.15 presents typical SEM images of the paste portion of HPC with or without SAP after 90 days curing taken at about 275 X magnification with M<sub>2</sub> used as a sample.

The part labelled A represents the sand particle (i.e. fine aggregate) in the paste and gave similar composition - Table 6.9 (Si - 47%, O<sub>2</sub> - 53%) as the coarse aggregate mentioned in the previous Section (Table 6.8 and Figure 6.14) classified as quartz.

The pattern of crack as shown in this specimen reveal that the aggregates are not the point of weakness for fracture in the HPCs but the crack is rather observed within the paste matrix and along the interfacial transition zone (ITZ). The portion labelled B (bright grey colour) is the alite (calcium silicate - C<sub>3</sub>S), C (white substance) is ferrite (C<sub>4</sub>AF), D is the paste matrix, E (bright grey colour) shows calcium and silicon with some contents of sulphur and other minor elements while F (bigger light grey in colour) is majorly calcium with some minor elements. Objects D, E and F are all from

the dark grey background and forms main products of cement hydration referred to as hydrates and their composition (which could be calcium silicate hydrate (C-S-H), calcium hydroxide (CH), or calcium sulfoaluminate phases).

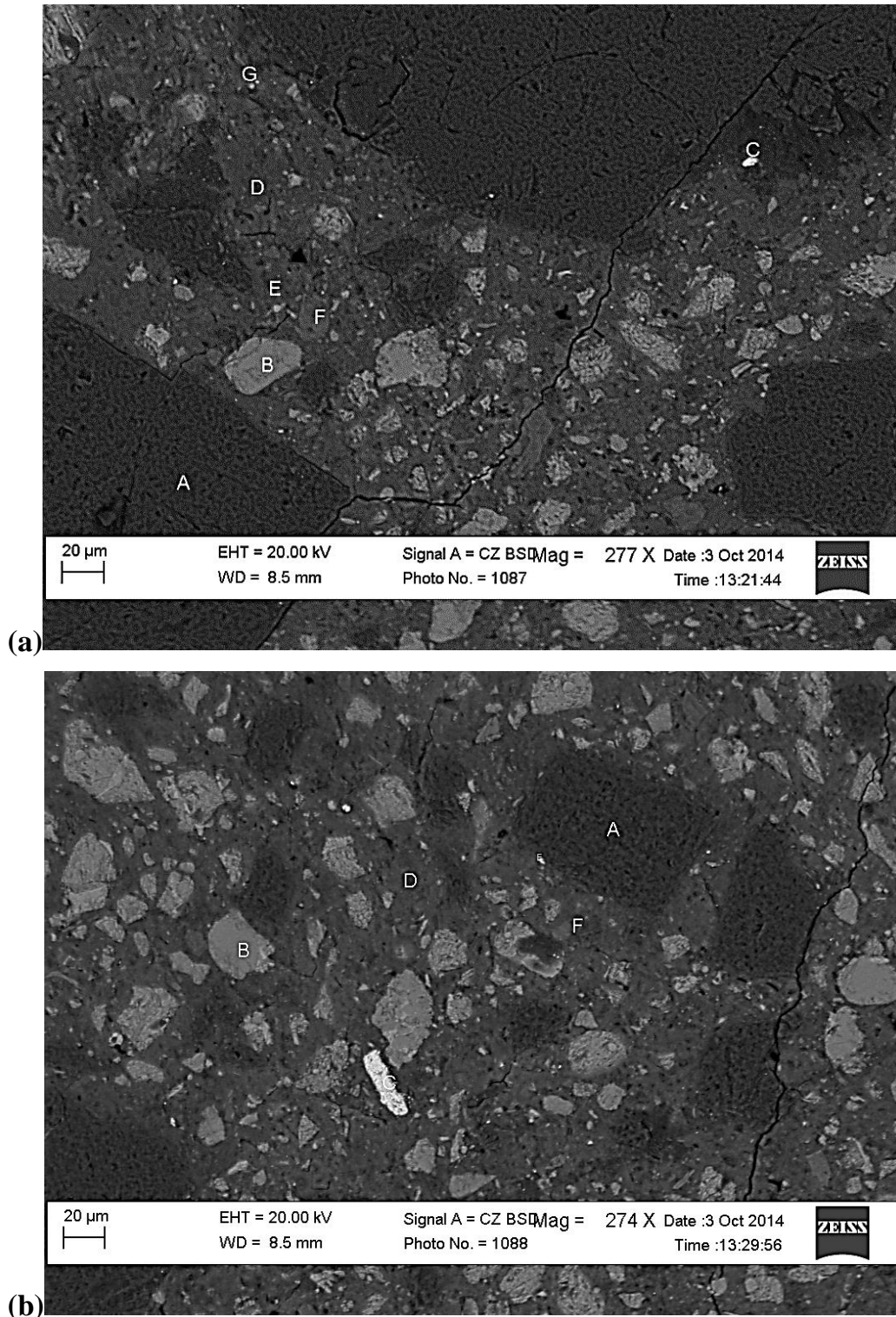


Figure 6-15: Typical SEM image of HPC paste portion ( $M_2$  as sample)

There composition is expected to be influenced by the binder type, W/B and the extent of curing provided (both internal - from SAP and external – from immersion in water). SAP type and content are the parameters of concern for curing variation in this study since all the HPCs are cured immersed in water.

**Table 6-9: Quantitative Analysis of a Typical M<sub>2</sub> – HPC SEM Image by Element Weight%**

Spectrum*	A	B	C	D	E	F	G
Mg	0.00	0.00	0.00	0.79	0.31	0.42	0.78
Al	0.00	0.84	0.30	3.42	0.97	0.00	7.33
Si	46.74	14.40	1.12	15.29	10.58	1.24	7.92
S	0.00	0.00	0.00	1.58	0.00	0.00	0.00
K	0.00	0.53	0.00	0.29	0.00	0.00	0.24
Ca	0.00	46.94	2.56	37.44	10.38	68.67	31.96
Ti	0.00	0.00	0.00	0.00	0.00	0.00	0.00
Cr	0.00	0.00	0.19	0.00	0.00	0.00	0.00
Mn	0.00	0.00	0.34	0.00	0.38	0.00	0.00
Fe	0.00	1.00	72.09	2.22	46.64	0.44	15.12
Mo	0.00	0.00	0.00	0.00	0.00	0.00	1.60
O	53.26	36.28	23.40	38.98	30.74	29.23	34.42
Total	100.00	100.00	100.00	100.00	100.00	100.00	100.00

\*Spectrum labelling in the Table represents the item labelling in SEM image of Figure 6.13

The results in Table 6.9 show these different portions of the cement hydration products in M<sub>2</sub> having compositions mainly of calcium (Ca), silicon (Si), aluminium (Al), iron (Fe) and oxygen (O<sub>2</sub>) with others minor elements such as magnesium (Mg), potassium (K), sulphur (S), titanium (Ti) and manganese (Mn).

The G label in Figure 6.15(a) shows tiny spots of bright grey colour within the cement paste which is clearly a different composition from the B (also of similar bright grey colour). Although the quantitative analysis shows G comprise of calcium and silicon as found in B, there is a considerable content of iron (Fe), aluminium (Al) and magnesium. The variation in the grey scale of objects in the HPCs becomes wider as the SAP contents, binder type and W/B changes (Appendix C).

Beyond using the grey scale for physical identification, is the need to access influence of the additives, admixtures and the change in W/B. Neville (2012) observed that the products of cement hydration may be influenced by compounds interactions and that the amount of water available in the

concrete could be a determinant for which of the calcium silicates ( $C_3S$  and  $C_2S$ ) results ultimately in the hydrate. Possibility of having several distinct calcium silicate hydrates (C-H-S) is further stressed by Neville (2012) and that if lime is absorbed or held in the solid particles the calcium / silica (C: S) ratio would be affected, and a strong evidence of this results in  $C_2S$  giving lime/silica ratio of 1.65 (Neville, 2012). Examination of the C: S ratio is specified as a way of distinguishing the calcium silicates with different test methods reported to yield diverse results for C: S ratio having a variation as wide as 1.5 to 2.0 while Electro-optical measurements (e.g. SEM) are known to yield low values of C: S ratio (Neville, 2012). A proper presentation of these results will serve well in understanding SAP influence on strength development of concrete especially the HPC.

The C-S-H which is referred to as the main hydrates nowadays is believed to have a C: S ratio of a rounded up value of 2 based on the mole ratio of water to silica taken to be a whole number (Neville, 2012). The work of Winter (2012) presents these results in atomic ratio plots using a minimum of about thirty analysis of an individual phase or spectrum for proper phase classification as other elements could have been packed together with the main phases during x-ray excitation and normalisation of results. The quantitative analysis of the SEM images and atomic ratio plot for Al/Ca vs. Si/Ca should show a C-S-H cluster in range of (0.04 - 0.08, 0.045 - 0.055) as control with some CH near the origin (Winter, 2012). Winter (2012) states also the S/Ca vs. Al/Ca plots as means of affirming the nature of the sulfoaluminate phases. This study thus adopts the use of the atomic ratios for an indication of the phases observed in the SEM analysis though time and schedule of the machine could not allow thirty repetitive analyses of individual phases; a plot of all the atomic ratios for the spectrum taken from phases of similar grey scale appearances in the reference HPCs mixtures with or without SAP is hereby adopted for phase identification and discussion.

### **6.2.3 Cement Hydration Products**

Three HPCs ( $M_{1F}$ ,  $M_2$  and  $M_3$ ) were examined after 90 days of curing and the results are discussed in the following sections.

### 6.2.3.1 Cement hydration products in $M_2$ – HPCs

The details of the atomic weight% composition of the various phases observed in the  $M_2$  – HPCs mixtures are presented in Appendix C while Figures 6.16 and 6.17 show the atomic ratio plots for both Al/Ca vs. Si/Ca and S/Ca vs. Al/Ca as suggested by Winter (2012) for proper identification of the various phases observed in the paste matrix of the HPC.

The results reveals that the phase labelled B and D are calcium silicate hydrates (C-S-H) with B clustering at 0.48 along the Si/Ca axis and 0.04 along the Al/Ca axis of Figure 6.16. D on the other hand displays a wider spread with two main clusters (0.46 and 0.64 along Si/Ca, 0.06 and 0.11 along the Al/Ca axis). The C: S ratios as reflected on Tables C1 and C3 of Appendix C for both phases fall within the range of 1.5 to 2.5 with B fitting better to a C: S rounded up value of 2. Figure 6.17 shows both clustering near the origin, thereby affirming they are C-S-H phases. The SEM image identification of B as light grey in colour and the lime: silica ( $\text{CaO}/\text{SiO}_2$ ) ratio generally of above 1.65 but about 2 places B appropriately as the impure  $\text{C}_3\text{S}$  – alite (i.e. un-hydrated cement particles) referred to by Winter (2012) as inner C-H-S phase while D known to be dark grey from the SEM image is the outer C-H-S phase. This is the portion which accounts for strength development of the cement paste.

The item labelled F clusters at the origin in both plots (Al/Ca vs. Si/Ca – Figure 6.16 and S/Ca vs. Al/Ca – Figure 6.17), an indication that it is the CH phase. G is however identified as the AFm phase from Figure 6.16 while Figure 6.17 shows it clearly as a monocarbonate (AFm) phase.

The composition by atomic weight% (Table C2, Appendix C) revealed C has dominantly iron (Fe – above 40%) and oxygen (about 45%). The item labelled C is therefore the ferrite phase of the paste.

The E label is observed in the  $M_2$  reference and  $M_2\text{SP}_1-0.2$  mixtures as made up of diverse small elements in combination with oxygen. While the E spectrum for  $M_2$  has some reasonable content of iron (Fe – 23.4%), the said spectrum in  $M_2\text{SP}_1-0.2$  does not contain iron at all but shows higher silicon and calcium than the E spectrum in  $M_2$ .

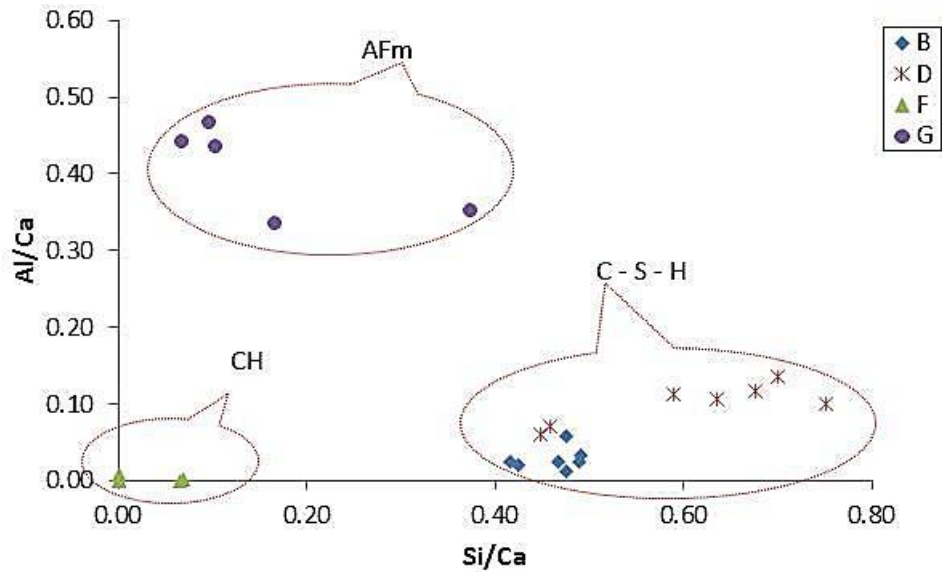


Figure 6-16: Atomic ratio plot (Si/Ca vs Al/Ca) for M<sub>2</sub> - HPC

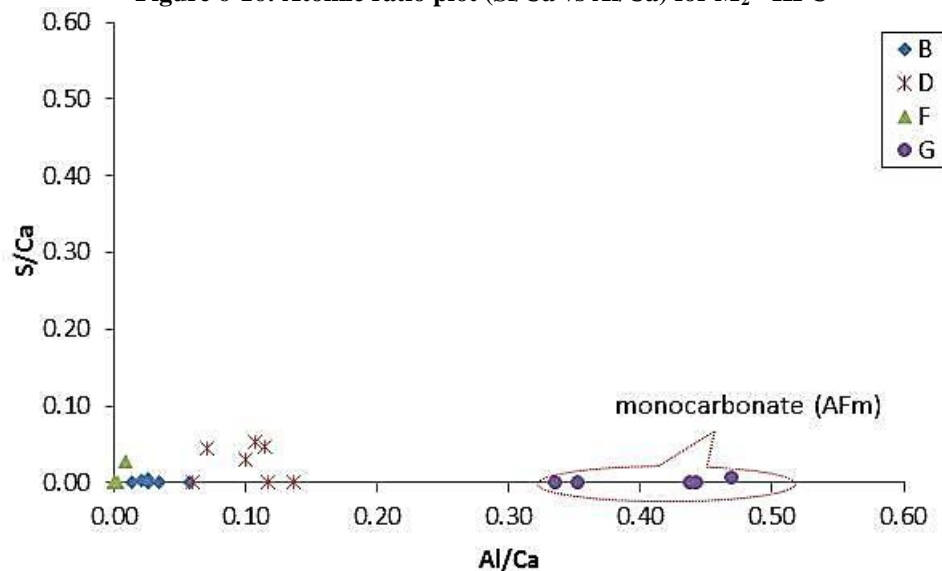


Figure 6-17: Atomic ratio plot (S/Ca vs Al/Ca) for M<sub>2</sub> - HPC

Other phases containing different minor elements such as lead (Pb), titanium (Ti), manganese (Mn), molybdenum (Mo) were noted in the SEM analysis of the HPCs as SAP contents increase. They are thereby presented only in their oxides form (Table C5 of Appendix C) and are perceived to possibly be products emanating from interaction of the SAP compounds and that of binders. Similar observations were recorded for M<sub>1F</sub> and M<sub>3</sub>. The Calcium silicate phases in the three HPC mixtures studied are thereby compared for a discussion on SAP, W/B or binder type influence on the cement hydration in the HPCs.

### 6.2.3.2 SAP, W/B and Binder Type Influence on Cement hydration

Tables 6.10 and 6.11 present summary results of the quantitative analysis of the calcium silicates phases (Spectrum B and D) for the three HPCs ( $M_2$ ,  $M_3$  and  $M_{1F}$ ) studied after 90 days curing in this work, while detailed results are shown in Appendix C (Tables C7 to C10). Results of some specimens (as observed in Tables 6.10) were however lost in the process of data gathering of the study.

**Table 6-10: Summary of Quantitative Analysis of Spectrum B**

HPC Type	Spectrum B	Ref	SP <sub>1</sub> -0.2	SP <sub>1</sub> -0.3	SP <sub>1</sub> -0.4	SP <sub>2</sub> -0.2	SP <sub>2</sub> -0.3	SP <sub>2</sub> -0.4
$M_2$ - Series 0.25 W/B Binary cement	Si/Ca	0.467	0.425	0.490	0.476	0.491	0.476	0.415
	Al/Ca	0.025	0.020	0.026	0.013	0.034	0.058	0.025
	S/Ca	0.000	0.002	0.005	0.000	0.000	0.000	0.000
	C: S	2.14	2.35	2.04	2.10	2.04	2.10	2.41
	CaO/SiO <sub>2</sub>	1.67	1.66	1.69	2.03	1.09	1.21	1.36
$M_3$ - Series 0.3 W/B Binary cement	Si/Ca	0.342	0.498		0.336		0.486	
	Al/Ca	0.023	0.016		0.017		0.010	
	S/Ca	0.001	0.005		0.000		0.000	
	C: S	2.92	2.01		2.98		2.06	
	CaO/SiO <sub>2</sub>	2.50	1.88		2.78		1.76	
$M_{1F}$ - Series 0.2 W/B Ternary cement	Si/Ca	0.471	0.491	0.391	0.338	0.346		0.491
	Al/Ca	0.028	0.027	0.025	0.020	0.019		0.032
	S/Ca	0.005	0.004	0.002	0.000	0.000		0.004
	C: S	2.12	2.04	2.55	2.96	2.89		2.03
	CaO/SiO <sub>2</sub>	1.98	1.90	2.39	2.76	2.72		1.90

**Table 6-11: Summary of Quantitative Analysis of Spectrum D**

HPC Type	Spectrum D	Ref	SP <sub>1</sub> -0.2	SP <sub>1</sub> -0.3	SP <sub>1</sub> -0.4	SP <sub>2</sub> -0.2	SP <sub>2</sub> -0.3	SP <sub>2</sub> -0.4
$M_2$ - Series 0.25 W/B Binary cement	Si/Ca	0.590	0.636	0.459	0.448	0.677	0.751	0.700
	Al/Ca	0.114	0.107	0.071	0.060	0.117	0.099	0.136
	S/Ca	0.047	0.053	0.044	0.000	0.000	0.030	0.000
	C: S	1.69	1.57	2.18	2.23	1.48	1.33	1.43
	CaO/SiO <sub>2</sub>	1.58	1.47	2.02	2.08	1.38	1.24	1.33
$M_3$ - Series 0.3 W/B Binary cement	Si/Ca	0.606	0.526		0.530		0.587	
	Al/Ca	0.097	0.075		0.088		0.131	
	S/Ca	0.031	0.036		0.028		0.040	
	C: S	1.65	1.90		1.89		1.70	
	CaO/SiO <sub>2</sub>	1.59	1.77		1.76		1.59	
$M_{1F}$ - Series 0.2 W/B Ternary cement	Si/Ca	0.674	0.784	0.731	0.959	0.650		0.588
	Al/Ca	0.138	0.244	0.120	0.158	0.160		0.065
	S/Ca	0.033	0.029	0.022	0.048	0.039		0.039
	C: S	1.48	1.28	1.37	1.04	1.54		1.70
	CaO/SiO <sub>2</sub>	1.38	1.19	1.23	0.97	1.42		1.59

The results (Tables 6.10 and 6.11) revealed that the C: S ratio in Spectrum B generally remained within the range 1.5 to 2.5 and a rounded value of 2 with few inconsistencies (as shown in red colour)

for all the HPCs with or without SAP addition. Spectrum D also maintained a C: S ratio generally below 2.0 and lots falling less than 1.50.

A plot of Al/Ca vs Si/Ca as shown in Figure 6.18 shows that the cluster of the calcium silicates within the range of 0.02 to 0.1 along Al/Ca and 0.37 to 0.07 along Si/Ca. The Spectrum B has the following clusters:  $M_2$  – 0.04 along Al/Ca and 0.46 along Si/Ca;  $M_3$  – 0.02 along Al/Ca and 0.43 along Si/Ca;  $M_{1F}$  – 0.02 along Al/Ca and 0.44 along Si/Ca. Spectrum D on the other hand has average clusters as:  $M_2$  – two clusters (0.07 and 0.10) along Al/Ca and (0.45 and 0.70) along Si/Ca;  $M_3$  – 0.10 along Al/Ca and 0.56 along Si/Ca;  $M_{1F}$  – 0.14 along Al/Ca and 0.68 along Si/Ca.

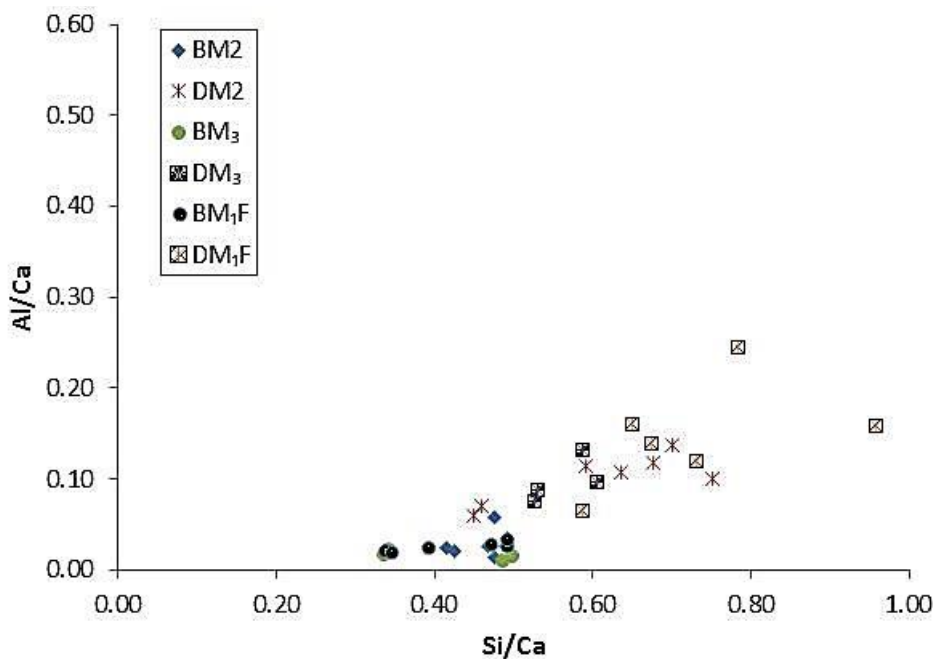


**Figure 6-18: Si/Ca vs Al/Ca plots of calcium silicates phases in the three HPCs**

The lime: silica ( $\text{CaO}/\text{SiO}_2$ ) ratio also varied greatly as the binder type or W/B varied. The SAP addition reflected some observed influence on the  $\text{CaO}/\text{SiO}_2$  ratio. The  $\text{CaO}/\text{SiO}_2$  generally decreased in Spectrum B as the SAP contents increased especially for the  $M_{1F}$  and  $M_2$  (0.2 and 0.25 W/B) HPCs with some inconsistencies – an indication of increased lime liberation as the SAP content increased. However for the  $M_3$  (0.3 W/B) HPC, SAP addition does not lead to increased  $\text{CaO}/\text{SiO}_2$  in Spectrum B. The influence of SAP on Spectrum D was however opposite. It thereby follows that as the SAP content increases the inner C-H-S (un-hydrated cement) decreases while the outer C-H-S (actual hydrated cement) increases.

## 6.2.4 Inferences

The findings from the study of the SEM on the low W/B concretes with SAP can be summarised as follows:

- i. The SEM image analysis of the HPCs reveals three internal phases categorised as aggregates, the paste matrix and air voids.
- ii. The aggregates were observed to be dark grey in colour, large, of irregular shape and often have small patterned grey spots within. The quantitative analysis reveals it as dominantly quartz which is often 100% silica ( $\text{SiO}_2$ ) as seen in this study and may sometimes contain feldspar and other minor materials.
- iii. The paste matrix shows diverse phases of objects with six prominent phases identified in all the HPCs.
- iv. The first of these phases identified as fine aggregate (Spectrum A) revealed similar composition of quartz (i.e. about 100%  $\text{SiO}_2$ ) as the coarse aggregate.
- v. Spectrum B and D were identified as the calcium silicate phases within the paste matrix known as the main product of cement hydration responsible for strength development and observed mechanical behaviour of the concrete.
- vi. SEM quantitative analysis affirmed B (bright grey colour) appropriately as the impure  $\text{C}_3\text{S}$  – alite (i.e. the un-hydrated cement particles) while D (dark grey in colour) is the outer C-H-S (i.e. the hydrated cement particles) of the paste matrix.
- vii. Other prominent phases observed are the C (white substance) which is dominantly iron – the ferrite ( $\text{C}_4\text{AF}$ ); E (also of bright grey colour) shows calcium and silicon with diverse small elements (including sulphur and sometimes iron) in combination with oxygen. F (bigger light grey in colour) is dominantly calcium and identified as the calcium hydroxide (CH) phase. G (tiny spots of bright grey colour within the paste matrix) is the monocarbonate (AFm) phase.

- viii. Other phases containing different minor elements such as lead (Pb), titanium (Ti), manganese (Mn), molybdenum (Mo) were noted in the SEM analysis of the HPCs as SAP contents increases.
- ix. SAP addition in the HPCs reflected some observed influence on the lime: silica ratio. The  $\text{CaO/SiO}_2$  generally decreases in Spectrum B as the SAP contents increases especially for the very low W/B HPCs (i.e.  $M_{1F} - 0.2$  W/B and  $M_2 - 0.25$  W/B) – an indication of increased lime liberation as the SAP content increased. SAP addition improves cement hydration and lead to reduction of the un-hydrated cement particle (i.e. alite - impure C-H-S) content present in this low W/B HPCs.

## 7

## *Conclusion and Recommendations*

The mechanical behaviour of HPC containing varying grain sizes and volumes of Superabsorbent Polymers (SAP) has been investigated with efforts made to evaluate the effect of SAP as an IC-agent. Experimental works were carried to study the impact of SAP addition on the rheology of the HPCs, identify and establish the effect of varying sizes and volume of SAP on rate of cement hydration and strength development. The work involved quantifying and modelling the mechanical behaviour (strength in compression, tension, elastic and fracture properties) of the low W/B (0.2 – 0.3) HPC (C55/67 –C100/115) with SAP. Microstructure and molecular interaction of the internal constituent of the HPC were also investigated using two non-destructive testing methods (i.e. the CT scanning and scanning electron microscopy). Findings of the study are hereby summarised in the following sections with conclusions drawn and appropriate recommendations made for future study.

### **7.1 Fresh and Early–Age Strength Properties**

- Cement pore solution (CPS) concentration (within the limits tested) does not have a significant influence on the SAP absorption capacity.
- SAP absorption capacity in CPS used for this study is 25 g/g (10 mins insertion in CPS) while the absorption in water is 230 g/g.
- Although the total W/B increases as SAP content increases by adding additional water for SAP absorption, the slump flow value remains in the same range for all HPC mixtures. This implies that SAP is mainly a water reservoir for IC of the HPC, absorbs all the additional water and stores it for IC of the concrete. SAP addition and the additional water provided in this study thereby have no significant influence on the consistency of the HPCs.
- SAP addition reduces the temperature difference increase resulting from concrete mixing in HPC production and hence helps to mitigate rapid heat development during cement hydration.

The swollen SAP within the HPC during concrete mixing and constituent agitation provides a means of reducing the temperature rise from the agitated solid constituents into the absorbed water within the SAP particles and hence lowers the internal concrete temperature.

- SAP addition in HPC resulted in a level of set retardation and thereby enhances longer slump retention time.
- The Kinetic of hydration (B) of all the HPC mixtures with or without SAP at the early-age conforms to the relationship as postulated in literature.

## 7.2 Mechanical Properties of HPC with SAP

- SAP addition to HPCs contribute to the air content in the concrete as the density of the HPCs decreases at relatively small rate as the SAP content increases.
- Compressive strength of low W/B HPCs decreases slightly as SAP contents increases. Higher SAP content with the additional water on basis of the tea-bag test result led to higher SAP created voids and hence reduces the HPC's ability to resist the force applied.
- SAP addition within the limits of the contents used in this study (0.2 to 0.4%  $b_{wob}$ ) in low W/B HPCs has no significant influence on the elastic and fracture properties of the concrete.
- SAP addition led to some reduction in compressive strength of HPC, correction made for void volume (SAP and air) using the Bolomey's formula and Powers' gel-space ratio was in agreement with the Powers' Model and hence makes possible a prediction of the effect of SAP on the compressive strength of HPC.

## 7.3 Non Destructive Tests on HPC with SAP

- Although SAP addition increases the air voids content in HPC, the influence on mechanical properties of the HPC will be minimal when the additional water for SAP absorption is kept within 12.5 g/g (i.e. half the 25 g/g obtained in the teabag test).
- Vibrating the HPCs with SAP for a longer time (10 minutes) reduces the SAP voids volume and the existence of large air voids. The longer vibration and agitation of the solid

constituents materials (especially the coarse aggregates) resulted in desorption of some of the absorbed water in the swollen SAP particles which escapes from the concrete as bleeding water and hence form part of the reason for reduction in SAP voids in the triplicate samples.

- The lime liberation in the low W/B HPCs increased as the SAP contents increased resulting in improved cement hydration and reduced un-hydrated cement particles content.

The findings from this research hereby propose that the 25 g/g SAP absorption capacity result of the tea-bag test over-estimates the actual amount of water used up by SAP in the IC of HPC considering the fact that the solid constituents of the concrete were not incorporated in the tea-bag test SAP absorption simulation. The revelation from the 3D void analysis of the HPC via CT scanning that SAP created voids in the HPC is only about half (i.e. 12.5 g/g) of the tea-bag test provision of 25 g/g affirms that the required additional water for SAP's effective IC of the low W/B HPC is 12.5 g/g. The excess water of 12.5 g/g above the required is the observed SAP created voids and the reason for the loss in compressive strength. The optimum additional water for SAP addition in the low W/B HPCs at no negative effect on mechanical properties is 12.5 g/g.

## 7.4 Recommendation

Based on the findings from this study the following is recommended:

- Additional water for SAP absorption should be kept as 12.5g/g in future studies for SAP addition in concrete especially HPC to minimise SAP's contribution to air voids in concrete.
- SAP addition within the limits stated above should be considered for slump retention in low W/B HPC at no negative effect on mechanical properties of the concrete.
- Further study to generate more experimental results on influence of SAP addition (with extra water) on fracture properties of HPC towards establishing a relationship is recommended.
- More detailed study on influence of SAP on the final products of hydration is recommended with a view to determine the contribution of SAP particles and its elements to the chemical interactions within the cement paste matrix at both the early-age and long term period.

## 8 References

- ACI THPC/TAC (1999), *ACI defines high performance concrete*, (the Technical Activities Committee Report (Chairman - H.G. Russell)). U.S.A: American Concrete Institute.
- Addis, B., & Goodman, J. (2009), Concrete mix design, In G. Owens (Ed.), *Fulton's concrete technology* (pp. 219 - 228), Midrand, South Africa: Cement and Concrete Institute.
- Aïtcin, P. C. (1998), *High performance concrete*, London & New York, E & FN Spon.
- American Concrete Institute (1992), *State-of-the-art report on high strength concrete (ACI 363R-92)*.
- American Concrete Institute (1998), *Guide to quality control and testing of high strength concrete, (ACI 363.2R-98)*.
- American Concrete Institute, (2008), *Guide to curing concrete*, (ACI Committee Report No. 308R-01(08)), U.S.A.
- American Concrete Institute, (2013), *Report on internally cured concrete using pre-wetted absorptive lightweight aggregate*, (ACI Committee Report No. 308-213 R13), U.S.A.
- American Standards and Test Methods (ASTM) International (2008), *ASTM C40/C403M - 08 - Standard test method for time of setting of concrete mixtures by penetration resistance*, USA, ASTM International.
- ASTM International (2010), *ASTM C469/C469M - 10 - Standard test method for static modulus of elasticity and Poisson's ratio of concrete in compression*, USA, ASTM International.
- Assmann, A., Mazanec, O., & Eissmann, D. (2014), Study on macroscopic viscosity for prediction of the swelling capacity of salt-insensitive superabsorbent polymers in cementitious materials. *International RILEM Conference on Application of Superabsorbent Polymers and Other New*

*Admixtures in Concrete Construction*, Technische Universitat Dresden, Dresden, Germany, *Pro* 095 105-114.

Bentur, A., Ingarashi, S., & Kovler, K., (2001), Prevention of autogenous shrinkage in high-strength concrete by internal curing using wet lightweight aggregates, *Cement Concrete Research*, 31 (11): 1587-1591.

Bentz, D. P., Geiker, M., & Jensen, O. M. (2002), On the mitigation of early age cracking, In: Proceeding 3<sup>rd</sup> International Seminar on Self-desiccation and its Importance in Concrete Technology, Persson, B., & Fagerlund, G. (eds.), Lund University, Lund, Sweden, 195-204

Beushausen, H., & Dehn, F. (2009), High-performance concrete, In G. Owens (Ed.) *Fulton's concrete technology* (Ninth ed., pp. 297-304). Midrand, South Africa: Cement and Concrete Institute.

Bolomey, J. (1935), Granulation and forecasting the resistance of concrete. ["Granulation et pr'évision de la r'esistance probable des b'etons,"] *"Travaux" (Works)*, 30, 228-232.

Braam, C. R., Van-der-Ham, H. W., & Koenders, E. A. (2006), Early-age shrinkage control and strength development of concrete, *International RILEM Conference on Volume Changes of Hardening Concrete: Testing and Mitigation*, Technical University of Denmark, Lyngby, Denmark. , *Proceeding Pro052(20-20 August)* 185--194.

Brandt, A. M. (1995a), *Cement-based composites: Materials, mechanical properties and performance*, London, E & FN Spon.

Brandt, A. M. (Ed.) (1995b), *Optimisation methods for material design of cement-based composites*, London, E & FN Spon.

British Standard Institution (2009), *Testing of fresh concrete, BS EN 12350 - 5 - Flow table test*, London, British Standard Institution (BSI).

British Standard Institution (2009), *Testing of fresh concrete, BS EN 12350 - 6 - Density*, London, BSI.

British Standard Institution (2009), *Testing of hardened concrete, BS EN 12390 - 1- shape, dimension and other requirement for specimens and mould*, London, BSI.

British Standards Institution (2009), *Testing of hardened concrete - making and curing specimen for strength tests, BS EN 12390-2*, London, BSI.

British Standard Institution (2009), *Testing of hardened concrete, BS EN 12390 - 3 - compressive strength test specimens*, London, BSI.

British Standard Institution (2009), *Testing of hardened concrete, BS EN 12390 - 4 -compressive strength, specification for testing machines*, London, BSI.

British Standard Institution (2009), *Testing of hardened concrete, BS EN 12390 - 6, Tensile splitting strength of test specimens*, London, BSI.

British Standard Institution (2009), *Testing of hardened concrete, BS EN 12390 - 7 - density of hardened concrete*, London, BSI.

British Standard Institution (2006), *BS EN 206 - Concrete: specification, performance, production and conformity*, London, BSI.

British Standard Institution (2004), *Eurocode 2: Design of concrete structures - Part 1-1: General rules*, London, BSI.

British Standard Institution (2000), *Cement- Composition, Specifications and Conformity Criteria for common Cements, BS EN 197- 1*, London, BSI.

British Standard Institution (1997), *Test for geometrical properties of aggregates, BS EN 933 - 1 - determination of particle size distribution (sieving method)*, London, BSI.

- Brühwiler, E., & Wittmann, F. H. (1990), The wedge splitting test, a new method for performing stable fracture mechanics test, *Engineering Fracture Mechanics*, Vol. 35(No. 1/2/3), 117-125.
- Craeye, B., & De Schutter, G. (2006), Experimental evaluation of mitigation of autogenous shrinkage by means of a vertical dilatometer for concrete, *In: RILEM Proceeding PRO 52 Volume Changes of Hardening Concrete: Testing and Mitigation*, Jensen, O. M., Lura, P. & Kovler, K. (eds.), RILEM Publications S.A.R.L., Bagnaux, France, 21-30.
- Craeye, B., Geirnaert, M., & Schutter, G. D. (2010), Super absorbing polymers as an internal curing agent for mitigation of early-age cracking of high-performance concrete bridge decks, *Construction and Building Materials*, 25(1), 1-13.
- Dehn, F. (2012), Constitutive concrete and durability models in the new fib model code 2010. *Encontro Nacional BETÃO ESTRUTURAL (National Concrete Structural) - BE2012 FEUP*, Portugal, (24 - 26 October) 1-12.
- DiStefano, C., Ferro, V., & Mirabile, S. (2010), Comparison between grain-size analyses using laser diffraction and sedimentation methods, *Biosystems Engineering*, 106, 205-215.
- Dudziak, L., & Mechtcherine, V. (2008), Mitigation of volume changes of ultra-high performance concrete (UHPC) by using super absorbent polymers, *Proceedings of 2<sup>nd</sup> International Symposium on Ultra High Performance Concrete*, E. Fehling et al., (eds.), Kassel University Press GmbH, 425-432.
- Dudziak, L., & Mechtcherine, V. (2010a), Reducing the cracking potential of Ultra-high performance concrete by using super absorbent polymers (SAP), *In: Van Zijl G. P. A. G. & Boshoff, W. P. (eds.), Proceedings of the International Conference on Advanced Concrete Materials*, Stellenbosch University, South Africa, 17-19 November, 2009.
- Dudziak, L., & Mechtcherine, V. (2010b), Enhancing early age resistance to cracking in high strength cement-based materials by means of internal curing using super absorbent polymers, *In:*

- Bramesshuber, W. (ed.), Proceedings of International Conference on Materials Science (MatSci), 6-10 September, 2010 (Aachen, Germany), RILEM Proc. PRO 77, Vol III, RILEM Publications S.A.R.L., Bagnaux, France, 129-139.
- du Plessis, A., Olawuyi, B. J., Boshoff, W. P., & le Roux, S. G. (2014), Simple and fast porosity analysis of concrete using X-ray computed tomography, *Materials and Structures*, online first (December).
- EDANA (2002), Recommended test: Free swell ratio, ERT 440.2-02.
- Esteves, L. P., Cachim, P., & Ferreira, V. M. (2007), Mechanical properties of cement mortars with superabsorbent polymers, *Advances in Construction Materials*, 451-462.
- Esteves, L. P. (2009), Internal curing in cement based materials, PhD Thesis, Aveiro University, Portugal.
- Esteves, L. P. (2014), Recommended method for measurement of absorbency of superabsorbent polymers in cement-based materials, *Materials and Structures*, published online 04 May 2014
- Fennis, S., Walvaren, J., & Den Uijl, J. (2012), Influence of particle packing on the strength of ecological concrete, *International Conference on Repair, Rehabilitation and Retrofitting (ICRRR) III*, Cape Town, South Africa, 486.
- FEI Visualisation Science Group (2013), *Avizo Fire (version 8.0) - 3D Analysis software for Scientific and Industrials Data*, [www.vsg3d.com](http://www.vsg3d.com)
- Friedemann, K., Stallmach, F., & Kärger, J. (2006), NMR diffusion and relaxation studies during cement hydration - a non-destructive approach to clarification of the mechanism of internal post-curing of cementitious materials, *Cement Concrete Research*, 36 (5): 817-826.

- Geika, M. R., Bentz, D. P., & Jensen, O. M. (2004), Mitigating autogenous shrinkage by IC, In Ries, J. P. & Holm, T. A. (Eds.), *High performance structural lightweight concrete* (Special Publication 218 ed., pp. 143-148), USA, ACI.
- Gils, M. A. J., Dortmans, L.J.M.G., & de With, G. (1995), Fictitious crack modelling of Kiln furniture ceramics, In: *Fracture Mechanics of Concrete Structures*, Wittmann, F. H. (eds.), Aedificatio Publishers, Freiburg, Germany, pp. 1261-1270.
- Guofan, Z., Hui, J., & Shilang, X. (1991), Study of fracture toughness and fracture energy by means of wedge splitting test specimens, In: *Brittle Matrix Composites*, Brand, A. M., & Marshal, I. H. (eds.), Elsevier Applied Science, London and New York, pp. 62-71.
- Habel, K., Charron, J., Braikey, S., Hooton, R.D., Gauvreau, P. & Massicotte, B. (2008), Ultra-High Performance Fibre Reinforced Concrete Mix Design in Central Canada. *Canadian Journal of Civil Engineering*, 35(2).
- Hansen, T. C. (1986), Physical structure of hardened cement paste: A classical approach, *Materials & Structures* 19 (6): 423-436.
- Hansen, E. A., Leive, M., Rodriguez, J., & Cather, R. (1996), Mechanical properties of high strength concrete - influence of test conditions, specimens and constituents. In I. Holand, & E. J. Sellevold (Eds.), *Proceedings of fourth international symposium on the utilization of high strength / high performance concrete* (pp. 187-196). Paris, France.
- Hasholt, M. T., Jespersen, M. H. S., & Jensen, O. M. (2010b), Mechanical properties of concrete with SAP, part II: Modulus of elasticity. *International RILEM Conference on use of Superabsorbent Polymers and Other Additives in Concrete*, Technical University of Denmark, Lyngby, Denmark. , *Proceedings Pro074* (15-18 August) 127--136.

- Hasholt, M. T., Jensen, O. M., Kovler, K., & Zhutovsky, S. (2012), Can superabsorbent polymers mitigate autogenous shrinkage of internally cured concrete without compromising the strength? *Construction and Building Materials*, 31, 226 - 230.
- Hasholt, M. T., Jespersen, M. H. S., & Jensen, O. M. (2010a), Mechanical properties of concrete with SAP - Part I: Development of compressive strength, *International RILEM Conference on Superabsorbent Polymers and Other Additives in Concrete*, Technical University of Denmark, Lyngby, Denmark. , *Proceeding Pro074*(15-18 August) 117--126.
- Henkensiefken, R., Nantung, T., & Weiss, J. (2011), Saturated lightweight aggregate for internal curing in low W/C mixtures: Monitoring water movement using x-ray absorption, *Strains* 47(s1): e432-e441.
- Hu, X. Z., & Wittmann, F. H. (1990), Experimental method to determine extension of fracture process zone . *Journal of Materials in Civil Engineering*, 2, 15-23.
- Hueste, M. B. D., Chompreda, P., Trejo, D., Celine, D. B. H., & Keating, P. B. (2004), Mechanical properties of high strength concrete for prestressed members. *ACI Structural Journal (Technical Paper)*, Jul.-Aug.(101-S45), 457-466.
- IBM® SPSS® Statistics Base (2015), Statistical Package for Social Sciences release version 22, IBM® SPSS® Statistics.
- Ingarashi, S., & Watanabe, A. (2006), Experimental study on prevention of autogenous deformation by IC using super-absorbent polymer particles, *International RILEM Conference on Volume Changes of Hardening Concrete: Testing and Mitigation*, Technical University of Denmark, Lyngby, Denmark. , *Proceeding Pro052*(20-23 August) 77-86.
- International Federation for Structural Concrete (fib). (2008), *Constitutive modelling of high strength /high performance concrete (HSC/HPC)*, (fib Bulletin 42), Lausanne:

International Federation for Structural Concrete (fib). (2012), *Model code 2010 (final version)*, (fib Bulletins 65 & 66), Lausanne: International Federation for Structural Concrete (fib).

International Union of Testing and Research Laboratories for Materials and Structures (RILEM) (1994), AAC13.1 - Determination of the specific fracture energy and strain softening of AAC 1992, TC51-ALC, 78-MCA, *RILEM technical recommendations for the testing and use of construction materials* (pp. 156-158), London, E & FN Spon.

International Union of Testing and Research Laboratories for Materials and Structures (RILEM) (1994), CPC4 - Compressive strength of concrete 1975, TC14-CPC, *RILEM technical recommendations for the testing and use of construction materials* (pp. 17-18), London, E & FN Spon.

International Union of Testing and Research Laboratories for Materials and Structures (RILEM) (1994), CPC8 - Modulus of elasticity of concrete in compression 1975, TC14-CPC, *RILEM technical recommendations for the testing and use of construction materials* (pp. 25-27), London, E & FN Spon.

Jensen, O. M. (1993), Autogenous deformation and RH-change - self-desiccation and self-desiccation shrinkage, *PhD Thesis*, Technical University of Denmark, Denmark.

Jensen, O. M., & Hansen, P. F. (2002), Water-entrained cement-based materials II: Experimental observations, *Cement and Concrete Research*, 32(6), 973--978.

Jensen, O. M., & Hansen, P. F. (2001), Water-entrained cement-based materials: I. principle and theoretical background, *Cement and Concrete Research*, 31(4), 647--654.

Jensen, O. M. & Lura, P. (2006), Techniques and materials for internal water curing of concrete, *Materials and Structures*, 39, 817 - 825.

- Jensen, O. M. (2008), Use of superabsorbent polymers in construction materials, *1<sup>st</sup> International Conference on Microstructure Related Durability of Cementitious Composites, October 13-15*, Nanjing, Peoples Republic of China.
- Jensen, O. M., Hasholt, M. T., & Laustsen, S. (Eds.). (2010), *Proceedings pro074: International RILEM conference on use of superabsorbent polymers and other new additives in concrete* RILEM Publications.
- Kadri, E. H., Aggoun, S., Kenai, S., & Kaci, A. (2012), The compressive strength of high-performance concrete and ultrahigh-performance. *Advance in Materials and Engineering*, (Article ID 361857), 1-7.
- Kakade, A. M. (2014), Measuring concrete surface pH - A proposed test method, *Concrete Repair Bulletin*, (March/April), 16-20.
- Kenter, P. (2012), Concrete sustainability requires coordinated research into hydration, beliefs expert, *Daily Commercial News and Construction Record (Online)*, 1.
- Kovler, K., & Jensen, O. M. (2007), *IC of concrete - state-of-the-art report of RILEM technical committee 196-ICC*, (RILEM STAR Report rep041), RILEM Publications.
- Kosmatka, S. H., Kerkhoff, B., & Panarese, W. C. (2002), Chapter 17: High performance concrete, *Design and control of concrete mixture: Engineering bulletin 001 (EB 001)* (Fourteenth ed., pp. 299-314), Illinois, USA: Portland Cement Association.
- Kowalenko, C. G., & Babuin, D. (2013), Inherent factors limiting the use of laser diffraction for determining particle size distribution of soil and related samples. *Geoderma*, 193 -194, 22-28.
- Kratz, M., Dudziak, L., & Mechtcherine, V. (2007), Plastic shrinkage of concretes with low and high W/C ratios, *Internal Technical Report*, Technical University, Dresden, Germany.

- Lam, L., Wong, Y. L., & Poon, C. S. (2000), Degree of hydration and gel/space ratio of high-volume fly ash/cement systems, *Cement and Concrete Research*, 30, 747-756.
- Lam, H., & Hooton, R. D. (2005), Effects of internal curing methods on restrained shrinkage and permeability, *Portland Cement Association, Research & Development Information Serial No.2620*, In: *Proceeding 4<sup>th</sup> International Seminar on Self-desiccation and its Importance in Concrete Technology*, Persson, B., Bentz, D., & Nilsson, L. O. (eds.), Lund University, Lund, Sweden, 201-228.
- Lausten, S., Hasholt, M. T., & Jensen, O. M. (2008), A new technology for air-entrainment of concrete, *1<sup>st</sup> International Conference on Microstructure Related Durability of Cementitious Composites*, 13-15 October, Nanjing, Peoples Republic of China, 1223-1230.
- Liu, B. D., Lv, W. J., Li, L., & Li, P. F. (2014), Effect of moisture content on static compressive elasticity modulus of concrete, *Construction and Building Materials*, 69, 133-142.
- Löfgren, I. (2005), Fibre Reinforced Concrete for Industrial Construction - a fracture mechanics approach to material testing and structural analysis, *PhD Thesis*, Chalmers University of Technology, Goteborg, Sweden 276pp.
- Löfgren, I., Stang, H., & Olesen, J. F. (2008), The WST method, a fracture mechanics test method for FRC, *Materials and Structures* 41: 197-211.
- Lura, P. (2003), Autogenous deformation and internal curing of concrete, PhD Thesis, Technical University, Delft, The Netherlands.
- Lura, P., Durand, F., Loukili, A., Kovler, K., & Jensen, O. M. (2006), Strength of cement pastes and mortars with superabsorbent polymers, *International RILEM Conference on Volume Changes of Hardening Concrete: Testing and Mitigation*, RILEM Proceedings PRO 52, RILEM Publications S.A.R.L., 117-126.

- Lura, P., & Lothenbach, B. (2010), Influence of pore solution chemistry on shrinkage of cement paste, *The 50-year Teaching and Research Anniversary of Prof. Sun Wei on Advances in Civil Engineering Materials*, Miao, C., Ye, G., & Chen, H. (eds.), RILEM Publications S.A.R.L., 191-200.
- Lyman, C. G. (1934), Growth and movement in Portland cement concrete, Oxford University Press, London.
- Maire, E., & Withers, P. J. (2014), Quantitative X-ray tomography, *International Materials Reviews*, 59(1), 1-43.
- Malhotra, V. M. (1994), *High-performance concrete: Proceedings, ACI international conference, Singapore*, Detroit, Mich.: American Concrete Institute.
- Maruyama, I., Kanematsu, M., Noguchi, T., Iikura, H., Teramoto, A., & Hayano, H. (2009), Evaluation of water transfer from saturated lightweight aggregates to cement paste matrix by neutron radiography, *Nuclear Instruments and Methods in Physics Research A: Accelerators, Spectrometers, Detectors and Associated Equipment*, 605 (1-2): 159-162.
- Masoero, E., Del Gado, E., Pelleng, R. J. M., Ulm, F. J., & Yip, S. (2012), Nanostructure and nanomechanics of cement: Polydisperse colloidal packing, *Physical Review Letters*, PR 109(155503), 1-4.
- Mechtcherine, V., & Müller, H. S. (1997), Fracture mechanical and fractological investigations on normal and high strength concrete, In A. M. Brand, V. C. Li & I. H. Marshall (Eds.), *Proceedings of the fifth international symposium on brittle matrix composites* (Bigraf/Warshaw ed., pp. 231-240), Cambridge, Woodhead Publishing Ltd.
- Mechtcherine, V., Dudziak, L., Schulze, J., & Staehr, H. (2006), Internal Curing by super absorbent polymers (SAP) - effects on material properties of self-compacting fibre-reinforced high performance concrete, *International RILEM Conference on Volume Changes of Hardening*

*Concrete: Testing and Mitigation*, Technical University of Denmark, Lyngby, Denmark. ,  
*Proceeding Pro052* (20-23 August) 87-96.

Mechtcherine, V., Dudziak, L., & Hempel, S. (2009), Mitigating early age shrinkage of Ultra-high performance concrete by using super absorbent polymers (SAP), *Creep, Shrinkage and Durability Mechanics of Concrete and Concrete Structures - CONCREEP-8*, T. Tanabe et. al. (eds.), Taylor & Francis Group, London, 843-853.

Mechtcherine, V., & Reinhardt, H. (eds.) (2012), Application of super absorbent polymers (SAP) in concrete construction, *RILEM State of the Art Reports*, 2

Mechtcherine, V., & Schroefl, C. (eds.) (2014), *Proceedings PRO 95: International RILEM conference on application of superabsorbent polymers and other new admixtures in concrete construction* (PRO 95 ed.). France: RILEM Publications S.A.R.L.

Mehta, P. K., & Monteiro, J. M. (2014), *Concrete microstructure properties and materials* (4th ed.), U.S.A.: McGraw-Hill Education.

Mönnig, S. (2005), Water saturated super-absorbent polymers used in high strength concrete, *Otto-Graf-Journal*, 16: 193-202.

Mönnig, S. (2009), Superabsorbing additions in concrete - applications, modelling and comparison of different internal water sources, PhD Thesis, University of Stuttgart, 164 pp.

Nawa, T., & Horita, T. (2004), Autogenous shrinkage of high-performance concrete, *In: Proceedings of the International Workshop on Microstructure and Durability to Predict Service Life of Concrete Structures*, February, Sapporo, Japan.

Nestle, K., Kühn, A., Friedemann, K., Horch, C., Stallmach, F., & Herth, G. (2009), Water balance and pore structure development in cementitious materials in internal curing with modified super-absorbent polymer studied by NMR, *Microporous Mesoporous Materials*, 125 (1-2): 51-57.

- Neville, A. M. (2012), *Properties of concrete* (Fifth ed.), England: Pearson Educational Limited.
- Neville, A. M., & Aitcin, P. C. (1998), High performance concrete - an overview, *Materials and Structures/Materiaux Et Constructions*, 31(Mars), 111-117.
- Neville, A. M., & Brooks, J. J. (2010), *Concrete technology* (2nd ed.), London: Prentice Hall.
- Nordic Innovative Centre (2005), Wedge Splitting Test Method: Fracture Testing of Fibre Reinforced Concrete (Mode I) - NT BUILD 511, Norway, 5pp.
- Ollivier, J. P., Carles-Gibergues, A., & Hanna, B. (1988), Pozzolanic activity and filling action of silica fume in high strength concrete matrices [Activite pouzzolanique et action de remplissage d'une fumee de silice dans les matrices de beton de haute resistance], *Cement and Concrete Research*, 18(3), 438-448.
- Persson, B. (1996), Hydration and strength of high performance concrete, *Advance Cement Based Materials*, 3, 107-123.
- Pierard, J., Pollet, V., & Cauberg, N. (2006), Mitigating autogenous shrinkage in HPC by IC using superabsorbent polymers, *International RILEM Conference on Volume Changes of Hardening Concrete: Testing and Mitigation*, Technical University of Denmark, Lyngby, Denmark. , *Proceeding Pro052(20-23 August)* 97-106.
- Portland Cement Association (2012), Specialty concrete - high end value materials. Retrieved from [www.cee.mtu.edu/~ljsutter/classes/cet1141/present/hvalue.ppt](http://www.cee.mtu.edu/~ljsutter/classes/cet1141/present/hvalue.ppt)
- Powers, T. C. (1958), Structure and physical properties of hardened Portland cement paste, [Article first published online 2nd June, 2006], *Journal of the American Ceramic Society*, 41(1), 1-6.
- Powers, T. C., & Brownyard, T. L. (2003a), Landmark series: Studies into physical properties of hardened Portland cement pastes, part 2, [originally published in the ACI JOURNAL, V. 18 No. 8, Apr. 1947], *Concrete International*, 25(9), 31-42.

- Powers, T. C., & Brownyard, T. L. (2003b), Landmark series: Studies of the physical properties of hardened cement paste, [originally published in the ACI JOURNAL, V. 18 No. 8, Apr. 1947] *Concrete International*, 25(8), 59-70.
- Rahimian, A., & Eilon, Y. (2012), The rise of one world trade centre, *STRUCTUREmag - Structural Engineering Magazine, Tradeshow*, Nov. 2012(1564)
- Ramezaniapour, A. A. (2014), Chapter 2: Fly ash. *Cement replacement materials: Properties, durability and sustainability* (pp. 47-156), Verlag Berlin Heidelberg: Springer Geochemistry/Mineralogy.
- Reinhardt, H., & Mönnig, S. (2006), Results of comparative study of the shrinkage behaviour of concretes with different internal water sources, *In: Jensen, O. M., Lura, P & Kovler, K. (eds.), Proceedings of International RILEM Conference on Volume Changes of Hardening Concrete: Testing and Mitigation*, (20-23 August), Technical University of Denmark, Lyngby, Denmark, 67-76.
- Reinhardt, W., Assmann, A., & Mönnig, S. (2008), Superabsorbent polymers (SAPs) - an admixture to increase the durability of concrete, *1<sup>st</sup> International Conference on Microstructure Related Durability of Cementitious Composites*, 13-15 October, Nanjing, Peoples Republic of China, 313-322.
- Schrofl, C., Mechtcherine, V., & Gorges, M. (2012), Relation between the molecular structure and the efficiency of superabsorbent polymer (SAP) as concrete admixture to mitigate autogenous shrinkage, *Cement and Concrete Research*, 42, 865-- 873.
- Sellevold, E. J., & Radjy, F. F. (1983), Condensed silica fume (microsilica) in concrete: Water demand and strength development, *Fly-Ash, Silica Fume, Slag and Other Mineral by- Products in Concrete ACI SP-79*,

Shetty, M. S. (2004), *Concrete technology - theory and practice*, New Dhelhi, India: S. Chand and Company Limited.

Siddique, R., & Khan, M. I. (2011), Chapter 2: Silica fume, *Supplementary cementitious materials* (XVI ed., pp. 67-119). Verlag Berlin Heidelberg: Springer.

Silica Fume Association (2005), *Silica fume Ushers' Manual*.

Siramanont, J., Vichit-Vadaka, W., & Siriwatwechakul, W. (2010), The impact of SAP structure on the effectiveness of IC, *International RILEM Conference on use of Superabsorbent Polymers and Other New Additives in Concrete*, Technical University Denmark, Lyngby, Denmark, *Proceeding Pro074* (15-18 August) 243--252.

Siriwatwechakul, W., Siramanont, J., & Vichit-Vadaka, W. (2010), Superabsorbent polymer structures, *International RILEM Conference on use of Superabsorbent Polymers and Other New Additives in Concrete*, Technical University Denmark, Lyngby, Denmark, *Pro074* (15-18 August) 253-262.

South African Bureau of Standards (2001), SANS 50197 - 1 - *Cement - Part 1: Composition, specifications and conformity criteria for common cements*, Pretoria, (SABS).

Trtik, P., Münch, B., Weiss, W. J., Kaestner, A., Jerjen, I., Josic, L., Lehmann, E., & Lura, P. (2011), Release of internal curing water from lightweight aggregates in cement paste investigated by neutron and X-ray tomography, *Nuclear Instruments and Methods in Physics Research A: Accelerators, Spectrometers, Detectors and Associated Equipment*, 651 (1): 244-249.

Trunk, B., Schober, G., Helbing, A. K., & Wittmann, F. H. (1999), Fracture mechanics parameters of autoclaved aerated concrete, *Cement and Concrete Research*, 29: 855-859

the IRON Platform (2014), Iuclid 5 composition and analysis guidance document: mill scale (EINECS number 266-007-8, CAS number 65996-74-9) - TWG117, pg. 2-3, [http://www.iron-consortium.org/assets/files/TWG/Analysis-MillScale-V2\\_100717.pdf](http://www.iron-consortium.org/assets/files/TWG/Analysis-MillScale-V2_100717.pdf)

Volume Graphics (2013), *VGStudio Max 2.2 - Application software for analysis and visualisation of industrial computed tomography/ voxel data*, [www.volumegraphics.com](http://www.volumegraphics.com)

Wang, F., Zhou, Y., Peng, B., Liu, Z., & Hu, S. (2009), Autogenous shrinkage of concrete with super absorbent polymer, *ACI Materials Journal*, 106 (2): 123-127.

Weber, S., & Reinhardt, H. W. (1997), A new generation of high performance concrete: concrete with autogenous curing, *Advanced Cement Based Materials*, 6 (2): 59-68.

Winter, N. B. (2012), *Scanning electron microscopy of cement and concrete*, Rendlesham, Woodbridge, UK: WHD Microanalysis Consultants Ltd.

Wille, K., Naaman, A. E., & Parra-Montesinos, G. J. (2011), Ultra-High Performance Concrete with Compressive Strength Exceeding 150 MPa (22 Ksi): A Simpler Way. *ACI Materials Journal*, 108(1), 23 June 2013.

Wittmann, F. H., Roelfstra, P. E., Mihashi, H., Huang, Y. Y., Zhang, X., & Nomura, K. (1987), Influence of age at loading, water-cement ratio and rate of loading on fracture energy of concrete, *Materials and Structures, Paris*, 20, 103-110.

Wyrzykowski, M., Gawin, D., Pesavento, F., & Lura, P. (2006), Multi-scale modelling of autogenous strains of an internally cured cementitious material, *International RILEM Conference on Volume Changes of Hardening Concrete Testing and Mitigation*, Technical University of Denmark, Lyngby, Denmark, *Proceeding Pro052* (20-23 August) 137-146.

Ye, G. (2003), Experimental study and numerical simulation of the development of the microstructure and permeability of cementitious materials, *PhD Thesis*, Delft University of Technology, Delft, Netherlands.

Zang, J. (2015), Developing non-heat treated UHPC in South Africa, PhD Thesis, University of Stellenbosch, Stellenbosch, South Africa.

Zhao, Z., Kwon, S. H., & Shah, S. P. (2008), Effect of specimen size on fracture energy and softening curve of concrete: Part I. experiments and fracture energy, *Cement and Concrete Research*, 38.

# Appendix A: Attachments to Chapter Four

**Table A1: for Specimen Designation of HPC Mixtures**

Specimen Designation	Binder Composition
	Binder Type 1 (binary cement) = CEM I 52.5 N(92.5%) + (SF (7.5%))
M <sub>2</sub>	Reference mixture for binder Type 1 (0.25 W/B)
M <sub>2</sub> SP <sub>1</sub> -0.2	M <sub>2</sub> + SAP Type 1 (0.2% b <sub>wob</sub> content)
M <sub>2</sub> SP <sub>1</sub> -0.3	M <sub>2</sub> + SAP Type 1 (0.3% b <sub>wob</sub> content)
M <sub>2</sub> SP <sub>1</sub> -0.4	M <sub>2</sub> + SAP Type 1 (0.4% b <sub>wob</sub> content)
M <sub>2</sub> SP <sub>2</sub> -0.2	M <sub>2</sub> + SAP Type 2 (0.2% b <sub>wob</sub> content)
M <sub>2</sub> SP <sub>2</sub> -0.3	M <sub>2</sub> + SAP Type 2 (0.3% b <sub>wob</sub> content)
M <sub>2</sub> SP <sub>2</sub> -0.4	M <sub>2</sub> + SAP Type 2 (0.4% b <sub>wob</sub> content)
M <sub>3</sub>	Reference mixture for binder Type 1(0.20 W/B)
M <sub>3</sub> SP <sub>1</sub> -0.2	M <sub>3</sub> + SAP Type 1 (0.2% b <sub>wob</sub> content)
M <sub>3</sub> SP <sub>1</sub> -0.3	M <sub>3</sub> + SAP Type 1 (0.3% b <sub>wob</sub> content)
M <sub>3</sub> SP <sub>1</sub> -0.4	M <sub>3</sub> + SAP Type 1 (0.4% b <sub>wob</sub> content)
M <sub>3</sub> SP <sub>2</sub> -0.2	M <sub>3</sub> + SAP Type 2 (0.2% b <sub>wob</sub> content)
M <sub>3</sub> SP <sub>2</sub> -0.3	M <sub>3</sub> + SAP Type 2 (0.3% b <sub>wob</sub> content)
M <sub>3</sub> SP <sub>2</sub> -0.4	M <sub>3</sub> + SAP Type 2 (0.4% b <sub>wob</sub> content)
Ternary cements (0.25 W/B)	
M <sub>1F</sub>	Reference mixture for binder Type 2 = CEM I 52.5 N (75.0%) + SF (7.5%) + FA (17.5%)
M <sub>1F</sub> SP <sub>1</sub> -0.2	M <sub>1F</sub> + SAP Type 1 (0.2% b <sub>wob</sub> content)
M <sub>1F</sub> SP <sub>1</sub> -0.3	M <sub>1F</sub> + SAP Type 1 (0.3% b <sub>wob</sub> content)
M <sub>1F</sub> SP <sub>1</sub> -0.4	M <sub>1F</sub> + SAP Type 1 (0.4% b <sub>wob</sub> content)
M <sub>1F</sub> SP <sub>2</sub> -0.2	M <sub>1F</sub> + SAP Type 2 (0.2% b <sub>wob</sub> content)
M <sub>1F</sub> SP <sub>2</sub> -0.3	M <sub>1F</sub> + SAP Type 2 (0.3% b <sub>wob</sub> content)
M <sub>1F</sub> SP <sub>2</sub> -0.4	M <sub>1F</sub> + SAP Type 2 (0.4% bwob content)
M <sub>1S</sub>	Reference mixture for binder Type 3 = CEM I 52.5 N (75.0%) + SF (7.5%) + CS (17.5%)
M <sub>1S</sub> SP <sub>1</sub> -0.2	M <sub>1S</sub> + SAP Type 1 (0.2% b <sub>wob</sub> content)
M <sub>1S</sub> SP <sub>1</sub> -0.3	M <sub>1S</sub> + SAP Type 1 (0.3% b <sub>wob</sub> content)
M <sub>1S</sub> SP <sub>1</sub> -0.4	M <sub>1S</sub> + SAP Type 1 (0.4% b <sub>wob</sub> content)
M <sub>1S</sub> SP <sub>2</sub> -0.2	M <sub>1S</sub> + SAP Type 2 (0.2% b <sub>wob</sub> content)
M <sub>1S</sub> SP <sub>2</sub> -0.3	M <sub>1S</sub> + SAP Type 2 (0.3% b <sub>wob</sub> content)
M <sub>1S</sub> SP <sub>2</sub> -0.4	M <sub>1S</sub> + SAP Type 2 (0.4% b <sub>wob</sub> content)

**Table A2: SAP Absorption**

time (min)	SAP1(g/g)						SAP2(g/g)					
	Water	CPS					Water	CPS				
		(W/C) 5.2	(W/C) 4.3	(W/C) 3.7	(W/C) 3.1	(W/C) 2.5		(W/C) 5.2	(W/C) 4.3	(W/C) 3.7	(W/C) 3.1	(W/C) 2.5
0.5	72.34	20.11	24.45	25.63	28.81	26.69	65.80	26.61	25.12	26.77	24.04	27.03
2	170.29	20.84	22.23	23.56	26.42	26.08	180.63	31.49	25.64	26.87	24.01	28.57
5	216.17	22.59	19.99	22.59	26.95	27.09	233.95	32.02	22.85	27.15	23.98	26.37
<b>10</b>	<b>228.44</b>	<b>24.30</b>	<b>21.64</b>	<b>24.08</b>	<b>22.77</b>	<b>27.24</b>	<b>258.22</b>	<b>33.93</b>	<b>24.45</b>	<b>27.85</b>	<b>23.61</b>	<b>24.09</b>
<b>15</b>	<b>242.00</b>	<b>31.64</b>	<b>21.02</b>	<b>25.08</b>	<b>21.93</b>	<b>24.07</b>	<b>284.49</b>	<b>35.80</b>	<b>23.96</b>	<b>24.41</b>	<b>22.99</b>	<b>24.14</b>
30	253.02	35.18	22.08	24.64	21.97	25.76	292.95	36.76	23.55	23.98	23.88	24.75
60	257.07	38.14	21.94	23.30	21.42	25.68	297.54	41.85	19.93	21.75	20.79	24.42
180	260.76	41.80	23.91	22.18	20.35	22.87	298.22	48.24	19.17	22.83	22.85	21.01

**Table A3: Setting Times and Strength Developments of HPC Mixtures**

Specimen	Setting Times				
	Initial	Final	Expression	R <sup>2</sup>	R
M <sub>2</sub>	535	675	2E-24X <sup>8.8671</sup>	0.9851	0.992522
M <sub>2</sub> Sp <sub>1</sub> -0.2	615	800	2E-21X <sup>7.626</sup>	0.9951	0.997547
M <sub>2</sub> Sp <sub>1</sub> -0.3	790	1030	2E-22X <sup>7.6766</sup>	0.9748	0.98732
M <sub>2</sub> Sp <sub>1</sub> -0.4	615	840	2E-18X <sup>6.5637</sup>	0.9790	0.989444
M <sub>2</sub> Sp <sub>2</sub> -0.2	555	695	6E-25X <sup>9.0245</sup>	0.9754	0.987623
M <sub>2</sub> Sp <sub>2</sub> -0.3	585	745	3E-24X <sup>8.676</sup>	0.9747	0.987269
M <sub>2</sub> Sp <sub>2</sub> -0.4	645	805	1E-27X <sup>9.7586</sup>	0.9856	0.992774
M <sub>3</sub>	490	625	1E-22X <sup>8.3387</sup>	0.9766	0.988231
M <sub>3</sub> Sp <sub>1</sub> -0.2	595	730	6E-27X <sup>9.6518</sup>	0.9891	0.994535
M <sub>3</sub> Sp <sub>1</sub> -0.3	650	845	3E-22X <sup>7.8352</sup>	0.9370	0.967988
M <sub>3</sub> Sp <sub>1</sub> -0.4	795	945	1E-33X <sup>11.522</sup>	0.9714	0.985596
M <sub>1F</sub>	485	580	4E-31X <sup>11.534</sup>	0.9809	0.990404
M <sub>1F</sub> Sp <sub>1</sub> -0.2	615	795	9E-23X <sup>8.1016</sup>	0.9775	0.988686
M <sub>1F</sub> Sp <sub>1</sub> -0.3	810	1095	3E-20X <sup>6.896</sup>	0.9586	0.979081
M <sub>1F</sub> Sp <sub>1</sub> -0.4	515	715	2E-17X <sup>6.3395</sup>	0.9566	0.978059
M <sub>1S</sub>	435	600	2E-16X <sup>6.1818</sup>	0.9362	0.967574
M <sub>1S</sub> Sp <sub>1</sub> -0.2	730	965	2E-21X <sup>7.4311</sup>	0.9376	0.968297
M <sub>1S</sub> Sp <sub>1</sub> -0.3	850	1090	6E-23X <sup>7.775</sup>	0.9509	0.975141
M <sub>1S</sub> Sp <sub>1</sub> -0.4	765	965	1E-24X <sup>8.4789</sup>	0.9546	0.977036
M <sub>1S</sub> Sp <sub>2</sub> -0.2	790	965	6E-29X <sup>9.9256</sup>	0.9882	0.994082
M <sub>1S</sub> Sp <sub>2</sub> -0.3	765	990	3E-21X <sup>7.3207</sup>	0.8964	0.946784
M <sub>1S</sub> Sp <sub>2</sub> -0.4	965	1150	5E-34X <sup>11.332</sup>	0.9564	0.977957

## Appendix B: Attachments to Chapter 5

### B1 Duncan Multiple Range Test Results for Early Age Properties

**Table B1.1: Duncan's multiple range effect of W/B Effects on Compressive Strength**

W/B	N	Subset		
		1	2	3
0.3	84	9.297958E1	1.062818E2	1.117036E2
0.25	84			
0.2	168			
Sig.		1.000	1.000	1.000

**Table B1.2: Duncan's multiple range effect of SAP contents on Compressive Strength**

SAP contents	N	Subset			
		1	2	3	4
0.4	96	9.476406E1	1.058031E2	1.090167E2	1.205024E2
0.3	96				
0.2	96				
0	48				
Sig.		1.000	1.000	1.000	1.000

**Table B1.3: Duncan's multiple range effect of SAP Type on Compressive Strength**

SAP type	N	Subset		
		1	2	3
1	144	1.020701E2	1.043191E2	1.205024E2
2	144			
0	48			
Sig.		1.000	1.000	1.000

**Table B1.4: Duncan's multiple range effect of Binder Type on Compressive Strength**

Binder type	N	Subset		
		1	2	3
1	168	9.963068E1	1.101398E2	1.132674E2
3	84			
2	84			
Sig.		1.000	1.000	1.000

**Table B1.5: Duncan's multiple range Effect of Curing Age on Compressive Strength**

Curing Age	N	Subset			
		1	2	3	4
7	84	8.180663E1	1.046660E2	1.154175E2	1.207785E2
28	84				
56	84				
90	84				
Sig.		1.000	1.000	1.000	1.000

Means for groups in homogeneous subsets are displayed based on observed means.  
The error term is Mean Square (Error) = 20.617.

## B2 Influence of SAP addition Compressive Strength of HPCs

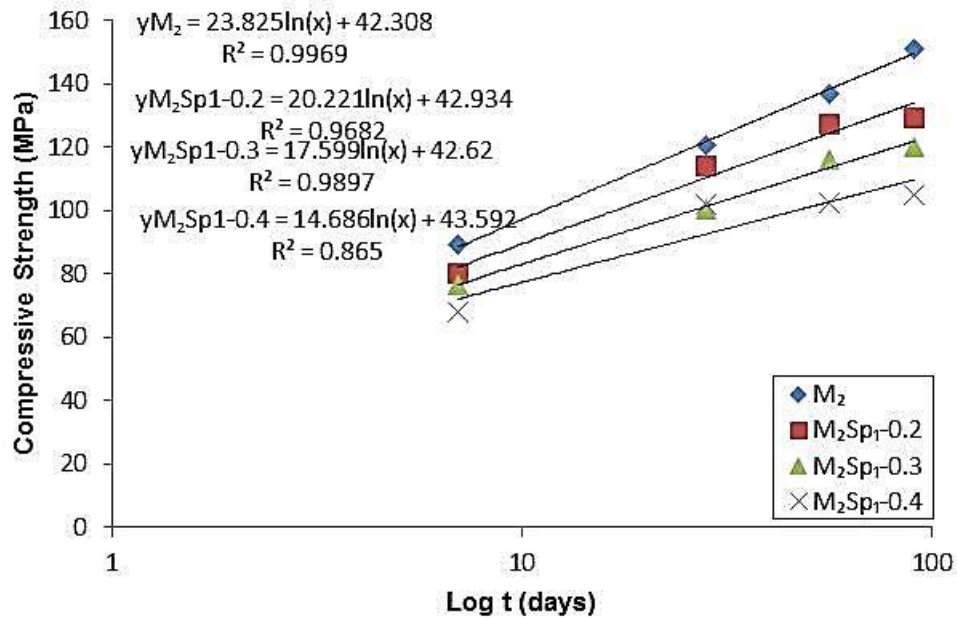


Figure B2.1: Compressive strength of  $M_2$  - HPCs with  $SP_1$  on log time scale

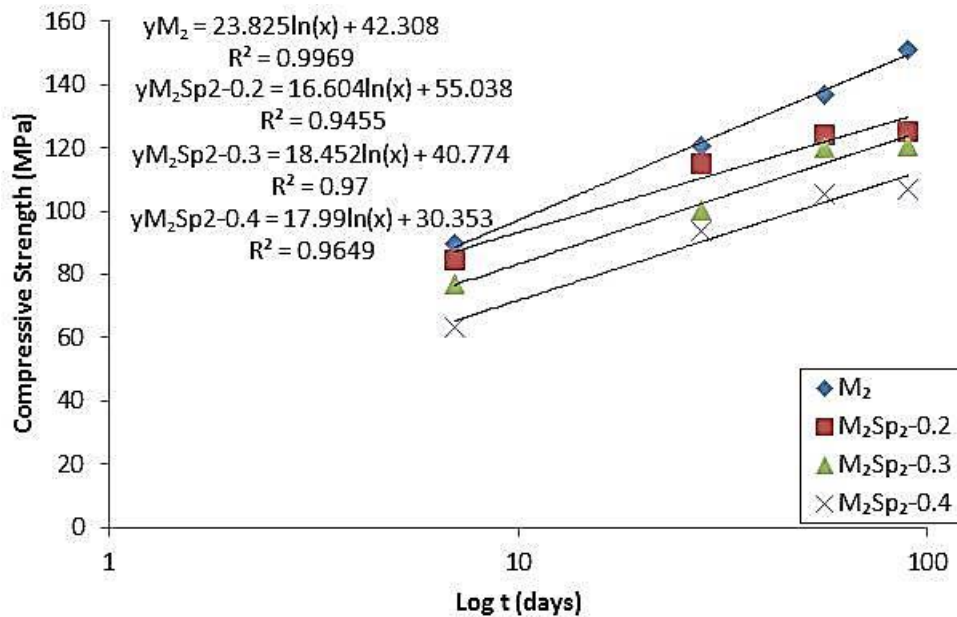


Figure B2.2: Compressive strength of  $M_2$  - HPCs with  $SP_2$  on log time scale

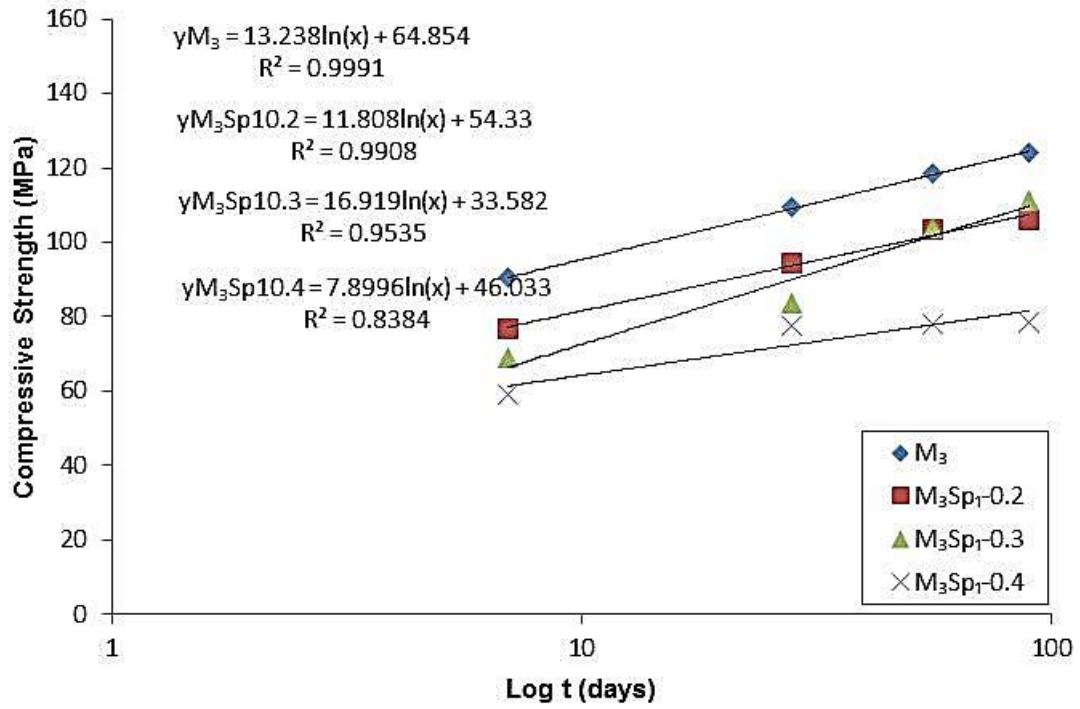


Figure B2.3: Compressive strength of M<sub>3</sub> - HPCs with SP<sub>2</sub> on log time scale

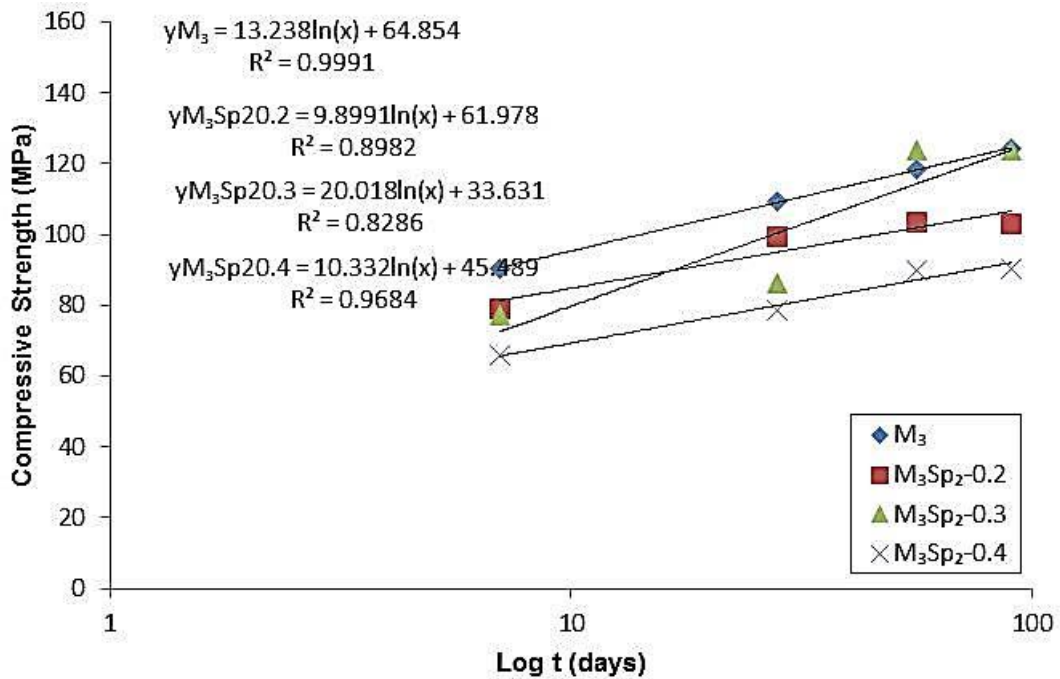


Figure B2.4: Compressive strength of M<sub>3</sub> - HPCs with SP<sub>2</sub> on log time scale

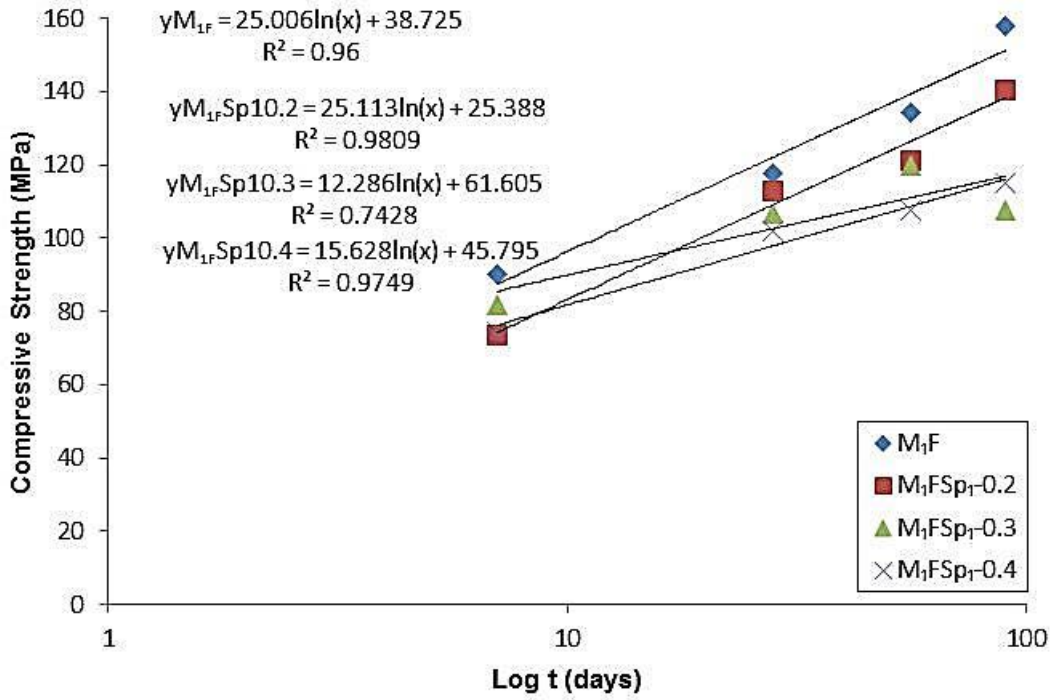


Figure B2.5: Compressive strength of M<sub>1F</sub> - HPCs with SP<sub>1</sub> on log time scale

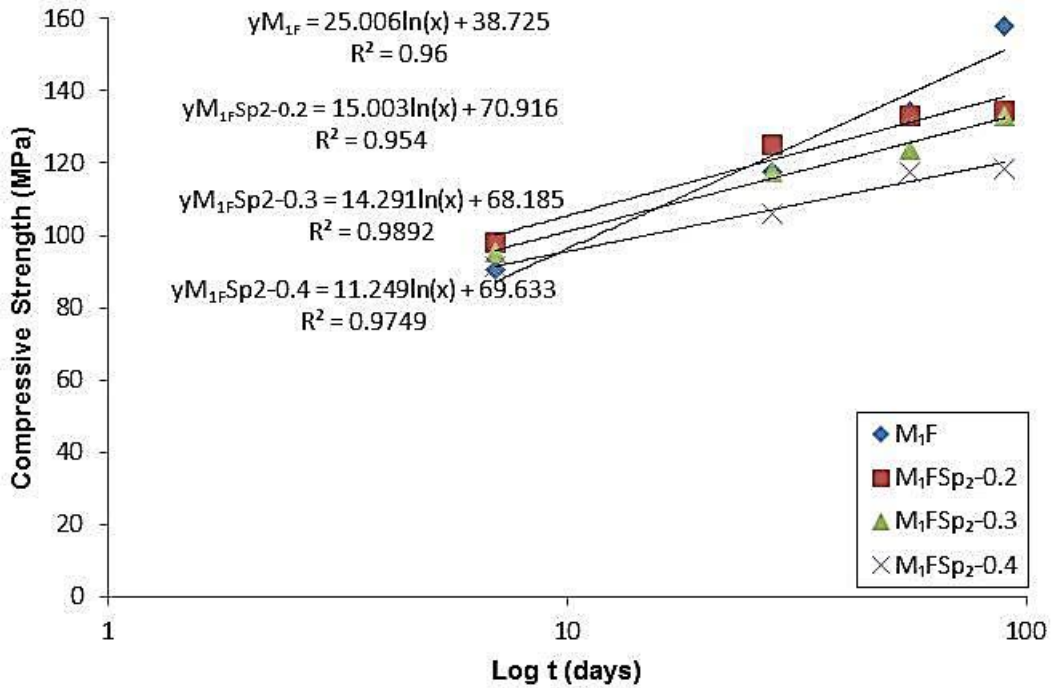


Figure B2.6: Compressive strength of M<sub>1F</sub> - HPCs with SP<sub>2</sub> on log time scale

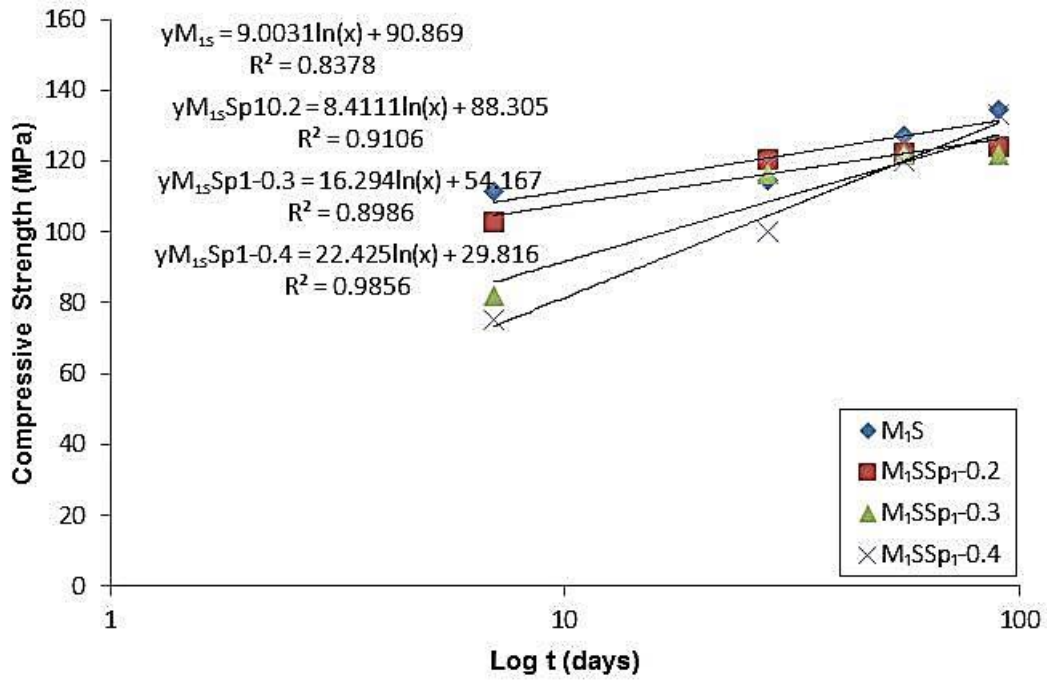


Figure B2.7: Compressive strength of M<sub>1S</sub> - HPCs with SP<sub>1</sub> on log time scale

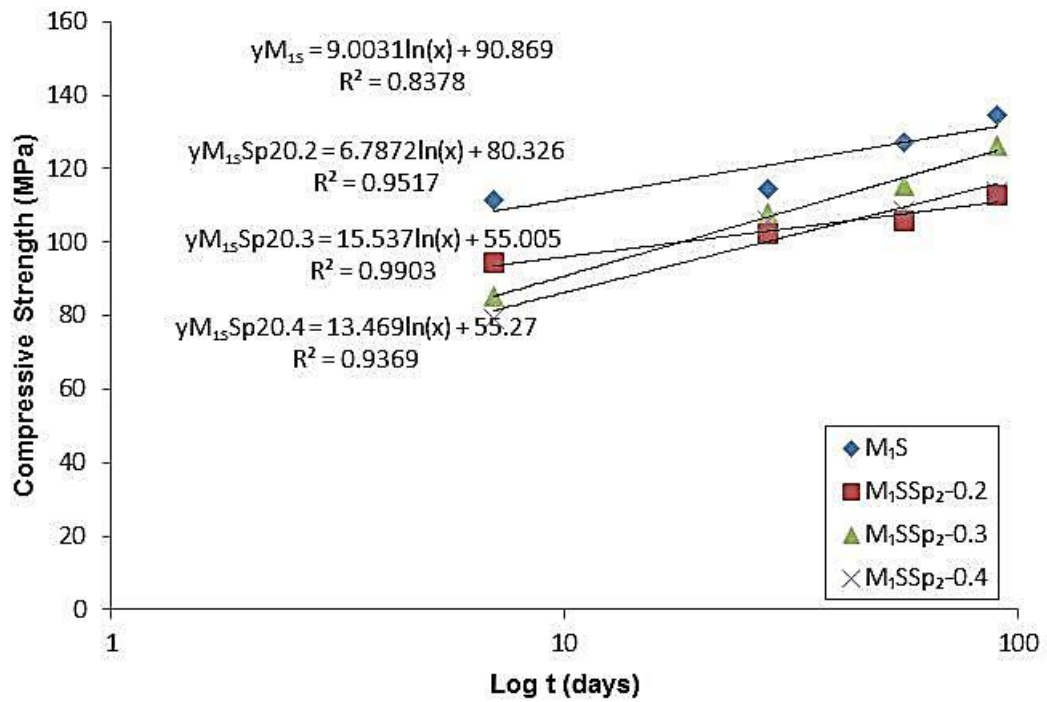


Figure B2.8: Compressive strength of M<sub>1S</sub> - HPCs with SP<sub>2</sub> on log time scale

### B3 Duncan Multiple Range Test Results for E-modulus of HPC

**Table B3.1: Duncan's multiple range effect of W/B Effects on E-modulus**

W/B	N	Subset		
		1	2	3
0.3	63	4.6766911E1	5.0272584E1	5.3728611E1
0.2	126			
0.25	63			
Sig.		1.000	1.000	1.000

**Table B3.2: Duncan's multiple range effect for SAP content Effects on E-modulus**

SAP content	N	Subset		
		1	2	3
0.4	72	4.8979484E1	5.0179033E1	5.2800817E1
0.3	72		5.0351677E1	
0.2	72			
0	36			
Sig.		1.000	.641	1.000

**Table B3.3: Duncan's multiple range effect of SAP type Effects on E-modulus**

SAP type	N	Subset	
		1	2
1	108	4.9528370E1	5.2800817E1
2	108		
0	36		
Sig.		.079	1.000

**Table B3.4: Duncan's multiple range effect of Binder type Effects on E-modulus**

Binder type	N	Subset		
		1	2	3
3	63	4.8245208E1	5.0247761E1	5.2299960E1
1	126			
2	63			
Sig.		1.000	1.000	1.000

**Table B3.5: Duncan's Multiple Range effect of Curing Age Effects on E-modulus**

Curing Age	N	Subset		
		1	2	3
90	84	4.7186068E1	4.7857662E1	5.5736787E1
56	84			
28	84			
Sig.		1.000	1.000	1.000

Means for groups in homogeneous subsets are displayed based on observed means.

The error term is Mean Square (Error) = 3.934.

### B4 Duncan Multiple range Test for Fracture Energy

**Table B4.1: Duncan<sup>a,b,c</sup> multiple range test on Fracture Energy with W/B**

W/B	N	Subset	
		1	
.20	95	151.8160	
.25	56	153.0893	
.30	52	153.2626	
Sig.		.706	

**Table B4.2: Duncan<sup>a,b,c</sup> multiple range test on Fracture Energy with SAP content**

SAP content	N	Subset	
		1	2
0	54	146.7170	
0	60	151.7014	151.7014
0	28	155.2023	155.2023
0	61		157.2903
Sig.		.056	.211

**Table B4.3: Duncan<sup>a,b,c</sup> multiple range test on Fracture Energy with SAP type**

SAP Type	N	Subset	
		1	
2	84	148.9072	
1	91	155.0693	
0	28	155.2023	
Sig.		.136	

**Table B4.4: Duncan<sup>a,b,c</sup> multiple range test on Fracture Energy with Binder Type**

Binder Type	N	Subset		
		1	2	3
2	50	142.3822		
1	108		153.1727	
3	45			162.2980
Sig.		1.000	1.000	1.000

**Table B4.5: Duncan<sup>a,b,c</sup> multiple range test on Fracture Energy with Curing Age**

Curing Age	N	Subset	
		1	
28	66	150.6234	
56	62	153.1797	
90	75	153.6919	
Sig.		.407	

Means for groups in homogeneous subsets are displayed based on observed means.

The error term is Mean Square (Error) = 400.581.

a. Uses Harmonic Mean Sample Size = 63.006.

b. The group sizes are unequal. The harmonic mean of the group sizes is used. Type I error levels are not guaranteed.

c. Alpha = 0.05.

## Appendix C: SEM image analysis of HPCs

### C1 Summary of SEM Quantitative Analysis for M<sub>2</sub> – HPC Series

**Table C1.1: Quantitative Analysis of Spectrum B in M<sub>2</sub> – HPC Series**

Atomic Ratio	M <sub>2</sub>	M <sub>2</sub> Sp <sub>1</sub> -0.2	M <sub>2</sub> Sp <sub>1</sub> -0.3	M <sub>2</sub> Sp <sub>1</sub> -0.4	M <sub>2</sub> Sp <sub>2</sub> -0.2	M <sub>2</sub> Sp <sub>2</sub> -0.3	M <sub>2</sub> Sp <sub>2</sub> -0.4
Mg		0.21	0.22	0.15	0.00	0.26	0.19
Al	0.67	0.55	0.65	0.35	0.92	1.44	0.68
Si	12.28	11.58	12.47	12.42	13.17	11.84	11.36
S	0.00	0.07	0.13	0.00	0.00	0.00	0.00
K	0.10	0.07	0.21	0.20	0.50	0.12	0.23
Ca	26.28	27.26	25.46	26.12	26.83	24.90	27.36
Ti	0.00	0.00	0.00	0.00	0.00	0.11	0.00
Fe	0.24	0.27	0.39	0.30	0.43	1.03	0.35
O	38.39	51.96	52.50	52.05	55.23	52.30	51.76
Si/Ca	0.467	0.425	0.490	0.476	0.491	0.476	0.415
Al/Ca	0.025	0.020	0.026	0.013	0.034	0.058	0.025
S/Ca	0.000	0.002	0.005	0.000	0.000	0.000	0.000
C: S	2.140	2.355	2.042	2.103	2.037	2.103	2.408
SiO <sub>2</sub>	31.66	30.43	33.26	32.94	34.59	31.20	29.74
CaO	64.95	66.75	62.72	64.64	61.12	61.24	66.84
CaO/SiO <sub>2</sub>	2.05	2.19	1.89	1.96	1.77	1.96	2.25

**Table C1.2: Quantitative Analysis of Spectrum D in M<sub>2</sub> – HPC Series**

Spectrum D	M <sub>2</sub>	M <sub>2</sub> Sp <sub>1</sub> -0.2	M <sub>2</sub> Sp <sub>1</sub> -0.3	M <sub>2</sub> Sp <sub>1</sub> -0.4	M <sub>2</sub> Sp <sub>2</sub> -0.2	M <sub>2</sub> Sp <sub>2</sub> -0.3	M <sub>2</sub> Sp <sub>2</sub> -0.4
Na	0.00	0.00	0.00	0.70	0.00	0.20	0.61
Mg	0.66	0.74	0.37	0.26	0.53	0.61	0.25
Al	2.39	2.18	1.71	1.44	2.47	1.89	2.62
Si	12.40	12.89	11.10	10.77	14.28	14.31	13.43
S	0.98	1.07	1.06	0.00	0.00	0.57	0.00
K	0.11	0.18	0.00	3.23	0.00	1.07	2.89
Ca	21.00	20.25	24.19	24.02	21.10	19.04	19.19
Fe	0.82	0.82	0.58	0.56	0.91	0.59	0.62
Mo	0.00	0.00	0.00	0.00	0.76	0.00	0.00
O	53.86	54.14	53.08	50.51	57.07	54.03	52.59
Si/Ca	0.59	0.64	0.46	0.45	0.68	0.75	0.70
Al/Ca	0.11	0.11	0.07	0.06	0.12	0.10	0.14
S/Ca	0.05	0.05	0.04	0.00	0.00	0.03	0.00
C: S	1.69	1.57	2.18	2.23	1.48	1.33	1.43
SiO <sub>2</sub>	33.64	35.14	29.68	28.23	36.31	39.22	36.26
CaO	53.17	51.54	60.08	58.77	50.08	48.70	48.34
CaO/SiO <sub>2</sub>	1.58	1.47	2.02	2.08	1.38	1.24	1.33

**Table C1.3: Quantitative Analysis of Spectrum C in M<sub>2</sub> – HPC Series**

Atomic Ratio	M <sub>2</sub>	M <sub>2</sub> Sp <sub>1</sub> -0.2	M <sub>2</sub> Sp <sub>1</sub> -0.3	M <sub>2</sub> Sp <sub>1</sub> -0.4	M <sub>2</sub> Sp <sub>2</sub> -0.2	M <sub>2</sub> Sp <sub>2</sub> -0.3	M <sub>2</sub> Sp <sub>2</sub> -0.4
Al	0.34	0.00	0.00	0.00	0.00	0.00	0.34
Si	1.26	0.45	0.75	0.71	1.34	1.29	1.29
S	0.00	0.00	0.00	0.00	0.00	0.00	0.00
Ca	1.92	0.79	1.35	1.54	1.58	1.67	1.87
Cr	0.12	0.00	0.00	0.00	0.00	0.00	0.00
Mn	0.20	0.29	0.00	0.25	0.23	0.23	0.20
Fe	40.05	42.70	41.73	41.21	40.72	40.70	40.13
O	45.29	44.68	44.86	44.52	45.21	45.18	45.29
Si/Ca	0.655	0.563	0.553	0.459	0.853	0.774	0.688
Al/Ca	0.178	0.000	0.000	0.000	0.000	0.000	0.184
S/Ca	0.000	0.000	0.000	0.000	0.000	0.000	0.000
C: S	1.527	1.775	1.809	2.177	1.172	1.293	1.453
SiO <sub>2</sub>	1.63	0.85	1.43	1.36	2.60	2.50	2.50
CaO	2.73	1.40	2.41	2.77	2.84	3.01	3.38
CaO/SiO <sub>2</sub>	1.67	1.66	1.69	2.03	1.09	1.21	1.36

**Table C1.4: Quantitative Analysis of Spectrum E in M<sub>2</sub> – HPC Series**

Atomic Ratio	M <sub>2</sub>	M <sub>2</sub> Sp <sub>1</sub> -0.2	Compound (Oxide)%	M <sub>2</sub>	M <sub>2</sub> Sp <sub>1</sub> -0.2
Mg	0.36	6.05	MgO	0.52	11.75
Al	1.01	5.83	Al <sub>2</sub> O <sub>3</sub>	1.83	14.31
Si	10.55	12.10	SiO <sub>2</sub>	22.64	35.02
S	0.00	0.81	SO <sub>3</sub>	0.00	3.14
K	0.00	0.28	K <sub>2</sub> O	0.00	0.63
Ca	7.26	12.82	CaO	14.53	34.61
Ti	0.19	0.14	TiO <sub>2</sub>	0.49	0.55
Fe	23.39	0.00	FeO	60.00	0.00
O	53.82	54.68			
Si/Ca	1.454	0.944	CaO/SiO <sub>2</sub>	0.642	0.988
Al/Ca	0.139	0.455			
S/Ca	0.000	0.063			
C: S	0.688	1.059			

**Table C1.5: Quantitative Analysis of Spectrum G in M<sub>2</sub> – HPC series**

Spectrum G	M <sub>2</sub>	M <sub>2</sub> Sp <sub>1</sub> -0.3	M <sub>2</sub> Sp <sub>1</sub> -0.4	M <sub>2</sub> Sp <sub>2</sub> -0.2	M <sub>2</sub> Sp <sub>2</sub> -0.3
Mg	0.78	1.56	1.52	1.56	1.62
Al	6.61	9.58	7.57	10.08	10.05
Si	7.02	1.43	3.74	2.36	2.05
S	0.15	0.00	0.00	0.00	0.15
Ca	18.77	21.63	22.58	23.05	21.47
Ti	0.16	0.42	0.33	0.26	0.26
Mn	0.00	0.25	0.22	0.34	0.21
Fe	6.63	7.52	5.69	6.96	6.16
Mo	0.40	0.00	0.00	0.00	0.00
O	51.38	49.03	49.49	52.27	49.62
Si/Ca	0.374	0.066	0.166	0.102	0.095
Al/Ca	0.352	0.443	0.335	0.437	0.468
S/Ca	0.008	0.000	0.000	0.000	0.007
C: S	2.675	15.093	6.032	9.789	10.485
SiO <sub>2</sub>	17.75	3.69	9.42	5.54	5.14
CaO	44.30	49.91	53.01	50.57	50.26
CaO/SiO <sub>2</sub>	2.496	13.529	5.629	9.136	9.786

**Table C1.6: Quantitative Analysis of other Phases observed in M<sub>2</sub> – HPC series**

Specimen	M <sub>2</sub> Sp <sub>2</sub> -0.3		M <sub>2</sub> Sp <sub>2</sub> -0.4		M <sub>2</sub> Sp <sub>1</sub> -0.3		M <sub>2</sub> Sp <sub>2</sub> -0.4		M <sub>2</sub> Sp <sub>1</sub> -0.4		
Spectrum	H	I	I1	J	J	L	M	N	O	P	Q
NaO	0.00	0.00	1.38	4.56	0.00	0.00	0.00	0.00	0.00	0.00	0.00
MgO	0.00	0.00	0.00	30.39	10.43	0.00	0.00	0.00	14.7	0.00	0.00
Al <sub>2</sub> O <sub>3</sub>	0.65	0.00	2.78	48.13	20.39	2.16	8.08	0.00	20.6	2.08	18.4
SiO <sub>2</sub>	8.64	0.51	7.60	0.00	36.89	19.39	10.72	0.64	35.6	31.0	65.9
SO <sub>3</sub>	15.6	0.00	0.00	9.49	0.00	0.00	28.66	50.8	0.00	0.00	0.00
K <sub>2</sub> O	0.00	0.00	0.22	0.00	8.24	0.00	1.03	0.00	0.00	0.00	15.7
CaO	25.4	0.00	0.25	0.00	0.00	0.00	1.81	0.00	0.00	29.3	0.00
TiO <sub>2</sub>	0.00	51.8	45.07	0.00	1.88	0.00	0.00	0.00	0.00	37.1	0.00
MnO	0.00	3.10	3.04	7.44	0.28	0.00	0.00	0.00	2.23	0.00	0.00
FeO	1.06	44.6	39.65	0.00	22.03	0.00	0.76	23.3	26.7	0.49	0.00
PbO	48.7	0.00	0.00	0.00	0.00	77.11	0.00	25.3	0.00	0.00	0.00
La <sub>2</sub> O <sub>3</sub>	0.00	0.00	0.00	0.00	0.00	0.00	10.22	0.00	0.00	0.00	0.00
Ce <sub>2</sub> O <sub>3</sub>	0.00	0.00	0.00	0.00	0.00	0.00	24.29	0.00	0.00	0.00	0.00
Nd <sub>2</sub> O <sub>3</sub>	0.00	0.00	0.00	0.00	0.00	0.00	8.82	0.00	0.00	0.00	0.00
ThO <sub>2</sub>	0.00	0.00	0.00	0.00	0.00	0.00	5.61	0.00	0.00	0.00	0.00
CaO/SiO <sub>2</sub>	2.94	0.00	0.03	0.00	0.00	0.00	0.17	0.00	0.00	0.94	0.00

**Table C1.7: Results of Quantitative Analysis of Spectrum B in M<sub>3</sub> - HPC**

Spectrum B	M <sub>3</sub>	M <sub>3</sub> Sp <sub>1</sub> -0.2	M <sub>3</sub> Sp <sub>1</sub> -0.3	M <sub>3</sub> Sp <sub>1</sub> -0.4	M <sub>3</sub> Sp <sub>2</sub> -0.2	M <sub>3</sub> Sp <sub>2</sub> -0.3	M <sub>3</sub> Sp <sub>2</sub> -0.4
Mg	0.52	0.14		0.43			0.00
Al	0.70	0.42		0.54			0.27
Si	10.41	13.33		10.45			13.30
S	0.03	0.13		0.00			0.00
K	0.02	0.17		0.00			0.11
Ca	30.41	26.78		31.10			27.37
Ti	0.06	0.06		0.05			0.00
Mn	0.00	0.00		0.00			0.00
Fe	0.34	0.27		0.23			0.22
O	53.36	55.04		53.75			54.65
Si/Ca	0.342	0.498		0.336			0.486
Al/Ca	0.023	0.016		0.017			0.010
S/Ca	0.001	0.005		0.000			0.000
C: S	2.921	2.009		2.977			2.058
SiO <sub>2</sub>	21.94	26.64		22.56			19.49
CaO	54.79	49.96		62.69			34.32
CaO/SiO <sub>2</sub>	2.50	1.88		2.78			1.76

**Table C1.8: Results of Quantitative Analysis of Spectrum D in M<sub>3</sub> - HPC**

Spectrum D	M <sub>3</sub>	M <sub>3</sub> Sp <sub>1</sub> -0.2	M <sub>3</sub> Sp <sub>1</sub> -0.3	M <sub>3</sub> Sp <sub>1</sub> -0.4	M <sub>3</sub> Sp <sub>2</sub> -0.2	M <sub>3</sub> Sp <sub>2</sub> -0.3	M <sub>3</sub> Sp <sub>2</sub> -0.4
F	0.00	0.00		1.19			0.00
Na	0.00	0.00		0.36			0.00
Mg	0.70	0.59		0.78			0.63
Al	2.12	1.75		1.99			2.81
Si	13.30	12.34		12.07			12.52
S	0.68	0.85		0.63			0.85
K	0.12	0.09		0.38			0.47
Ca	21.94	23.43		22.78			21.35
Ti	0.06	0.08		0.10			0.09
Mn	0.00	0.00		0.00			0.00
Fe	0.98	0.88		0.99			0.77
O	55.61	54.96		54.16			54.98
Si/Ca	0.606	0.526		0.530			0.587
Al/Ca	0.097	0.075		0.088			0.131
S/Ca	0.031	0.036		0.028			0.040
C: S	1.651	1.900		1.887			1.704
SiO <sub>2</sub>	21.67	18.25		19.49			16.62
CaO	34.39	32.36		34.32			26.44
CaO/SiO <sub>2</sub>	1.59	1.77		1.76			1.59

**Table C1.9: Results of Quantitative Analysis of Spectrum B in M<sub>3</sub> - HPC**

Spectrum B	M <sub>1</sub> F	M <sub>1</sub> FSp <sub>1</sub> -0.2	M <sub>1</sub> FSp <sub>1</sub> -0.3	M <sub>1</sub> FSp <sub>1</sub> -0.4	M <sub>1</sub> FSp <sub>2</sub> -0.2	M <sub>1</sub> FSp <sub>2</sub> -0.3	M <sub>1</sub> FSp <sub>2</sub> -0.4
F	0.00	1.05	1.22	0.00	0.00		0.00
Na	0.00	0.00	0.00	0.00	0.00		0.00
Mg	0.18	0.14	0.34	0.45	0.39		0.42
Al	0.76	0.70	0.71	0.62	0.60		0.84
Si	12.67	12.95	11.30	10.38	10.71		12.77
P	0.00	0.08	0.00	0.00	0.00		0.12
S	0.13	0.11	0.07	0.00	0.00		0.11
K	0.22	0.27	0.07	0.00	0.00		0.41
Ca	26.91	26.34	28.88	30.72	30.93		25.99
Ti	0.06	0.05	0.04	0.00	0.00		0.08
Mn	0.00	0.00	0.00	0.00	0.00		0.00
Fe	0.32	0.37	0.36	0.30	0.35		0.44
O	54.51	54.58	53.57	53.17	53.99		54.66
Si/Ca	0.471	0.491	0.391	0.338	0.346		0.491
Al/Ca	0.028	0.027	0.025	0.020	0.019		0.032
S/Ca	0.005	0.004	0.002	0.000	0.000		0.004
C: S	2.125	2.035	2.555	2.960	2.887		2.035
SiO <sub>2</sub>	21.98	28.38	24.09	17.48	22.94		22.54
CaO	43.59	53.91	57.49	48.29	62.31		42.81
CaO/SiO <sub>2</sub>	1.98	1.90	2.39	2.76	2.72		1.90

**Table C1.10: Results of Quantitative Analysis of Spectrum D in M<sub>3</sub> - HPC**

Spectrum D	M <sub>1</sub> F	M <sub>1</sub> FSp <sub>1</sub> -0.2	M <sub>1</sub> FSp <sub>1</sub> -0.3	M <sub>1</sub> FSp <sub>1</sub> -0.4	M <sub>1</sub> FSp <sub>2</sub> -0.2	M <sub>1</sub> FSp <sub>2</sub> -0.3	M <sub>1</sub> FSp <sub>2</sub> -0.4
F	0.00	1.26	1.26	0.00	0.91		0.00
Na	0.00	0.00	0.30	0.00	0.35		0.00
Mg	0.68	0.49	0.42	0.61	0.67		0.65
Al	2.81	4.40	2.34	2.66	3.19		1.44
Si	13.69	14.10	14.28	16.11	12.97		13.08
P	0.00	0.00	0.06	0.00	0.00		0.00
S	0.68	0.51	0.44	0.80	0.77		0.87
K	0.15	0.22	1.18	0.00	0.51		0.14
Ca	20.31	17.99	19.52	16.81	19.94		22.25
Ti	0.04	0.00	0.10	0.09	0.07		0.12
Mn	0.00	0.00	0.00	0.00	0.00		0.00
Fe	0.72	0.87	0.62	0.78	0.78		0.95
O	55.51	55.80	55.00	57.00	55.01		55.08
Si/Ca	0.674	0.784	0.731	0.959	0.650		0.588
Al/Ca	0.138	0.244	0.120	0.158	0.160		0.065
S/Ca	0.033	0.029	0.022	0.048	0.039		0.039
C: S	1.483	1.276	1.367	1.043	1.538		1.701
SiO <sub>2</sub>	18.69	23.71	24.07	23.41	20.12		17.73
CaO	25.71	28.24	29.57	22.79	28.57		28.14
CaO/SiO <sub>2</sub>	1.376	1.191	1.228	0.974	1.420		1.588